# THE OXIDATION OF LIQUID ALUMINIUM AND THE POTENTIAL FOR OXIDES IN GRAIN REFINEMENT OF ALUMINIUM ALLOYS

by

# Elizabeth Mary Hinton

A thesis submitted to the University of Birmingham for the degree of DOCTOR OF PHILOSOPHY

School of Metallurgy and Materials
College of Engineering and Physical Sciences
University of Birmingham
August 2014

# UNIVERSITYOF
# BIRMINGHAM

**University of Birmingham Research Archive**

**e-theses repository**

**Abstract**

Aluminium and their alloys readily react with air to form surface oxides and films. If they become entrained in a casting, they form double oxide film defects that reduce the mechanical properties of the component. It is important to determine the nature and behaviour of the films formed, so that defects can be avoided or their internal gas volumes reduced. The reaction of common additions and impurities that may be present in aluminium alloys were melted at 750 °C in air and nitrogen, to determine thickness, composition and structure of possible films that may form in a defect. The effects of molybdenum were also investigated.

It has also been suggested that oxides formed on aluminium alloys may act as heterogeneous nucleation points for solidification. Spinel containing copper layers were manufactured by electro-codeposition, and added to commercial purity aluminium to test its potential as a grain refiner. It was compared with non-refined aluminium and aluminium refined with standard Al-5Ti-1B  refiner. The lattice parameters of oxides formed were also compared with that of aluminium to ascertain their potential as nucleation centres. The results are discussed in this work.

It was found that Superpure Al grew an oxide of up to 0.37 μm over 24 hours and formed alumina structures of γ –alumina with traces of α-alumina by this time. The growth did not appear to follow the parabolic law, but may have followed a hyperbolic law. Alloying additions and impurities affected the oxidation rate in different ways. The additions of 4 wt.% Mg, 7 wt.% Si-0.3 wt.% Mg, 4 wt.% Cu, 0.3 wt.% Sr, and powdered Mo all increased the oxidation rate by forming permeable surface oxides layers. In contrast, additions of 1 wt.% Fe reduced the oxidation rate and 7 wt.% Si appeared to have no effect on the rate. The addition of 1 wt.% Mo to Al also did not appear to change the rate, but the addition to Al-7 wt.% Si-0.3 wt.% Mg increased the rate and formed a few different oxide structures within the layer. A nitrogen atmosphere led to the formation of aluminium nitride on pure Al but with a thicker surface layer. Al-4 wt.% Mg had a much lower oxidation rate than in air as, did Al-7 wt.% Si-0.3 wt.% Mg. As a result it was concluded that the likely layers to assist with closure of double oxide film defects were those formed on superpure Al, Al-Mg, Al-Cu , Al-Sr and Al-Mo.

The lattice parameters of the formed oxides were assessed to determine their ability to act as grain refiners for Al alloys. In order of effectiveness they were $MoO_2$, $MoO_3$, MgO and α-alumina.

2

Electro-codeposition was carried out to form a layer of copper with particles of $MgAl_2O_4$ within it. The layer with the most particles (8.5 wt. %) was formed using a pulse reverse frequency of 200 Hz with an electrode rotation speed of 1000 rpm. The addition of several samples made this way was added to commercial purity Al (~50 ppm in total) and the result of the grain size analysis compared to the addition of 125 ppm of a commercial Al-5Ti-1B refiner and commercial purity Al with no additions. The additions of $MgAl_2O_4$ and Al-5Ti-1B reduced grain size by 23% and 36% respectively.

**Acknowledgements**

## Introduction

Aluminium is a reactive metal, immediately oxidising on contact with air. These oxides can become entrained in the bulk of a casting during surface turbulence, causing double oxide film defects and reducing the mechanical properties. The double oxide film defect effectively acts as a large crack or hole in a cast component as the two surface come in to contact. The temperature of the aluminium melts are not high enough to enable the two oxide surfaces to bond together, leaving an inherent weak point in the cast part. They are also often the cause of shrinkage porosity, as the part solidifies and the oxide is pulled apart to leave a large defect. Therefore, it is important to understand the nature of these films in order to determine how they may behave in a defect with regards to defect closure. (Campbell 2003).

Oxidation of aluminium is affected by many variables. It is influenced by temperature, with a higher temperature leading to an increase in the thickness of the oxide. When liquid aluminium oxidises in air it first forms an amorphous oxide, which crystallises to form γ-alumina which, after time, forms α-alumina. This α-alumina has a smaller volume than γ-alumina and this leads to cracks in the oxide, exposure of the liquid metal underneath the oxide layer and an increase in the oxide layer (Bergsmark et al 1989, Blackburn and Gulbransen 1960, Drouzy and Mascré 1969, Impey et al 1993).

Additional elements added to aluminium affect how the metal oxidises. The addition of elements like magnesium and copper has been shown to increase the oxidation rate of aluminium. Elements such as beryllium have been shown to reduce the oxidation rate. It is important to know how alloying and possible impurity elements would affect oxidation of the liquid metal and so how they would behave in a casting (Agema and Fray 1989, Scamans and Butler 1975, Thiele 1962).

The atmosphere in the casting environment affects how the oxide forms. If argon and nitrogen make up the surrounding atmosphere the oxidation of aluminium slows, as little to no oxygen would be present in the atmosphere, and so the oxidation would not be able to occur. Humid atmospheres tend to result in a higher overall oxide thickness. The effects of atmosphere on the oxidation is an important issue, not only for surface oxides and castings, but for how the atmosphere in a double oxide film defect would change its behaviour (Cochran et al 1977. Raeiszadeh 2005).

It has been suggested that oxides may act as grain refiners in castings. The benefits of a small grain size on mechanical properties of cast parts, such as increased tensile strength and ductility, have been widely reported. The size of internal defects is also reduced, which in turn reduces scrap rates and cost savings (Cook 1998, Fan et al 2011). Grain refinement in castings is generally achieved by the addition of refiners containing titanium diboride. These react to form titanium aluminide compounds that act as heterogeneous nuclei. The ability for oxides to act as nucleants would provide the potential for the recycling of aluminium, which is currently difficult and expensive (Fan et al 2009, Perepezko & LeBeau 1981).

Oxides and traditional grain refiners (e.g. $MgAl_2O_4$ and 5:1 Ti:B ) can be added as master alloys made by electro co-deposition. Pulse reverse plating can be used to manufacture layers of metal substrate containing small oxide particles. The pulse reverse process makes it possible to attract particles of different charges to make up the same composite layer. These composite layers can be added to liquid metal to so that the oxide particles ($MgAl_2O_4$) can act as nucleation centres for solidification (Podlaha & Landolt 1997, Weston et al 2011).

The effects of holding time was observed on samples of aluminium, both as a pure metal and with additions of magnesium, silicon (both and separately), copper, iron, strontium and titanium. They were held at 750 °C for logarithmic times in air. The samples were observed using scanning electron microscopy, energy dispersive x-ray analysis and x-ray diffraction in order to ascertain the thickness, composition and structure of the different alloys. The effects of molybdenum as powder and as an alloying element was also observed. The pure aluminium, aluminium-magnesium and aluminium-silicon-magnesium alloys were also melted in a nitrogen atmosphere.

To discover the potential of oxides as grain refiners, layers of copper with alumina-magnesia spinel were made using electro-codeposition methods. The layers were optimised for maximum spinel content and added to aluminium melts which were cast in to test bar moulds. The test bars were compared with non-refined aluminium and a standard grain refiner.

The oxides and nitrides formed in the experiments were judged for their ability to help reduce the volume of double oxide film defect. Their lattice parameters were compared to that of aluminium and the mismatch observed for their potential as nucleants for solidification of aluminium.

## 1 - Literature Review

Aluminium (Al) is a reactive metal, and forms an oxide skin immediately on contact with air. Surface turbulence can draw the oxide skin into a casting, leaving a weak point in the component (Campbell 2003). Therefore, it is important that the formation and growth of oxides on metals is understood as much as possible. The ideal situation of having no surface oxide could be impossible to achieve, but through understanding the nature of the oxides, it may be possible to have a degree of control over them, and minimise them as much as possible.

## 1.1 - Oxidation of Aluminium and its Alloys

### 1.1.1 - Structure and the Effect of Temperature on the Oxide

Oxidation of aluminium is complex, with temperature, impurities and experimental technique all affecting its behaviour (Bergsmark et al 1989). Pure aluminium reacts immediately on contact with air, forming an amorphous layer of aluminium oxide or alumina ($Al_2O_3$). This amorphous film quickly develops crystals within the layer, initially forming $\gamma$-$Al_2O_3$. This is a protective film and its growth is controlled principally by diffusion of Al ions through the $\gamma$-alumina layer, so the oxidation rate slows. After an induction period (which decreases with increasing temperature) the $\gamma$-$Al_2O_3$ transforms to corundum, or $\alpha$-$Al_2O_3$, which is denser and less protective (Impey et al 1993, Drouzy & Mascré 1969). The $\alpha$-$Al_2O_3$ has a smaller volume than the $\gamma$-$Al_2O_3$ resulting in cracks forming in the oxide layer. This leads to a much faster rate of oxidation, as the liquid metal beneath the oxide becomes exposed to air. These react and lead to the growth of more oxide in the cracks. This is known as breakaway oxidation. There is a higher mobility of O ions within the layer, with O diffusion dominating the growth, and so the rate of the $\alpha$-alumina growth is slower. It is more the formation of cracks that increases the rate (Agema & Fray 1989). A schematic of oxide growth is shown in Figure 1.
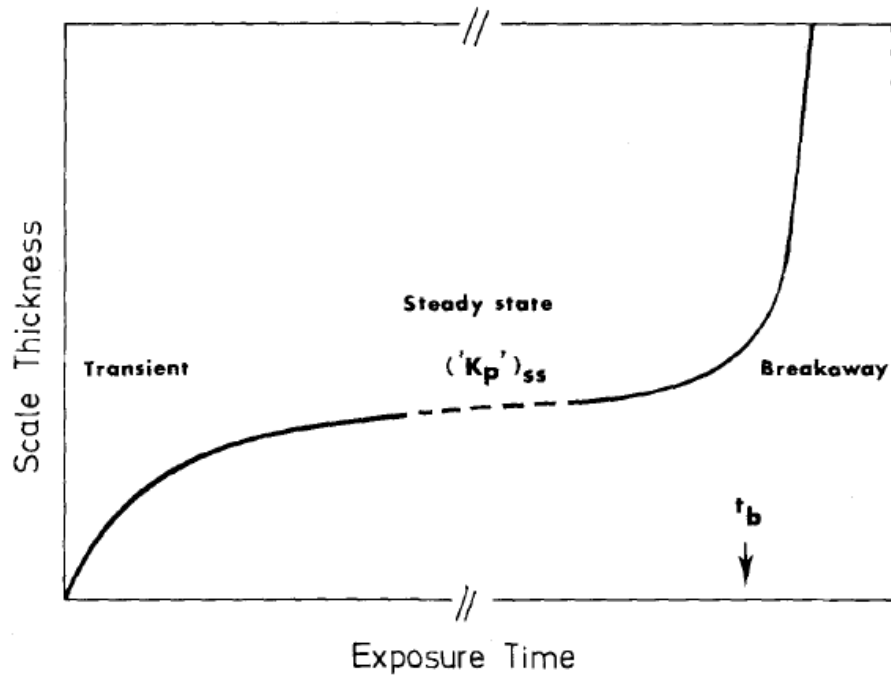
**Figure 1 - A schematic of oxide growth of a protective oxide (Hindam & Whittle 1982)**

The rate of oxidation very much depends on temperature and composition of the surrounding environment. Up to around 350°C, the reaction can be described as inverse logarithmic. From 350°C to 450°C it is thought to grow parabolically (Beck et al 1967). At higher temperatures the growth can be complex, including linear growth and other non-parabolic growth patterns (Blackburn & Gulbransen 1960, Sleppy 1961).
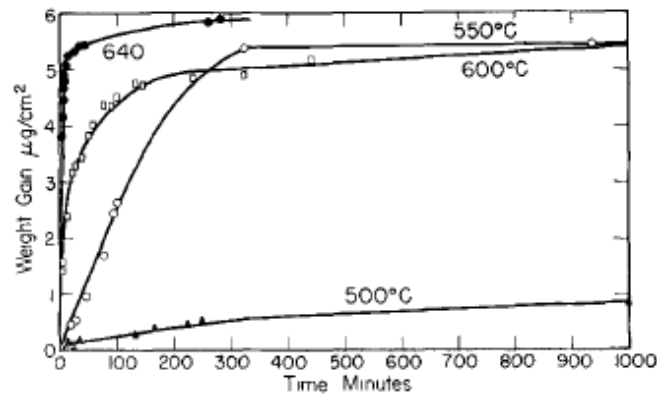


**Figure 2 – Effect of temperature on the rate of aluminium oxidation in 0.1 atm O2 (Blackburn & Gulbransen 1960)**

Temperature has a marked effect on oxidation rate. Figure 2 shows the effect of temperature on the oxidation rate of aluminium in dry oxygen. It can be generally seen that the oxidation rate increases with increasing temperature. The figure shows that the rate of initial oxidation increases rapidly with increased temperature. This corresponds to the growth of crystalline γ-alumina, which grows on amorphous alumina. At the end of this fast period of growth, the

11

crystalline γ-Al$_2$O$_3$ growth rate can be seen to level off, which is likely to be a result of the γ-Al$_2$O$_3$ becoming a continuous oxide and therefore more protective. This occurs after only a few seconds at 640°C, whereas at 500°C it is difficult to see where the transition is due to the slow rate of the initial oxidation. The rate of the second, slower stage of oxidation also increases with temperature, also meaning the induction period before the formation of α-Al$_2$O$_3$ decreases (Blackburn & Gulbransen 1960). Thiele also reported that weight gain due to oxidation greatly increased with temperature, with an oxide on a 99.9% aluminium alloy having grown more than double at 800°C than at 700°C. Also the rate is much quicker, as after 1 hour the thickness of the γ-Al$_2$O$_3$ oxide layer was ~9000Å at 700°C, remaining stable for up to 25 hours before oxidation resumed. At 800°C the oxide grew to ~10,000 to 20,000Å and suppressed further oxidation for ~8 hours, after which the growth rate increased and the decreased in a signoidal manner. Above 900°C the corundum may form not only from the γ-Al$_2$O$_3$ but directly from the amorphous film, due to the pronounced increase in growth rate (Agema & Frey 1990, Thiele 1962).
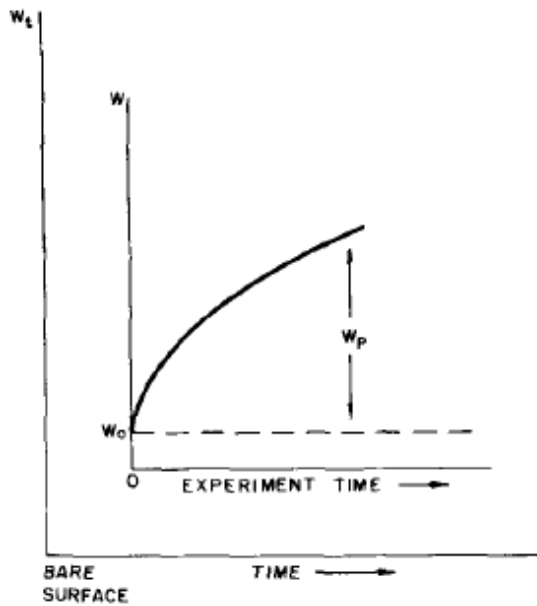


**Figure 3 - Schematic diagram of oxide growth on aluminium (Sleppy 1961)**

A schematic of the growth of oxide on aluminium can be seen in Figure 3, where W is experimentally measured oxide growth, $W_t$ is the oxide growth from the bare metal surface, $W_p$ is oxide growth controlled by diffusion and $W_o$ is the rapid oxidation that occurs in the early stages of reaction (all in μg/cm$^2$). Sleppy in 1961 determined that oxide growth at 660-700°C in a vacuum corresponds to a direct logarithmic law:

$$W = K \ln(at + 1) \qquad (1)$$

12

where $K$ = a constant, $a$ = a constant with dimensions time$^{-1}$ and $t$ = time. It was also determined that the oxide at 750°C follows a modified parabolic law of:

$$W^2 + K_1 W = K_2 t + K_3 \qquad (2)$$

It was found that $W_p$ from Figure 3 obeys the law set out in equation (2) and so can be rearranged:

$$\frac{dW_p}{dt} = \frac{K_p K_c C_o}{K_c W_p + K_p} \qquad (3)$$

where $K_p$ = physical constant related to transport of matter across the oxide film, $K_c$ = chemical constant and $C_o$ = concentration of diffusing species at the metal-oxide interface. If equation (3) is intergrated, it gives:

$$^1/_2 K_C W_p^2 + K_p W_p = K_p W_c C_o t + K' \qquad (4)$$

$$W_p^2 + k_1 W_p = K_2 t + k_3 \qquad (5)$$

$W_p$ is then substituted in terms of $W$ ( $W_p = W - W_o$, experimentally derived) to give:

$$W^2 - 2WW_o^2 + W_o + k_1 W - k_1 W_o = K_2 t + k_3 \qquad (6)$$

$W_o$ can be considered a constant, and so will not change with time. Equation (6) can be rearranged and then simplified to give:

$$W^2 + (k_1 - 2W_o) + (W_o^2 - k_1 W_o) = K_2 t + k_3 \qquad (7)$$

$$W^2 + K_1 W = K_2 t + K_3 \qquad (2)$$

Parabolic growth is generally described in Scully (1990) as:

$$y^2 = Kt \qquad (8)$$

where $K$ is parabolic oxidation rate constant and $y$ is thickness of the oxide. There are two driving forces for parabolic growth, i.e. concentration and electric potential gradients, as they account for diffusion and migration across the oxide film. Both of the rates are inversely proportional to the thickness of the oxide, so it can be shown that:

$$\frac{dy}{dt} = \frac{K_{diffusion}}{y} + \frac{K_{migration}}{y} \qquad (9)$$

where $K_{diffusion} + K_{migration} = K$. As long as boundary conditions are ignored and the field does not act on particles asymmetrically, both cases have the same energy dissipated. Parabolic oxidation can therefore be considered from a diffusion or electrical migration viewpoint.

The derivation of equation (8) can be done from Fick's law of diffusion:

$$\frac{dm}{dt} = DA \frac{dc}{dx} \qquad (10)$$

13

where dm = amount of matter diffused by distance dx in time dt, D = diffusion constant, A = area, dc = change in concentration across dx. This can then be integrated:

$$m = DA\frac{dc}{dx}t + \text{constant} \qquad (11)$$

The term m can be defined:

$$m = \frac{yA\rho nM}{W} \qquad (12)$$

where m = mass of species diffusing through the oxide, $\rho$ = density of oxide, n = number of atoms of diffusing species contained in a molecule of oxide, M = atomic weight of species diffusing and W = molecular weight of oxide.

If the m from equation (11) is replaced by that from equation (12), where dx=y:

$$\frac{yAMn\rho}{W} = DA\frac{dc}{y}t \qquad (13)$$

which can be rearranged to give equation (8):

$$y^2 = Kt \qquad (8)$$

Where $K = \frac{WDdc}{Mn\rho}$.

The growth of oxides for most metals seems to conform to parabolic growth. Oxide growth is a temperature dependant as it is dominated by diffusion of ions. The rate constant has an exponential relationship with temperature:

$$K = K_0\exp\left({-Q}/{RT}\right) \qquad (14)$$

where Q = activation energy for the diffusion, R = gas constant, T = temperature, $K_0$ = constant (Scully 1990).

In 1956, Hart concluded that the initial fast oxidation of Al followed the direct logarithmic law, as set out in equation (1). He also concluded that the slower region of growth follows an inverse logarithmic law, and this was derived by Evans (1960). It is derived from the general equation for passage across a uniform film. It is taken that the potential gradient across the film is only electrical in nature.

$$\frac{1}{y} = K_1 - K_2\ln(a(t - t_0) + 1)$$

14

This is the reverse logarithmic law, and oxidation of aluminium in dry was thought to follow this law, but little evidence has been found to support it. The law appears to only be applicable at low temperatures (below 350 °C) and is not relevant for high temperature oxidation.

1.1.2 - Atmospheric Effects

Atmospheric conditions affect oxidation and its rate. Figure 4 shows how different combinations of oxygen, water vapour and hydrogen can change the oxidation rate. It has been concluded that additions of oxygen and hydrogen to water vapour did not change the reaction rate very much. However, it was noted that water vapour reacts quickly with the surface aluminium and increases the initial oxidation rate and formation of crystalline oxide. The oxidation rate is then slowed by the presence of water vapour with the incubation period increasing. However, this results in a higher overall weight gain as can be seen by comparing Figure 5a and Figure 5b (Blackburn & Gulbransen 1960).
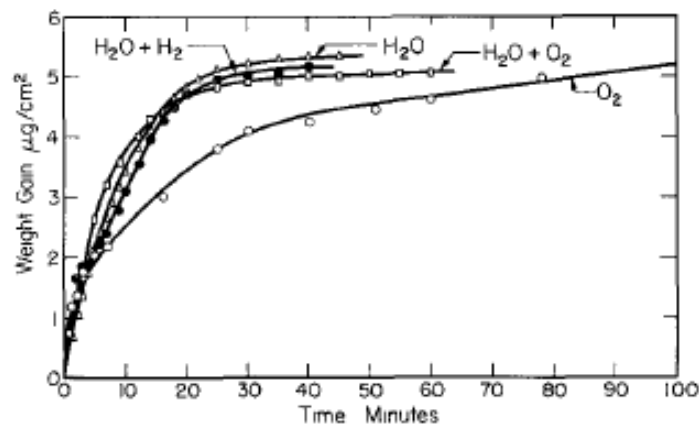


**Figure 4 - Effect of different atmospheres on oxidation rate at 600 °C (Blackburn & Gulbransen 1960)**

Other atmospheric conditions can also affect the oxidation behaviour. The addition of nitrogen ($N_2$) to the oxygen atmosphere prolongs the period of slow oxidation before the onset of breakaway oxidation. Argon (Ar) has a similar effect of slowing oxidation, but the effects are not as pronounced when used in similar quantities (typically 4 parts to 1 of air). These effects can be seen in Figure 6a. Carbon dioxide ($CO_2$) also slows the onset of breakaway oxidation. It has been shown that when 65% $CO_2$ atmosphere (air balance) is used, breakaway oxidation can be halted for around 16-18 hours, but with 50% $CO_2$ or less it occurs after around 1 hour. Flue gas containing water vapour, $N_2$ and $CO_2$ was also found to slow oxidation, although it did not have as strong an effect as $CO_2$ alone (Cochran et al 1977).
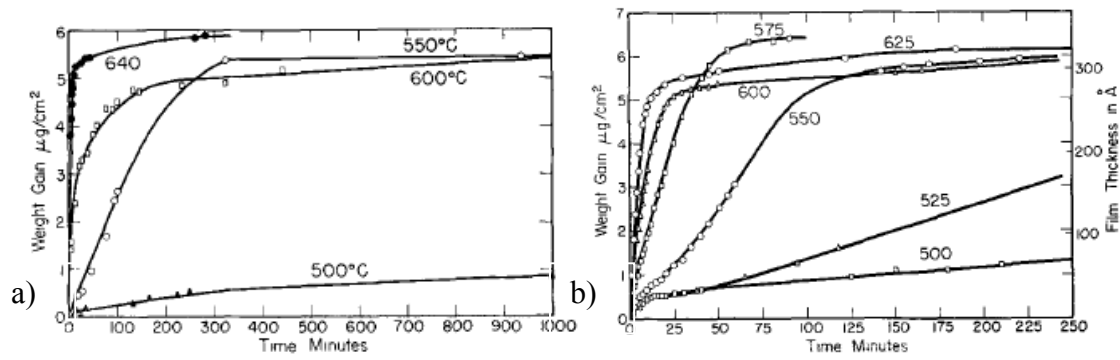
**Figure 5 - Oxidation of aluminium in a) 0.1 atm oxygen and b) 0.1 atm water vapour (Blackburn & Gulbransen 1960)**

It has been found that sulphur hexafluoride (SF$_6$) has an effect on the oxidation rate of magnesium alloys, and so could have a similar effect on aluminium. Under an atmosphere of SF$_6$, the liquid magnesium wets the solid magnesium oxide (MgO) particle that formed from initial contact with oxygen. This means that the MgO particles draw up the liquid Mg up their sides by capillary action, as seen in Figure 7a. Capillary forces, F$_c$, then draw together the oxide particles forming a "raft" of oxide particles floating on the metal surface, and can be seen in Figure 7b. This results in the minimum amount of liquid Mg being exposed to oxygen, reducing the overall oxidation rate (Cashion et al 2002).
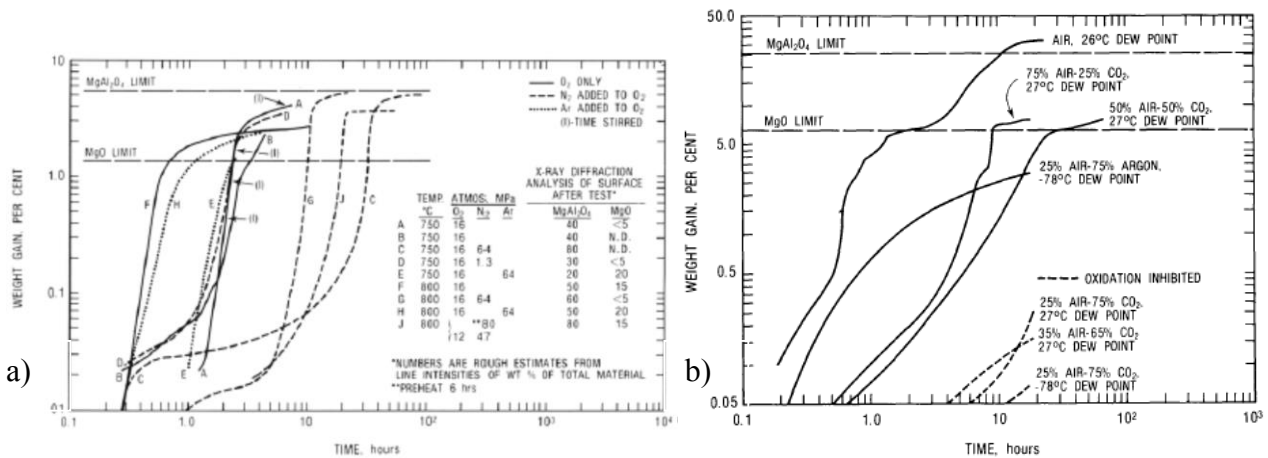


**Figure 6 - Effects of different gases on oxidation of aluminium a) nitrogen and argon b) carbon dioxide in different quantities (Cochran et al 1977)**
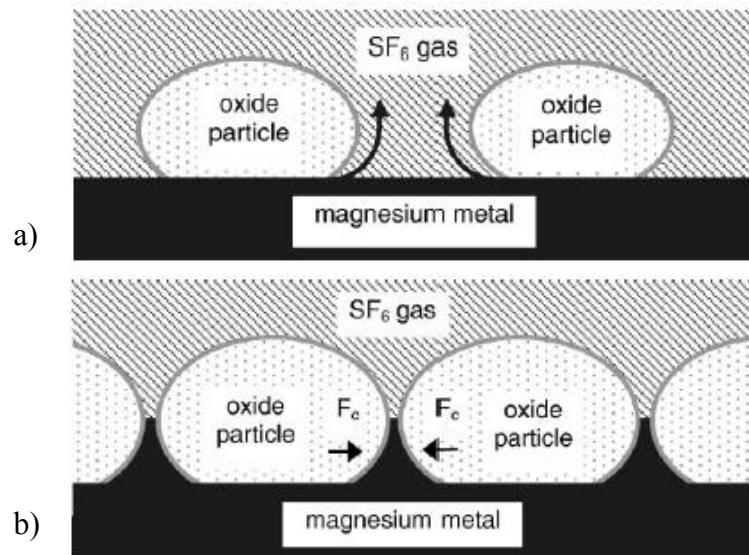
**Figure 7 - An illustration of how SF$_6$ protects molten magnesium from oxidation a) wetting of the oxide particles b) drawing together of particles by capillary forces, F$_c$ (Cashion et al 2002)**

Nitrogen has been observed to have an effect on the oxidation of aluminium. Various authors found that Al and N$_2$ react to form AlN. Gerrard and Griffiths (2014) saw that if a sample is held in N$_2$ at 700 °C prior to being held in hydrogen (H$_2$), the H$_2$ pores formed had a film of AlN within them. This suggested that AlN had formed prior to the H$_2$ being introduced. It has also been noted that when a bubble of air is held in liquid aluminium for an extended time, the oxygen will react first to form alumina. When the atmosphere of the bubble contained 5% O$_2$ or less, the aluminium would then react with nitrogen to form AlN. This suggested that once most of the oxygen present within the air bubble had been used up in the oxidation reaction, the remaining nitrogen is able to react with the liquid Al to form AlN (Raeiszadeh 2005).

1.1.3 - Alloying and Additional Elements

Alloying elements can have a marked effect on the oxidation behaviour of aluminium. They often incorporate their own oxides into the oxide layer of aluminium, which is why they can change the oxidation rate. An element can give another protective oxide layer on top, mix with the existing Al$_2$O$_3$ layer therefore lowering the rate, or increase ion mobility within the oxide layer itself (Agema & Fray 1989). Beryllium (Be) has a strong effect on the oxidation rate, as shown for an Al-magnesium alloy in Figure 8. Even in small amounts such as 0.001wt%, Be has been found to significantly hinder the onset of breakaway oxidation for many hours (Cochran et al 1977). Elements such as sodium, calcium and selenium have been shown to increase the oxidation rate of pure aluminium, whilst a presence of boron or titanium can result in a thicker oxide (Thiele 1962, Drouzy & Mascré 1969).
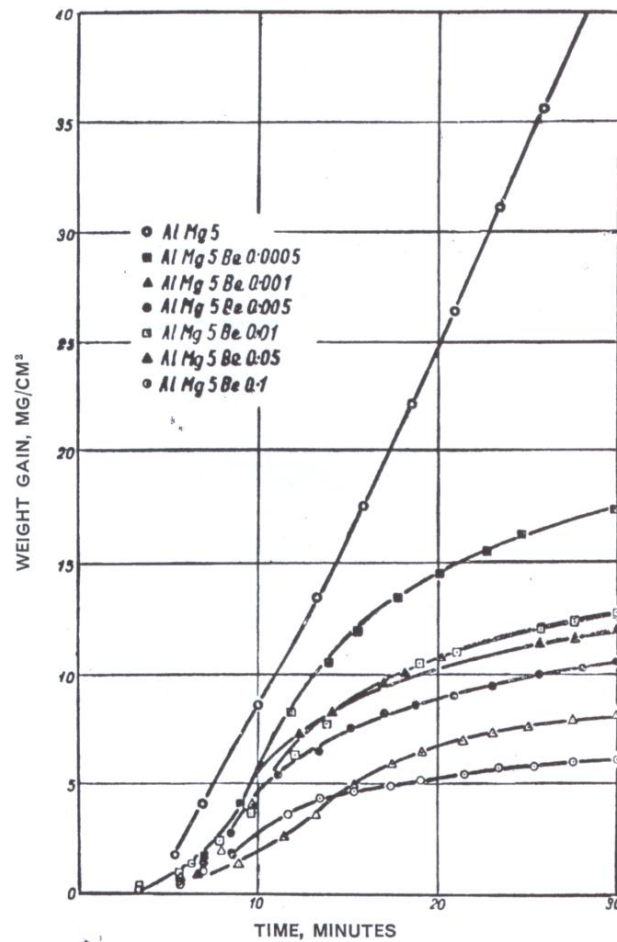
**Figure 8 - Effects of beryllium on oxidation rate of aluminium at 700 °C (Drouzy & Mascré 1969)**

Other common alloying additions and impurities can have an effect on the oxidation behaviour of Al alloys, and this was summarised by Thiele (1962) in

Figure 9. It has been found that Si alone, has little effect in the oxidation rate. Oxide growth was similar to that formed on commercial purity Al. Additions of 1 at. % (Thiele 1962) and 12.5 wt.% (Partington et al 1998) have been added to Al, and both authors found little difference in the oxide growth.
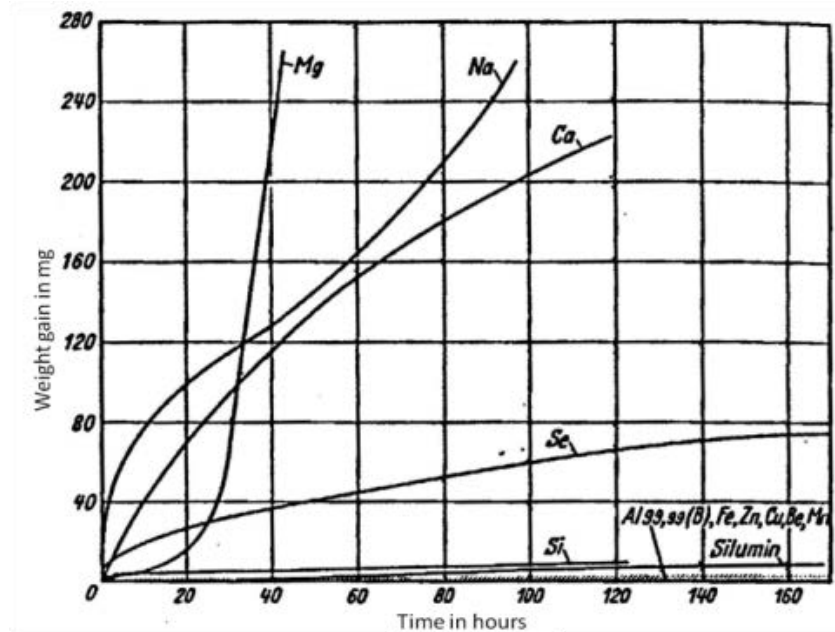
**Figure 9 - The effect of different elemental additions on Al at 700 °C, (additions levels of 1 at.%, except Si, Na 0.029 at.%, Se 0.0034 at.%) (Thiele 1962)**

The presence of Cu in Al has been shown to increase the oxidation rate (Saunders and Pryor 1968). Brock and Pryor (1973) discovered the how growth of the oxide on an Al-Cu alloy progresses. Initially, an amorphous alumina grows parabolically, via Al and electrons migrating towards the surface and reacting with air to form an amorphous oxide. The presence of Cu (a 2+ cation, as opposed to the 3+ cation of Al) reduces the overall charge of the lattice, as the positive (cation) and negative (O) sub-lattices are now not balanced. At temperatures over 525 °C, the number of anion vacancies is increased as oxygen ions are removed from the O sub-lattice in order to restore the charge balance. The oxygen ions migrate inwards through defective regions in the amorphous lattice, leaving a number of anion vacancies. Crystalline oxide develops at the metal-oxide interface as a rod-like structure which then grows and causes undulations in the surface oxide. This is shown in Figure 10 (Brock & Pryor 1973).
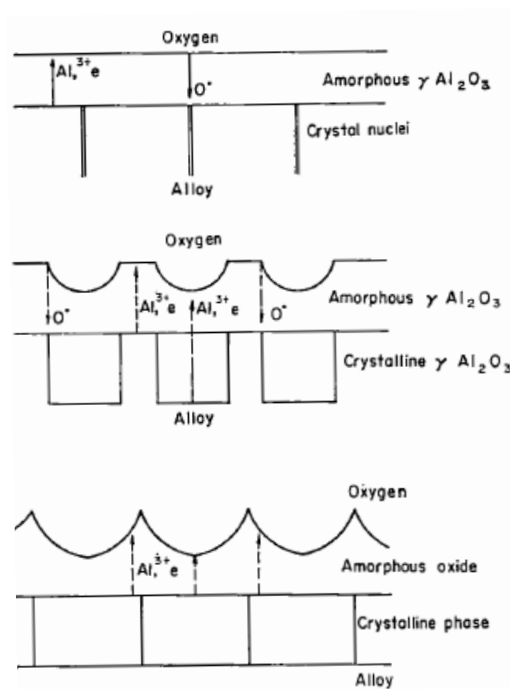
**Figure 10 - Schematic of oxide growth on Al-Cu alloys (Brock & Pryor 1973)**

The addition of zinc (Zn) increases the incubation period before breakaway oxidation, thought to be done by increasing the number of anion vacancies in the amorphous oxide layer, similar to Cu. This would prevent ingress of oxygen towards the oxide/metal interface. It is thought it may also reduce the cation vacancies in the crystalline $Al_2O_3$. The lack of vacancies and reduction of movement of oxygen particles throughout the oxide film would mean a low rate of growth. If the film is charge neutral, ions will not migrate through the lattice and react to thicken the oxide (Scamans & Butler 1975). In order for the oxide to grow, there must be transport of ions and electrons within the oxide, as shown in

Figure 11. The aluminium ions move out towards the atmosphere and the oxygen ions move in towards the metal. As the ions move by diffusion, movement of ions between vacant lattice sites determines its rate as shown in equation (11). Aluminium oxide is deficient in anions and so the anion lattice contains vacancies. This means that electrons moving through the oxide are maintained within the structure and the charge remains balanced. However additions affect how the ions move in the oxide and this is how the oxidation rate is changed. Aluminium has a valency of +3, and additions that have a higher valency provide more electrons to the lattice (Scully 1990).
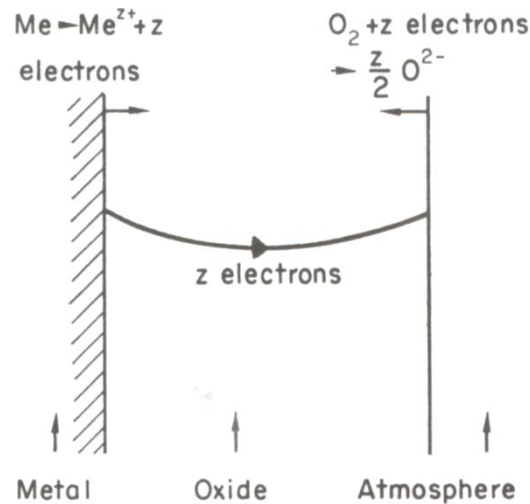
**Figure 11 - Ionic movement during parabolic growth of aluminium oxides, from which the growth laws are taken (Scully 1990)**

When Strontium (Sr) is present in Al alloys, it forms its own oxide SrO. A356 alloy (Al-7 wt.% Si-0.35 wt.% Mg) with an addition of 0.4 wt. % Sr was sand cast at 710-730 °C and contained pores covered with alumina, $MgAl_2O_4$, with Sr-Si intermetallics. Porosity in Al-Sr alloys is an issue, and is thought to be due to Sr reacting with moisture and forming pores (Miresmaeili et al 2005). Even low additions of 660 ppm formed an oxide of $Al_2SrO_3$. This forms during melting, as sr has a high affinity for oxygen (Liu et al 2003)

Al-Fe alloys tend to oxidise more slowly than pure Al. An Al-4.8 wt.% Fe alloy was melted at 800 °C in a damp hydrogen atmosphere for 450 minutes (7 hours) and formed γ-alumina (Grace & Seybolt 1958). Whereas pure Al had started to form α-alumina at 320 minutes (5.3 hours) (Thiele 1962). It has been shown that the composition of the oxide changes with increase oxidation time. Over an eleven minute period, the elemental composition of the oxide on an FeCrAl alloy changed. As the oxide grew, the amount of oxygen and Al increased, as the amount of Fe and Cr decreased. This suggests the growth of oxide in this case is dominated by Al ions moving outwards from the oxide and the O ions moving in, meaning the oxide becomes enriched in Al (Hou 2003). Oxide growth was found to decrease with the addition of Yttrium(Y). The presence of Y seemed to supress the outward diffusion of Al ions, and prevented void formation at the metal/oxide interface. This occurred even at high temperatures of 1200 °C for 5 hours. It was concluded that oxidation was likely to occur via diffusion on grain boundaries (Mennicke et al 1998). This was also concluded by Prescott & Graham (1992).

Prescott & Graham (1992) stated that the growth of γ-alumina was dominated by transport of Al and O ions through the layer and it was this transport processes that determined the thickness

21

of the oxide. Y also changes how the oxide growth, encouraging a columnar growth rather than equiaxed, which deform more easily and lead to higher oxidation rate (Prescott 1992 & Graham).

Oxidation rate can be affected by the strength and deformation of the oxide layer. Oxide strength plays an important role when the liquid underneath the layer is moving. If a continuous oxide layer has poor strength properties, it will rupture many times upon movement of the underlying liquid. This will lead to fresh liquid becoming exposed to the atmosphere, which will itself become oxidised, leading to an increase in the oxidation rate. The strength decreases as oxidation temperature and time increase, meaning cracks will initiate more easily at high temperatures and long exposure times. Additions also change the strength of the oxide layer, with elements such as calcium (Ca), sodium (Na), lithium (Li) and magnesium (Mg) increasing the strength, and elements such as beryllium (Be), silicon (Si), antimony (Sb) and strontium (Sr) decreasing it (Agema & Fray 1989). The addition of Y increases the deformation resistance of the oxide scale, whilst the presence of sulphur (S), chlorine (Cl) and phosphorus (P) reduce the adhesion between the oxide and the substrate, which also increases the oxidation rate. If adhesion is poor, the oxide is more easily detached from the underlying metal, leaving the liquid metal surface exposed to further oxidation. Yttrium segregates to the interface and improves adhesion (Prescott & Graham 1992)

### *1.1.3.1 - Aluminium-Magnesium Alloys*

One of the main alloying elements used with aluminium is magnesium. It is used in different amounts depending on the properties required of the alloy. Magnesium is a reactive metal and as such changes how the oxide forms and behaves. The oxidation rate tends to increase with increasing amount of Mg additions. When Mg is present in the alloy it oxidises preferentially to the aluminium, so the amorphous $Al_2O_3$ forms magnesium oxide (MgO) instead of $\gamma$-$Al_2O_3$ or $\alpha$-$Al_2O_3$ as oxidation continues. Mg also segregates towards the surface, meaning more oxidation in that area and poor oxidation resistance (Esposto et al 1994). The MgO can form from direct growth at the oxide/oxygen interface (primary oxide) or by reduction of $Al_2O_3$ at the metal/oxide interface (secondary oxide) (Agema & Fray 1989, Scamans & Butler 1975). The oxide forms as an amorphous layer consisting of a duplex film of primary and secondary MgO which helps to provide protection against oxidation (Impey et al 1990). As this reaction proceeds and the amorphous layer starts to crystallise, the composition of Mg falls and so a spinel ($MgAl_2O_4$) structure forms in the oxide layer. The spinel nucleates and grows much more quickly than the $\gamma$-$Al_2O_3$ as inward diffusion of oxygen increases when Mg is present in the

oxide layer (Scamans & Butler 1975). It consists of a fine mix of the two oxides and tends to form in randomly oriented crystals. It also grows at the expense of the $Al_2O_3$ in the amorphous layer (Shimizu et al 1998). This layer can be thick and this effect is increased with large Mg compositions (Drouzy & Mascré 1969). The layer also thickens with temperature, as the ions and vacancies within the layer are more mobile at higher temperatures enabling growth to occur more quickly (Wakefield & Sharp 1991).
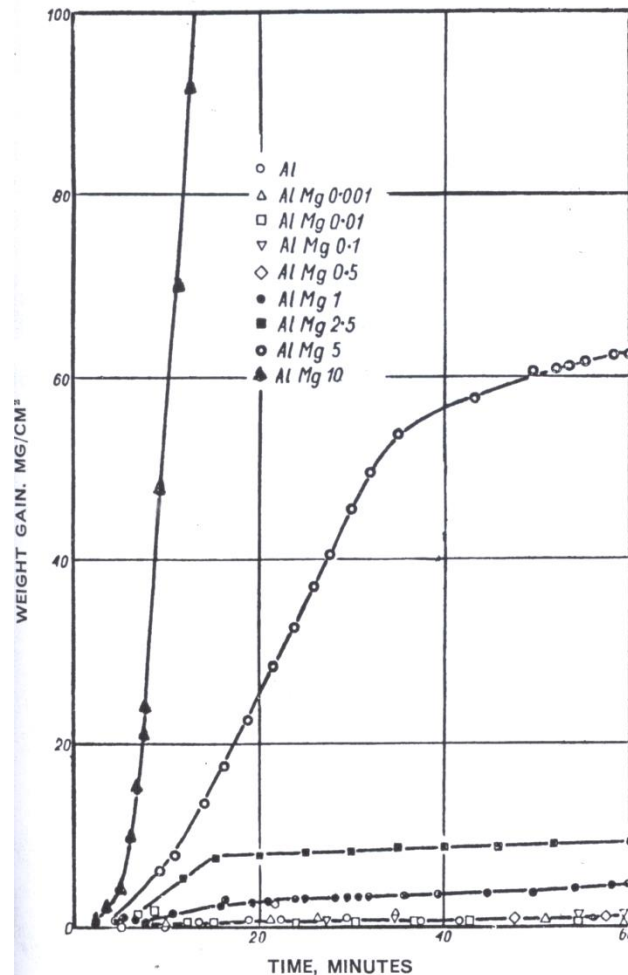


**Figure 12 - Effects of magnesium on the oxidation rate of aluminium at 700 °C (Drouzy & Mascré 1969)**

Even additions of Mg to an Al alloy will increase the oxidation rate. Al-7%Zr and Al-6%Zn-3%Mg were found to have different oxidation behaviour. While Al-7%Zr had an increased incubation period of 35 minutes at 475 °C between the formation of γ and α-alumina (compared to 5 minutes in pure Al), Al-6%Si-3%Mg had an incubation period of less than 1 minute. It was concluded the formation of MgO was the reason for the increased oxidation rate (Scamans & Butler 1975). Additions of Mg also increase oxidation on Al alloys containing Si. During a rise in furnace temperature at a rate of 250 °C/hour, the formation of different oxide species was observed. An Al-12.5% Si alloys grew undetectable levels of oxide. Al-5 wt.% Si- 5 wt.% and Al-6 wt.% Si-4 wt.% Mg alloys formed spinel and alumina structures formed at 900 °C and

23

1230 °C, 950 °C and 1223 °C respectively. This suggests that the higher level of Mg in the alloy, the higher the oxidation rate (Partington et al 1998).

*1.1.3.2 – Gibbs Free Energy of Formation and the Pilling Bedworth Ratio*

The preferential oxidation of alloying elements in Al alloys is due to the Gibbs Free Energy of Formation for each element. The oxide species with the lowest energy are thermodynamically more favourable to form. Oxidation of metals follow the general reaction shown in equation (15) (Scully 1990).

$$M + O_2 \rightarrow MO_2 \tag{15}$$

with the basic mechanisms

$$M \rightarrow M^{n+} + ne^- \tag{16}$$

$$O_2 + 4e^- \rightarrow 2O^{2-} \tag{17}$$
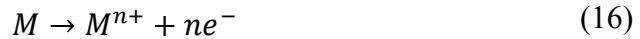
Where M = metal

The Standard Free Energy of Formation for the reaction in (15), $\Delta G°$, is related to the enthalpy of the reaction, $\Delta H°$, the entropy, $\Delta S°$ and the temperature, T. The reaction is given in equation (18).

$$\Delta G° = \Delta H° - T\Delta S° \tag{18}$$

The standard Free Energies of Formation are given in the Ellingham diagram Figure 13. From this, the energies of formation can be worked out. $\Delta G°$ of common oxides include $Al_2O_3$ = -907 kJ/mol, MgO = -985 kJ/mol and $MgAl_2O_4$ = -939 kJ/mol (at 727 °C). From these values it can be seen that an Al-Mg alloy would form MgO first, followed by $MgAl_2O_4$ and $Al_2O_3$ as the energies dictate that the reactions are less thermodynamically favourable from MgO to alumina (Scully 1990).
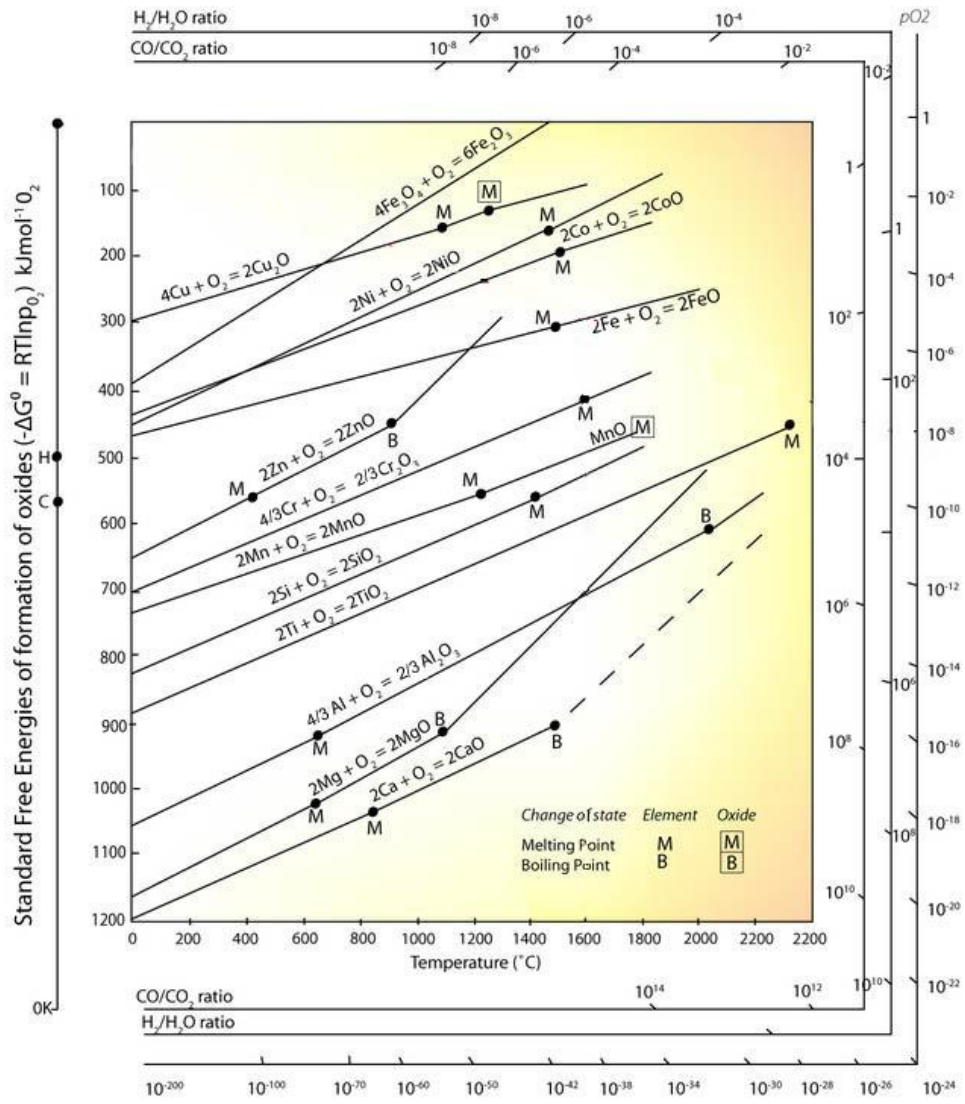
**Figure 13 - Ellingham diagram showing the Standard Free Energy of Fomation of various oxides (Cambridge 2014)**

The Pilling Bedworth Ratio, R, indicates a surface layer's ability to become passivating. It is a ratio of the equivalent volumes of the oxide and the metal and is shown in (19, as is the calculation for alumina (from Xu & Gao 2000).

$$R = \frac{Md}{XmD} = \frac{V \ (one \ mole \ Al_2O_3)}{V \ (two \ moles \ Al)} \tag{19}$$

$$V \ (Al_2O_3) = \frac{M}{D} = \frac{102}{3.987}$$
$$= 25.58 \ cm^3$$

where

$$V \ (Al) = \frac{Na^3}{n} \tag{20}$$

$$= \frac{2 \times (6.02 \times 10^{23}) \times (4.04 \times 10^{-7})^3}{4}$$
$$= 19.85 \ cm^3$$

so

$$R = \frac{25.58}{19.85} = 1.28 \tag{21}$$

Where, M = molecular weight of the oxide ($M_aO_b$), m = atomic weight of the metal, d = density of the metal, D = density of the oxide, X = number of metallic moles in the oxide, V = volume. The Pilling Bedworth ratios can then be calculated as 1.28 for $Al_2O_3$ (shown in equations (**20**) and (**21**)) and 0.81 for MgO. A ratio of more than 1 means that the oxide will passivate and become protective, whereas a ratio of less than one means that the oxide will not passivate and will allow for further oxidation of the metal underneath (German & Munir 1974, from Xu & Gao 2000).

1.1.4 - Surface Condition

Surface condition of the metal prior to melting can change oxidation behaviour. It has been found that polished surfaces can encourage surface oxidation, with electropolishing having a significant effect on aluminium, as can be seen in Figure 14. Surface preparation tends to remove the oxide layer and so can encourage rapid oxidation to take place. It seems to be that the smoother the surface of a specimen, the greater degree of oxide development. It has been suggested that stress levels at the surface increase with surface preparation, influencing how the oxide film behaves, meaning that it is more likely to break up during oxidation, leading to an increase in the oxidation rate. However, in the case of Al-Mg alloys the effect is slightly different. Oxidation occurs more quickly on machined surfaces than on polished ones, the opposite to pure aluminium. The build-up of stress increases the surface temperature of the polished samples, which encourages magnesium to settle near the surface. This region would be the first to melt upon heating, relieving the stress at the surface caused by preparation. This means the oxide growing would be less likely to break up and reveal fresh surface to then be subsequently oxidised. Rapid oxidation can be avoided by ensuring the protective surface is maintained (Impey et al 1993).
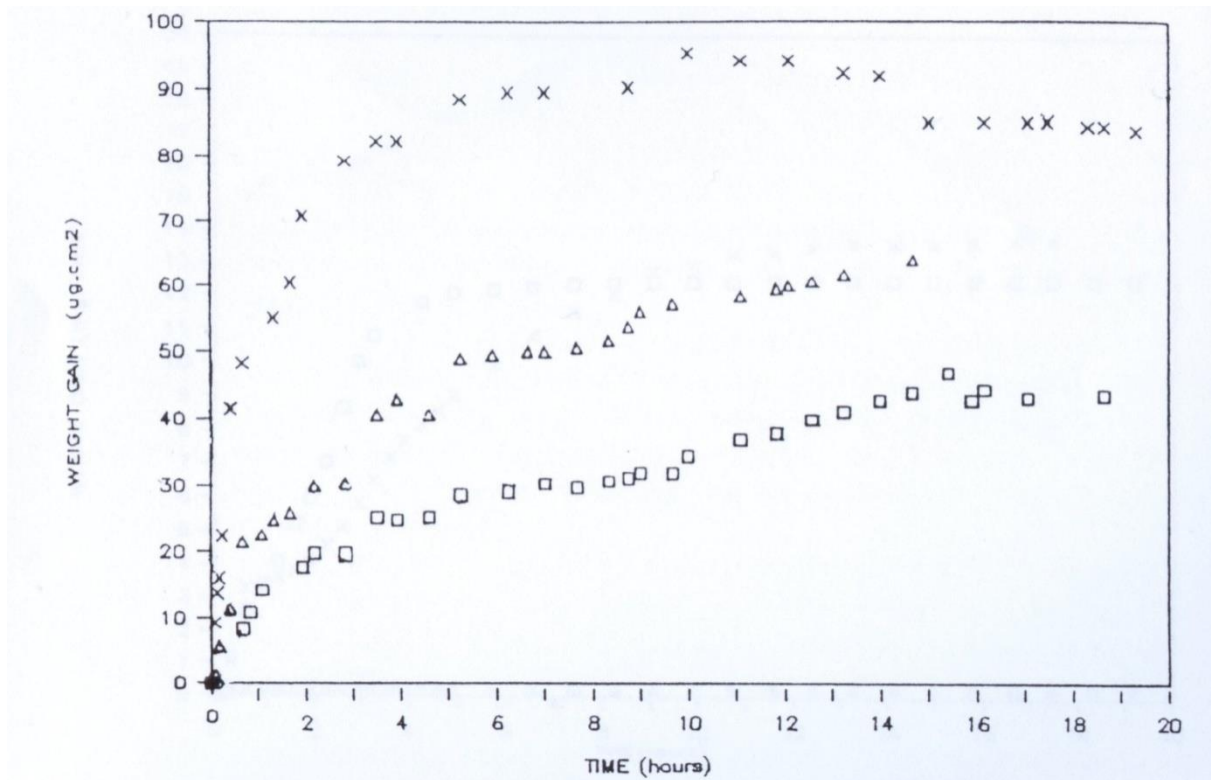
**Figure 14 - Effect of surface finish on oxidation in air of aluminium at 750 °C ✕ = electropolish, Δ = diamond polish (1µm), ☐ = machined, (Impey et al 1993)**

## 1.1.5 - Crystallography of Oxides

Crystallography of the oxides is of great interest when assessing how they grow. Doherty & Davis (1963) undertook a study of the crystallography of both amorphous and crystalline oxides on pure aluminium. They discovered that particles of an amorphous oxide grew by the same amount (50Å) on the (100), (110) and (111) planes when heated to 500 °C for 15 minutes. However, it was noted that the appearance of oxides were different, with oxides on the (100) plane having a uniform thickness, whereas the oxides on the (110) and (111) planes had a regular variation in thickness. The (111) plane oxides formed a "hillock" appearance only when very near the surface of the oxide, but (110) plane oxides formed a ridged surface at different orientations of the plane. The crystalline oxides also showed some variation on structure on different planes. The surface of the (100) plane grew a polycrystalline oxide, with the (110) and (111) tending to form single crystal oxides (Doherty & Davis 1963).

The interface between γ-alumina and the Al matrix has been shown to have an epitaxial relationship. On the (110) and (111) planes of aluminium, (111)[110] of the matrix is parallel to (110)[110]. On the (110) of aluminium, (110)[110] of the matrix is parallel to (110)[110] of the oxide. On the (100) plane of aluminium, (110)[100] of the matrix is parallel to (100)[100] (Hart & Maurin 1970).

27

As aluminium is commonly alloyed with magnesium, it is important to consider the crystallographic relationship between MgO and the matrix. The relationship has been shown to be that the most closely packed planes around the interface, <1$\bar{2}$10> of the Mg matrix and <01$\bar{1}$> of the oxide, are parallel to each other. The planes that are most densely packed, {0002} of the Mg matrix and {111} of MgO, are only displaced by an angle of 2° (Fan et al 2009a).

## 1.2 - Grain Refinement

a)                                    b)
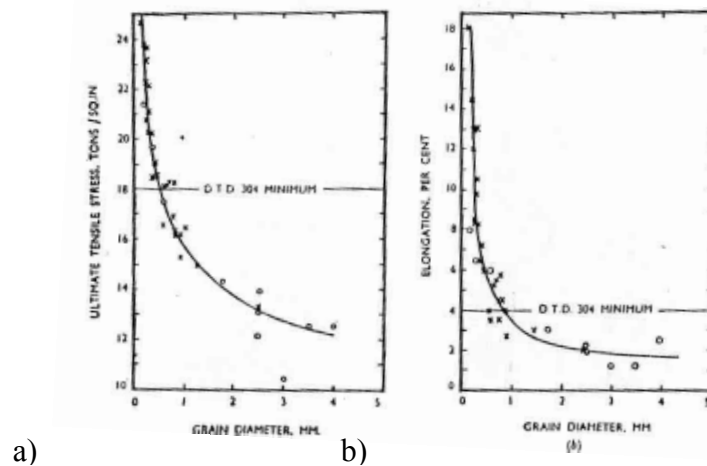
**Figure 15 - Effect of grain size on a) tensile strength b) elongation for an Al-4.8Cu alloy (Cibula 1952)**

For a metal to have good mechanical properties, it is desirable for the grain structure to be uniform and small in size. An equiaxed grain structure is a good structure for the majority of components. Castings with large and columnar grains tend to have poor mechanical properties and a finer grain size also reduce defect sizes (Easton & StJohn 1999). The effect of grain size on mechanical properties can be seen in Figure 15. It has been observed that an equiaxed structure gives uniform mechanical properties, leads to even distribution of inclusions or second phases (which in turn improves machinability), increased strength and fatigue life, and allows for more effective feeding of castings. One way of achieving this is to refine the grains using an inoculant in order to initiate simultaneous nucleation. The use of grain refinement in liquid aluminium using inoculants has been shown to have great effect. It can be seen in Figure 16 that the addition of a grain refiner makes the grain size of a casting much smaller and also ensures a uniform shape and small size range (McCartney 1989). Inoculation is described as "the use of additives to ensure that a material solidifies to a fine, equiaxed grain structure" with a large majority of castings having been grain refined in this way (Kelton & Greer 2010).
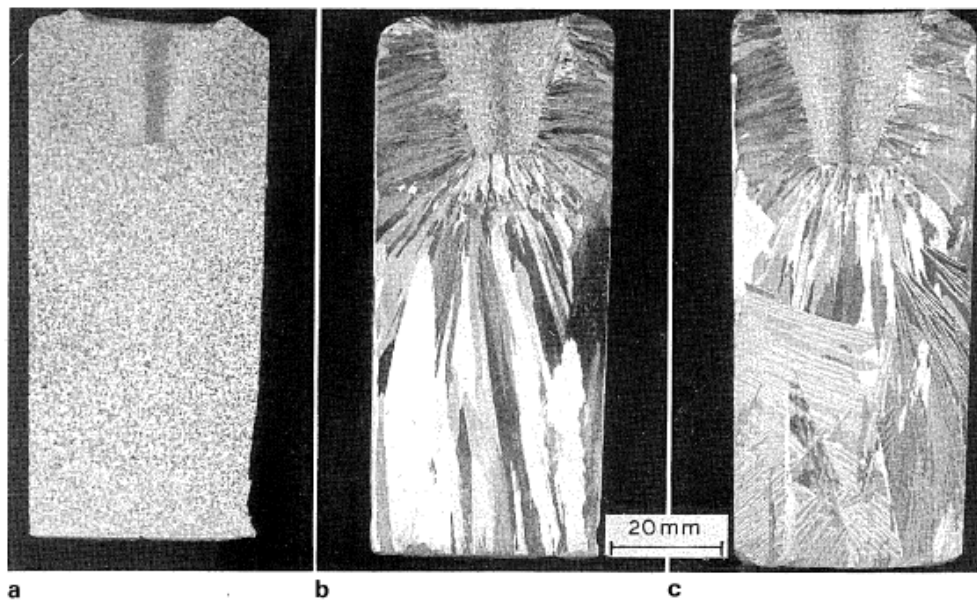
**Figure 16 - The effect of a grain refiner on casting grain structure a) grain refiner added, fine structure b) no refiner, columnar grains c) no refiner, twinned columnar (feather) grains (McCartney 1989)**

Grain refinement needs to reduce columnar growth, as seen in Figure 16b, and form equiaxed grains instead, seen in Figure 16a. The grain refiner is required to promote the "columnar to equiaxed transition" (McCartney 1989). In principle, the grain refinement mechanism is straightforward. Potential nucleation sites become dispersed in the melt (number 1 in Figure 17) with many becoming active during solidification, and so nucleate the solid. When a master alloy (Al metal containing a large proportion of one or more elements in solution, e.g. Al-Ti5-B contains 5% Ti and 1% B in an Al solution) is added to a melt, the intermetallic particles are released when the master alloy melts, and these then act as nucleants. In an Al-Ti alloy the particles that act as nucleants are $TiAl_3$. It dissolves when it comes in to contact with the Al and so the liquid at the interface become enriched in Ti (number 2 in Figure 17). Al-Ti alloys can solidify above the melting temperature of Al, so the initial solidification will take place on the aluminide particle. The physical and chemical characteristics of these particles and the reactions that occur with them in the melt are still somewhat disputed. In order to attempt to understand grain refinement, basic concepts that are necessary for grain refinement need to be considered (Sigworth & Kuhn 2007, Mohanty & Gruzleski 1995, McCartney 1989).

29
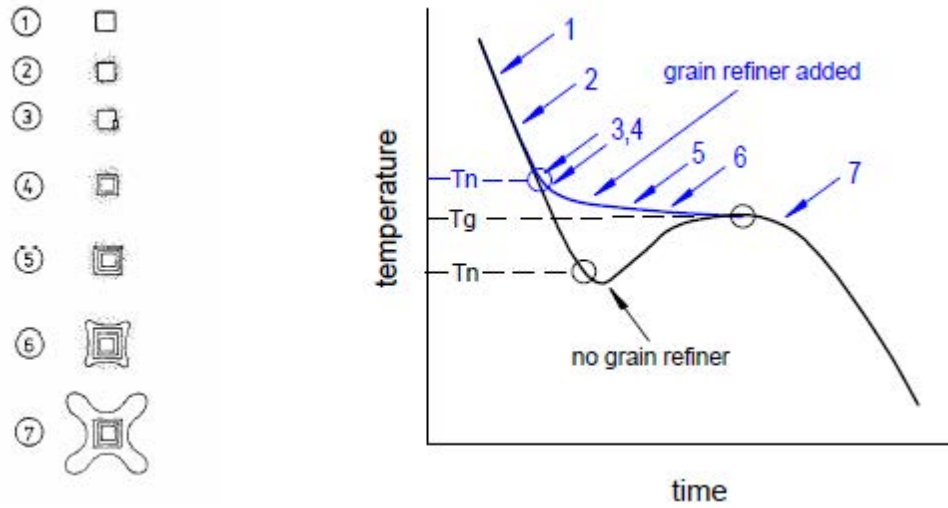
**Figure 17 - Growth of nucleation sites of TiAl₃ in Al grains corresponding to the solidification curve (Sigworth & Kuhn 2007)**

There are various mechanisms and theories that may explain how the grain refining effect may occur. Both nucleation and growth restriction are thought to be important concepts, and are discussed in later sections. Substrates and solute both appear to play an important role in the grain refining mechanism. There is also an important effect regarding the size of grain refiner particles and melt undercooling (Easton & StJohn 1999, Greer et al 2000).

## 1.3 - Nucleation and Growth
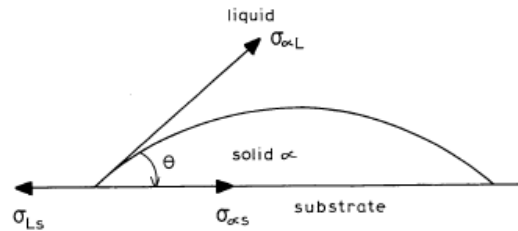


**Figure 18 - A Schematic of the formation of a cap of solid α on a substrate. Surface tension forces and contact angles are shown and are explained below (McCartney 1989)**

When pure materials solidify, homogeneous nucleation is occurring and the critical radius of a nucleus ($r^*_{ho}$) and critical free energy of nucleation ($\Delta G^*_{ho}$) is derived by the following (all taken from McCartney 1989):

$$r^*_{ho} = -\frac{2\sigma_{\alpha L}}{\Delta G_v} \tag{22}$$

$$\Delta G^*_{ho} = \frac{16\pi\sigma^3_{\alpha L}}{3\Delta G_v^2} \tag{23}$$

where $\sigma_{\alpha L}$ = surface energy per unit area between $\alpha$ and liquid (in $Jm^{-2}$) and $\Delta G_v$ = chemical free energy change for liquid to solid transformation at undercooling $\Delta T$ (in $Jm^{-3}$), as shown in Figure 18. The same can be derived for heterogeneous nucleation:

$$r_{he}^* = -\frac{2\sigma_{\alpha L}}{\Delta G_v} \tag{24}$$

$$\Delta G_{he}^* = \frac{16\pi\sigma_{\alpha L}^3}{3\Delta G_v^2} f(\theta) \tag{25}$$

where $f(\theta) = (2 - 3\cos\theta + \cos^3\theta)/4$ , a function of the contact angle. The most potent nucleation sites for heterogeneous nucleation have $\theta$ close to zero (McCartney 1989).

From the above expressions, a term for homogeneous and heterogeneous nucleation can be identified. Reasonable estimates of $\Delta T/T_m$ ($T_m$ = melting temperature in K) for homogeneous nucleation are in the region of 0.2-0.25. Undercooling for most aluminium alloys are about 1-2 K, suggesting that it is heterogeneous nucleation that is occurring. An expression for heterogeneous nucleation ($I_{he}^V$) is given in $m^{-3}$ $s^{-1}$:

$$I_{he}^V = 10^{18} N_V^p \, exp\left[-\frac{16\pi\sigma_{\alpha L}^3 f(\theta)}{3K_b\Delta S^2\Delta T^2}\right] \tag{26}$$

where $N_p^V$ = number of nucleants particles per unit volume ($m^{-3}$), $K_b$ = Boltzmann's constant (J $K^{-1}$) and $\Delta S$ = entropy for the liquid to solid phase transformation (J $m^{-3}$ $K^{-1}$). This equation allows for estimation of $\theta$ values for potent nucleants. When values of $\Delta T = 1.5$, $I_{he}^V = 10^6$ $m^{-3}$ $s^{-1}$ and $N_p^V = 10^{11}$- $10^{12}$ $m^{-3}$ were used, McCartney (1989) calculated that $\theta = \pi/30$ radians (standard values were used for other constants). A graph of $I_{he}^V$ vs. $\Delta T$ is shown in Figure 19. For any value of $\theta$, it is possible to calculate $\Delta T_n$ (critical undercooling below equilibrium liquidus temperature for heterogeneous nucleation on a substrate in K). Below this value, $I_{he}^V$ is basically zero, but rises when critical undercooling is reached (McCartney 1989).
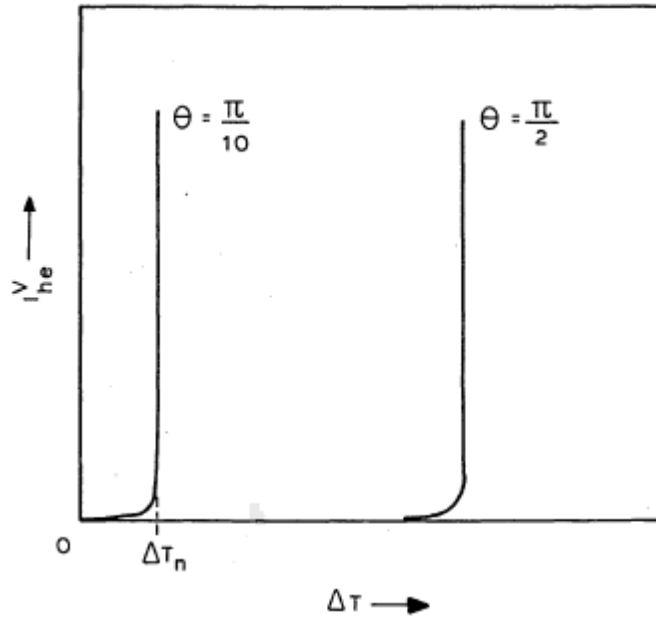
**Figure 19 - $I_{he}^V$ vs. $\Delta T$ for different contact angles (McCartney 1989)**

The nature of the growth front between the solid (and semi-solid) and liquid phases depends on the variables such as alloy composition, convection within the liquid or presence of any heterogeneous nuclei. If $G_L$ (temperature gradient in the liquid, K m$^{-1}$)/V (growth rate at solid/liquid interface) is large enough, the liquid and solid phases are separated by a planar front. Dendritic growth occurs below a critical value of $G_L/V$. The dendrites grow away from heat sink during columnar growth, and dendrites grow radially from multiple centres during equiaxed growth, releasing heat in to the liquid. Both of these types of growth require undercooling. The undercooling at the dendrite tip is dependent on temperature gradient, growth rate and composition of the metal (McCartney 1989). It has been shown that this value can be expressed:

$$\Delta T_c = \frac{D G_L}{V_c} + C_1 V_c^{1/2} \qquad (27)$$

where D = solute diffusion in liquid (m$^2$ s$^{-1}$), $V_c$ = growth rate of columnar growth front (m s$^{-1}$) and $C_x$ = proportional constant between undercooling and velocity for an alloy (K m$^{-1/2}$ s$^{1/2}$). For many casting methods $DG_L/V_c$ is in region of $0.05\Delta T_c$, and so $\Delta T_c \propto V_c^{1/2}$ (Burden & Hunt 1974, McCartney 1989).

Equiaxed growth tends to be more complicated. Growth from the nucleation centre starts out in a spherical manner, which then transforms to fully dendritic growth. Growth impingement of the equiaxed grain also needs to be considered at later stages of solidification. When the temperature gradient is near zero, and the growth is dendritic, a growth law can be used:

32

$$\Delta T_e = C_2 V_e^{1/2} \qquad\qquad (28)$$

where $\Delta T_e$ = undercooling below liquidus temperature during equiaxed growth, K and $V_e$ = radial growth rate of equiaxed dendrite, m s$^{-1}$ (Burden & Hunt 1974, McCartney 1989).

1.3.1 - Columnar to Equiaxed Transition (CET)

The grain refining inoculant is required to bring about the columnar to equiaxed transition. Work has been done to try and understand what affects this transition. When the growth of equiaxed grains ahead of a growth front of columnar grains during directional solidification, it is assumed that the columnar front is growing at undercooling $\Delta T_c$ (as in equation (27)). It is also assumed that equiaxed grains nucleate instantaneously at a required undercooling, $\Delta T_n$. If $\Delta T_n < \Delta T_c$ and then equiaxed growth is favourable above columnar growth. While taking impingement in to account, it was found that an equiaxed grain volume fraction of more than 0.66 at $\Delta T_c$ allows for equiaxed growth to occur, whereas a volume fraction of less than 0.0066 leads to full columnar growth (Hunt 1984, McCartney 1989).
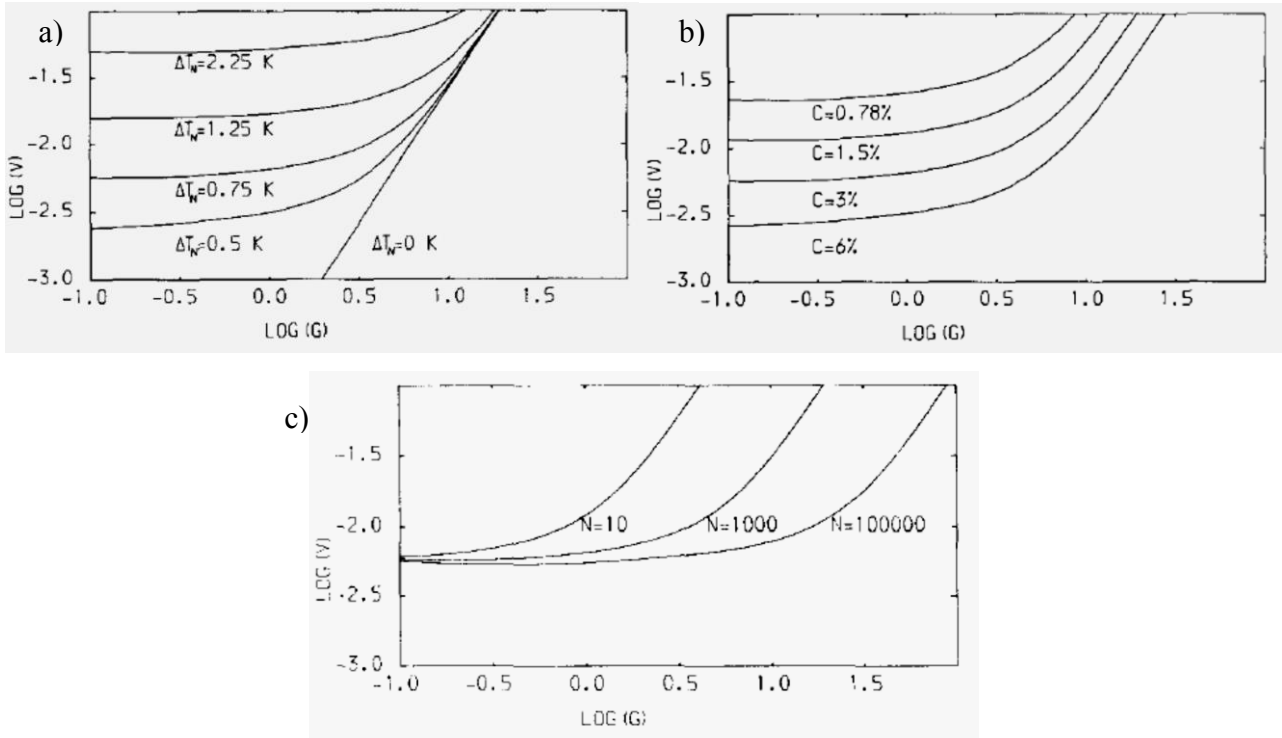


**Figure 20 - Plots of growth rate V vs. temperature gradient G for different variables a) undercooling b) composition and c) number of nucleation sites (equiaxed growth occurs above lines) (Hunt 1984)**

It can be seen in Figure 20 that factors such as undercooling, alloy composition and number of nucleation sites have an effect on the CET. It can be seen in Figure 20a that an increased undercooling increases the CET, meaning that a low undercooling is good for equiaxed growth.

Increasing the amount of an alloying element in the alloy can decrease the CET, meaning that less-pure alloys tend to form equiaxed grains, as shown in Figure 20b. Figure 20c shows how the number of nucleation sites increases the amount of equiaxed grains by reducing the CET. It is these factors that show how grain refinement can be used to improve the grain structure of a casting (Hunt 1984).

1.3.2 - Mechanisms of Grain Refinement

The principles of grain refinement are relatively simple. An inoculant is added to a metal in order for many potent heterogeneous nuclei to be dispersed throughout the melt. These sites become active during solidification, due to requirements of heat and fluid flow being met, and nucleate the solid. Care must be taken with growth rates, because if growth proceeds too quickly the first grains to grow will consume other potential nucleation sites. Exactly which particles act as the prominent nucleation sites, their physical and chemical characteristics and the subsequent reaction with the melt are still somewhat disputed. However there are a few main theories of how grain refinement occurs.

*1.3.2.1 - Peritectic Theory*

This theory puts forward the idea that nucleation occurs through a peritectic reaction:

$$L + TiAl_3 \rightarrow \alpha - Al \ (solid \ solution) \tag{29}$$

When a molten metal cools, the crystals of the primary phase form and these then react in a peritectic way with the liquid as cooling continues. This peritectic reaction at least partially transforms crystals of the primary phase into secondary phase crystals, which act as nucleation centres during subsequent solidification. As the peritectic reaction takes place the primary crystals break up and these also act as nuclei. The most potent nuclei arise from fine dendritic crystals. It has been suggested that a peritectic reaction is required in order to achieve significant grain refinement (Crossley & Mondolfo 1951). It is thought that the TiAl crystals dissolve in the Al, which gradually fades over time. This fading effect can be reduced by the addition of boron (B) in to the melt, taking the peritectic composition closer to the Al end of the phase diagram (Figure 21) and so more stable at lower temperatures (McCartney 1989). However, it has been suggested that the peritectic reaction does not directly lead to grain refinement in all Al alloys. A study observing grain refinement in Al-Zr alloys noted that no grain refinement was observed for the Al-Zr, compared to the Al-Ti alloy. It was also noted that the addition of B did not improve refinement of an Al-Zr alloy (Delamore & Smith 1971).

34
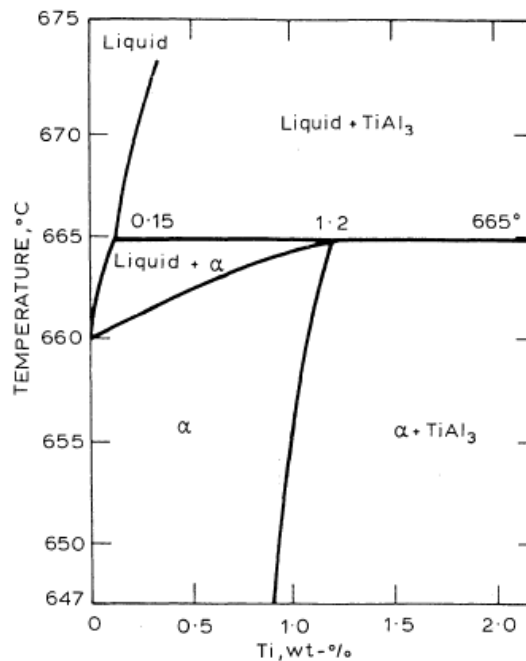
**Figure 21 - Al-Ti phase diagram (McCartney 1989)**

*1.3.2.2 - (Carbide-Boride) Particle Theory*

This theory suggests that the addition of Al-Ti master alloys to the melt reacts with residual carbon to form TiC which acts as a heterogeneous nucleant. The TiC phase can form even when C is present at ppm level. If Ti-Al-$B_2$ is added, $TiB_2$ particles will also be present, acting as a nucleation centre. This effect fades but only due to the particles agglomerating or settling within the melt. However some issues can be found with this theory. The only phases generally discussed are the $TiB_2$, $AlB_2$ or $(Al, Ti)B_2$ phases. $AlB_2$ has been shown to be a poor grain refiner in pure aluminium and only nucleates in hypereutectic alloys. This suggests that $TiB_2$ is a better nucleant than $TiAl_3$, when there is evidence to the contrary. The Ti/B ratio has to have an excess of Ti in order for the particle to act as a good nucleant (McCartney 1989, Mohanty & Gruzleski 1995).

The presence of the complex phase of $(Al, Ti)B_2$ has led to the proposal of a metastable boride theory. The $(Al, Ti)B_2$ phase disappears after a long holding time and so is thought to be a metastable phase. This phase increases grain refinement either by acting as a nucleant or by nucleating $TiAl_3$. It is not clear if the $(Al, Ti)B_2$ phase is stable or metastable, even though the $TiB_2$ and $AlB_2$ are both stable (Mohanty & Gruzleski 1995) The complex borides of Al and Ti were found to substitute each other in the lattice, plus $TiB_2$ and $AlB_2$ have been shown to be isomorhpous. This continuous solid solubility suggests that the $(Al, Ti)B_2$ could be a stable phase (Guzowski et al 1987). During the holding of the liquid master alloy, the $(Al, Ti)B_2$ phase transforms to $TiB_2$. During this transformation some of the boride particles become attached to

35

the aluminide crystals and are trapped when the aluminide duplex particles grow. The duplex particles increase grain refinement in the alloy (Kiusalaas & Bäckerud 1987).

*1.3.2.3 - Hypernucleation Theory*

This theory suggests that Ti in solution promotes nucleation on boride particles present in the melt. 'Pseudo' crystals form at the interface between the metal and the boride particles, forming on solutes (e.g. Ti) that segregate there. The solidification structure in these regions are similar to α-Al. The atoms that form at the interface restrict the mobility of the aluminium in the surrounding area, and so the area structure becomes similar to α-Al. The 'pseudo' crystals are stable above the liquidus temperature, and may grow as the temperature falls below the liquidus. This would mean no undercooling would be required to start nucleation. It has been observed that thermal traces deviate just above the liquidus temperature (in Al inoculated with Al-5Ti-B) which may suggest this effect may play a role in grain refinement. It has also been seen that liquid Xenon particles, in contact with α-Al, had well defined layers at the solid/liquid interface. There was no long range periodicity, but there was order at the interface, suggesting a similar structure to pseudo-crystals on certain liquids (Jones & Pearson 1976, Quested 2004).

This theory has been disputed, thermodynamically, and the mechanisms were not fully described in Jones & Pearson (1976). Thermodynamics dictate that chemical potentials must be in equilibrium, but the theory suggests that there would be an activity gradient, which is not correct. There is also no experimental evidence to support the theory (Murty et al 2002).

*1.3.3.4 - Growth Restriction*

It is possible that the addition of refiners not only assists with nucleation of the solid phase, but also helps to restrict growth of nucleated grains during solidification. The solute diffusion limits the growth of grains and is defined by the growth restriction factor, Q:

$$Q = m(k-1)C_0 \qquad (30)$$

where m = liquidus slope in the solute-Al phase diagram, k = partition coefficient, $C_0$ = solute content (Quested & Greer 2004). However, this is only relevant to simple alloys, i.e. those with only one solute element. It needs to be understood in terms of multicomponent alloys. The components of equation **(30)** can be evaluated for individual solutes (i):

$$Q_{\sum bin} = \Sigma Q_{bin,i} = \Sigma m_{bin,i}(k_{bin,i} - 1)C_{0,i} \qquad (31)$$

36

However, simply summing up the individual values from different binary phase diagrams does not give accurate results. A gradient of the liquidus surface can be calculated for a multidimensional component from partial derivatives and partition coefficients, which come from the equilibrium tie line. The growth restriction factor for a multicomponent alloy can be calculated as:

$$Q_{multi} = \Sigma m_i(k_i - 1)C_{0,i} \tag{32}$$

The growth restriction factor can also calculated from thermodynamic values;

$$Q_{true} = \left(\frac{\delta(\Delta T_{cs})}{\delta f_s}\right)_{f_s \to 0} \tag{33}$$

$$\text{where } \Delta T_{cs} = m(c_0 - c_L^*) \tag{34}$$

where $T_{cs}$ = constitutional supercooling , $f_s$ = phase fraction of the growing solid phase, $c_0$ = liquidus point and $c_L$ = liquid interface composition (from phase diagram). Growth restriction is subject to both solute content and temperarure. It is also important to note that Q involves the presence of intermetallics and compounds in melt in order for it to become relevant in grain refinement (Schmid-Fetzer & Kozlov 2011).

Work by Johnsson (1995) suggested that when the growth restriction factor goes above 20, the effectiveness of the grain refiner reduces. Some common solutes were assessed for their growth restriction values. A comparison of growth restriction factor and grain size is shown in Figure 22 (Johnsson 1995).
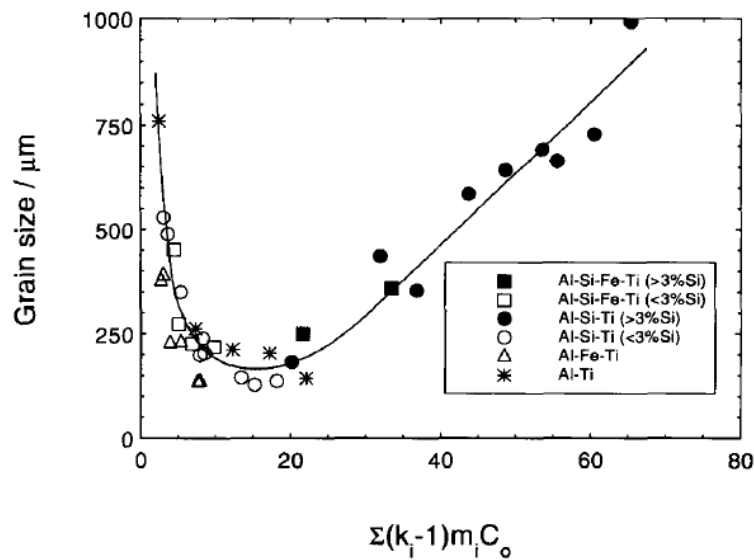


**Figure 22 - Grain size compared to various solutes, and thier growth resriction values (Johnsson 1995)**

The theories outlined suggest a number of ways grain refinement can occur in liquid metals, and there is not yet one definitive answer to how the mechanisms of grain refinement operate.

1.3.3 - Grain Refiners

The most common grain refiners tend to contain Ti and B, as described above, they are good grain refiners. The refining compounds used include $Al_3Ti$, which is thought to partake in the peritectic reaction, and TiC, $TiB_2$ and $AlB_2$ which follow the particle theories (Perepezko & LeBeau 1981). Elements such as Niobium (Nb) and Zirconium (Zr) have good effects on grain refinement. $NbAl_3$ is a stable particle with agglomeration and settling reducing its effect (which is less than that of Ti). Hyperperitectic compositions are required for Nb to be an effective refiner. But as it is less effective and more expensive than using the Ti particles, it is not widely used as a grain refiner. Zirconium forms particles of $ZrAl_3$, which dissolve quickly in the bulk alloy. These types of grain refiner react with the bulk Al to form the fresh $XAl_3$ compounds, which are important for grain refinement (Robert & Cupini 1987). Chromium can also be a good grain refiner, particularly in pure melts, but only at low concentration. It has been found that an excess of Cr in a grain refiner (~2 wt. %) will poison the effect of a grain refiner, leading to a coarsening of the grain structure (Rao et al 1996).

The ideal size of an inoculant particle has been predicted to be in the region of 1-2 μm, as seen in Figure 23 (Kelton & Greer 2010).
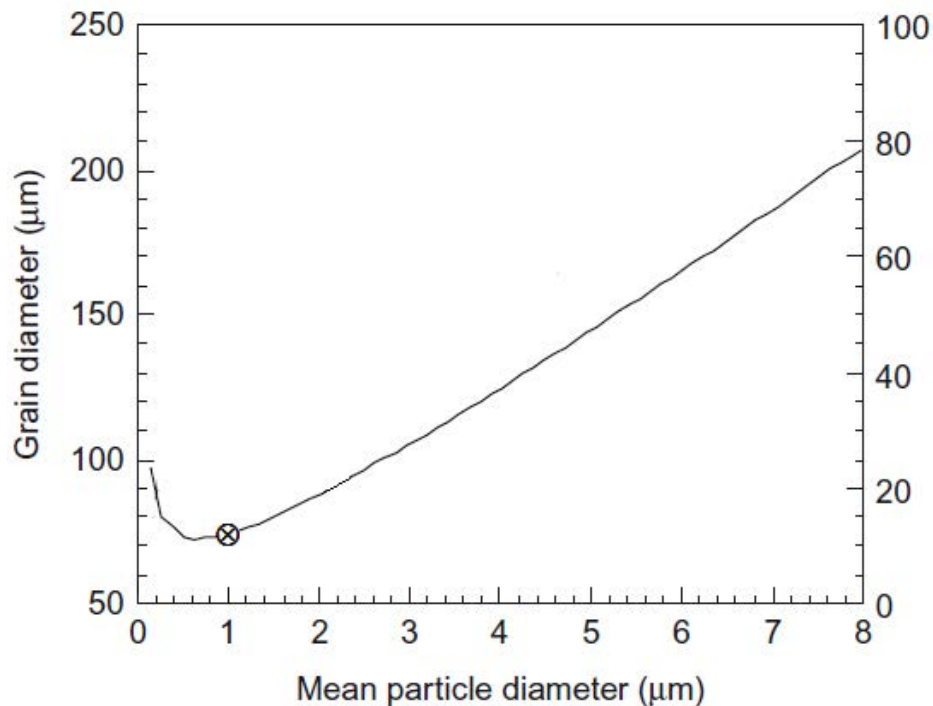


**Figure 23 - Effect of inoculant particle diameter on grain size (modified from Kelton and Greer 2010)**

<u>1.3.4 - Grain Refinement without Inoculation</u>

The majority of grain refinement techniques use inoculants in order to encourage heterogeneous nucleation. However, grain refinement can also take place without the presence of an inoculant in the melt. It is expected that the growth of grains in this case is columnar but if the solidification occurs within certain undercooling ranges, the result is a fine equiaxed structure. It is thought that dendrite break up is a contributing factor in the refining process in these systems. Grain refinement has been shown to occur at lower undercoolings and large supercoolings, as can be seen in Figure 24. It must be noted that grain refinement at small undercoolings has only been recorded in alloys and not pure metals. However the solute content required can be very low e.g. 0.01 at% $O_2$ in nickel. It is thought that the solute promotes the growth of dendrites by assisting local remelting. It may also involve some fluid flow as a result of solidification shrinkage (Kelton & Greer 2010).
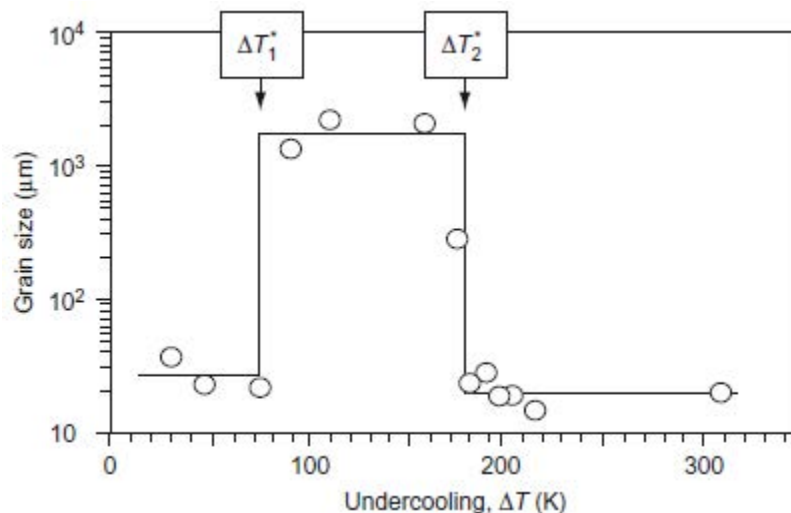


**Figure 24 - Grain size of a Cu/Ni alloy at different undercoolings (Kelton 2010)**

Grain refinement is also found at large supercoolings, for both pure metals and alloys. It was observed for nickel melts, that a large undercooling of 140-150 K the grain sizes were a tenth of those formed at small undercoolings, where columnar growth dominates. The solid that forms at large undercoolings can be stressed and this could be a driving force for recrystallisation. In most metals, it is thought that grain refinement is a result of solidification followed by recrystallisation. The grain refining effect can be linked to dendrite break up, as with the cases using small undercoolings. It has even been suggested that the orientation of the broken dendrites may affect the refinement process. The methods of break-up have been widely discussed but unresolved. A simple mechanism has been proposed, however, for grain refinement in both large and small undercoolings. The solidification occurs, when rapid growth occurs to with some recalescence. The partially solidified drop has a dendritic structure has a

constant temperature from the equilibrium between the drop and the liquid. During this equilibrium period, the dendrites can grow and may then break in to fragments. This does not occur at medium undercoolings and columnar structures form are found in the solid (Kelton & Greer 2010).

Nickel and copper can be grain refined from the oxides that form within the melt. It has been proposed that the same can be done for aluminium and its alloys (Fan et al 2009a).

## 1.4 - Melt Conditioning

Aluminium oxides may act as a grain refiner for aluminium. Fan et al (2009a) discovered that this may be achievable when the melt is processed in a certain way. A melt conditioning method is used on the liquid metal before casting, and involves passing the metal through extruder screws. The two screws are co-rotating and fully intermeshed. The barrel is also heated to maintain melt temperature. This introduces high amounts of turbulence and shearing to the metal and breaks down any oxide into individual particles. The intensive shear that occurs within the barrel, and this means that the temperature, composition and the dispersion of any inclusions are all uniform. When magnesium was put through this process, the MgO particles were dispersed and the particles small in size, around 100-200 nm in diameter. It seemed to be that the small MgO particles are semi-coherent with the $\alpha$-Mg and the $Al_8Mn_5$ particles in the alloy, and they appeared to be potent sites for heterogeneous nucleation. Also, unlike many grain refiners, the effects to the small oxides did not fade with holding times. Whilst the evidence is, as yet, insufficient to support this theory, the good crystallographic matching indicates that it could be correct. If so, there are possibilities regarding recycling of light alloys, which currently is impractical for many manufacturers. Aluminium is difficult to recycle as impurity elements (e.g. Fe) are detrimental to the mechanical properties. They are difficult and can be expensive as the metal would need to be purified chemically, by flux-based processing, hydrometallurgy or other reduction processes. It has been shown that the grain refining method increases the tolerance of the Al to these elements, potentially meaning that more metal will be able to be recycled without the need for expensive purification techniques (Fan et al 2009a, Fan et al 2009b).
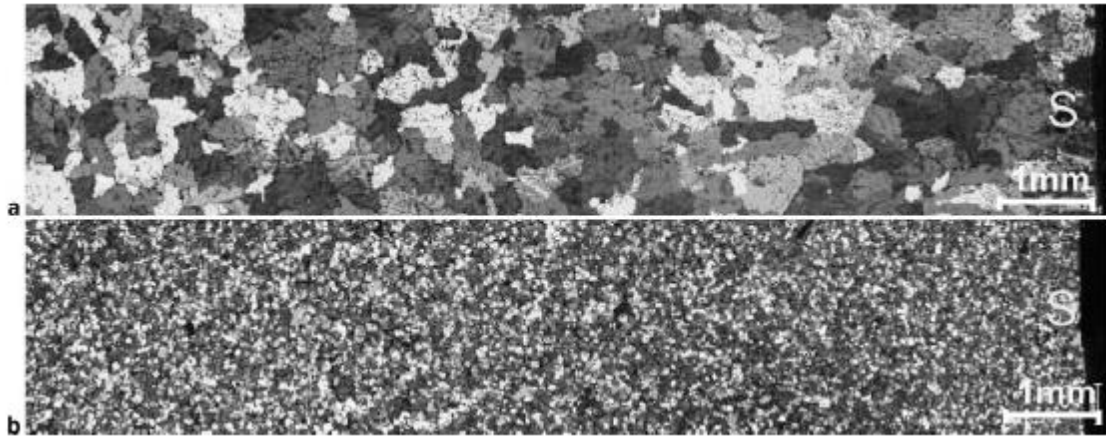
**Figure 25 - Microstructure of an Al alloy a) conventional die cast b) after melt conditioning (S represent the surface of the casting) (Fan et al 2009b)**

The work was also carried out on an Al alloy. The resulting grain refinement can be seen in Figure 25. The smaller, more uniform grains improve the mechanical properties of the castings, as seen in Figure 26 (Fan et al 2009b).
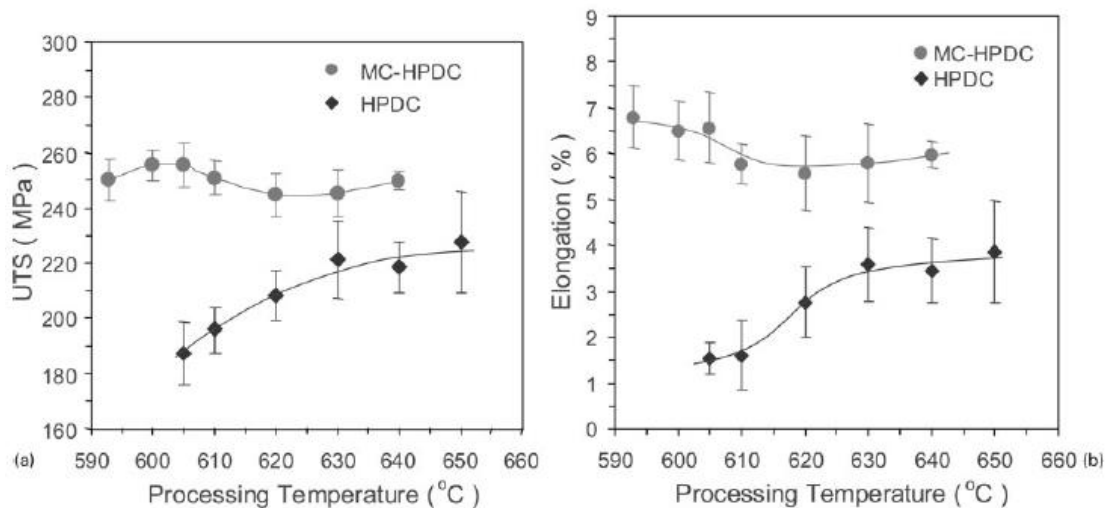


**Figure 26 - Comparison of mechanical properties for high pressure die cast (HPDC) and melt conditioned HPDC a) tensile strength b) elongation (Fan et al 2009b)**

The mechanism of the nucleation of an alloy melt conditioned metal on the oxides has been theorised. It has been reported that the oxides do act as nucleation sites for many intermetallics but not for the Al-matrix itself. It is thought that the melt shearing causes the oxide and the other particles to disperse in the melt, leading to a narrow distribution of particle size. The melt shearing can force wetting of the oxide particles by the liquid by helping to overcome the barrier for wetting. During cooling, intermetallic phases nucleate on the oxides. The primary Al phase then nucleates on the intermetallics. It may also be that the primary phase will nucleate directly on the oxide in pure metals, when no intermetallic phases are present (Fan et al 2009c).

41

**1.5 - Codeposition of Inoculant Particles**

1.5.1 - Codeposition Theory

Inoculant particles can be introduced into a molten melt via a master alloy. One method of producing a master alloy is to use electro-codeposition to put alumina-based particles into a base alloy. Electrodeposition is often used for depositing composite coatings onto different components and has been used for many years to apply coatings with improved mechanical properties (Garcia et al 2001, Greenberg et al 2004, Mishra et al 2004). Many theories of codeposition have been suggested including electrophoresis (the motion of particles relative to a fluid in an electric field), mechanical entrapment, adsorption and convective-diffusion (Low et al 2006).

The theory put forward by Guglielmi looks at the influence of current density and particle concentration within the electrolyte on particle incorporation rates. It states that the codeposition rate is mainly influenced by the attractive forces in and near the diffusion layer, so that the particle is held at the surface until enough metal has been deposited to entrap it within the layer. However, it does not fully take all variables in to consideration. It only empirically considers things like the size, type or effect of pre-treatment on particles, temperature or pH of the plating bath or any hydrodynamic effects (Guglielmi 1972, Roos et al 1990).

Another theory was put forward by Celis et al (1987). It was designed on the hypothesis that "A particle will be embedded only if a certain fraction of the adsorbed ions on the particle's surface is reduced" (Roos et al 1990). The model was based on the fact that codeposition can be viewed as a 5 step process, as shown in Figure 27:

1) An adsorbed double layer forms around each particle in the bulk of the solution

2) The particle is transferred by convection to the boundary layer

3) The particle reaches the surface of the cathode by diffusion

4) At the cathode, free and adsorbed electro-active ions are reduced

5) When a certain fraction of the ions originally present on the particle's surface is reduced, the particle is captured                  (all taken from Roos et al (1990))
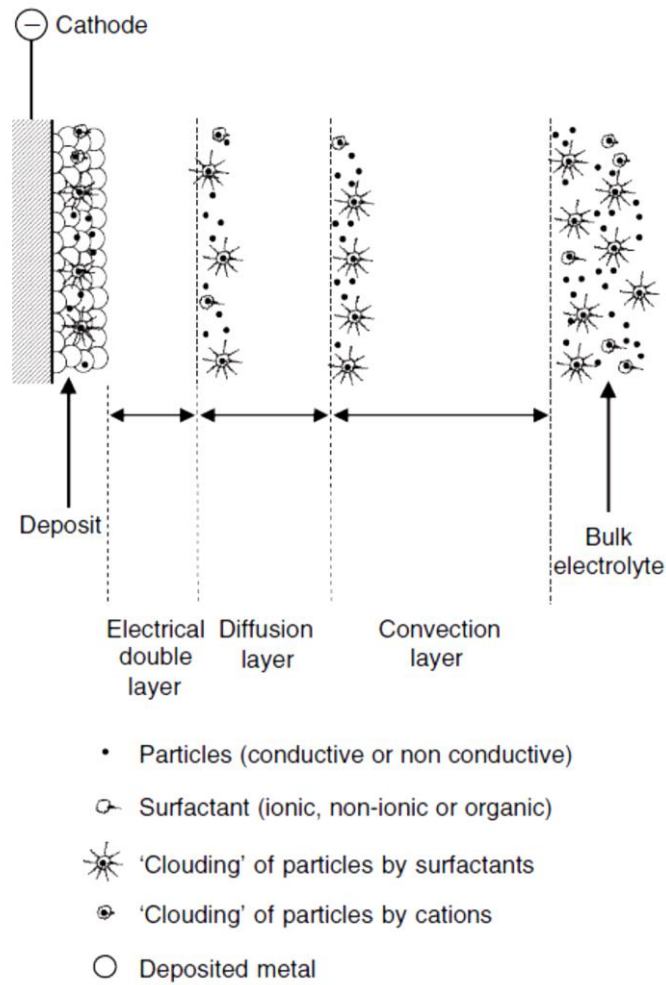
Figure 27 - Schematic of the codeposition mechanism (Low et al 2006)

The model is therefore based on the statistics of a particle being incorporated into a layer, and attempts to predict the amount of particle codeposited there:

$$\alpha_v = \frac{G'PJ}{G + G'PJ} \qquad (35)$$

Where $\alpha_v$ = volume fraction of embedded particles, $G'$ = weight of one particle, $P$ = probability for a particle crossing the diffusion layer at the working electrode to become incorporated, $J$ = number of particles arriving at the working electrode per unit time and surface area and $G$ = weight increase due to the deposited metal per unit time and surface area. The model had been found to be particularly valid for the $Cu-Al_2O_3$ codeposition system (Low et al 2006, Roos et al 1990).

The theories above have led to the development of three main techniques of depositing particles in a metal coating: Direct current plating, pulse plating and reverse pulse plating.

1.5.2 - Direct Current (DC) Plating

DC deposition involves a constant DC current being used to attract metal particles (for the coating matrix). Two electrodes are immersed in a solution and a DC current is applied across

them. The metal ions are then drawn to the cathode and form a metal layer on the substrate (Kanani 2004). A schematic can be seen in Figure 28.
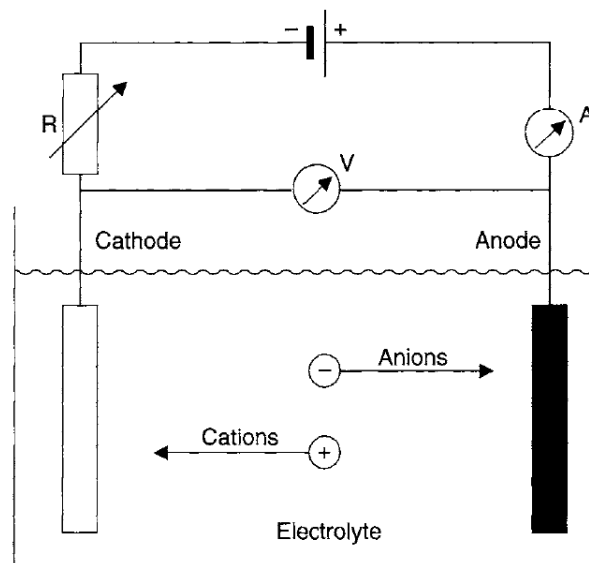


**Figure 28 - A basic schematic of a DC current plating system (Kanani 2004)**

The DC plating technique has been used for the deposition of alumina in copper and has been found that it follows the law predicted by Guglielmi (1977) when a sulphate bath is used (Celis & Roos 1977). The method involves a constant current being applied across the system, as shown in Figure 28. The metal ions are attracted to the cathode and the layer is deposited. The particles are surrounded by metal ions and are attracted to the cathode at the same time (Low et al 2006)
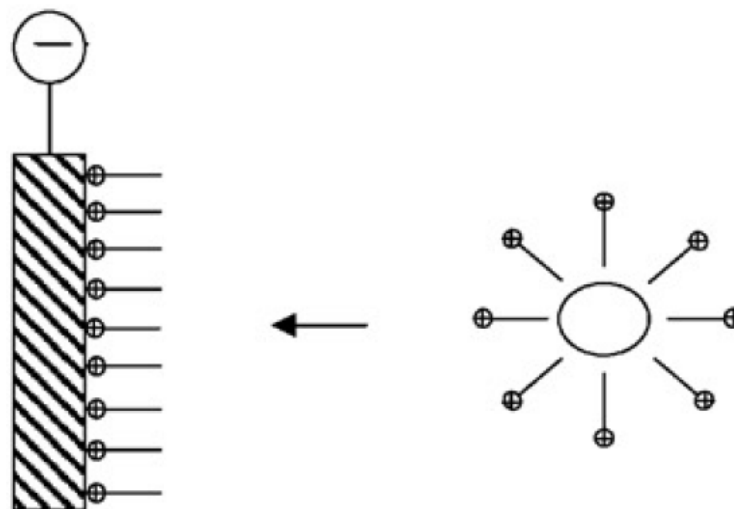


**Figure 29 - Schematic how a surfactant works in DC plating (Weston et al 2011)**

The deposition of the particles can be enhanced by the use of a surfactant. Surfactants work by surrounding the particles to be coated, and as they have a strong charge, the particles will be

attracted to the electrode. They also help stop the particles clustering via the repulsive forces between the surfactant chains (Kanani 2004, Weston et al 2011). This can be seen in Figure 29.

In order to further increase the pickup of particles and quality of the coating, the DC plating technique has been further developed so that the electrolysis is pulsed.

### 1.5.3 - Pulsed Plating (PP)

Pulsed plating had been shown to give greater control of and to increase the mechanical properties of the coatings made using this method. The grain structures of PP coatings tend to be finer, as higher current densities are often used, leading to improved nucleation rates. (Guo et al 2006). It also improves the amount of particle drawn in to the coating, with less agglomeration of those particles. It also leads to better pickup of smaller sized particles (when a range of particle sizes are used in the electrolyte), which may also contribute to the smaller microstructure be pinning grain boundaries (Steinbach & Ferkel 2001).
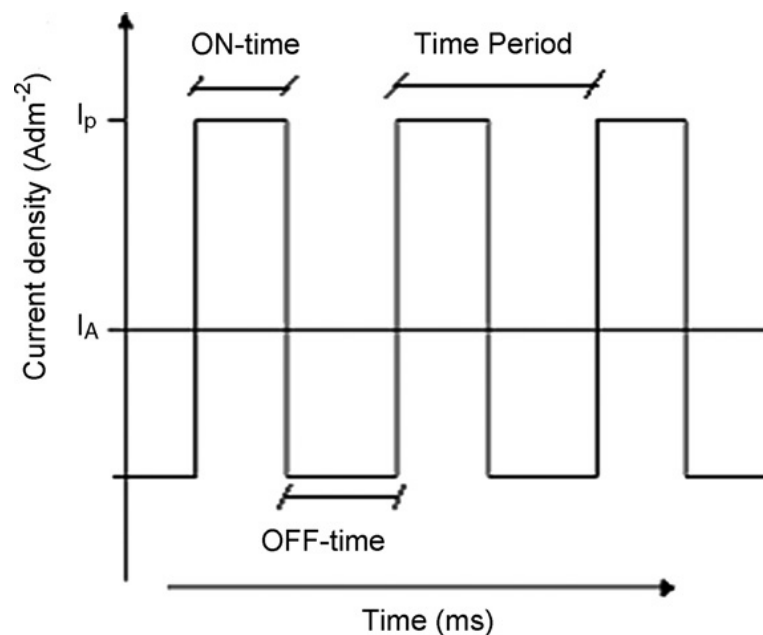


**Figure 30 - The basic current cycle of a pulse plating method (Chandrasekar & Pushpavanam 2008)**

The technique of pulsed plating works by having an 'On' time ($t_{on}$) and an 'Off' time ($t_{off}$). The $t_{on}$ is when a normal DC plating method is applied across the system, and the $t_{off}$ is when the plating is switched off. The cycle is shown in Figure 30. These factors, plus the peak current density are the three variables that control the rate of deposition (Chandrasekar & Pushpavanam 2008).

The duty cycle is the ratio of $t_{on}$ and $t_{off}$ and an important variable in pulse plating:

$$Duty\ cycle\ (\%) = \frac{t_{on}}{t_{on} + t_{off}} \times 100 \qquad (36)$$

It is related to the pulse frequency, which gives the amount of on/off cycles per second:

$$Frequency\ (Hz) = \frac{1}{t_{on}+t_{off}} = \frac{1}{t} \qquad (37)$$

(all from Chandrasekar & Pushpavanam 2008)

It has been found that the duty cycle has an effect on the amount of particles that will be deposited in a coating. A duty cycle of between 10% and 20% leads to higher amounts of alumina and $ZrB_2$ when compared to higher duty cycles of up to 90%. The pulse frequency also has an effect on the particles deposited. Pulse frequencies of 7-8 Hz led to a higher amount of alumina particles being deposited than those with pulse frequencies of 1-2 Hz. But high pulse frequencies (up to 2000 Hz) were used on $ZrB_2$ particles and resulted in lower particle pickup than frequencies of 200 Hz (Thiemig et al 2007, Guo et al 2006).

The idea of pulse plating has been taken further by pulse reverse plating, where instead of a period of time where the current is switched off, the current is reversed so that the electrode charge will attract particles of opposite charge to the metal ions.

1.5.4 - Pulse Reverse Plating (PRP)

Pulse reverse plating (PRP) was developed to get a larger pickup of particles during deposition of the metal layer. It involves a cathodic current during the on time and an anodic during the off time and the waveform can be seen in Figure 31. A higher pickup of particles is achieved with PR plating when compared to pulse plating (PP). The reverse step stops the small amount of metal from depositing during the off time, which tends to occur with PP. In fact it tends to lead to partial dissolution of the metal layer. This leads to similar, smaller sized particles being deposited in the layer, as larger particles are lost during this dissolution, but smaller ones are still deposited (Podlaha & Landolt 1997, Low et al 2006).
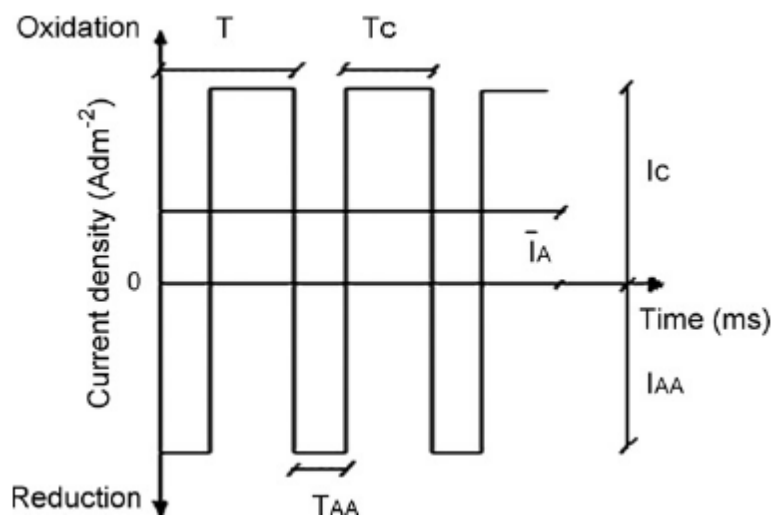
**Figure 31 - A typical waveform of pulse reverse plating (Chandrasekar & Pushpavanam)**

The incorporation of particles is affected by similar parameters as PP plating. The duty cycle is an important parameter, with a lower duty cycle (~20%) leading to the highest concentration of particles. Also the cathodic time has been shown to have an effect on particle pickup. A shorter cathodic time has given a high concentration of particles, due to the fact that less of the metal matrix can be deposited during one cycle, meaning that more particles can become entrapped. This is seen in Figure 32 (Podlaha & Landolt 1997, Weston et al 2011).
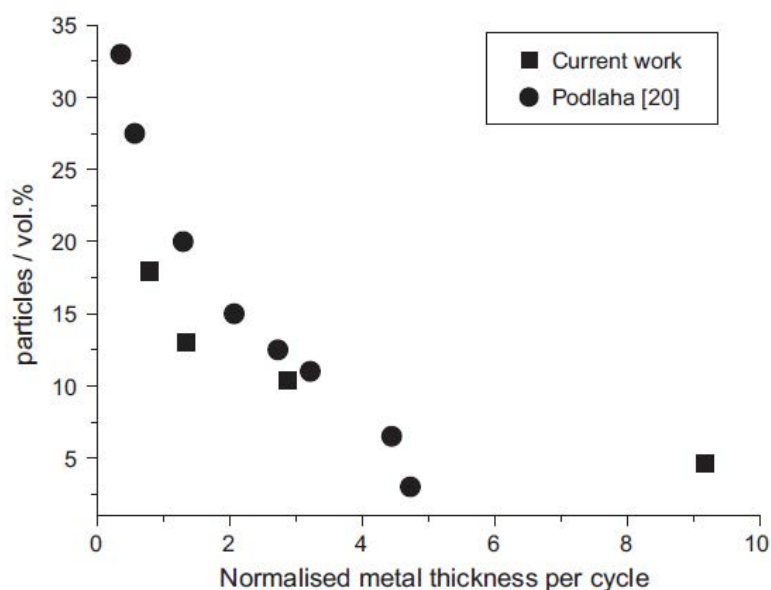


**Figure 32 - Volume fractions of WS$_2$ particles in Co and Al$_2$O$_3$ in Cu (Podlaha & Landolt 1997) showing the particle pickup of different metal thicknesses (Weston et al 2011)**

## 2 - Experimental Methods

## 2.1 - Construction of Oxidation Cell

In order to establish how changes in oxidation conditions affect the oxide, an oxidation cell was constructed. It enabled repeatable changes to be made to the atmosphere.
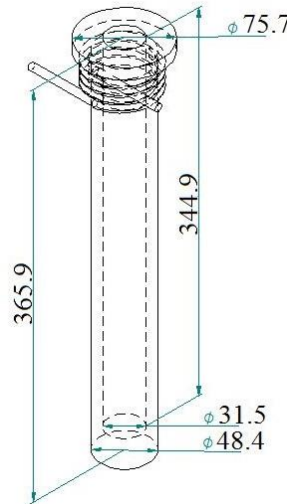


**Figure 33 - Dimensions of oxidation cell (in mm)**

The dimensions of the oxidation cell are shown in Figure 33. The cell was constructed using 316 grade stainless steel bar so that it resulted in a thick wall tube (stainless steel was chosen as it would retain reasonable strength at the required experimental temperatures). A cylinder of steel was welded on to the base of the tube to complete the basic cell shape.

A flange was welded to the top of the cell, and a lid of the same dimensions was made to fit it. This enables the inside of the cell to be sealed to allow for experimentation with controlled atmospheres. For the same purpose, a small groove was made in the flange so a rubber o-ring could be inserted to make an airtight seal, as shown in Figure 34b. Three valves were placed in the lid of the cell, two for inlet and outlet of gases, and one for a thermocouple, to allow for the monitoring of cell temperature during experiments involving gases, as shown in Figure 34c.
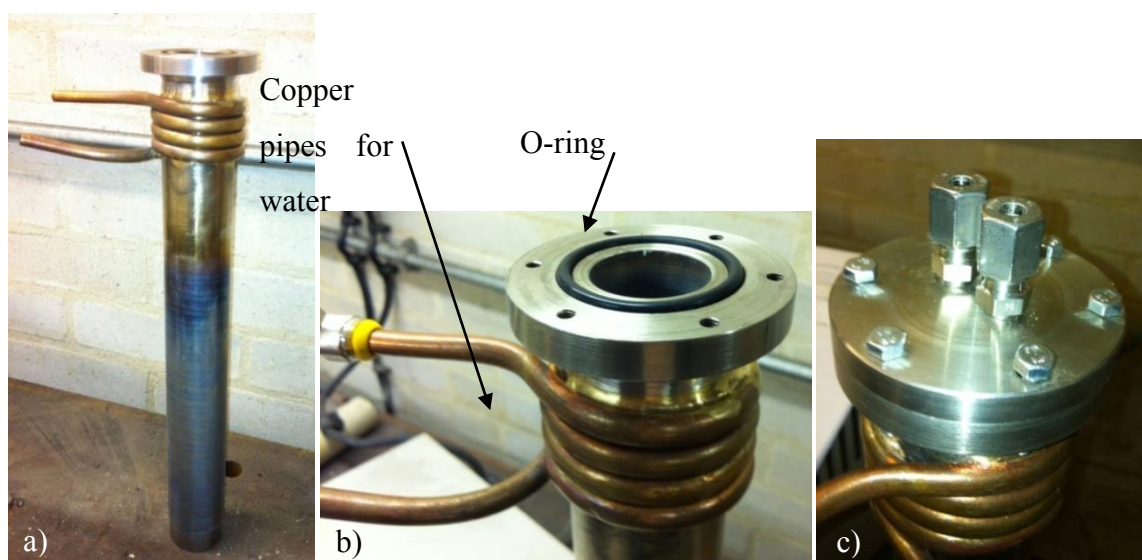
**Figure 34 - Oxidation cell a) basic layout of the cell b) the o-ring and water cooling c) lid of cell showing the valves for gas exchange**

A coiled copper tube was brazed around the top of the cell. This was used to water-cool the top of the cell preventing overheating of the cell and allow for easier handling of the hot cell, as shown in Figure 34a.

## 2.2 - Preparation of Alloys

Different aluminium alloys were made up by adding the required amounts of alloying additions to 1 or 2 kg of superpure aluminium (SP-Al, 99.9999 wt.% purity) or by mixing the superpure Al with the required amount of master alloy. The different alloys made, and the method used can be seen in Table 1 (compositions confirmed with x-ray fluorescence – see appendix 1). For the Al-7wt. %Si-0.3wt. %Mg alloy, a commercial alloy was purchased from Coleshill Aluminium Ltd. (all percentage compositions in this thesis are wt. % unless otherwise stated).

**Table 1 - Different alloy compositions made and the purity of the additions made**

| Alloy made (wt. %) | Elements added (purity) |
|---|---|
| Al 7%Si | Silicon 76g (99.99%) |
| Al 4%Mg | Magnesium 42g (99.95%) |
| Al 4%Cu | Copper 42g (99.99+ %) |
| Al 1%Fe | Iron 11g (99.99+ %) |
| Al 0.3%Sr | Strontium 31g of master alloy Al 10%Sr (99.95%) |
| Al 0.25%Ti | Titanium 2.5g (99.99+ %) |

The SP-Al was melted to 900 ˚C in an induction furnace and the appropriate amount of alloying addition was poured into the molten metal. This temperature was required in order to ensure higher melting point additions (e.g. Ti) would be able to dissolve properly. The mixture was allowed to sit for 1 hour, to allow the additions to melt in to the aluminium and become fully mixed. The molten alloy was then poured into a 1 or 2 kg mould and allowed to cool in air.

## 2.3 - Melt Experiments

Prior to the oxidation experiments, the temperature inside the cell during heating and cooling was monitored. A cylindrical furnace was used to conduct the oxidation cell experiments (made by Carbolite, serial no. 8/97/1843, type 15/50/175), as shown in Figure 35. A data logger running Labview software was used to monitor the temperature inside the cell over time and with different cooling methods for two empty runs. This was done using an Inconel sheathed type K thermocouple of diameter 0.5mm. The cooling methods measured were air cooling and quenching in a water bath at room temperature. The empty cell was heated, with the lid off to a temperature of 750 ˚C.



**Figure 35 - Cylindrical furnace used to heat the oxidation cell (shown inserted)**

A crucible (from Multilab) made from high purity sintered alumina was used to melt the charges and is shown in Figure 36a. This shape was chosen as a pseudo-constant composition that can be achieved during the test due to the high volume to surface area ratio. It had an upper outer

50

diameter of 25mm, a lower inner diameter of 15mm and a height of 30mm. This was placed carefully in the base of the cell. Later experiments were undertaken using cylindrical crucibles, with the dimensions of 20mm outer diameter, 16mm inner diameter and height 30mm. This can be seen in Figure 36b. The change was made to acquire a flatter top surface and so make later analysis easier.
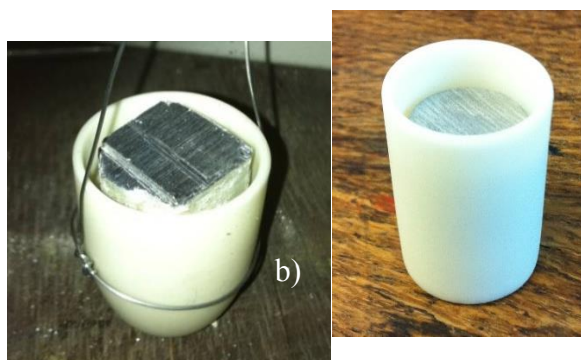


**Figure 36 - The alumina crucible used for melting a) conical shape b) cylindrical shape**

First the cooling tubes were connected to mains water to make for constant cooling during the experiment. The cell containing the crucible was lowered in to the cylindrical furnace. The furnace was turned off as this point. A thermocouple was inserted in to the cell so that it sat next to the crucible rather than inside it.

### 2.3.1 - Sample Preparation

A cylinder of the required metal was milled to a diameter of 15mm. The samples were cut to fit in the crucibles. To remove as much old surface oxide as possible, prior to melting the samples were immersed in hydrofluoric acid (2% HF in water) for 5 minutes then washed using water and dried. Typical intervals between cleaning and initiation of the melting cycle were in the order of 300 to 450 seconds.

### 2.3.2 - Melting Protocol

The furnace was switched on and set to the required temperature for the experiment. Once the temperature inside the cell had reached the correct temperature, the metal was held for the required time. The holding times for each sample are shown in Table 2. The humidity and temperature of the atmosphere around the furnace was also noted for reference only. Some samples were melted using a small oven-type furnace (Pyrotherm, model no. ECON 10/8). These were samples that had shorter holding times, and the furnace was used to ensure the aluminium was molten before the holding time was started. This was less of an issue for the longer holding times so the oxidation cell was used for these. The ramping temperature for both

furnace was in the region of 50 °C/min. The holding times are designed so that a logarithmic range of results can be recorded. A temperature of 750 °C was used as previous work (Thiele 1962) suggested that at this temperature the formation of γ and α-alumina would occur over the times used. Several melts were repeated, to check the melting procedure was repeatable, and they are also noted in Table 2.

**Table 2 - Holding times and temperatures for the samples (750 ˚C)**

| Sample comp. | Sample no. (no. of repeats) | Holding Time (s) | Melting method | Room Temp. (˚C) | Relative Humidity | Cooling method |
|---|---|---|---|---|---|---|
| SP Al | 1 | 300 (5 min) | Furnace | 22.5 | 31% | Air cool |
| | 2 (2) | 1000 (17 min) | Furnace | 22.1 | 32% | Air cool |
| | 3 (3) | 3600 (1 hour) | Oxidation cell | 22.3 | 29% | Quench |
| | 4 (2) | 10 800 (3 hour) | Oxidation cell | - | - | Quench |
| | 5 (2) | 25 200 (7hours) | Oxidation cell | 22.5 | 27% | Quench |
| | 6 (3) | 86 400 (24 hours) | Oxidation cell | 22.5 | 44.2% | Quench |
| Al 4wt.%Mg | 1 | 300 (5 min) | Furnace | 21.4 | 29% | Air cool |
| | 2 | 1000 (17 min) | Furnace | 21.4 | 29% | Air cool |
| | 3 (2) | 3600 (1 hour) | Oxidation cell | 21.4 | 25% | Quench |
| | 4 (2) | 10 800 (3 hour) | Oxidation cell | 20.8 | 28% | Quench |
| | 5 | 25 200 (7hours) | Oxidation cell | 21.4 | 32% | Quench |
| Al 7wt.%Si | 1 | 300 (5 min) | Furnace | 21.2 | 31% | Air cool |

| | 2 | 1000 (17 min) | Furnace | 21.2 | 31% | Air cool |
|---|---|---|---|---|---|---|
| | 3 (2) | 3600 (1 hour) | Oxidation cell | 21.6 | 25% | Quench |
| | 4 | 10 800 (3 hour) | Oxidation cell | 21.2 | 31% | Quench |
| | 5 | 25 200 (7hours) | Oxidation cell | 21.8 | 44% | Quench |
| | 6 | 86 400 (24 hours) | Oxidation cell | 21.4 | 22% | Quench |
| Al 7wt.%Si 0.3wt.%Mg | 1 | 300 (5 min) | Furnace | 25 | 24% | Air cool |
| | 2 | 1000 (17 min) | Furnace | 25 | 24% | Air cool |
| | 3 (2) | 3600 (1 hour) | Oxidation cell | 25.8 | 21% | Quench |
| | 4 (2) | 10 800 (3 hour) | Oxidation cell | 21.4 | 27% | Quench |
| | 5 | 86 400 (24 hours) | Oxidation cell | 23.6 | 32% | Quench |
| Al 4wt.%Cu | 1 | 300 (5 min) | Furnace | 23.5 | 45% | Air cool |
| | 2 | 1000 (17 min) | Furnace | 23.5 | 45% | Air cool |
| | 3 (2) | 3600 (1 hour) | Oxidation cell | 24.5 | 31% | Quench |
| | 4 | 10 800 (3 hour) | Oxidation cell | 23.6 | 40% | Quench |
| | 5 | 25 200 (7hours) | Oxidation cell | 23.2 | 38% | Quench |
| | 6 | 86 400 (24 hours) | Oxidation cell | 22.5 | 30.6% | Quench |
| Al 1wt.%Fe | 1 | 300 (5 min) | Furnace | 23.6 | 32% | Air cool |

| | 2 | 1000 (17 min) | Furnace | 23.6 | 32% | Air cool |
|---|---|---|---|---|---|---|
| | 3 | 3600 (1 hour) | Oxidation cell | 23.6 | 32% | Quench |
| | 4 | 10 800 (3 hour) | Oxidation cell | 22.8 | 41% | Quench |
| | 5 | 265 200 (7hours) | Oxidation cell | 23.9 | 37% | Quench |
| | 6 | 86 400 (24 hours) | Oxidation cell | 22.9 | 23.8% | Quench |
| Al 0.3wt.%Sr | 1 | 300 (5 min) | Furnace | 21.8 | 31.7% | Air cool |
| | 2 | 1000 (17 min) | Furnace | 21.8 | 31.7% | Air cool |
| | 3 | 3600 (1 hour) | Oxidation cell | 18.9 | 24% | Quench |
| | 4 | 10 800 (3 hour) | Oxidation cell | 19.5 | 20% | Quench |
| | 5 | 25 200 (7hours) | Oxidation cell | 19.9 | 22% | Quench |
| | 6 | 86 400 (24 hours) | Oxidation cell | 22.7 | 23% | Quench |
| Al 0.25wt.%Ti | 1 | 300 (5 min) | Furnace | 21.8 | 31.7% | Air cool |
| | 2 | 3600 (1 hour) | Oxidation cell | 22.1 | 22% | Quench |
| | 3 | 86 400 (24 hours) | Oxidation cell | 23.6 | 22% | Quench |

After holding at temperature the cell and samples were either quenched or air cooled, to see if this affected the structure. The cooling methods used for each sample are also shown in Table 2. When quenched the cell was placed in a bath of water at room temperature and held still with a lid. Quenching was used for samples in the oxidation cell, as removing the small crucible from the cell and air cooling it was attempted but proved difficult. Quenching enabled a good

cooling rate within the cell and around the sample. When air cooled, the cell was placed in a stand, the base resting on a fire brick until cool. Air cooling was used for the samples held in the smaller furnace, and done at room temperature (noted in Table 2). This meant that the cooling rate was comparable for each melting method. Once cooled, the metal was removed from the cell and examined using various techniques.

### 2.3.3 - Nitrogen Atmosphere

To observe how nitrogen may change the resulting layer, experiments were carried out on samples at 750 °C in a nitrogen atmosphere. The cell seen in Figure 34 had an air tight seal, so gases can be introduced to the system. The set up allowed the respective inlet of helium and nitrogen in to the cell.

Prior to melting, a Mixcheck helium/oxygen analyser by Vandagraph (model no. 238138, oxygen sensor no. 314364) was calibrated using compressed air, to set the oxygen level to 20.9%.

The samples were introduced to the cell after 5 minute etch in 2% HF solution. The cell was then sealed using the sealing o-ring and a series of screws, as seen in Figure 34c. The $He/O_2$ analyser was attached to the gas outlet pipe attached to the cell. A bottle of Helium and a bottle of oxygen free nitrogen (99.9998% min. $N_2$ level) were fed in to the cell via a t-junction valve, allowing for rapid change between the feeding gases. Helium was passed through the system until the analyser read that 100% Helium was being expelled from the cell. The gas outlet pipe was removed from the analyser and the gas supply was switched to nitrogen. The gas was passed through at a rate of ~13 $cm^3$/min.

At this point the experiment followed the same procedure as used for the oxidation experiments. The alloys used in the nitrogen cell were SP-Al, Al 4% Mg and Al 7%Si 0.3%Mg as described in Table 1, as these are the most common aluminium alloys used in industrial applications.

### 2.3.4 - Mo Experiments

A series of experiments were undertaken to observe the effects of molybdenum on the oxide layer. SP-Al was melted in the small furnace used previously. The surface of the molten metal was removed from one half of the samples before 3g of 99.9+% pure Mo powder was placed on the surface of the melt. The other half had the Mo powder added without having the surface

removed. The samples were held for 5 minutes, 1 hour and 24 hours (holding times) and taken out to air cool after being held.

Two alloys were made up of Al 1%Mo and an alloy using the Al 7%Si 0.3%Mg alloy used in the oxidation experiments above containing 1wt% Mo. The experiments were done at 750 °C, and the undertaken in both air and $N_2$ atmospheres. The conditions (and those repeated) are shown in Table 3.

Table 3 - Experiements done to determine the effects of Mo on the oxidation of SP-Al (all done at 750 °C)

| Sample no. (no. of repeats) | Sample comp. | Holding Time (s) | Melting method | Room Temp. (˚C) | Relative Humidity | Cooling method |
|---|---|---|---|---|---|---|
| AMo1 | Al + 3g Mo powder | 300 (5 min) | Furnace | 21.7 | 23% | Air cool |
| AMo2 | | 1000 (17 min) | Furnace | 21.7 | 23% | Air cool |
| AMo3 (2) | | 3600 (1 hour) | Furnace | 21.7 | 23% | Air cool |
| AMo4 (3) | | 10 800 (3 hour) | Furnace | 21.4 | 27% | Air cool |
| AMo5 | | 25 200 (7hours) | Furnace | 24.3 | 21% | Air cool |
| AMo6 | | 86 400 (24 hours) | Furnace | 21.5 | 22% | Air cool |
| AlMo1% 1 | Al 1% Mo | 300 (5 min) | Furnace | 22.9 | 30.7% | Air cool |
| AlMo1% 3 | | 3600 (1 hour) | Oxidation cell | 22.9 | 30.7% | Quench |
| AlMo1% 6 | | 86 400 (24 hours) | Oxidation cell | 21.5 | 29.8% | Quench |
| ASMMo1% 1 | Al 7%Si 0.3%Mg 1% Mo | 300 (5 min) | Furnace | 21.7 | 31.5% | Air cool |
| ASMMo1% 3 (2) | | 3600 (1 hour) | Furnace | 21.6 | 31.7% | Air cool |
| ASMMo1% 6 | | 86 400 (24 hours) | Furnace | 21.6 | 31.7% | Air cool |

## 2.4 - Crystallographic and Structural Observations

*SEM – Preparation for and Use*

Cooled samples were then cut to sizes appropriate for mounting in conductive Bakelite. They were cut from top to bottom so that the oxide surface was perpendicular to the cut surface. A Struers Accutom-50 cuttig machine with a silicon carbide cutting wheel. The samples were then mouted using am ATM Opal-480 hot mounting press and mounted in Bakelite. To avoid

observing the effects of damage on the oxide layers, the samples were gently ground down in an attempt to ensure the oxide visible was not in the region cut by the machine. Samples were ground and polished initially using an auto-polisher (to the final finish) and by hand for further final polish. SiC grinding papers of 800 (5 minutes), 1200 (5 minutes) and 4000 (5 minutes) grits were used before polishing using MD-Mol with a 3μm DP suspension diamond solution (2 minute intervals – progress depended on alloy mix) then MD-Chem with a 0.04μm OP suspension diamond solution (2 minute intervals – progress depended on alloy mix). Following each step in the preparation samples were cleaned in acetone using an ultrasonic bath for 3 minutes, to ensure no residue from polishing remained on the surface.

## 2.5 - Characterisation

### 2.5.1 - Scanning Electron Microscopy

Samples were viewed using a Jeol 7000 Field Emission Gun (FEG) scanning electron microscope (SEM). The samples were observed perpendicular to the oxide layer. An accelerating voltage of 10kV was used where possible (sometimes higher had to be use when the microscope was not functioning correctly) and a spot size in region of 6-6.5. Where possible, backscattered electron imaging was used (on composition setting), but sometimes this was not possible due to the microscope sometimes not being at full functionality. Energy Dispersive X-ray (EDX) spectroscopy was conducted on each sample surface, with an attempt to get analysis of the top oxide layer and the bulk metal in the sub-surface region. The oxide thickness was measured by analysis of the images obtained during SEM. Zeiss Axiovision (LE) software was used to measure the thickness of the oxides in the images. The scale bar was input as the pixel ratio and several measurements were taken for each image, with a minimum of 3 images being taken for each sample. Only regions of even, uniform thickness with no evidence of spalling or damage. An average thickness was then calculated from the images. Errors were calculated from the standard deviation of the measured thicknesses and divided by √sample size.

### 2.5.2 - XRD

The samples were observed using x-ray diffraction (XRD) in order to acquire the crystal structure of the surface layers formed during the experiments. The top surface areas of samples were cut in to small pieces, around 3 mm, in order for them to be made into powder suitable for the XRD analysis machine. The pieces were milled using a Spex CertiPrep Freezer Mill 6750, which is a cryogenic mill that uses liquid nitrogen to cool samples before a magnetic rod is used to crush the pieces to a powder. The amount of powder used was enough to ensure a reasonable

coverage of the sample holder's assessment area (10 mm diameter) and was placed between two layers of amorphous tape. The samples were then observed using a D8 Autosampler XRD machine. It observed each sample for $2\theta$ values between 20° and 90° with a stepsize of 0.02. The spectra were compared to published data (from work verified as having reliable results) using EVA 2 software, and as so the confirmed species signals sometimes differed between samples of the same alloy as the reference signals came from different data sets.

## 2.6 - Grain Refinement Tests

*Electrolytic Codeposition*

A method to incorporate small particles of suspected Al-Mg spinel ($MgAl_2O_4$) grain refiners into a copper based master alloy was used. They were made using a process of electro-codeposition of spinel particles in a copper coating. Several experiments were undertaken to determine the most efficient method for particle deposition. The spinel was sourced from Sigma Aldrich and had a grain size range of 1-5 μm.

A solution of 0.25M $CuSO_4{\cdot}5H_2O$ and 0.3M $C_6H_5Na_3O_7{\cdot}2H_2O$ was used for all experiments, from work done by Podlaha and Landolt (1997). The initial deposition was carried out on brass stubs of 8 mm diameter, mounted within rotating electrode apparatus. The solution above was made up, 100 ml of which was put in to a beaker and the equivalent of 10 g/l of spinel particle were added (1-5 μm size distribution) and stirred using a magnetic stirrer set to 530 rpm. The brass stub had its surface made rough by grinding it with a 400 grit SiC paper, prior to being placed in the solution. A copper counter electrode and an Ag/AgCl reference electrode were also placed in the solution. Nova 1.6 software was used to control the current density and cycle times and attached to the electrodes. A combination of DC and fast pulse reverse (FPR) currents were used for deposition. A duty cycle of 20%, with a positive current of 0.01A and negative of -0.5A, was used for FPR cycles. The initial experiments are shown in Table 4.

**Table 4 - Inital codeposition experiments, using no surfacant and 10 g/l spinel**

| Type of deposition used | Experimental parameters | Rotating electrode speed (rpm) | Time at negative/positive (s) (if applicable) |
|---|---|---|---|
| DC | -20 mA/cm$^2$, 30 mins | 500 | - |
| DC | -20 mA/cm$^2$, 30 mins | 800 | - |
| FPR | 50 Hz | 800 | 0.002/0.018 |
| FPR | 50 Hz | 1000 | 0.002/0.018 |
| FPR | 50 Hz, pre-roughed with 220 grit paper | 1000 | 0.002/0.018 |
| FPR | 50 Hz | 1200 | 0.002/0.018 |
| FPR | 200 Hz | 800 | 0.0005/0.0045 |

The use of surfactants was also studied. The surfactant of sodium dodecyl sulphate (SDS) was used to judge the effectiveness of surfactants on the experiment. It was added in a quantity of 0.4 ml (0.2 g/l), along with 4 g of spinel (50 g/l) to see the effect of particle concentration on pickup. This stage of experiments can be seen in Table 5.

**Table 5 - Secondary codeposition experiments, using 0.2 g/l SDS and 50 g/l spinel**

| Type of deposition used | Experimental parameters | Rotating electrode speed (rpm) | Time at negative/positive (s) (if applicable) |
|---|---|---|---|
| DC | -20 mA/cm$^2$, 30 mins | 800 | - |
| FPR | 50 Hz | 800 | 0.002/0.018 |
| FPR | 200 Hz | 800 | 0.0005/0.0045 |
| FPR | 200 Hz | 1000 | 0.0005/0.0045 |
| FPR | 200 Hz | 1200 | 0.0005/0.0045 |
| FPR | 200 Hz, 50 °C | 800 | 0.0005/0.0045 |
| FPR | 50 Hz | 2000 | 0.002/0.018 |

Minitab software was used to design a series of experiments to determine the optimum technique to deposit the largest amount of spinel particles present in the copper coating. The FPR technique was studied and the variables of 50-200Hz pulse speed and 800-2000 rpm rotation speed were used for the design. The experimental design used a solution of 100 ml of 0.25M $CuSO_4 \cdot 5H_2O$ and 0.3M $C_6H_5Na_3O_7 \cdot 2H_2O$ which was added to a beaker along with 0.4 ml (equivalent to 0.2 g/l) of SDS and 50 g/l of $MgAl_2O_4$. The series of experiments undertaken can be seen in Table 6.

**Table 6 – Experimental design undertaken to determine the best deposition method for spinel particles in a copper matrix**

| Experiment order | Reverse-pulse speed (Hz) | Rotating electrode speed (rpm) | Time at negative/positive (s) |
|---|---|---|---|
| 1 | 200 | 2000 | 0.0005/0.0045 |
| 2 | 125 | 1400 | 0.0008/0.0072 |
| 3 | 50 | 2000 | 0.002/0.018 |
| 4 | 231.66 | 1400 | 0.00043/0.0039 |
| 5 | 125 | 550 | 0.0008/0.0072 |
| 6 | 18.9 | 1400 | 0.00529/0.0476 |
| 7 | 125 | 2248 | 0.0008/0.0072 |
| 8 | 200 | 1000 | 0.0005/0.0045 |
| 9 | 200 | 800 | 0.0005/0.0045 |
| 10 | 50 | 800 | 0.002/0.018 |
| 11 | 200 | 1200 | 0.0005/0.0045 |

The cathodic current density was set at $-5mA/cm^2$ and the anodic current density was set at $10mA/cm^2$ for all experiments and electrodeposition occurred for 30 minutes.

The percentage of spinel was calculated using EDX techniques, analysing large areas of the layers in the SEM. The levels of Mg and Al were used to calculate the percentage spinel in the Cu layer and the sample with the highest pickup, had its method used to produce the samples for grain refinement tests. Samples for grain refinement tests were made using the best method but the codeposition occurred for 2 hours, and four samples were made so that a good enough particle count was present in the metal in order for grain refinement to take place. The layers were removed by cutting them from the brass stubs using a Steurs Minitom, in order to ensure a gentle removal of the layers.

### 2.6.1 - Grain refinement Tests

To determine if the spinel and MgO embedded in Cu coatings worked as grain refiners, a series of experiments were performed comparing the grain structures of unrefined metal (a sample containing spinel embedded coatings, made using the above method) to those containing a standard grain refiner ( Al-5Ti-B),. The metal was melted in the charges shown in Table 7. The melt temperature of 750 °C was used to match the holding temperatures used in the oxidation experiments.

Table 7 - Charges of the metals melted in grain refinement tests

| Alloy melted | Charge Make-up | Melt temperature (°C) |
|---|---|---|
| Commercial Purity Al (CP-Al) | 2247g CP-Al | 750 (transfer at 760) |
| CP-Al + Al-5Ti-B (in copper layer) | 2298g CP-Al<br>457g 5:1 TiB$_2$ | 750 (transfer at 757) |
| CP-Al + Spinel particles | 2223 g CP-Al<br>4 spinel containing Cu coatings | 750 (transfer at 760) |

The moulds shown in Figure 37 were used to cast the metal. The mould was made from 25kg silica sand, mixed with binding agents and placed in two halves of the pattern to give the required mould shape. The two halves were then stuck together using Corfix 22 and allowed to set. Once hard, the mould was placed in a rolling frame as seen in Figure 38. A sand mould was used due to time constraints. Only a small amount of the Al-Mg spinel was able to be made, so a TP1 type test was unfeasible. Industrial levels (125-150 ppm) were unable to be made during the experimental period so only the equivalent of 50 ppm was added. The superheat was not controlled, and no chills were used. The moulds did not allow for any superheat control, plus the castings were representative of a commercial castings setup.

. CP-Al was melted to the conditions in Table 7, and the required additions made. The amount of Al-Mg spinel present in the melt was the equivalent of 12.5 ppm. The molten metal was transferred at the temperatures shown in Table 7. The metal was poured in to the mould and when full it was rolled so to ensure the bars would be filled with metal upon solidification.



**Figure 37 - Measurements of the mould used to assess potency of grain refiners (dimensions in mm)**
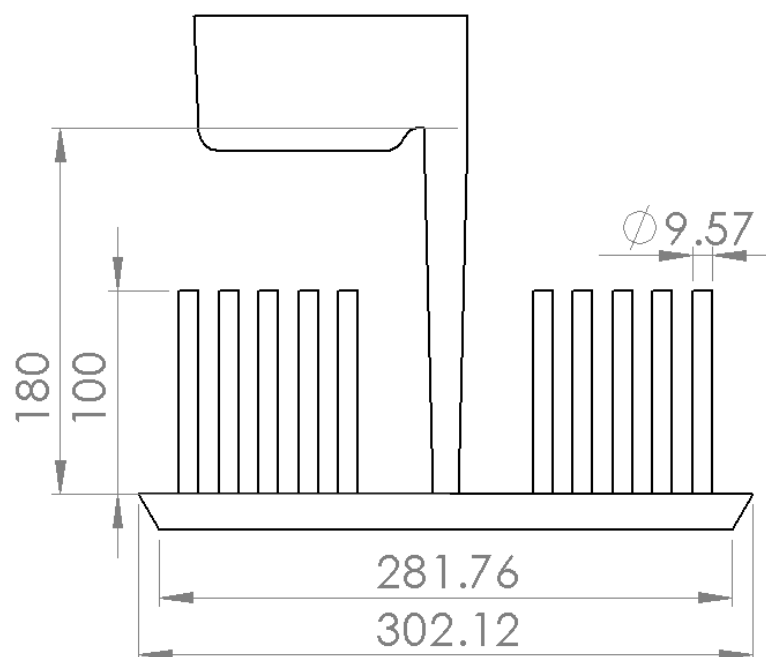
**Figure 38 - The frame used to roll the mould over to ensure proper filling**

The solid bars were cut from the main casting. They were then cut, mounted, polished (as described previously) and etched in Keller's etch for 10-15 seconds (this was the technique recommended by technicians. Samples were observed using optical microscopy analysis. The grain size was measured using Zeiss Axiovision software by drawing several lines across the images. Where the grain boundaries crossed the line, was counted as a measurement (with the scale bar on the image used as reference). Measurements were taken from a minimum of 3 images from different areas of the sample with 3 lines across each image.

# 3 – Results

## 3.1 - Oxidation of Aluminium Alloys
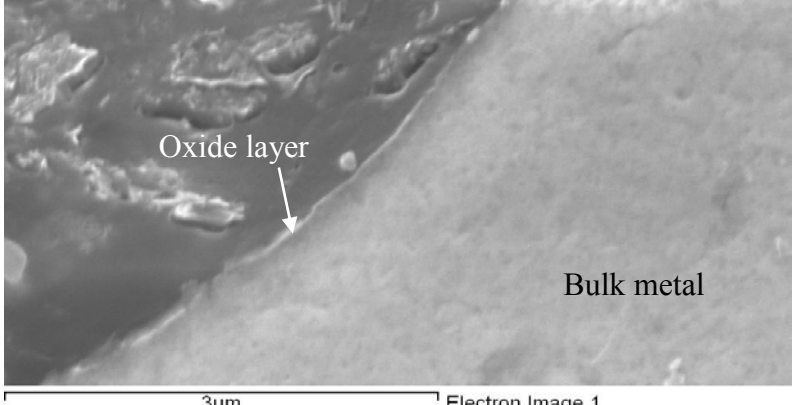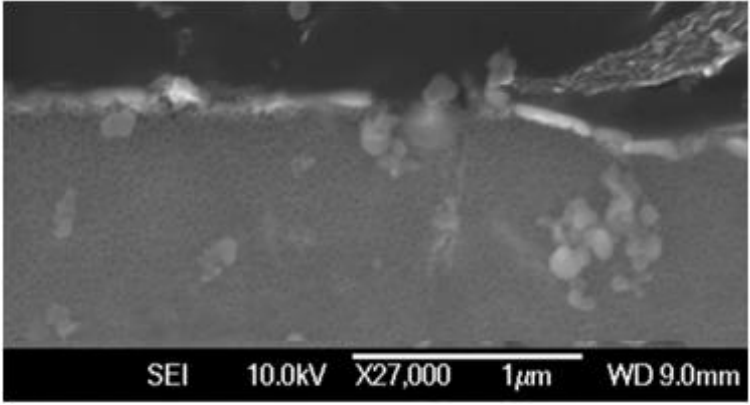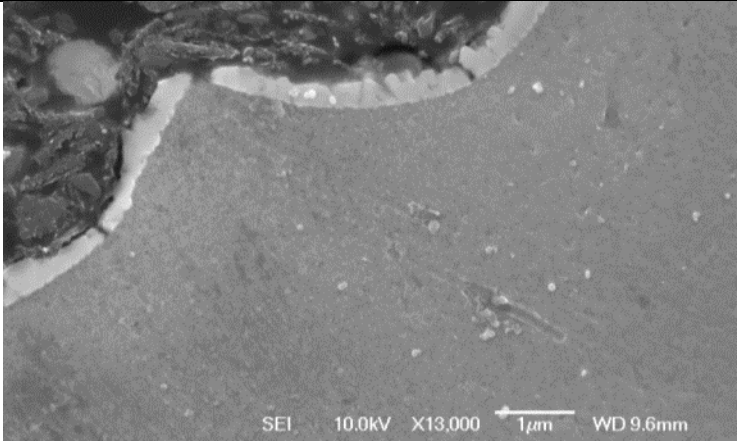
Samples from the oxidation experiments of Al and its alloys were observed using a combination of techniques. Scanning electron microscopy (SEM) analysis was used to observe the oxide layer and to measure it. The layers were analysed using energy dispersive x-rays (EDX) to determine the composition of the oxides present. The outer oxides were manufactured in to powders and analysed using x-ray diffraction (XRD) in order to determine the structure of the oxides. The results are described in the following section

Some samples were quenched and others air cooled. There seemed to be little difference in oxidation due to this, as both room temperature and temperature of quenching water was within a few degrees of each other (as the water was always at room temperature). Humidity readings were for information only, any water vapour present near the samples would have evaporated during heating. Repeated samples all had oxide thickness values similar to the ones noted, showing the method was repeatable. Images were taken from each sample and the results averaged. The thicknesses given are an average of all thickness measurements taken. Care was taken to ensure the samples were polished perpendicular to the direction of the oxide layer, in an attempt to minimise the effect of different polishing angles on the oxide. Thickness measurements were taken across a range of the sample at different places, and several measurements made at each chosen area. This ensured an average thickness measurements across all samples, to give an accurate measurement.

### 3.1.1 - Superpure Aluminium (SP-Al)

The initial SEM work was done on SP-Al samples in order to ascertain the nature of the oxides on liquid Al when grown in air. Samples held at 750 ˚C were assessed and images representative of the structures observed are summarised in Figure 39.

**Figure 39 - Images of SP-Al held at 750ºC, at different times for superpure Al. The thickness of the oxide layer is also noted**

| Sample | Image |
|---|---|
| 1<br><br>750 ºC 5 min hold<br><br>Oxide layer ≈ 0.05 μm |  |
| 2<br><br>750 ºC 17 min hold<br><br>Oxide layer ≈ 0.1μm |  |
| 3<br><br>750 ºC 1 hour hold<br><br>Oxide layer ≈ 0.35 μm |  |

| | |
|---|---|
| 4<br><br>750 ºC 3 hour hold<br><br>Oxide layer ≈ 0.55 μm | <br>COMPO   10.0KV   X7,500   1μm   WD 9.3mm |
| 5<br><br>750 ºC 7 hour hold<br><br>Oxide layer ≈ 0.42 μm | <br>2μm                    Electron Image 1 |
| 6<br><br>750 ºC 24 hour hold<br><br>Oxide layer ≈ 0.37 μm | <br>2μm                    Electron Image 1 |
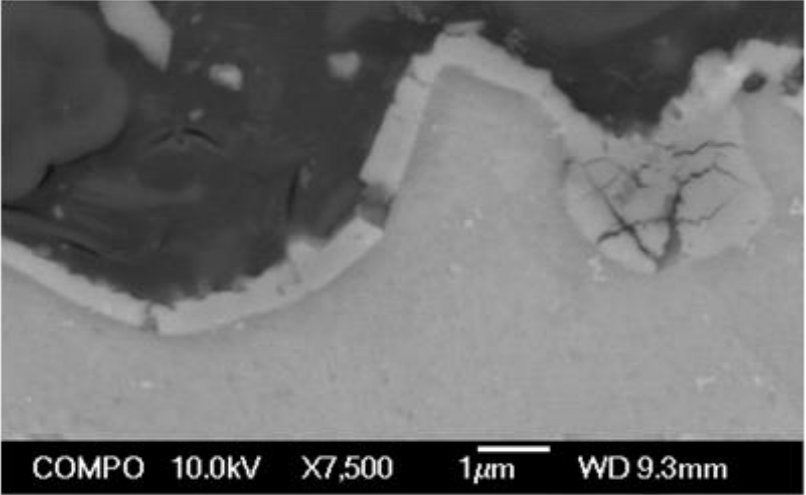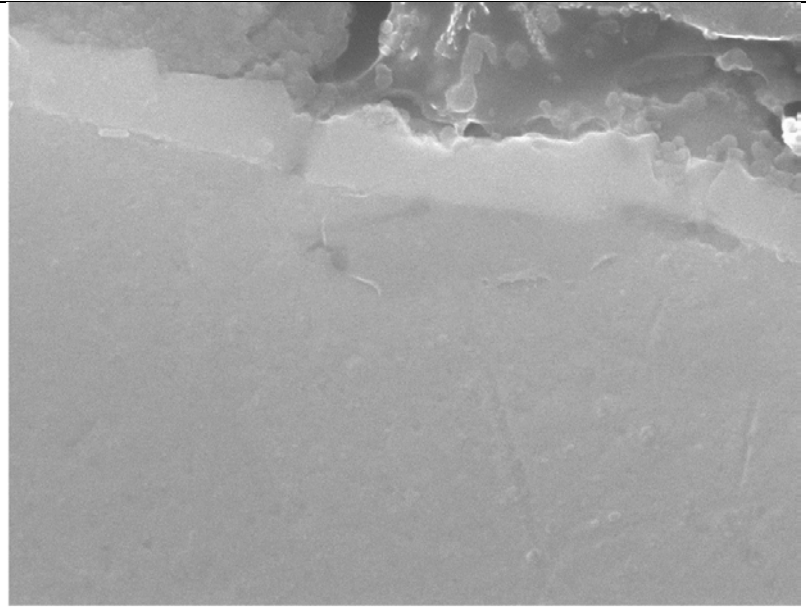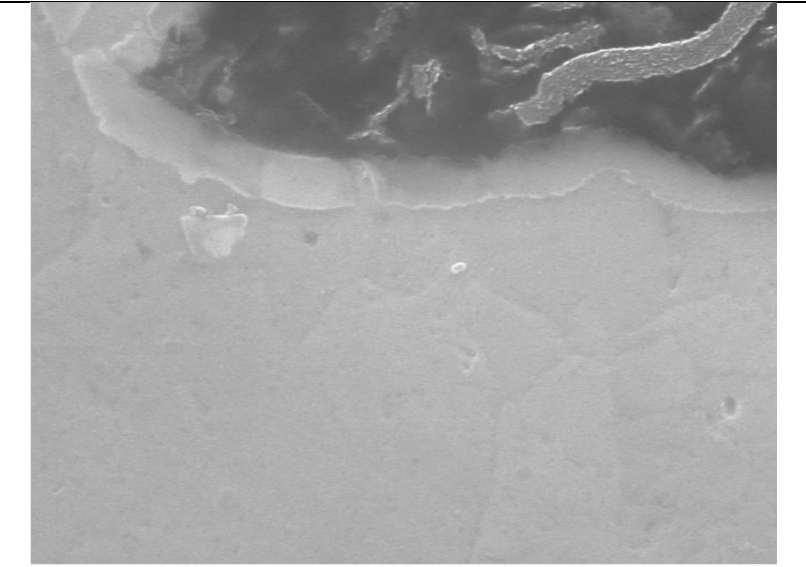
**Figure 39 continued - Images of SP-Al held at 750ºC, at different times for superpure Al. The thickness of the oxide layer is also noted**

It can be seen that the thickness of the oxide layer generally increased with holding time, as previously shown by Thiele (1962), and this is summarised in Table 8 and Figure 40. There was an increase until the 3 hour holding time, which then decreased in 7 hour and then levelled off (considering the error bars).

**Table 8 - Summary of oxide thicknesses for superpure Al held at 750oC**

| Melt Conditions | Oxide Thickness |
|---|---|
| 750$^{\circ}$C 5 min hold | 0.05 μm |
| 750$^{\circ}$C 17 min hold | 0.10 μm |
| 750$^{\circ}$C 1 hour hold | 0.30 μm |
| 750$^{\circ}$C 3 hour hold | 0.53 μm |
| 750$^{\circ}$C 7 hour hold | 0.42 μm |
| 750 $^{\circ}$C 24 hour hold | 0.37 μm |
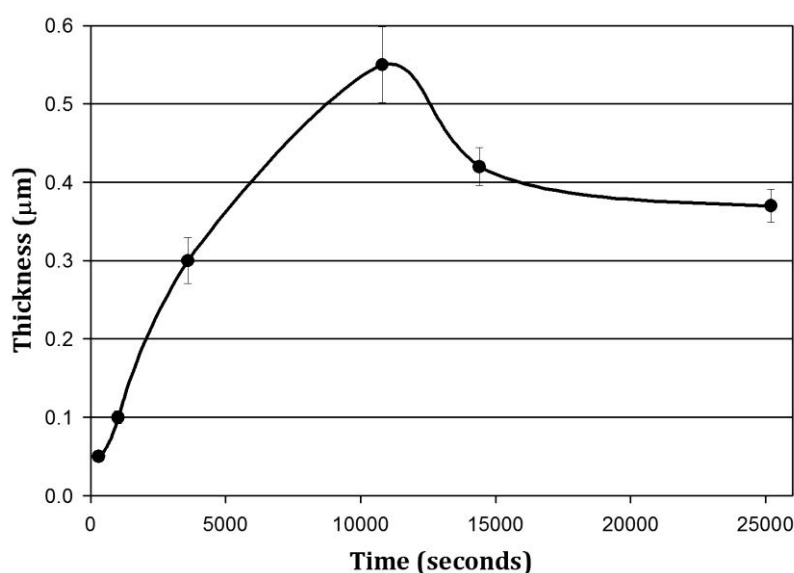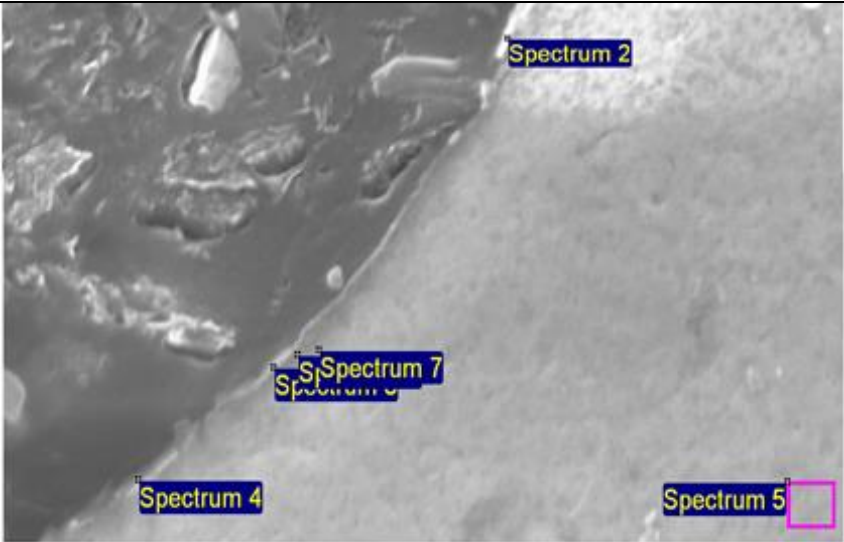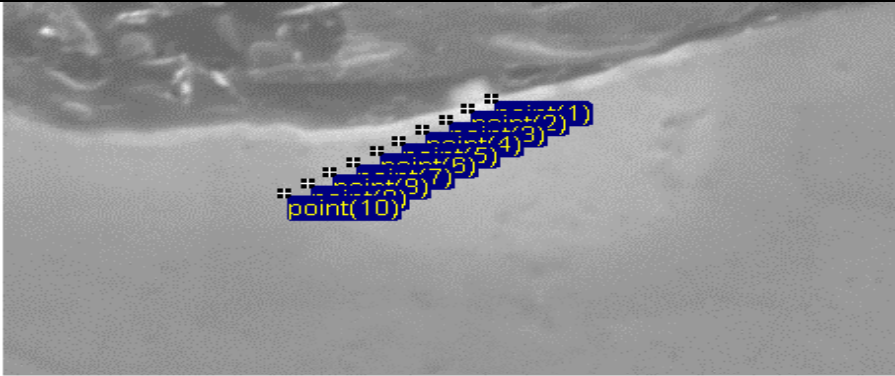


**Figure 40 - Thickness of oxide layer vs. holding time for superpure Al samples held at 750 °C**

It can be seen that the thickness of the oxide layers of the samples increased with holding time. It is also apparent that there is a point where the rate increased more rapidly, between 5 minutes and 1 hour. There is an increase in rate up to 1 hour oxidation (7.5 x $10^{-5}$ μm/s) which then plateaus. This could be due to the forming of γ-$Al_2O_3$, once a continuous layer formed the oxidation rate slowed the oxygen in contact with the liquid Al is reduced as the permeability of the oxide layer is decreased.

Low resolution EDX analysis was done on the surface of the samples using a tungsten filament field emission gun (FEG) SEM. The results are shown in Figure 41.

**Figure 41 - EDX analysis of superpure Al samples**

| Sample | Analysis |
|---|---|
| 1<br><br>750 °C 5 min hold<br><br>Oxide layer ≈ 0.05 μm | <br><br>Spectrum 2<br>Element / Weight%<br>O 44.03 / Al 55.97<br><br>Spectrum 3<br>Element / Weight%<br>O 42.31 / Al 57.69<br><br>Spectrum 4<br>Element / Weight%<br>O 39.22 / Al 60.78<br><br>Spectrum 5<br>Element / Weight%<br>O 0.86 / Al 99.14<br><br>Spectrum 6<br>Element / Weight%<br>O 37.97 / Al 62.03<br><br>Spectrum 7<br>Element / Weight%<br>O 30.5 / Al 69.5 |
| 2<br><br>750 °C 17 min hold<br><br>Oxide layer ≈ 0.1μm | <br><br>Point 1<br>Element / Weight%<br>O 29.32 / Al 70.68<br><br>Point 2<br>Element / Weight%<br>O 29.58 / Al 70.42<br><br>Point 3<br>Element / Weight%<br>O 26.13 / Al 73.87<br><br>Point 4<br>Element / Weight%<br>O 21.31 / Al 78.69<br><br>Point 5<br>Element / Weight%<br>O 12.97 / Al 87.03<br><br>Point 6<br>Element / Weight%<br>O 7,66 / Al 92.34<br><br>Point 7<br>Element / Weight%<br>O 5.78 / Al 94.22<br><br>Point 8<br>Element / Weight%<br>O 4.19 / Al 95.81<br><br>Point 9<br>Element / Weight%<br>O 4.95 / Al 95.05<br><br>Point 10<br>Element / Weight%<br>O 3.48 / Al 96.52 |

| 3<br><br>750 ºC 1 hour hold<br><br>Oxide layer ≈ 0.35 μm | <br>2μm    Electron Image 1 |
|---|---|

**Point 1**

| Element | Weight% |
|---|---|
| O | 33.22 |
| Al | 66.78 |

**Point 2**

| Element | Weight% |
|---|---|
| O | 38.10 |
| Al K | 61.90 |

**Point 3**

| Element | Weight% |
|---|---|
| O | 27.59 |
| Al | 72.41 |

**Point 4**

| Element | Weight% |
|---|---|
| O | 9.77 |
| Al | 90.23 |

**Point 5**

| Element | Weight% |
|---|---|
| O | 5.75 |
| Al | 94.25 |

**Point 6**

| Element | Weight% |
|---|---|
| O | 4.26 |
| Al | 95.74 |

**Point 7**

| Element | Weight% |
|---|---|
| O | 1.43 |
| Al | 98.57 |

| 4<br><br>750 ºC 3 hour hold<br><br>Oxide layer ≈ 0.6 μm | <br>7μm    Electron Image 1 |
|---|---|

**Point 1**

| Element | Weight% |
|---|---|
| O | 45.54 |
| Al | 54.46 |

**Point 2**

| Element | Weight% |
|---|---|
| O | 43.25 |
| Al K | 56.75 |

**Point 3**

| Element | Weight% |
|---|---|
| O | 32.6 |
| Al | 67.4 |

**Point 4**

| Element | Weight% |
|---|---|
| O | 7.07 |
| Al | 92.93 |

**Point 5**

| Element | Weight% |
|---|---|
| O | 2.63 |
| Al | 97.37 |

**Point 6**

| Element | Weight% |
|---|---|
| O | 1.09 |
| Al | 98.91 |

**Point 7**

| Element | Weight% |
|---|---|
| O | 0.72 |
| Al | 99.28 |

**Figure 41 - EDX analysis of superpure Al samples**

| 5 |
| :---: |
| 750 ºC 7 hour hold |
| Oxide layer ≈ 0.42 μm |



2μm          Electron Image 1

| Spectrum 1 | | Spectrum 2 | | Spectrum 3 | | Spectrum 4 | |
| --- | --- | --- | --- | --- | --- | --- | --- |
| Element | Weight% | Element | Weight% | Element | Weight% | Element | Weight% |
| O | 28.68 | O | 28.05 | O | 24.40 | O | 11.14 |
| Al | 71.32 | Al | 71.95 | Al | 75.60 | Al | 88.86 |

| Spectrum 5 | | Spectrum 6 | | Spectrum 7 | | Spectrum 8 | |
| --- | --- | --- | --- | --- | --- | --- | --- |
| Element | Weight% | Element | Weight% | Element | Weight% | Element | Weight% |
| O | 6.94 | O | 6.34 | O | 5.32 | O | 4.76 |
| Al | 93.06 | Al | 93.66 | Al | 94.68 | Al | 95.24 |

| 6 |
| :---: |
| 750 ºC 24 hour hold |
| Oxide layer ≈ 0.37 μm |
| Composition vs. depth profile shown |



2μm          Electron Image 1



| Spectrum 1 | | Spectrum 2 | | Spectrum 3 | | Spectrum 4 | |
| --- | --- | --- | --- | --- | --- | --- | --- |
| Element | Weight% | Element | Weight% | Element | Weight% | Element | Weight% |
| O | 5.59 | O | 25.50 | O | 28.72 | O | 26.01 |
| Al | 94.41 | Al | 74.50 | Al | 71.28 | Al | 73.99 |

| Spectrum 5 | | Spectrum 6 | | Spectrum 7 | | Spectrum 8 | |
| --- | --- | --- | --- | --- | --- | --- | --- |
| Element | Weight% | Element | Weight% | Element | Weight% | Element | Weight% |
| O | 19.31 | O | 11.60 | O | 6.36 | O | 4.85 |
| Al | 80.69 | Al | 88.40 | Al | 93.64 | Al | 95.15 |

**Figure 41 continued - EDX analysis of superpure samples**

It can be seen from Figure 41 that oxygen levels are higher at the surfaces, and that they decrease further away from the oxide layer, as shown in the composition vs. depth profile seen in sample 6. This shows that the way oxide grows on aluminium samples in air follows the trends that have been noted in the literature; as the holding time generally increased the thickness of the oxide did also (Blackburn and Gulbransen 1960). Using a 10 kV acceleration voltage, the penetration depth would have been a maximum of 1.32 μm. The EDX spots would have penetrated the oxide layer, parallel to the oxide/metal interface. Some subsurface material would have been detected. EDX analysis also struggles to detect light elements, such as $O_2$, accurately. As such, the oxygen is taken as a guide to what elements were present in the oxide and sub-surface region, rather than to determine the exact composition of any surface layer. The results are used in conjunction with XRD analysis, which would give a clearer idea of the structure of the surface region.

XRD analysis was undertaken on the 5 minute, 1 hour and 24 hour samples and are shown in Figure 42, Figure 43 and Figure 44. The peaks appear to have weak signals, probably due to the small amount of oxide within the sample compared to the bulk Al. The same reference data was used for each spectra as much as possible, so it was the same crystal structures being compared between the samples.
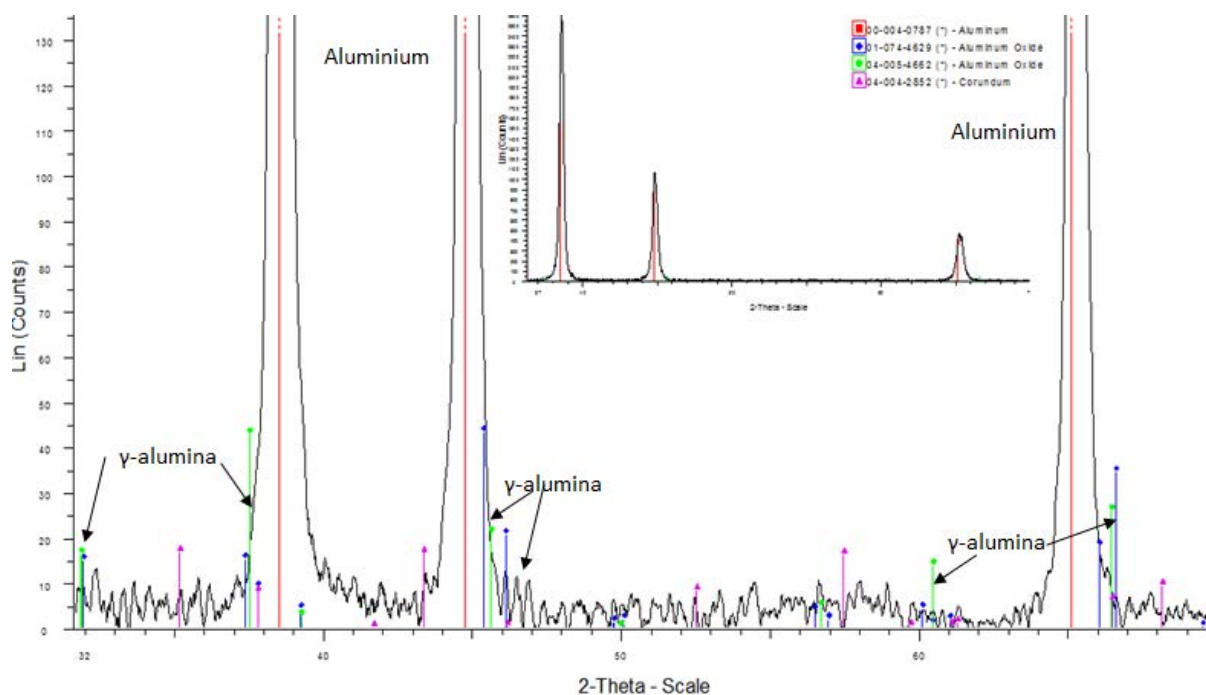


**Figure 42 - The XRD spectra for SP-Al held for 5 minutes at 750 °C (zoomed out spectra inset)**
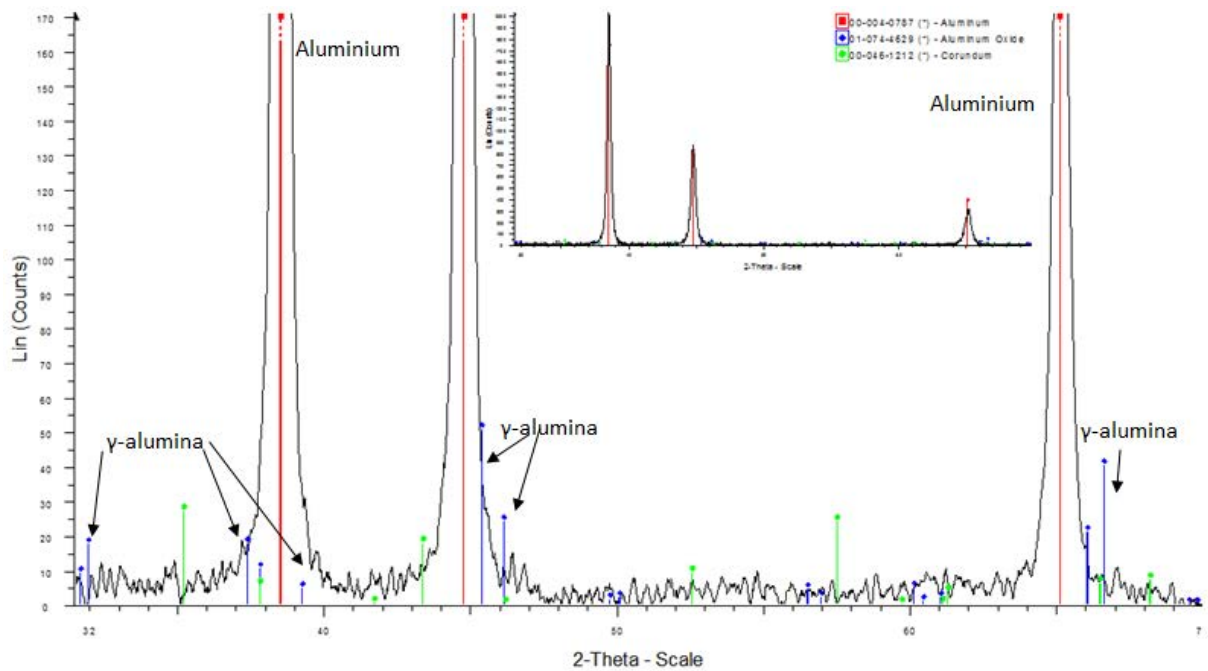
**Figure 43 - The XRD spectra for SP-Al held for 1 hour at 750 °C (zoomed out spectra inset)**
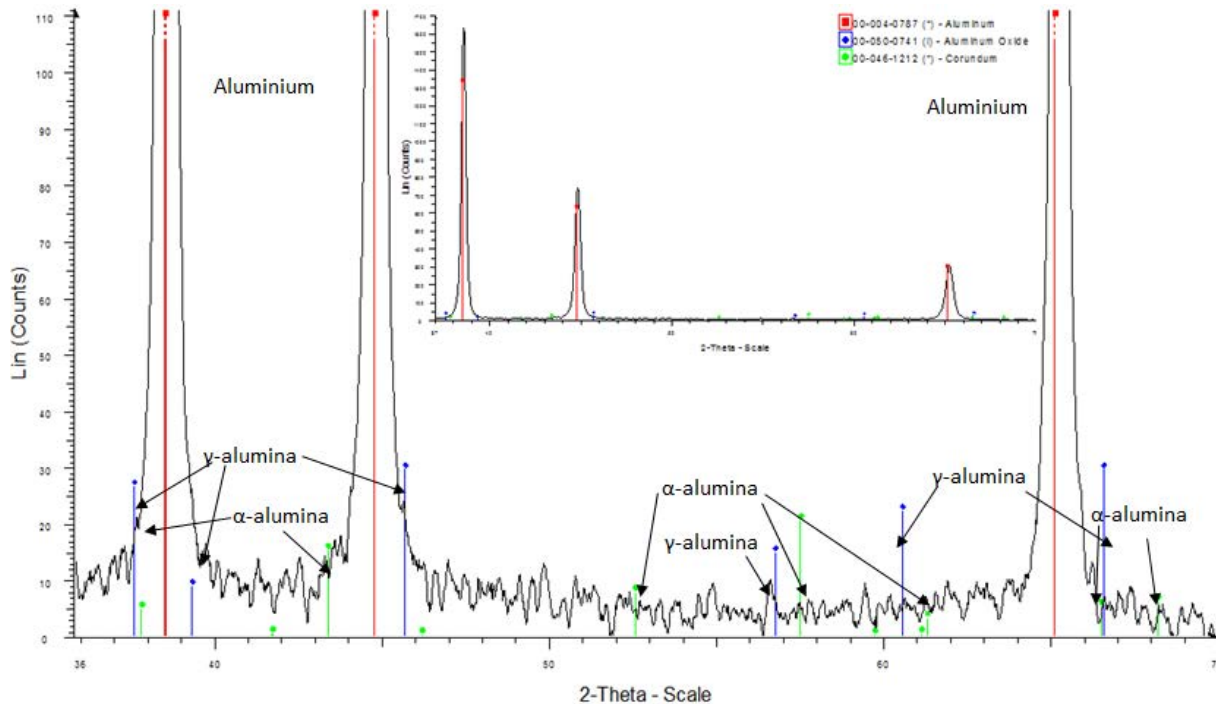


**Figure 44 - The XRD spectra for SP-Al held for 24 hours at 750 °C (zoomed out spectra inset)**

The SEM images of the 5 and 17 minute samples shown in Figure 39, suggest a discontinuous oxide, with a continuous oxide at 1 hour, which makes this likely. The rate increase due to the formation of $\alpha$-Al$_2$O$_3$, which has an associated change in volume, does not seem to have occurred (Agema & Fray 1989). The XRD analysis in Figure 42, Figure 43 and Figure 44 shows that Al$_2$O$_3$ was present at all stages of the oxidation process, as the $\gamma$-phase. It seems that $\gamma$-Al$_2$O$_3$ was the same structure in Figure 42 and Figure 43, but the signals did seem to shift slightly in Figure 44. Traces of $\alpha$-Al$_2$O$_3$ were formed in the 24 hour sample (Figure 44). The main Al peak (red line) is firstly offset by the presence of alumina, shown in Figure 44. There

71
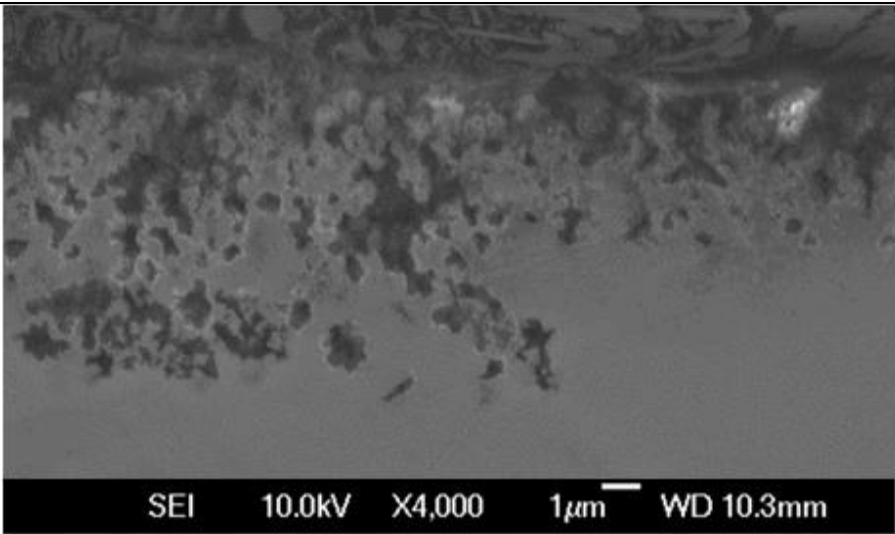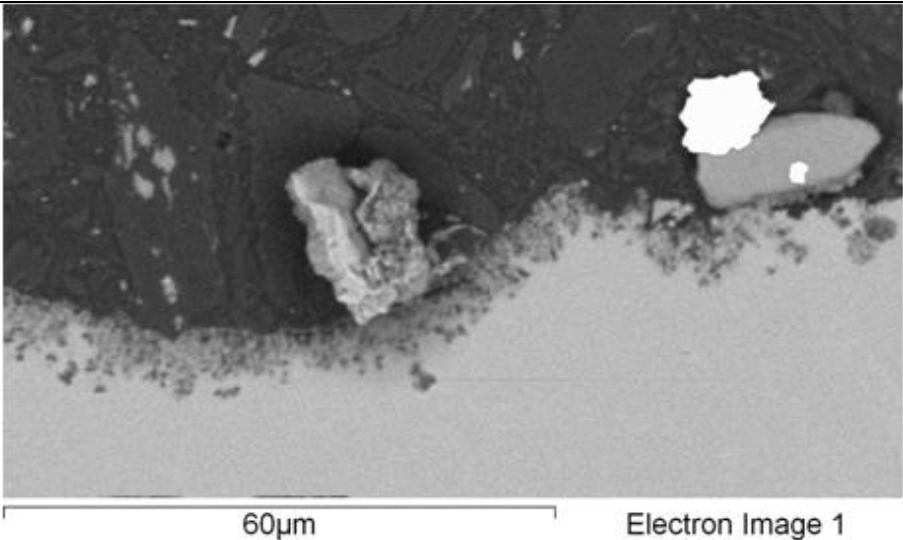
also appears to be some small peaks around the Al peaks. This matches the theory that the γ-alumina forms initially, but the α-alumina did not form until longer holding times.

### 3.1.2 - Effects of Alloying Elements

#### *3.1.2.1 – Al-4%Mg*

SEM examination showed how the oxide became thicker and much more porous with longer holding times, as shown in Figure 45.

**Figure 45 – Images of Al-4%Mg melted at 750 °C for different times**
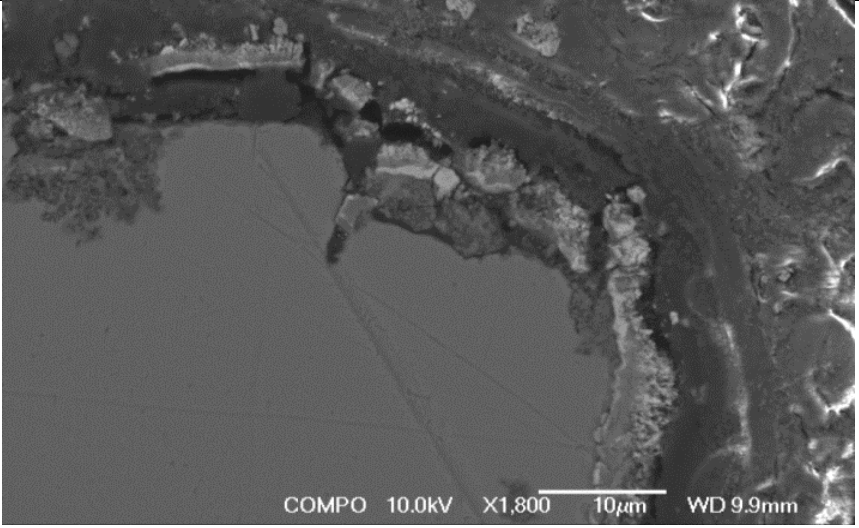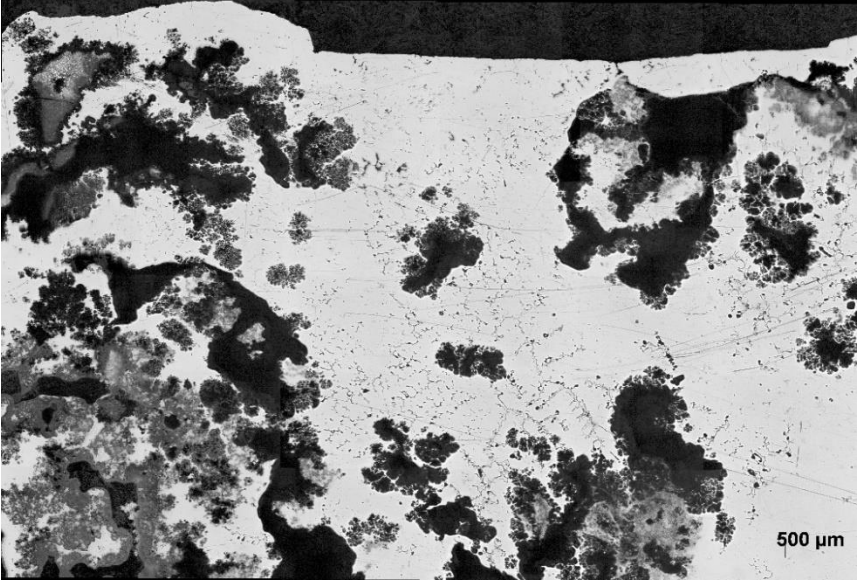
| Sample | Image |
|--------|-------|
| 1<br><br>750 °C 5 min hold<br><br>Oxide layer ≈ 5.25 μm | <br>SEI  10.0kV  X4,000  1μm  WD 10.3mm |
| 2<br><br>750 °C 17 min hold<br><br>Oxide layer ≈ 6.15 μm | <br>60μm  Electron Image 1 |

| | |
|---|---|
| 3<br><br>750 °C 1 hour hold<br><br>Oxide layer ≈ 7.15 μm | <br>COMPO 10.0kV X1,800 10μm WD 9.9mm |
| 4<br><br>750 °C 3 hour hold<br><br>Oxide layer ≈ total oxidation of samples<br><br>Longer holding times had a similar appearance | <br>500 μm |

**Figure 45 - Images of Al-4%Mg melted at 750 °C for different times**

The Al-Mg alloy the oxide thickness increased with holding time, as with the SP-Al samples, but at a faster rate. The oxide layer increased by ~2.1 μm at 1 hour holding, with the samples being completely oxidised over 3 hours. The change in oxide layer thickness with time is summarised in Table 9 and Figure 46 (only samples up to 1 hour are used in the graph, being the only measurable oxide thicknesses – total oxidation occurred so actual thickness cannot be determined). The 3 hour sample was oxidised to such a degree that the oxide was present throughout the sample, from surface to the bottom of the sample.

**Table 9 - Summary of oxide thicknesses for Al-4%Mg at 750 °C (* indicates that the entire specimen was oxidised)**

| Melt Conditions | Oxide Thickness |
|---|---|
| 750°C 5 min hold | 5.25 μm |
| 750°C 17 min hold | 6.15 μm |
| 750°C 1 hour hold | 7.15 μm |
| 750°C 3 hour hold | oxidised* |
| 750°C 7 hour hold | oxidised* |
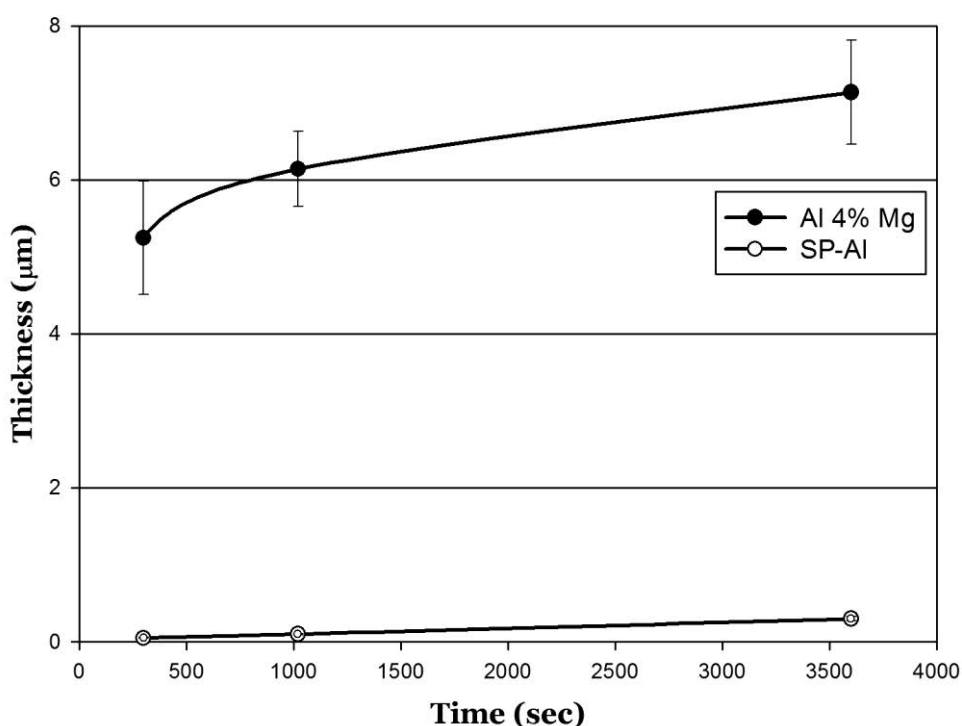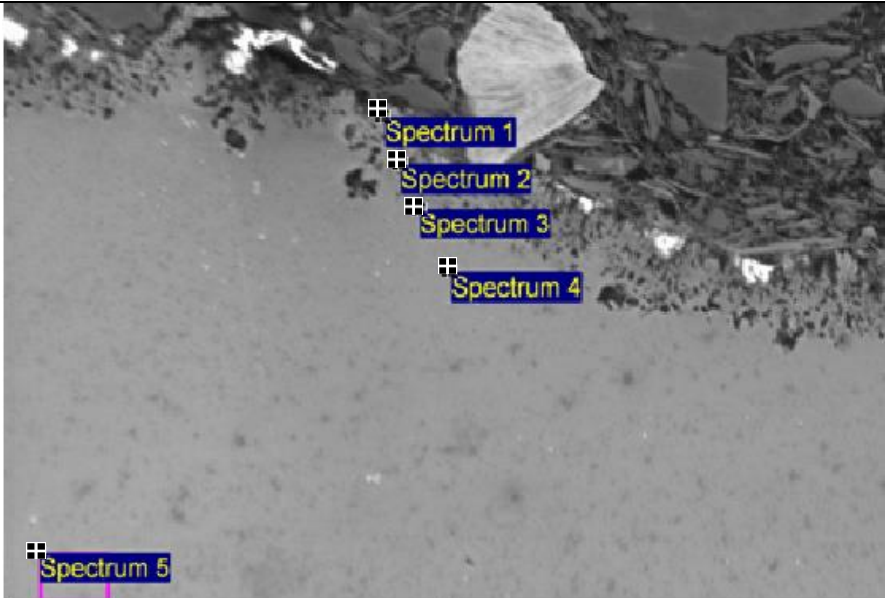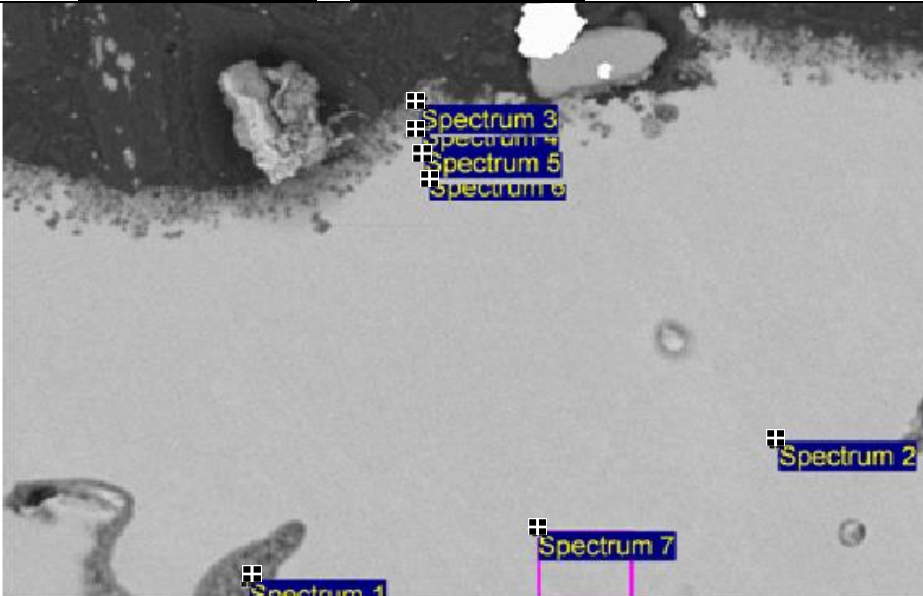


**Figure 46 - Thickness of oxide layer vs. holding time for Al-4%Mg samples held at 750 °C, compared with SP-Al over the same time period (5, 17 minutes and 1 hour samples shown)**

The oxide growth was much more rapid than that in SP-Al, an effect of the addition of Mg. The oxide was also much more porous, shown in Figure 45 sample 1 and 2, which would mean that oxygen was able to react with the liquid metal more readily than with a continuous, non-porous oxide layer, which was particularly noticed in the 3 hour sample in Figure 45. The thickness rate was $1.25 \times 10^{-3}$ μm/s between 5 and 17 minutes, $3.8 \times 10^{-4}$ μm between 17 minutes and 1 hour. This is demonstrated in Figure 46. After this the oxide thickness increases until the entire sample had oxidised. Magnesium oxide (MgO) is a porous, non-passivating oxide (with a Pilling Bedworth ratio of 0.81) and so oxidation of the liquid metal beneath the oxide layer occurs much more quickly. EDX analysis of the oxide layers can be seen in Figure 47.

**Figure 47 - EDX spectra for the Al-4%Mg samples melted at 750 °C**

| Sample | Analysis |
|---|---|

**Sample 1 — 750 ºC, 5 min hold, Oxide layer ≈ 5.25 μm**



Spectrum 1
| Element | Weight% |
|---|---|
| O | 21.05 |
| Mg | 31.02 |
| Al | 47.92 |

Spectrum 2
| Element | Weight% |
|---|---|
| O | 31.82 |
| Mg | 41.47 |
| Al | 26.71 |

Spectrum 3
| Element | Weight% |
|---|---|
| O | 3.39 |
| Mg | 9.14 |
| Al | 87.47 |

Spectrum 4
| Element | Weight% |
|---|---|
| O | 0.00 |
| Mg | 5.17 |
| Al | 94.83 |

Spectrum 5
| Element | Weight% |
|---|---|
| O | 0.00 |
| Mg | 3.06 |
| Al | 96.94 |

**Sample 2 — 750 ºC, 17 min hold, Oxide layer ≈ 6.15 μm**



Spectrum 1
| Element | Weight% |
|---|---|
| O | 46.18 |
| Mg | 0.54 |
| Al | 53.28 |

Spectrum 2
| Element | Weight% |
|---|---|
| O | 22.19 |
| Mg | 5.17 |
| Al | 72.64 |

Spectrum 3
| Element | Weight% |
|---|---|
| O | 30.27 |
| Mg | 42.69 |
| Al | 27.04 |

Spectrum 4
| Element | Weight% |
|---|---|
| O | 27.07 |
| Mg | 36.02 |
| Al | 36.91 |

Spectrum 5
| Element | Weight% |
|---|---|
| O | 0.00 |
| Mg | 5.1 |
| Al | 94.9 |

Spectrum 6
| Element | Weight% |
|---|---|
| O | 0.00 |
| Mg | 4.65 |
| Al | 95.35 |

Spectrum 7
| Element | Weight% |
|---|---|
| O | 0.00 |
| Mg | 2.19 |
| Al | 97.81 |

| 3

750 ºC

1 hour

hold

Oxide

layer ≈

7.15 μm |
|---|



30µm     Electron Image 1

Point 1

| Element | Weight% |
|---|---|
| O | 40.51 |
| Mg | 57.73 |
| Al | 1.77 |

Point 2

| Element | Weight% |
|---|---|
| O | 40.16 |
| Mg | 59.37 |
| Al | 0.47 |

Point 3

| Element | Weight% |
|---|---|
| O | 41.03 |
| Mg | 58.97 |
| Al | 0.00 |

Point 4

| Element | Weight% |
|---|---|
| O | 40.11 |
| Mg | 59.09 |
| Al | 0.81 |

Point 5

| Element | Weight% |
|---|---|
| O | 1.48 |
| Mg | 13.93 |
| Al | 84.58 |

| 4

750 ºC

3 hour

hold

Oxide

layer ≈

total

oxidation |
|---|



1mm     Electron Image 1

Spectrum 2

| Element | Weight% |
|---|---|
| O | 48.75 |
| Mg | 31.51 |
| Al | 19.74 |

Spectrum 3

| Element | Weight% |
|---|---|
| O | 41.42 |
| Mg | 30.96 |
| Al | 27.62 |

Spectrum 4

| Element | Weight% |
|---|---|
| O | 55.26 |
| Mg | 7.56 |
| Al | 37.18 |

Spectrum 5

| Element | Weight% |
|---|---|
| O | 58.44 |
| Mg | 17.98 |
| Al | 23.58 |

Spectrum 6

| Element | Weight% |
|---|---|
| O | 65.9 |
| Mg | 10.6 |
| Al | 23.5 |

Spectrum 7

| Element | Weight% |
|---|---|
| O | 0.86 |
| Mg | 0.77 |
| Al | 98.37 |

Spectrum 8

| Element | Weight% |
|---|---|
| O | 0.81 |
| Mg | 0.68 |
| Al | 98.51 |

Spectrum 9

| Element | Weight% |
|---|---|
| O | 47.03 |
| Mg | 49.97 |
| Al | 3.00 |

**Figure 47 continued - EDX spectra for the Al-4%Mg samples melted at 750 °C**

It can be seen in Figure 47 that the oxides of all samples contained Al, Mg and O, which suggests that a mixture of, Mg and Al oxides or a spinel ($MgAl_2O_4$) was present. There was also a high concentration of Mg in the subsurface region which is particularly apparent in the 1 hour sample. This is likely to be due to mobility of elements within the alloy, causing them to move towards and through the oxide layer, as elements diffuse to vacancies within the amorphous oxide layer (Kooi et al 2002, Ritchie et al 1971). This may also account for the lack of Al in the oxide layer at the oxide-metal interface in the 1 hour sample. XRD analysis of the 5 minute, 1 hour and 7 hour samples can be seen in Figure 48, Figure 49 and Figure 50.
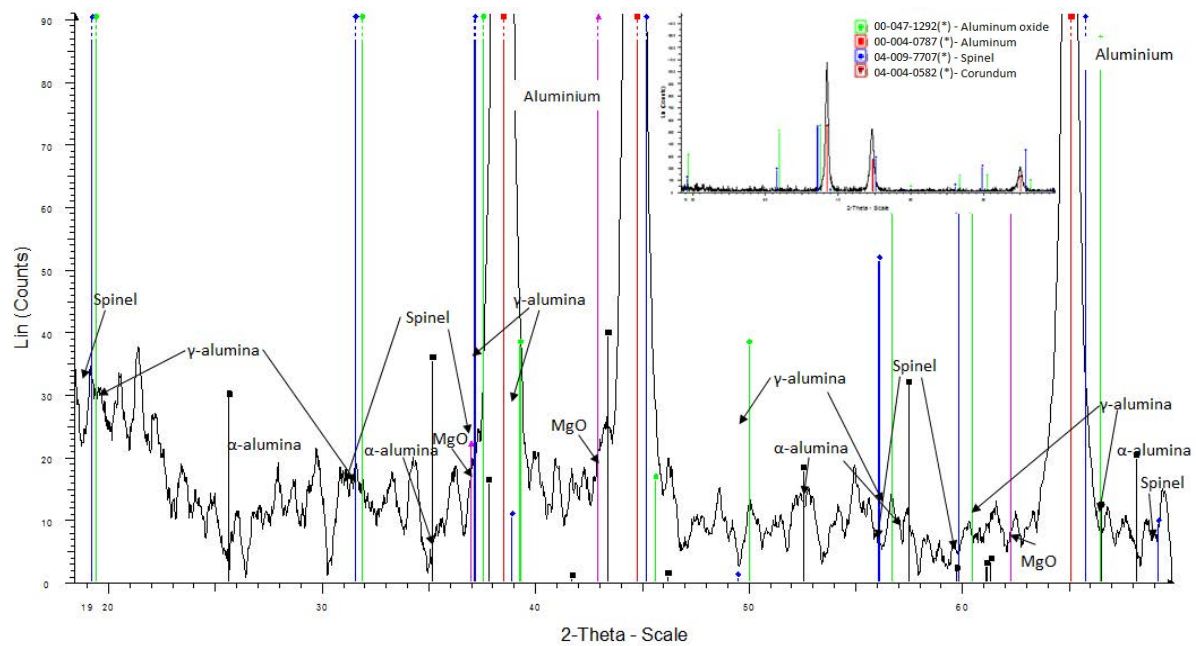


**Figure 48 - The XRD spectra for Al-4%Mg held for 5 minutes at 750 °C (zoomed out spectra inset)**
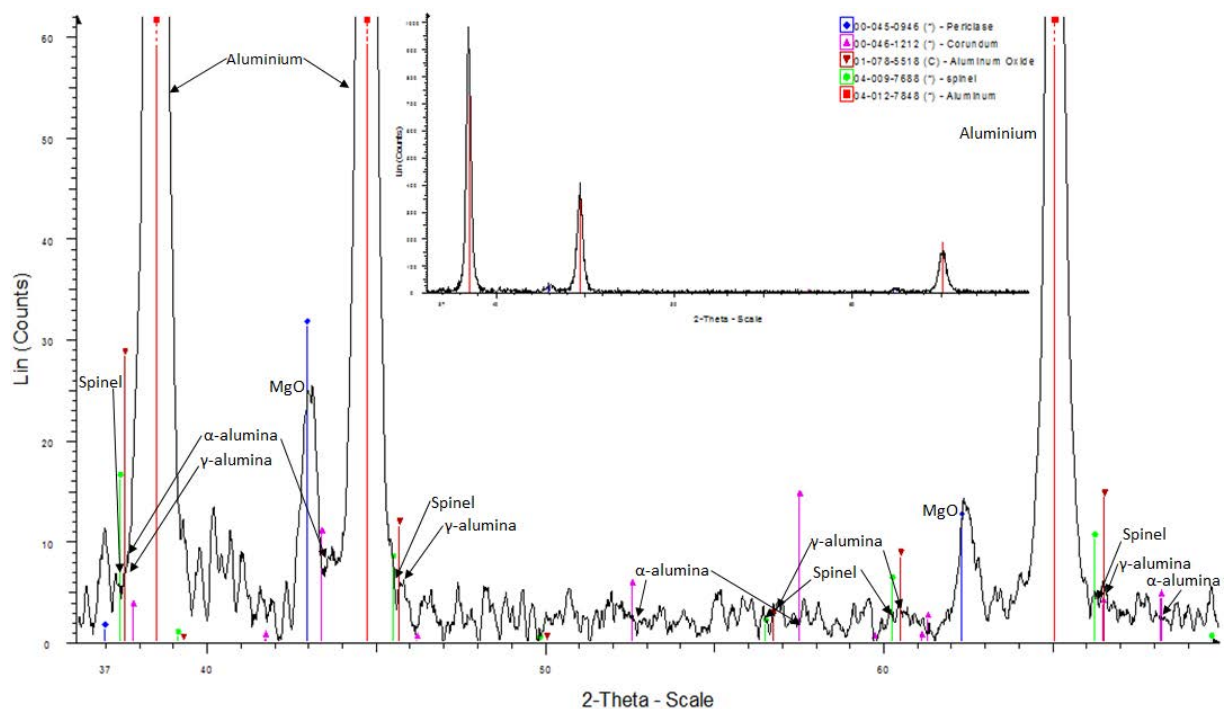


**Figure 49 - The XRD spectra for Al-4%Mg held for 1 hour at 750 °C (zoomed out spectra inset)**
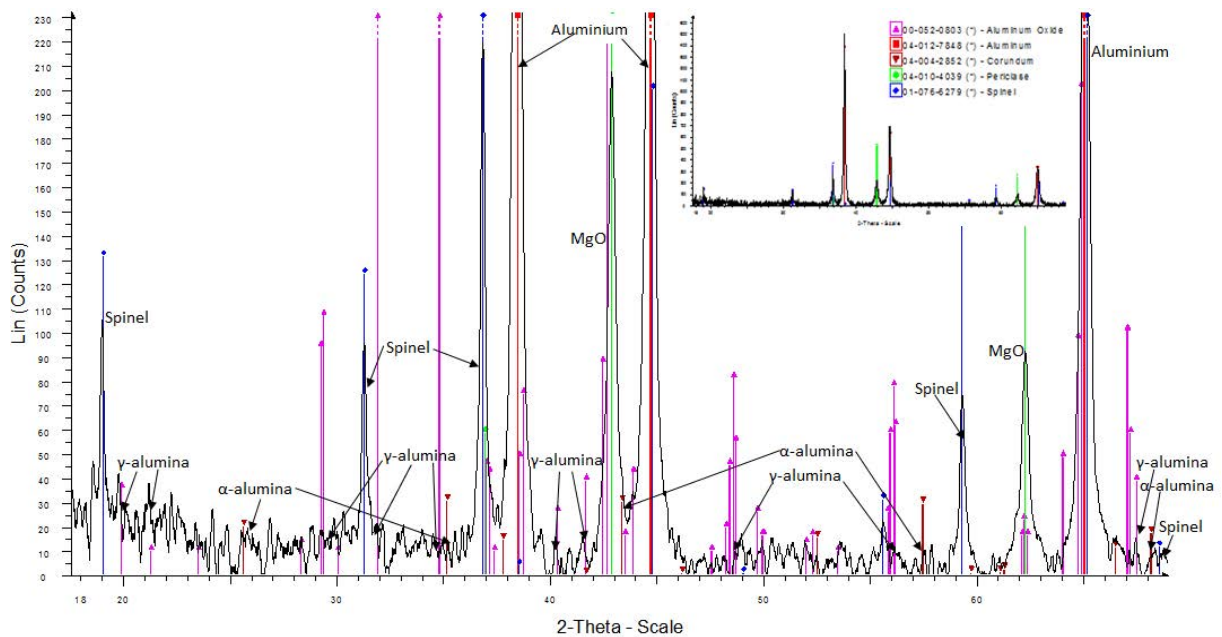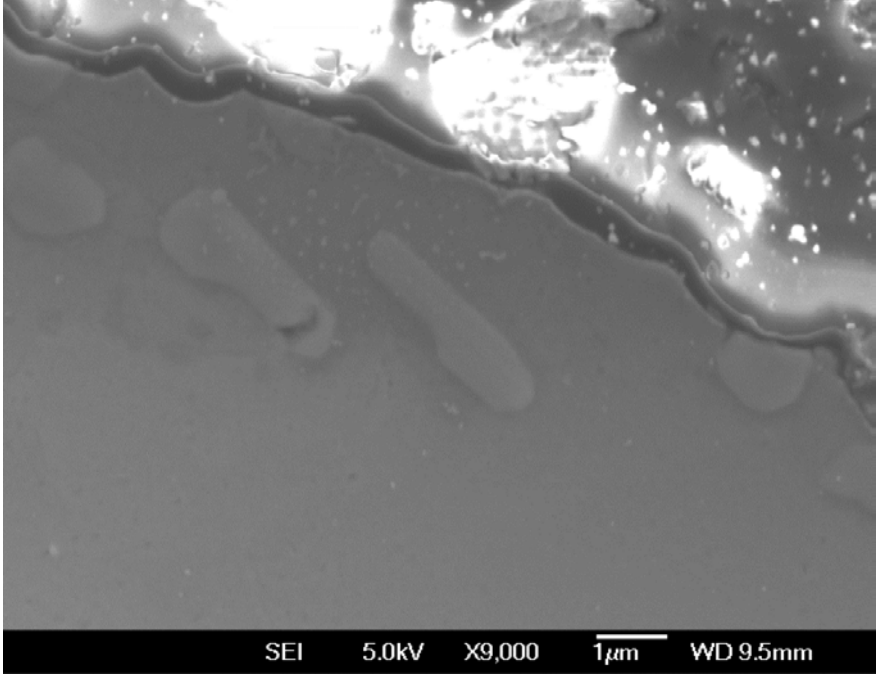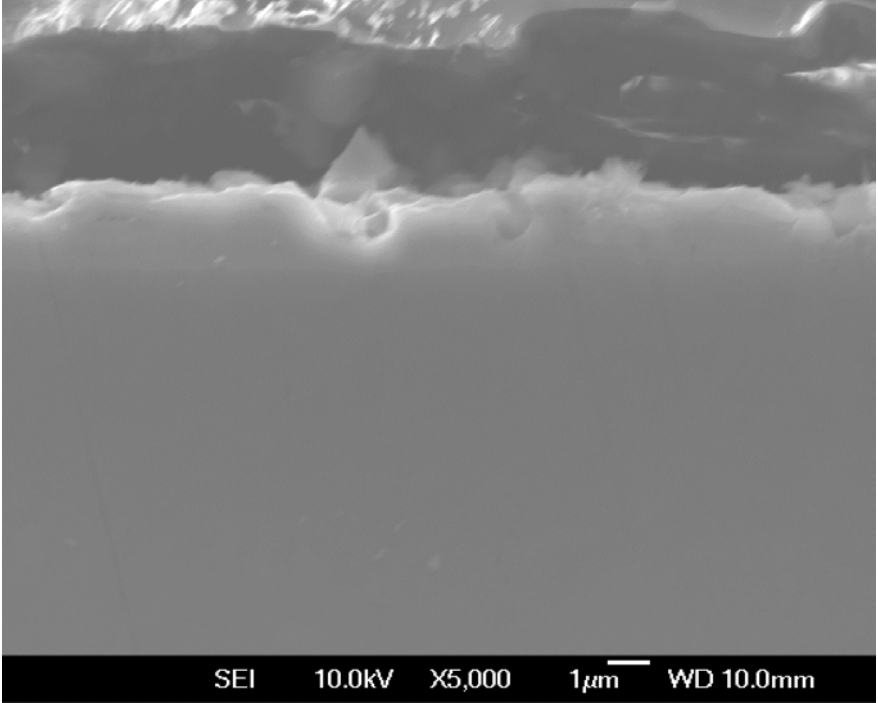
**Figure 50 - The XRD spectra for Al-4%Mg held for 7 hours at 750 °C (zoomed out spectra inset)**

From the XRD analysis, it can be seen that the initial oxide on the 5 minute sample consisted of a mix of spinel, $\gamma$-$Al_2O_3$ and traces of $\alpha$-alumina and MgO (Figure 48). This suggested that the Mg shown in the EDX results came from the MgO present in the spinel and MgO. The 1 hour sample contained some MgO oxide which suggested that initially, the MgO present in the spinel grew more quickly in comparison to the $\gamma$-alumina, as it had a stronger signal, shown in Figure 49, along with peaks for spinel. The 7 hour sample spectra had strong peaks for MgO and spinel. From these results, as shown in Figure 50, and the EDX and SEM results, the MgO grew more in the 7 hour sample than in the 1 hour sample, and the spinel signal was also stronger, suggesting more is present in the sample. This suggests that as the MgO grew, the oxide became permeable allowing air to diffuse through it. The Al in the bulk (underneath the newly formed MgO layer) started to react to form alumina. This formed in and around the porous MgO that had already formed, rather than forming $\gamma$-alumina in a different area. It would have also been forming at the same time as more MgO was growing. The fact that small amounts of $\alpha$-alumina were detected also suggests that alumina was not able to grow as quickly as MgO or spinel, due to the preferential oxidation of the Mg present in the sample.

78

## 3.1.2.2 – Al 7%Si

SEM images of the Al-7%Si alloy held at different holding times can be seen in Figure 51.

**Figure 51 - Images of Al-7%Si melted at 750 °C for different times**
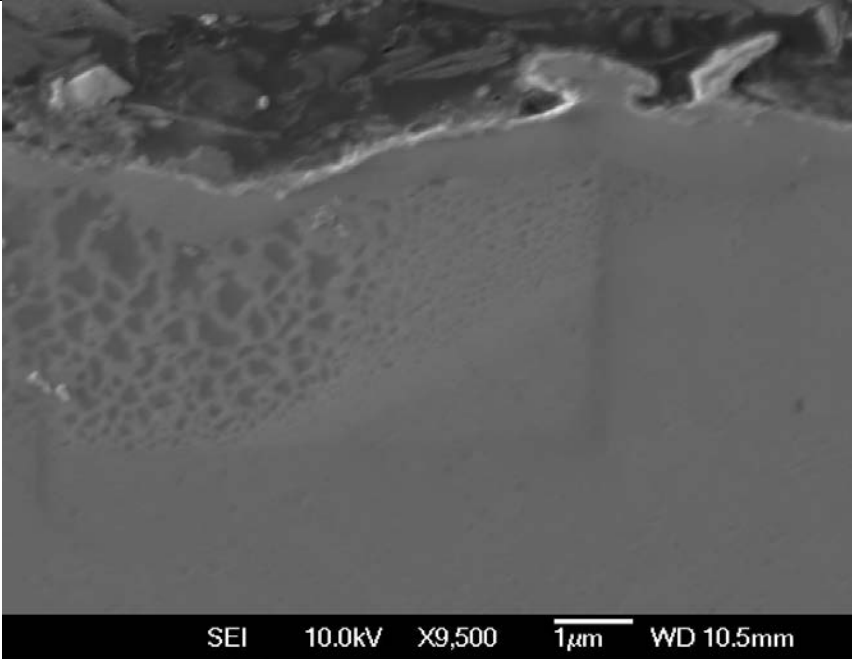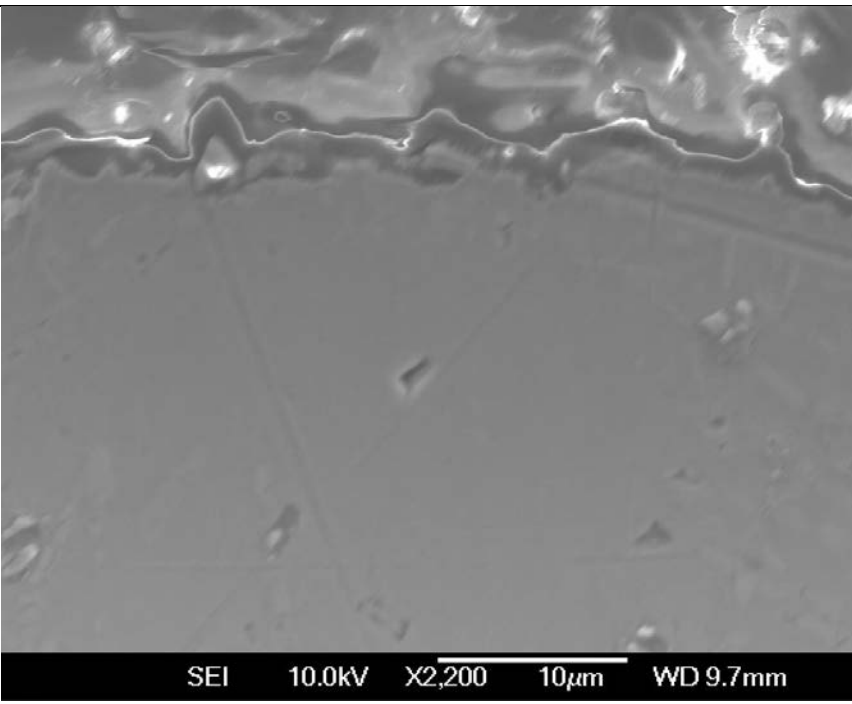
| Sample | Image |
|---|---|
| 1<br><br>750 ºC 5 min hold<br><br>Oxide layer ≈ 0.12 μm | <br>SEI  5.0kV  X9,000  1μm  WD 9.5mm |
| 2<br><br>750 ºC 17 min hold<br><br>Oxide layer ≈ 0.14 μm | <br>SEI  10.0kV  X5,000  1μm  WD 10.0mm |

| 3 750 ºC 1 hour hold Oxide layer ≈ 0.15 μm |  |
|---|---|
| 4 750 ºC 3 hour hold Oxide layer ≈ 0.4 μm |  |

**Figure 51 continued – Images of Al-7%Si melted at 750 °C for different times**
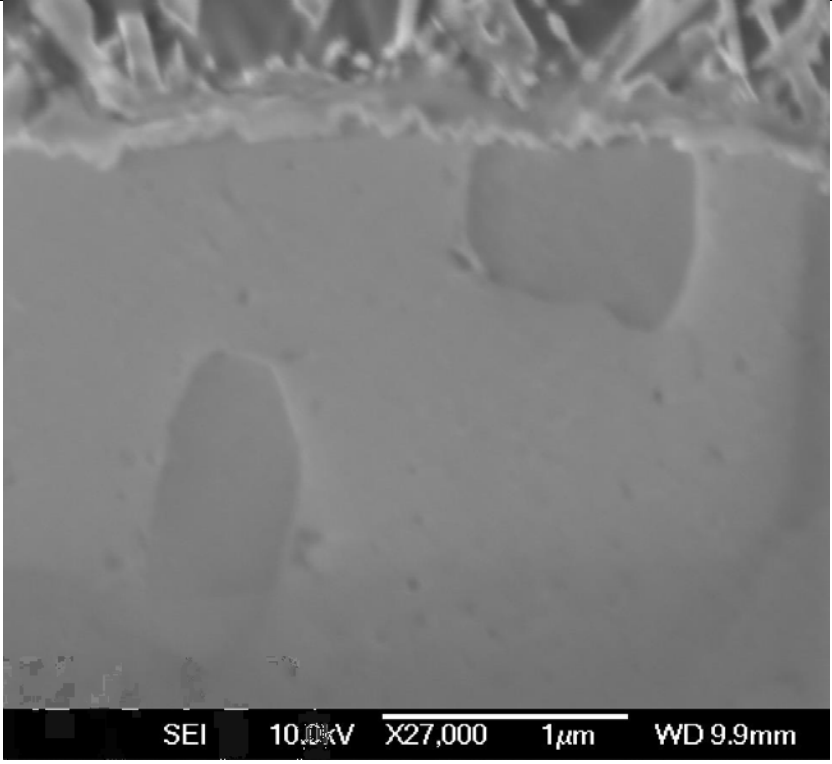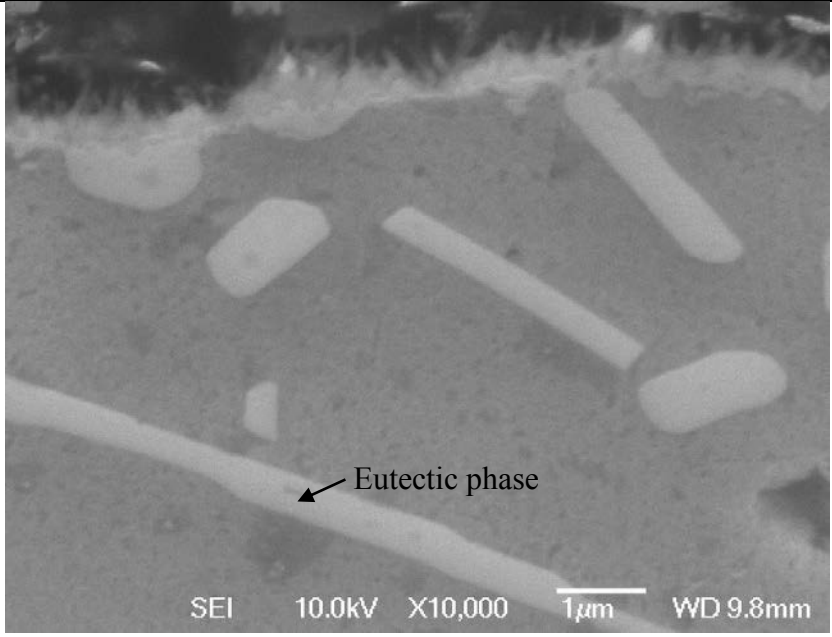
| | |
|---|---|
| 5<br><br>750 °C 7 hour hold<br><br>Oxide layer ≈ 0.1 μm |  |
| 6<br><br>750 °C 24 hour hold<br><br>Oxide layer ≈ 0.39 μm |  |

**Figure 51 continued – Images of Al-7%Si melted at 750 °C for different times**

The presence of Si had little effect on the oxide growth. The thickness of the oxide layers are summarised in Table 10 and Figure 52 and were similar to those for SP-Al. The oxide thickness increased by ~0.27 μm from 5 minutes to 24 hours.

**Table 10 - Thicknesses of oxides for Al-7%Si melted at 750 °C**

| Melt Conditions | Oxide Thickness |
|---|---|

| | |
|---|---|
| 750ºC 5 min hold | 0.12 μm |
| 750ºC 17 min hold | 0.14 μm |
| 750ºC 1 hour hold | 0.15 μm |
| 750ºC 3 hour hold | 0.4 μm |
| 750ºC 7 hour hold | 0.1 μm |
| 750 °C 24 hour hold | 0.39 μm |
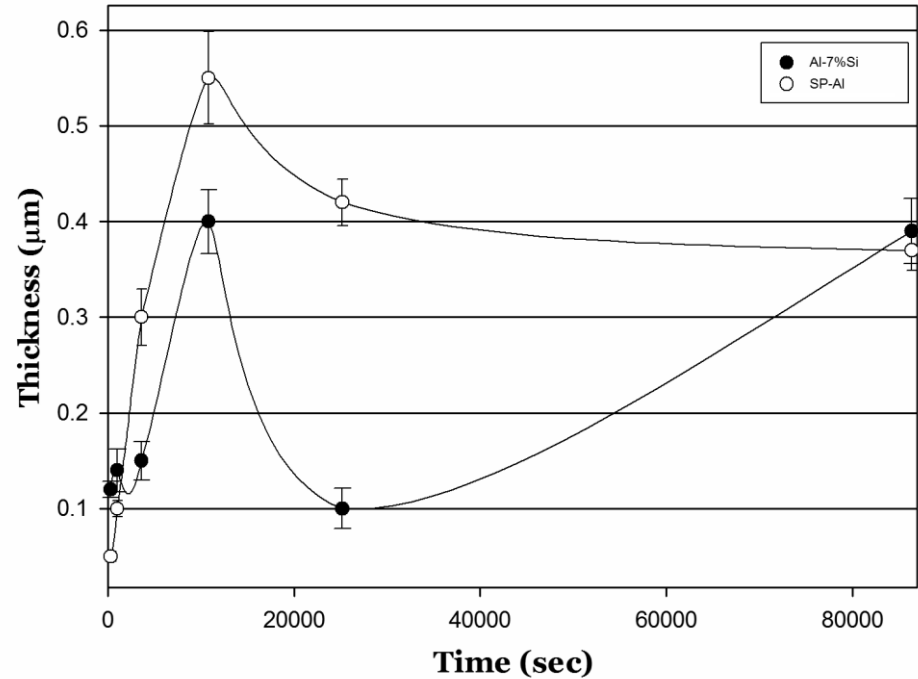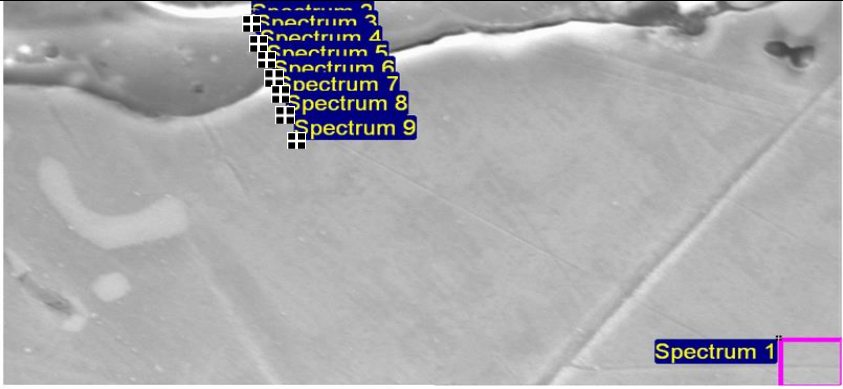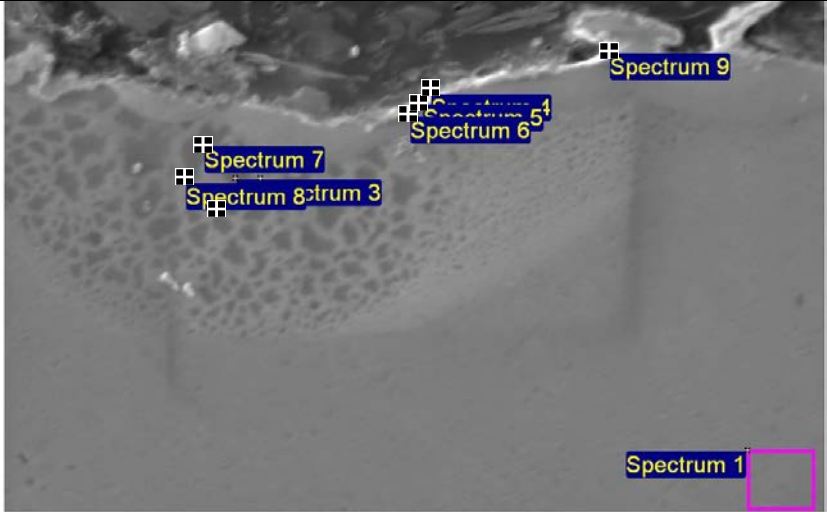


**Figure 52 - Thickness of oxide layer vs. holding time Al 7%Si samples held at 750 °C, compare with SP-Al over the same time period**

The oxide growth was rather slow in the presence of 7wt. % Si. This was alluded to in previous work where it was shown that Si in the melt leads to slow oxide growth up to ~100 hours (Thiele 1962). The EDX results are shown in Figure 53.

**Figure 53 - EDX spectra for the Al-7%Si samples melted at 750 °C**

| Sample | Analysis |
|---|---|

| | |
|---|---|
| 1<br><br>750 ºC 5 min hold<br><br>Oxide layer ≈ 0.12 μm | <br><br>Electron Image 1 |

Spectrum 1

| Element | Weight % |
|---|---|
| O | 0.49 |
| Al | 98.17 |
| Si | 1.34 |

Spectrum 2

| Element | Weight % |
|---|---|
| O | 65.80 |
| Al | 34.20 |
| Si | 0.00 |

Spectrum 3

| Element | Weight % |
|---|---|
| O | 68.35 |
| Al | 31.65 |
| Si | 0.00 |

Spectrum 4

| Element | Weight % |
|---|---|
| O | 81.83 |
| Al | 13.16 |
| Si | 5.01 |

Spectrum 5

| Element | Weight % |
|---|---|
| O | 73.69 |
| Al | 17.02 |
| Si | 9.29 |

Spectrum 6

| Element | Weight % |
|---|---|
| O | 54.61 |
| Al | 39.04 |
| Si | 6.35 |

Spectrum 7

| Element | Weight % |
|---|---|
| O | 51.98 |
| Al | 41.47 |
| Si | 6.55 |

Spectrum 8

| Element | Weight % |
|---|---|
| O | 26.47 |
| Al | 52.12 |
| Si | 21.41 |

Spectrum 9

| Element | Weight % |
|---|---|
| O | 2.22 |
| Al | 74.68 |
| Si | 23.11 |

| | |
|---|---|
| 2<br><br>750 ºC 1 hour hold<br><br>Oxide layer ≈ 0.15 μm | <br><br>Electron Image 1 |

Spectrum 1

| Element | Weight % |
|---|---|
| O | 0.00 |
| Al | 98.31 |
| Si | 1.69 |

Spectrum 2

| Element | Weight % |
|---|---|
| O | 0.98 |
| Al | 93.75 |
| Si | 5.27 |

Spectrum 3

| Element | Weight % |
|---|---|
| O | 0.75 |
| Al | 90.31 |
| Si | 8.94 |

Spectrum 4

| Element | Weight % |
|---|---|
| O | 25.21 |
| Al | 31.40 |
| Si | 43.39 |

Spectrum 5

| Element | Weight % |
|---|---|
| O | 19.84 |
| Al | 28.49 |
| Si | 51.67 |

Spectrum 6

| Element | Weight % |
|---|---|
| O | 6.50 |
| Al | 28.04 |
| Si | 65.46 |

Spectrum 7

| Element | Weight % |
|---|---|
| O | 1.40 |
| Al | 79.92 |
| Si | 18.69 |

Spectrum 8

| Element | Weight % |
|---|---|
| O | 0.87 |
| Al | 98.11 |
| Si | 1.02 |

Spectrum 9

| Element | Weight % |
|---|---|
| O | 31.58 |
| Al | 51.34 |
| Si | 17.08 |

| | | | |
|---|---|---|---|
| 3<br><br>750 ºC 3 hour hold<br><br>Oxide layer ≈ 0.4 μm | <br><br>20µm — Electron Image 1 | | |

**Spectrum 1**

| Element | Weight % |
|---|---|
| O | 0.77 |
| Al | 97.84 |
| Si | 1.39 |

**Spectrum 2**

| Element | Weight % |
|---|---|
| O | 92.82 |
| Al | 4.42 |
| Si | 2.76 |

**Spectrum 3**

| Element | Weight % |
|---|---|
| O | 53.43 |
| Al | 40.09 |
| Si | 6.48 |

**Spectrum 4**

| Element | Weight % |
|---|---|
| O | 46.51 |
| Al | 49.94 |
| Si | 3.55 |

**Spectrum 5**

| Element | Weight % |
|---|---|
| O | 46.27 |
| Al | 49.70 |
| Si | 4.03 |

**Spectrum 6**

| Element | Weight % |
|---|---|
| O | 5.39 |
| Al | 84.61 |
| Si | 10.00 |

**Spectrum 7**

| Element | Weight % |
|---|---|
| O | 48.47 |
| Al | 45.19 |
| Si | 6.34 |

**Spectrum 8**

| Element | Weight % |
|---|---|
| O | 0.89 |
| Al | 87.05 |
| Si | 12.06 |

4

750 ºC 7 hour hold

Oxide layer ≈ 0.1 μm



2µm — Electron Image 1

**Spectrum 1**

| Element | Weight % |
|---|---|
| O | 0.66 |
| Al | 95.81 |
| Si | 3.53 |

**Spectrum 2**

| Element | Weight % |
|---|---|
| O | 0.62 |
| Al | 40.83 |
| Si | 58.55 |

**Spectrum 3**

| Element | Weight % |
|---|---|
| O | 5.40 |
| Al | 19.54 |
| Si | 75.06 |

**Spectrum 4**

| Element | Weight % |
|---|---|
| O | 23.05 |
| Al | 76.20 |
| Si | 0.75 |

**Spectrum 5**

| Element | Weight % |
|---|---|
| O | 16.83 |
| Al | 82.62 |
| Si | 0.55 |

**Spectrum 6**

| Element | Weight % |
|---|---|
| O | 11.95 |
| Al | 87.64 |
| Si | 0.41 |

**Spectrum 7**

| Element | Weight % |
|---|---|
| O | 9.35 |
| Al | 90.18 |
| Si | 0.47 |

**Spectrum 8**

| Element | Weight % |
|---|---|
| O | 6.14 |
| Al | 93.86 |
| Si | 0.00 |

**Spectrum 9**

| Element | Weight % |
|---|---|
| O | 20.61 |
| Al | 78.81 |
| Si | 0.58 |

**Spectrum 10**

| Element | Weight % |
|---|---|
| O | 28.65 |
| Al | 70.36 |
| Si | 0.99 |

**Spectrum 11**

| Element | Weight % |
|---|---|
| O | 2.41 |
| Al | 97.10 |
| Si | 0.49 |

**Spectrum 12**

| Element | Weight % |
|---|---|
| O | 0.94 |
| Al | 98.16 |
| Si | 0.91 |

**Figure 53 - EDX spectra for the Al-7%Si samples melted at 750 °C**

| 5<br><br>750 ºC<br>24 hour<br>hold<br><br>Oxide<br>layer ≈<br>0.39 μm |  |

**Figure 53 continued - EDX spectra for the Al-7%Si samples melted at 750 °C**

| Spectrum 1 | |
| --- | --- |
| Element | Weight % |
| O | 0.00 |
| Al | 25.61 |
| Si | 74.39 |

| Spectrum 2 | |
| --- | --- |
| Element | Weight % |
| O | 0.00 |
| Al | 98.23 |
| Si | 1.77 |

| Spectrum 3 | |
| --- | --- |
| Element | Weight % |
| O | 44.08 |
| Al | 53.23 |
| Si | 2.69 |

| Spectrum 4 | |
| --- | --- |
| Element | Weight % |
| O | 37.81 |
| Al | 62.19 |
| Si | 0.00 |

| Spectrum 5 | |
| --- | --- |
| Element | Weight % |
| O | 4.06 |
| Al | 94.56 |
| Si | 1.38 |

| Spectrum 6 | |
| --- | --- |
| Element | Weight % |
| O | 8.09 |
| Al | 91.3 |
| Si | 0.61 |

| Spectrum 7 | |
| --- | --- |
| Element | Weight % |
| O | 27.49 |
| Al | 71.95 |
| Si | 0.56 |

| Spectrum 8 | |
| --- | --- |
| Element | Weight % |
| O | 30.29 |
| Al | 68.44 |
| Si | 1.27 |

| Spectrum 9 | |
| --- | --- |
| Element | Weight % |
| O | 31.45 |
| Al | 66.85 |
| Si | 1.7 |

| Spectrum 10 | |
| --- | --- |
| Element | Weight % |
| O | 42.11 |
| Al | 57.14 |
| Si | 0.75 |

It can be seen from Figure 53 that, particularly at shorter holding times, Si is present in the oxide and in the oxide subsurface region, seemingly having migrated there during oxidation, as suggested in previous work (Kooi et al 2002). It seems that the oxide may have prevented the movement of oxygen through the layer and inwards towards the liquid metal, but it does not seem to have affected the oxidation. To ascertain the type of oxide present in the samples, XRD analysis was performed, and the spectra are shown in Figure 54 and Figure 55.
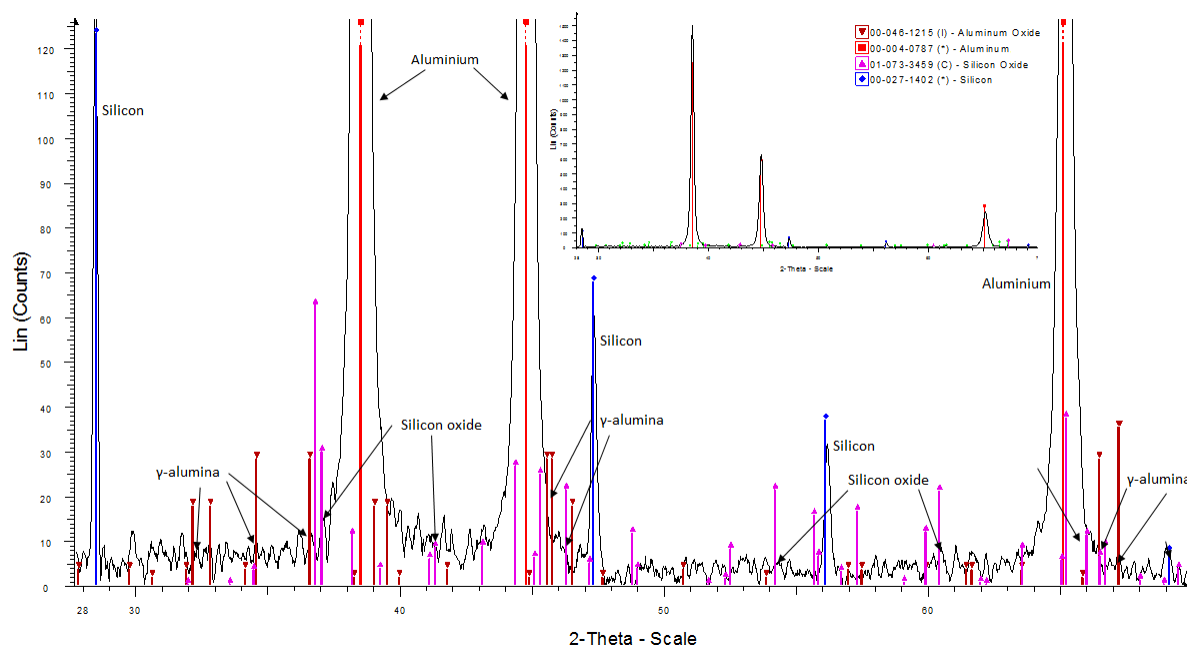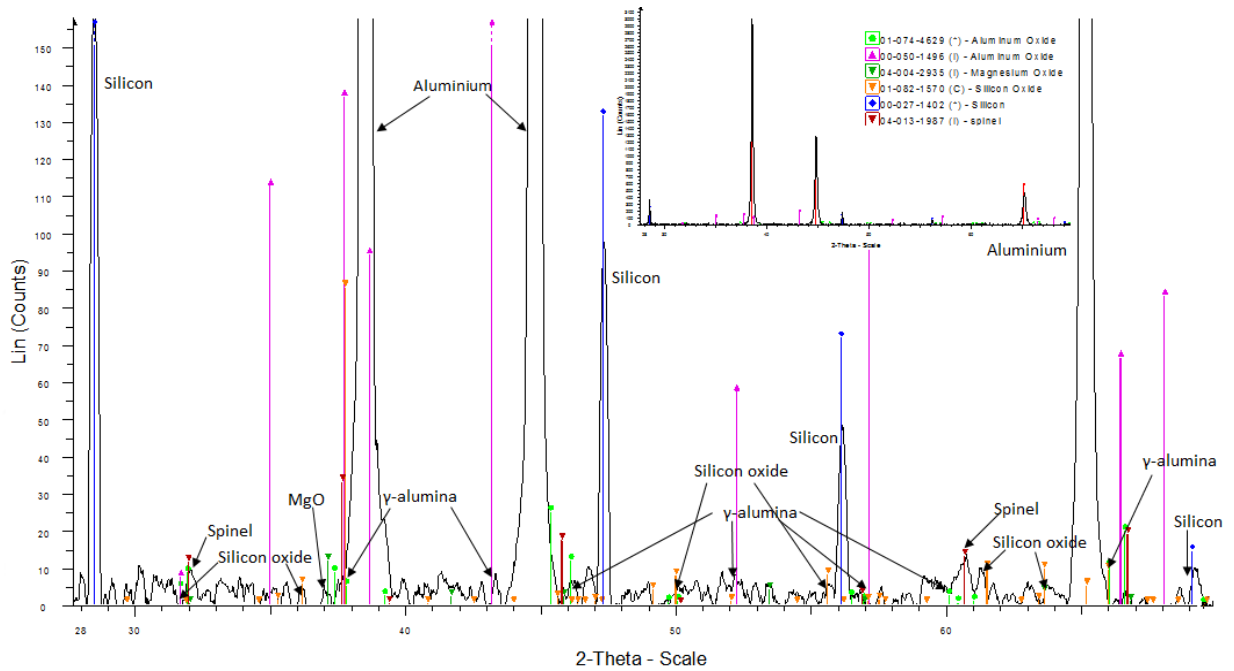
**Figure 54 - The XRD spectra for Al-7%Si held for 5 minutes at 750 °C (zoomed out spectra inset)**
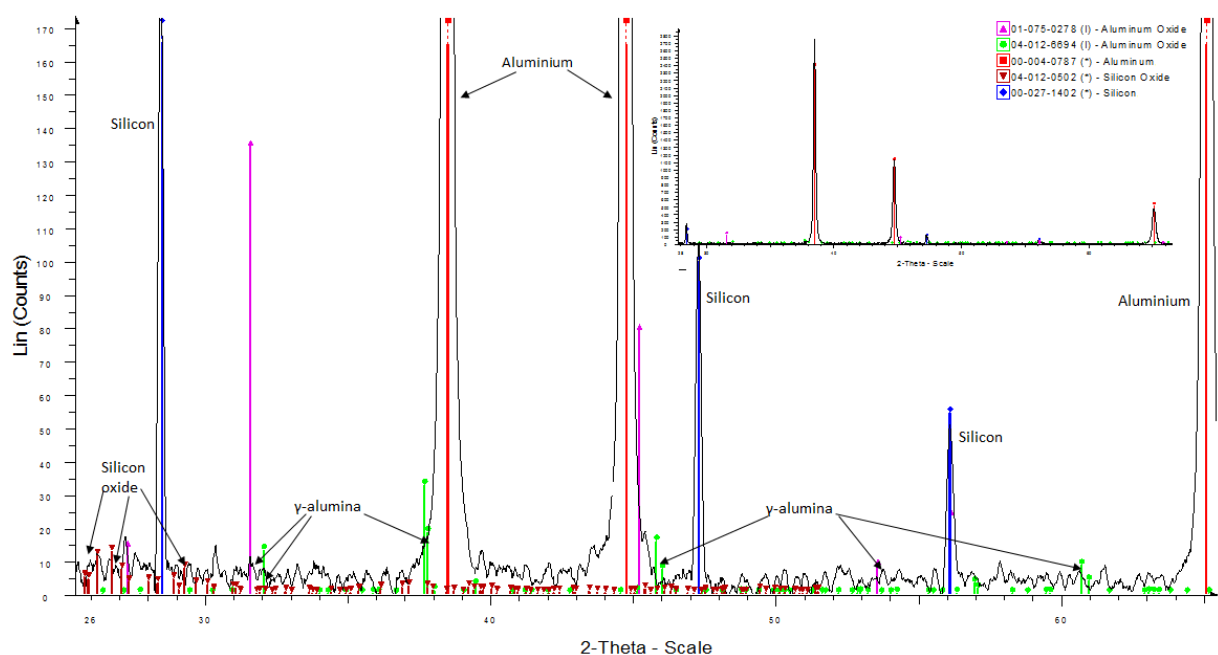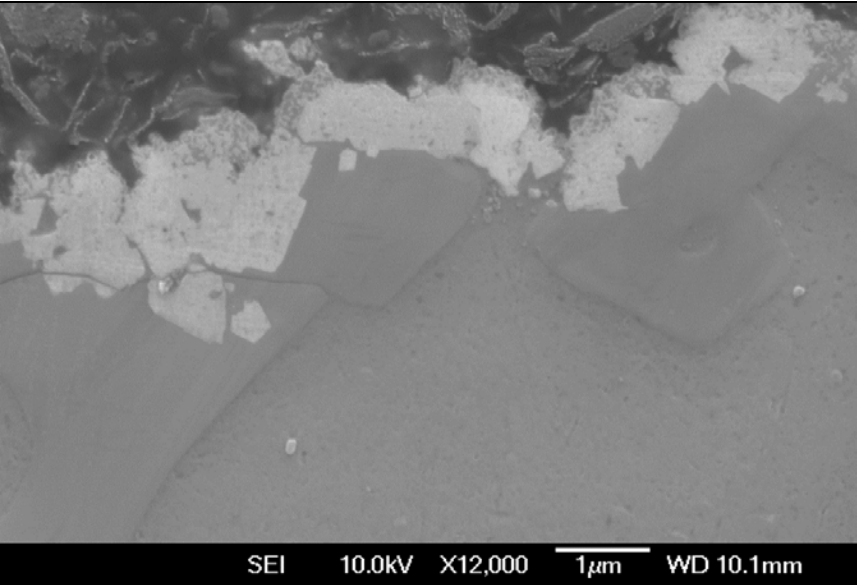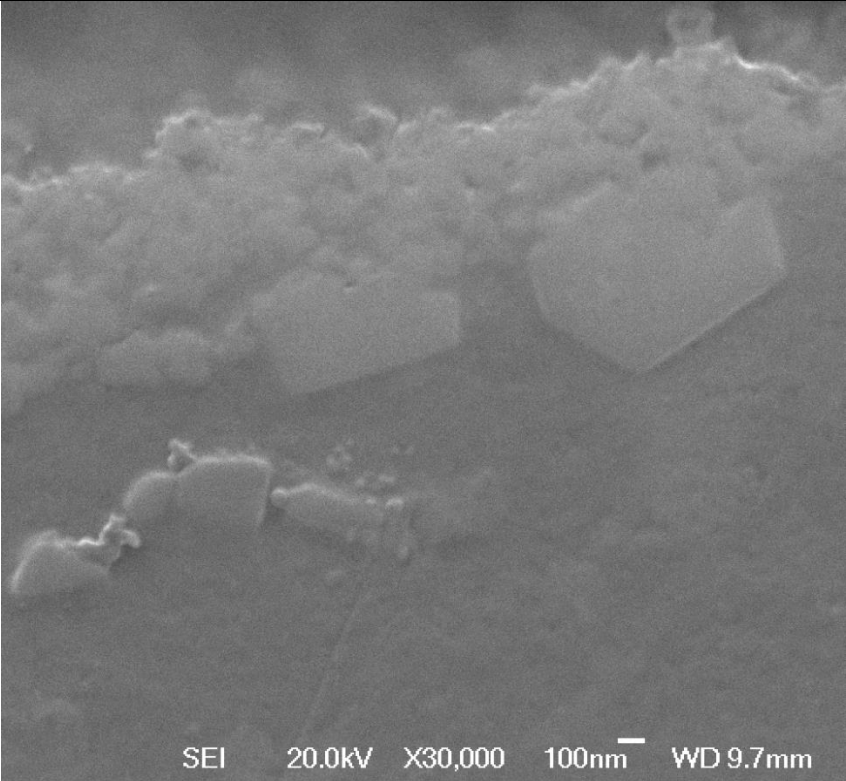


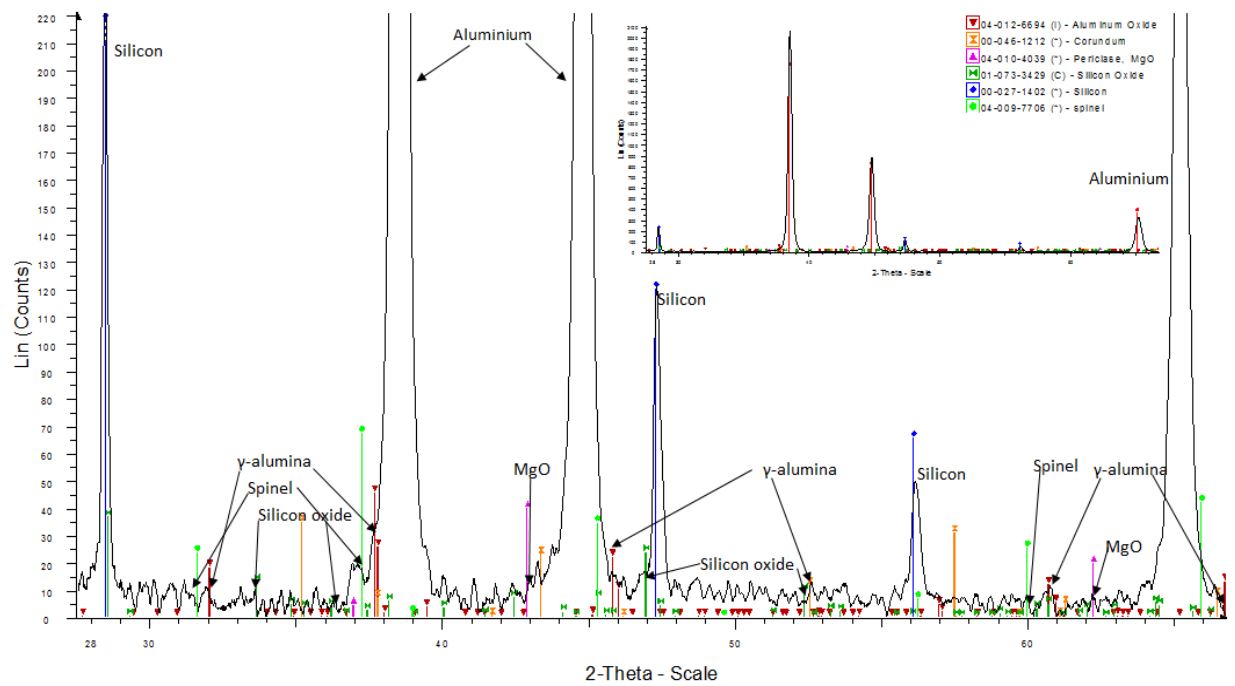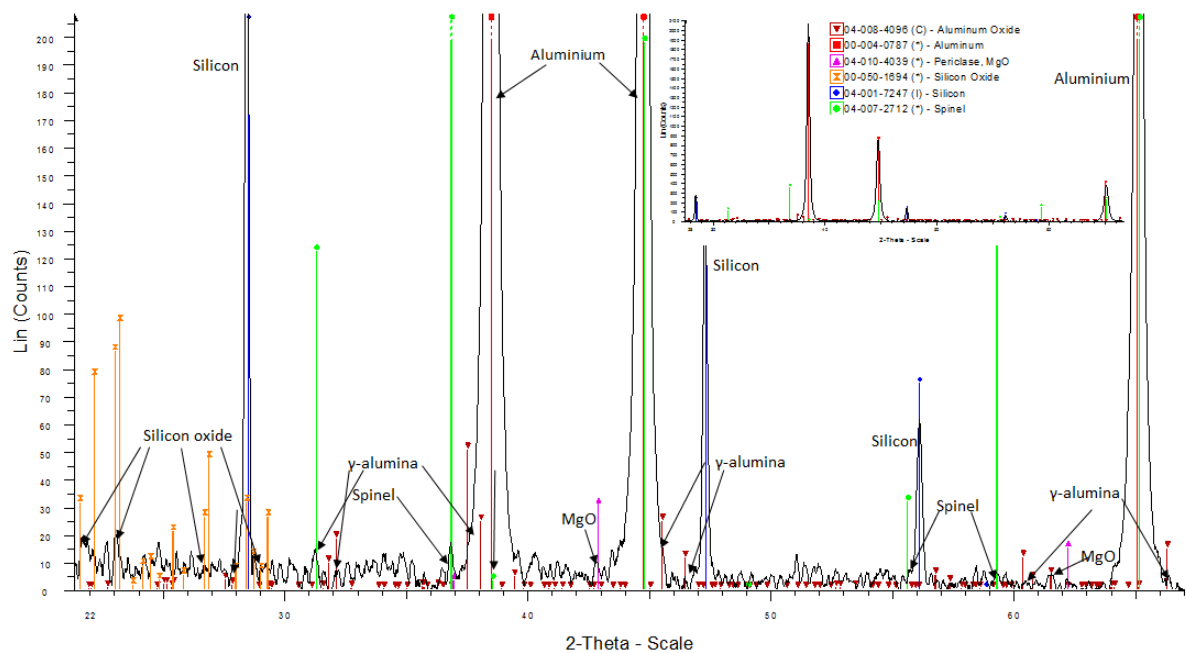**Figure 55 - The XRD spectra for Al-7%Si held for 24 hours at 750 °C (zoomed out spectra inset)**

The XRD analysis in Figure 54 and Figure 55 showed that γ-alumina formed the oxide layer, along with traces of $SiO_2$ but this seems not to have affected the oxidation rate. No α-alumina was detected. There also appeared to be Si present. This Si was likely present in the solution and came out in the eutectic phases, which can be seen in sample 6 of Figure 51. The Si present was likely detected as an element as it was not in a compound with another and did not form part of the detected $SiO_2$ oxide.

## 3.1.2.3 – Al 7%Si 0.3%Mg

SEM images of Al-7%Si-0.3%Mg alloy held at different holding times are shown in Figure 56.

**Figure 56 - Images of Al-7%Si-0.3%Mg melted at 750 °C for different times**
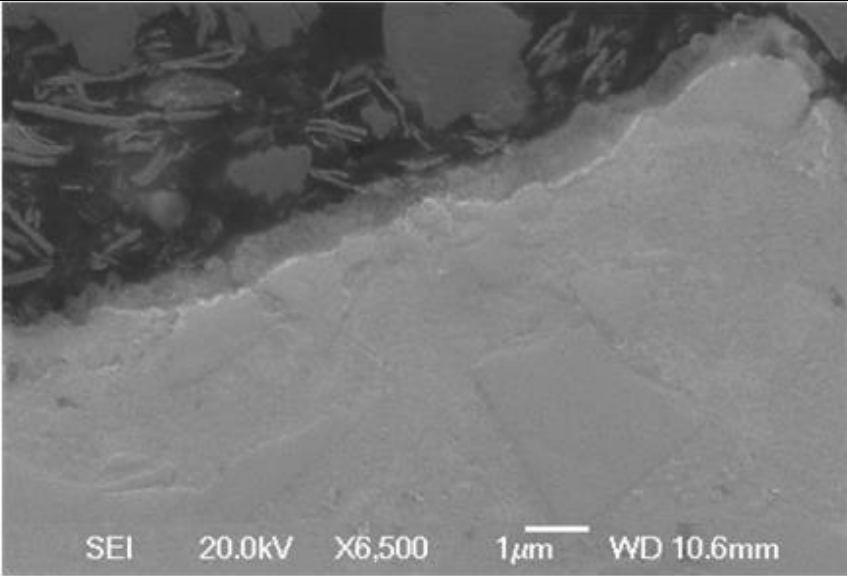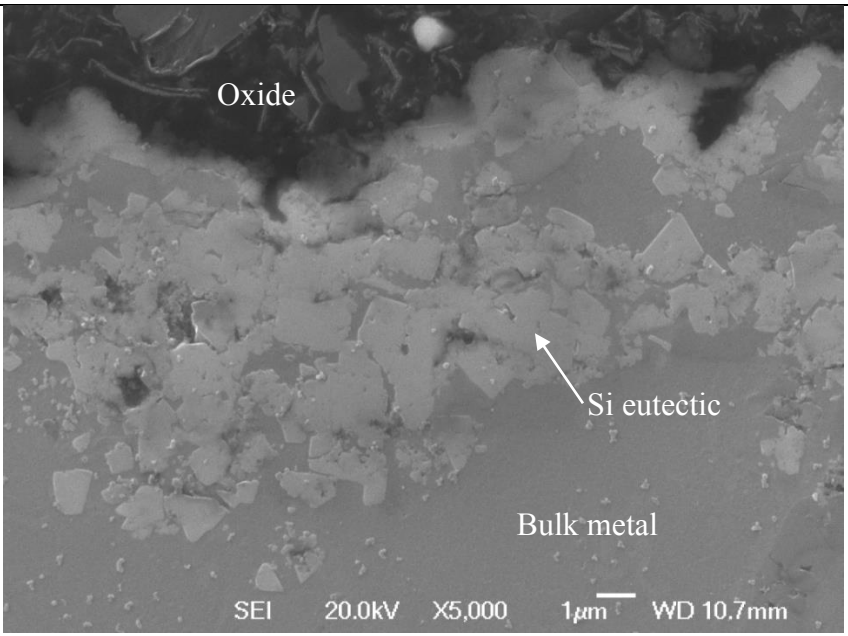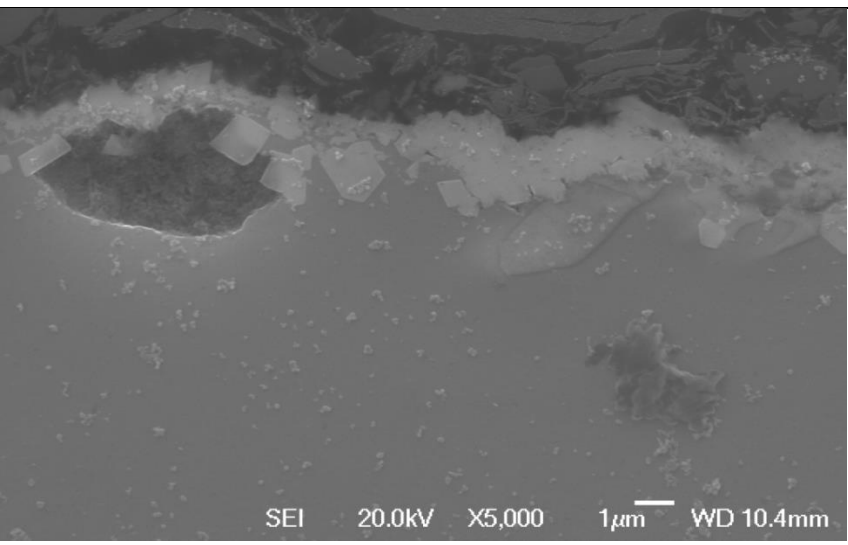
| Sample | Image |
|---|---|
| 1<br><br>750 °C 5 min hold<br><br>Oxide layer ≈ 0.65 μm |  |
| 2<br><br>750 °C 17 min hold<br><br>Oxide layer ≈ 0.60 μm |  |

| | |
|---|---|
| 3<br><br>750 ºC 1 hour hold<br><br>Oxide layer ≈ 0.67 μm |  |
| 4<br><br>750 ºC 3 hour hold<br><br>Oxide layer ≈ 0.73 μm |  |
| 5<br><br>750 ºC 24 hour hold<br><br>Oxide layer ≈ 1.55 μm |  |

**Figure 56 continued - Images of Al-7%Si-0.3%Mg melted at 750 °C for different times**

The oxide thickness increased over time in Al-7%Si-0.3%Mg, with an increase of ~0.96 μm over the total oxidation time. The oxide thickness can be seen in Table 11 and Figure 57. The growth followed a similar pattern to SP-Al, but was thicker over the total oxidation period (1.56 μm compared to 0.37 μm in SP-Al). There seemed be a cubic structure just beneath the oxide layer, possibly a eutectic. The growth patterns can be seen in Table 11 and Figure 58.

**Table 11 - Thicknesses of oxides for Al-7%Si-0.3%Mg melted at 750 °C**

| Melt Conditions | Oxide Thickness |
|---|---|
| 750°C 5 min hold | 0.65 μm |
| 750°C 17 min hold | 0.6 μm |
| 750°C 1 hour hold | 0.67 μm |
| 750°C 3 hour hold | 0.73 μm |
| 750 °C 24 hour hold | 1.56 μm |
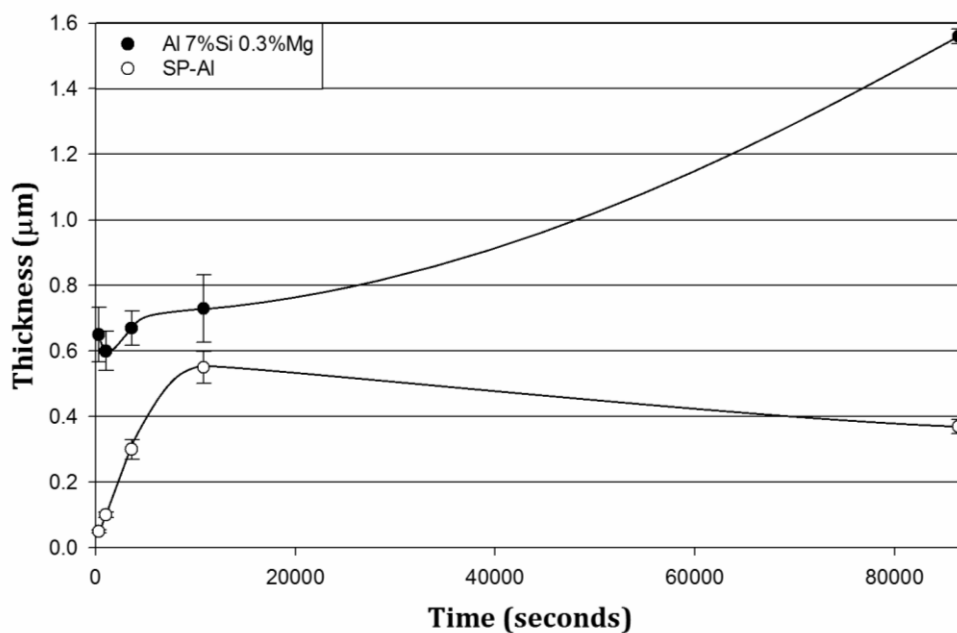


**Figure 57 - Thickness of oxide layer vs. holding time Al 7%Si 0.3%Mg samples held at 750 °C**

The resulting growth pattern, seen in Figure 57, suggested that the oxide growth may have occurred similarly to SP-Al. However, if the error bars are taken in to consideration, the growth may have been more linear than the graph suggests, as the errors could put the thicknesses at very similar levels, below 3 hours of oxidation time. The large increase in the oxide layer thickness implies that for oxidation times up to 3 hours, the oxide layer was non-protective and non-continuous. The growth rate decreased after this point, suggesting that the oxide had become continuous and protective. The presence of Mg in the Al-4%Mg alloy greatly increased

the thickness of the oxide over time, as shown in Figure 45. The presence of Si in the Al-7%Si alloy seemed to have little effect, as shown in Figure 51. It seems that even the small amount of Mg present in the Al-7%Si-0.3%Mg alloy had a large effect on the oxidation rate. The initial growth rate between 5 minutes and 3 hours was $4.8 \times 10^{-5}$ µm/s and $6.5 \times 10^{-6}$ µm/s between 3 and 24 hours. The initial rate of growth for the SP-Al was $7.5 \times 10^{-5}$ µm/s, higher initially than Al-7%Si-0.3%Mg but this plateaued after 1 hour with no further growth after 1 hour. The EDX spectra, in Figure 58, show the elemental composition of the oxide layers.

**Figure 58 - EDX spectra for the Al-7%Si-0.3%Mg samples melted at 750 °C**

| Sample | Analysis |
|---|---|
| 1<br><br>750 °C 5 min hold<br><br>Oxide layer ≈ 0.65 µm |  |

Point 1

| Element | Weight % |
|---|---|
| O | 26.33 |
| Mg | 24.07 |
| Al | 49.60 |
| Si | 0.00 |

Point 2

| Element | Weight % |
|---|---|
| O | 21.27 |
| Mg | 22.07 |
| Al | 54.96 |
| Si | 1.70 |

Point 3

| Element | Weight % |
|---|---|
| O | 18.27 |
| Mg | 18.96 |
| Al | 56.07 |
| Si | 6.70 |

Point 4

| Element | Weight % |
|---|---|
| O | 18.00 |
| Mg | 18.43 |
| Al | 53.22 |
| Si | 10.34 |

Point 5

| Element | Weight % |
|---|---|
| O | 7.07 |
| Mg | 9.51 |
| Al | 26.13 |
| Si | 57.29 |

Point 6

| Element | Weight % |
|---|---|
| O | 3.30 |
| Mg | 4.76 |
| Al | 13.15 |
| Si | 78.79 |

Point 7

| Element | Weight % |
|---|---|
| O | 1.46 |
| Mg | 1.63 |
| Al | 11.30 |
| Si | 85.61 |

Point 8

| Element | Weight % |
|---|---|
| O | 0.00 |
| Mg | 0.00 |
| Al | 57.49 |
| Si | 42.51 |

| 2

750 ºC 17 min hold

Oxide layer ≈ 0.60 μm |  |

Spectrum 1
| Element | Weight % |
|---|---|
| O | 0.00 |
| Mg | 0.00 |
| Al | 98.48 |
| Si | 1.52 |

Spectrum 2
| Element | Weight % |
|---|---|
| O | 2.74 |
| Mg | 0.84 |
| Al | 40.27 |
| Si | 56.14 |

Spectrum 3
| Element | Weight % |
|---|---|
| O | 5.32 |
| Mg | 2.08 |
| Al | 64.50 |
| Si | 28.10 |

Spectrum 4
| Element | Weight % |
|---|---|
| O | 0.00 |
| Mg | 0.00 |
| Al | 79.85 |
| Si | 20.15 |

Spectrum 5
| Element | Weight % |
|---|---|
| O | 12.27 |
| Mg | 6.75 |
| Al | 33.05 |
| Si | 47.93 |

Spectrum 6
| Element | Weight % |
|---|---|
| O | 13.02 |
| Mg | 5.33 |
| Al | 49.41 |
| Si | 32.24 |

---

3

750 ºC 1 hour hold

Oxide layer ≈ 0.67 μm



Spectrum 1
| Element | Weight % |
|---|---|
| O | 0.00 |
| Mg | 0.00 |
| Al | 69.89 |
| Si | 30.11 |

Spectrum 2
| Element | Weight % |
|---|---|
| O | 0.00 |
| Mg | 1.43 |
| Al | 25.59 |
| Si | 72.98 |

Spectrum 3
| Element | Weight % |
|---|---|
| O | 24.85 |
| Mg | 26.05 |
| Al | 41.7 |
| Si | 7.4 |

Spectrum 4
| Element | Weight % |
|---|---|
| O | 23.9 |
| Mg | 28.57 |
| Al | 41.93 |
| Si | 5.6 |

Spectrum 5
| Element | Weight % |
|---|---|
| O | 22.4 |
| Mg | 23.63 |
| Al | 51.99 |
| Si | 1.98 |

Spectrum 6
| Element | Weight % |
|---|---|
| O | 12.02 |
| Mg | 9.17 |
| Al | 39.57 |
| Si | 39.24 |

Spectrum 7
| Element | Weight % |
|---|---|
| O | 0.00 |
| Mg | 0.00 |
| Al | 39.52 |
| Si | 60.48 |

Spectrum 8
| Element | Weight % |
|---|---|
| O | 10.92 |
| Mg | 10.98 |
| Al | 19.85 |
| Si | 58.25 |

**Figure 58 continued - EDX spectra for the Al-7%Si-0.3%Mg samples melted at 750 °C**

| 4

750 ºC 3 hour

hold


Oxide layer ≈

1.16 μm | |

| Spectrum 1 | | Spectrum 2 | | Spectrum 3 | | Spectrum 4 | |
|---|---|---|---|---|---|---|---|
| Element | Weight % | Element | Weight % | Element | Weight % | Element | Weight % |
| O | 0.00 | O | 9.23 | O | 38.65 | O | 33.25 |
| Mg | 0.82 | Mg | 3.91 | Mg | 14.85 | Mg | 12.70 |
| Al | 98.00 | Al | 85.42 | Al | 45.68 | Al | 50.40 |
| Si | 1.18 | Si | 1.44 | Si | 0.81 | Si | 3.65 |

| Spectrum 5 | | Spectrum 6 | | Spectrum 7 | | Spectrum 8 | |
|---|---|---|---|---|---|---|---|
| Element | Weight % | Element | Weight % | Element | Weight % | Element | Weight % |
| O | 18.01 | O | 34.56 | O | 42.73 | O | 37.41 |
| Mg | 2.58 | Mg | 12.50 | Mg | 19.00 | Mg | 16.63 |
| Al | 78.57 | Al | 28.65 | Al | 38.27 | Al | 44.05 |
| Si | 0.84 | Si | 24.29 | Si | 0.00 | Si | 1.91 |

| Spectrum 9 | | Spectrum 10 | |
|---|---|---|---|
| Element | Weight % | Element | Weight % |
| O | 40.82 | O | 39.58 |
| Mg | 16.52 | Mg | 14.46 |
| Al | 41.94 | Al | 45.96 |
| Si | 0.72 | Si | 0.00 |



5

750 ºC 24 hour

hold


Oxide layer ≈

1.56 μ m

| Spectrum 1 | | Spectrum 2 | | Spectrum 3 | |
|---|---|---|---|---|---|
| Element | Weight % | Element | Weight % | Element | Weight % |
| O | 0.00 | O | 39.91 | O | 25.79 |
| Mg | 0.00 | Mg | 23.01 | Mg | 17.65 |
| Al | 100.00 | Al | 36.16 | Al | 54.48 |
| Si | 0.00 | Si | 0.92 | Si | 2.09 |

| Spectrum 4 | | Spectrum 5 | | Spectrum 6 | |
|---|---|---|---|---|---|
| Element | Weight % | Element | Weight % | Element | Weight % |
| O | 15.66 | O | 16.79 | O | 41.44 |
| Mg | 13.72 | Mg | 20.33 | Mg | 25.06 |
| Al | 53.00 | Al | 46.25 | Al | 33.50 |
| Si | 17.62 | Si | 16.63 | Si | 0.00 |

**Figure 58 continued - EDX spectra for the Al-7%Si-0.3%Mg samples melted at 750 °C**

As with previous alloys, Mg and Si seemed to have migrated towards the surface (as shown in the EDX data of Figure 58) and were present in high levels, up to ~20% Mg within the oxide layer and up to ~70% Si in the subsurface region. a series of subsurface features in most samples. The presence of Mg in particular is likely to be the reason for the high oxide thicknesses (compared to SP-Al). There also appeared to be a high-silicon phase which had a pseudo-cubic appearance in the SEM micrographs (see sample 1, 4 and 5 of Figure 58) that could be a eutectic phase. The XRD analysis for the 5 minute, 1 hour and 24 hours sample's oxide regions are seen in Figure 59, Figure 60 and Figure 61.
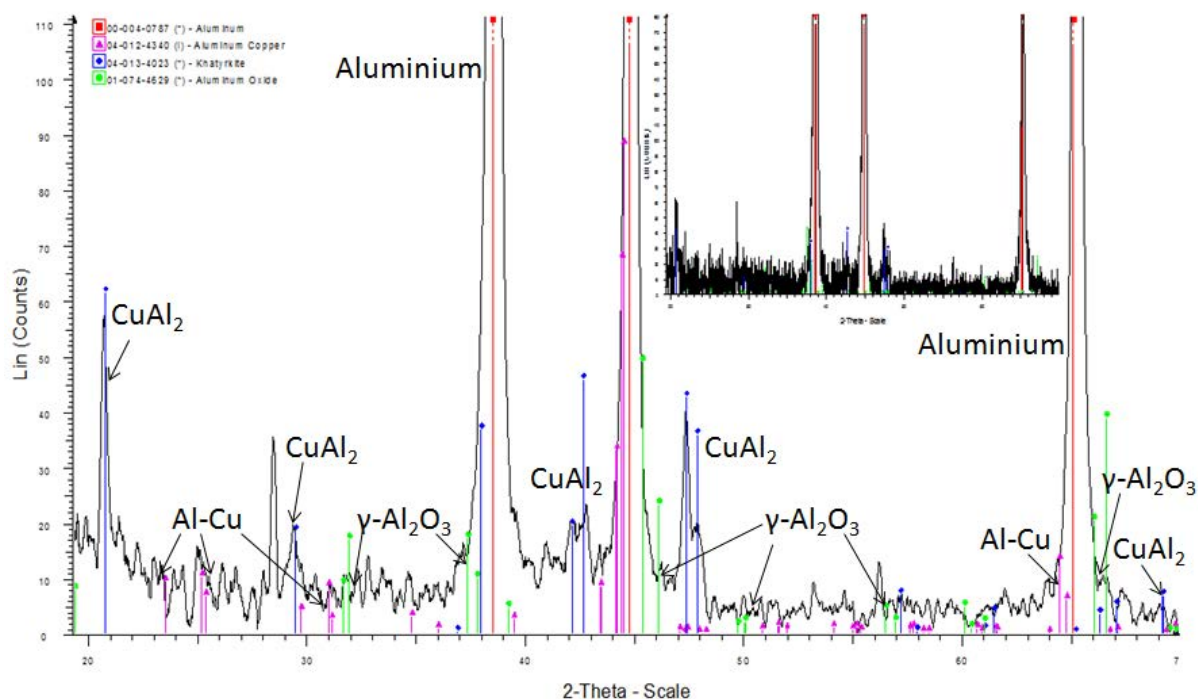


**Figure 59 - The XRD spectra for Al-7%Si-0.3%Mg held for 5 minutes at 750 °C (zoomed out spectra inset)**

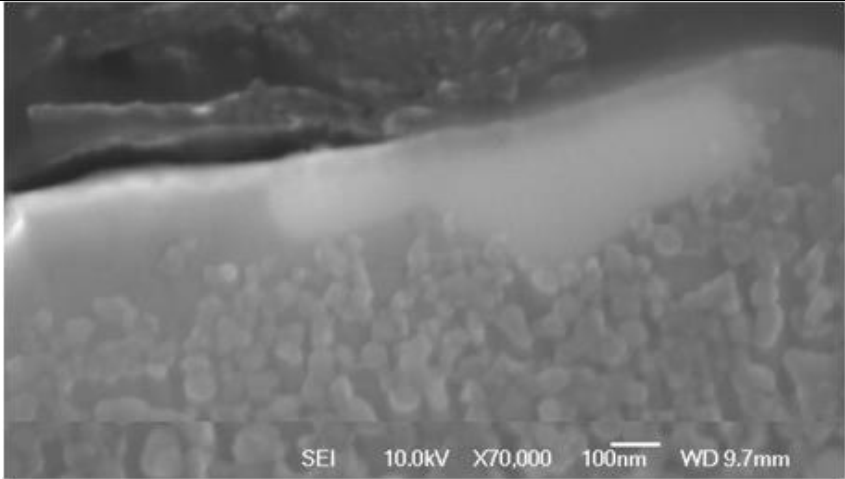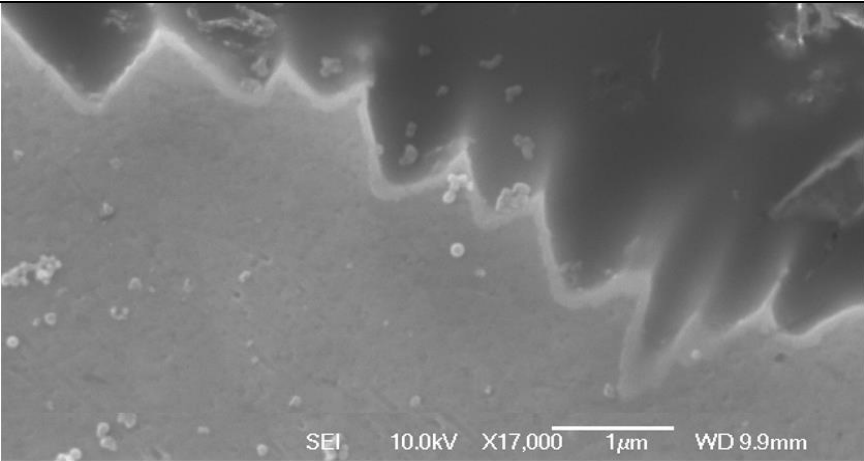**Figure 60 - The XRD spectra for Al-7%Si-0.3%Mg held for 1 hour at 750 °C (zoomed out spectra inset)**



**Figure 61 - The XRD spectra for Al-7%Si-0.3%Mg held for 24 hours at 750 °C (zoomed out spectra inset)**
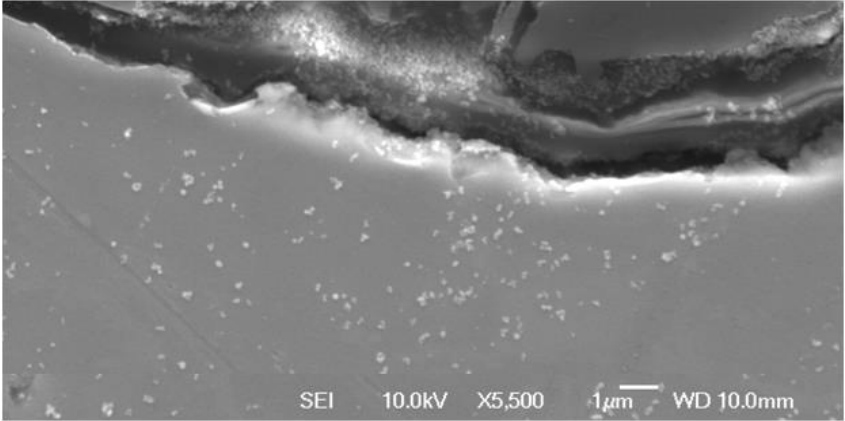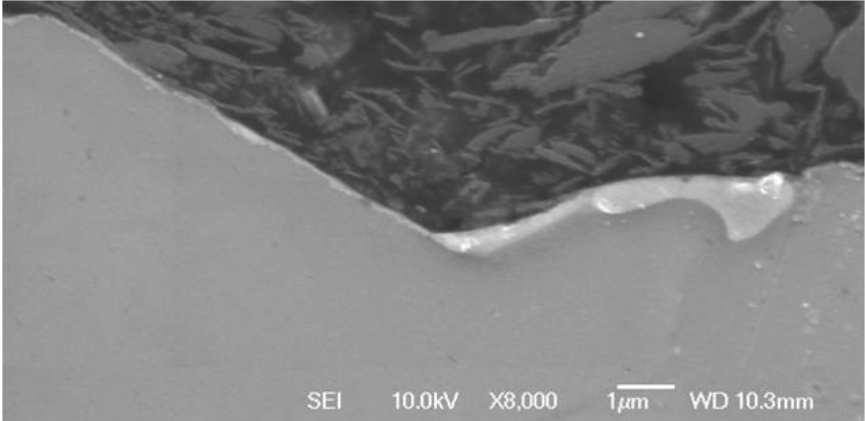
The XRD results suggest that the oxides present in the samples were γ-alumina, with stronger counts indicating a greater amount with the longer oxidation times, spinel and traces of MgO and $SiO_2$. This suggests that γ-alumina was present at 5 minutes, and grew during the fast oxidation period to become protective after 3 hours. Si also showed a strong signal in all samples, suggesting it was present in increased amounts in the surface region. This may have been a eutectic phase, whose structure was not determined. These may have corresponded to the cubic sub-surface features seen in SEM micrographs. The spectra also show signals for spinel and MgO, suggesting that they were growing simultaneously. This could be an influence

94
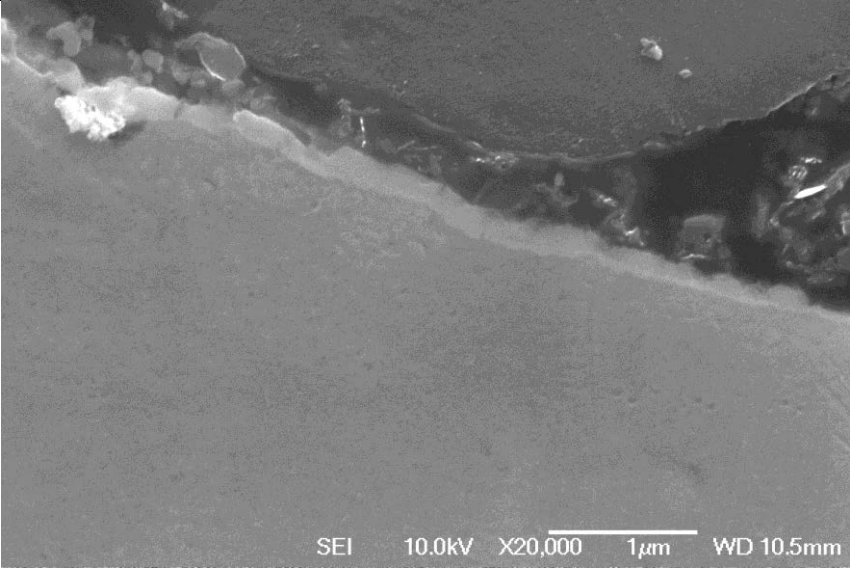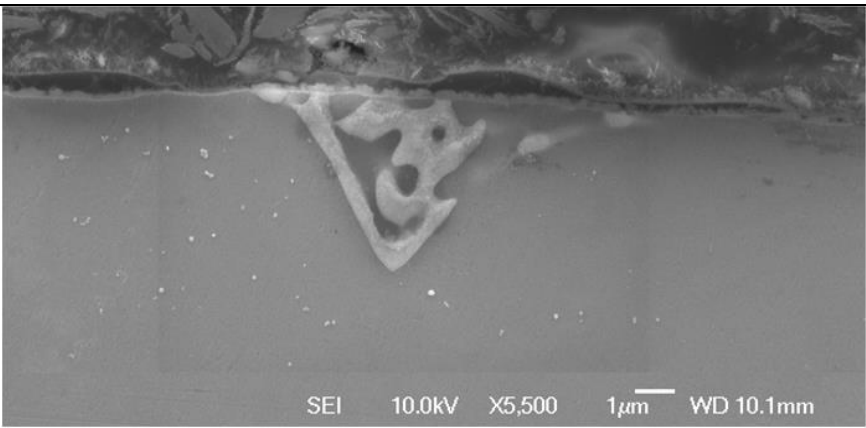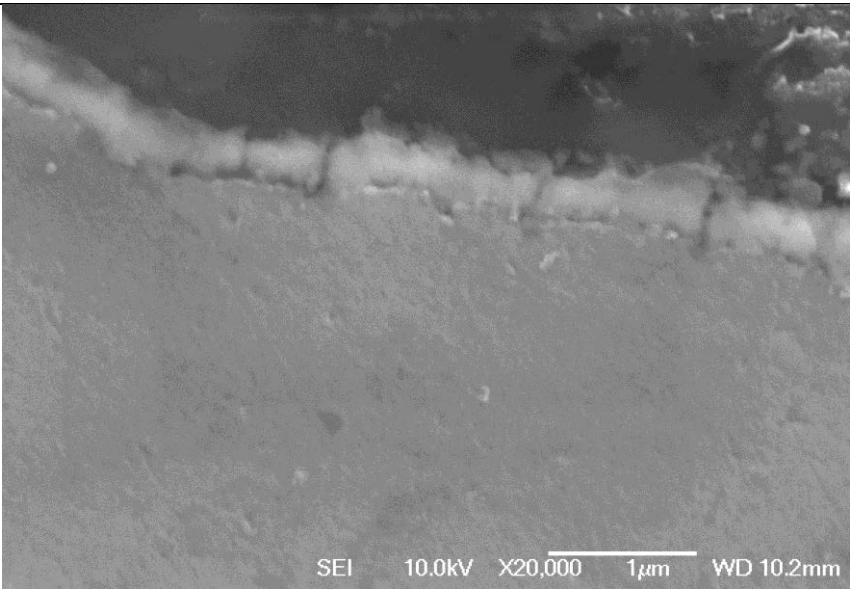
of Si on the oxidation, but the low concentration of Mg in the alloy also will mean its effect will be smaller. The Pilling Bedworth ratio for MgO, is 0.81, therefore the oxide is porous and non-passivating, suggesting that MgO contributed to the increase in oxide thickness, but $SiO_2$, with a Pilling Bedworth ratio of 1.88, would have helped to slow the growth down.

### 3.1.2.4 – Al 4%Cu

SEM images of the Al-4%Cu alloy held at different holding times can be seen in Figure 62.

**Figure 62 - Images of Al-4%Cu melted at 750 °C for different times**

| | Image |
|---|---|
| 1<br><br>750 °C 5 min hold<br><br>Oxide layer ≈ 0.31 μm | SEI 10.0kV X5,500 1μm WD 10.0mm |
| 2<br><br>750 °C 17 min hold<br><br>Oxide layer ≈ 0.36 μm | SEI 10.0kV X8,000 1μm WD 10.3mm |

| | |
|---|---|
| 3<br><br>750 ºC 1 hour hold<br><br>Oxide layer ≈ 0.21 μm | <br>SEI  10.0kV  X20,000  1μm  WD 10.5mm |
| 4<br><br>750 ºC 3 hour hold<br><br>Oxide layer ≈ 0.22 μm | <br>SEI  10.0kV  X5,500  1μm  WD 10.1mm |
| 5<br><br>750 ºC 7 hour hold<br><br>Oxide layer ≈ 0.39μm | <br>SEI  10.0kV  X20,000  1μm  WD 10.2mm |

| 6 |  |
|---|---|
| 750 °C 24 hour hold<br><br>Oxide layer ≈ 1.72 μm | |

**Figure 62 - Images of Al-4%Cu melted at 750 °C for different times**

The oxide thickness in the Al-4%Cu alloy is summarised in Table 12 and Figure 63. The growth rate was initially slower than in SP-Al, $3.2 \times 10^{-6}$ μm/s compared to the initial oxidation rate of $7.5 \times 10^{-5}$ μm/s for SP-Al, but increased between 7 and 24 hours holding to $2.2 \times 10^{-5}$ μm/s. The oxide layer changed by 0.18 μm at 7 hours. The longest oxidation time of 24 hours had a thicker oxide of 1.72 μm, leading to a total oxide change of ~1.5 μm over the oxidation period.

**Table 12 - Thicknesses of oxides for Al-4%Cu melted at 750 °C**

| Melt Conditions | Oxide Thickness |
|---|---|
| 750°C 5 min hold | 0.31 μm |
| 750°C 17 min hold | 0.36 μm |
| 750°C 1 hour hold | 0.21 μm |
| 750°C 3 hour hold | 0.22 μm |
| 750°C 7 hour hold | 0.39 μm |
| 750 °C 24 hour hold | 1.72 μm |
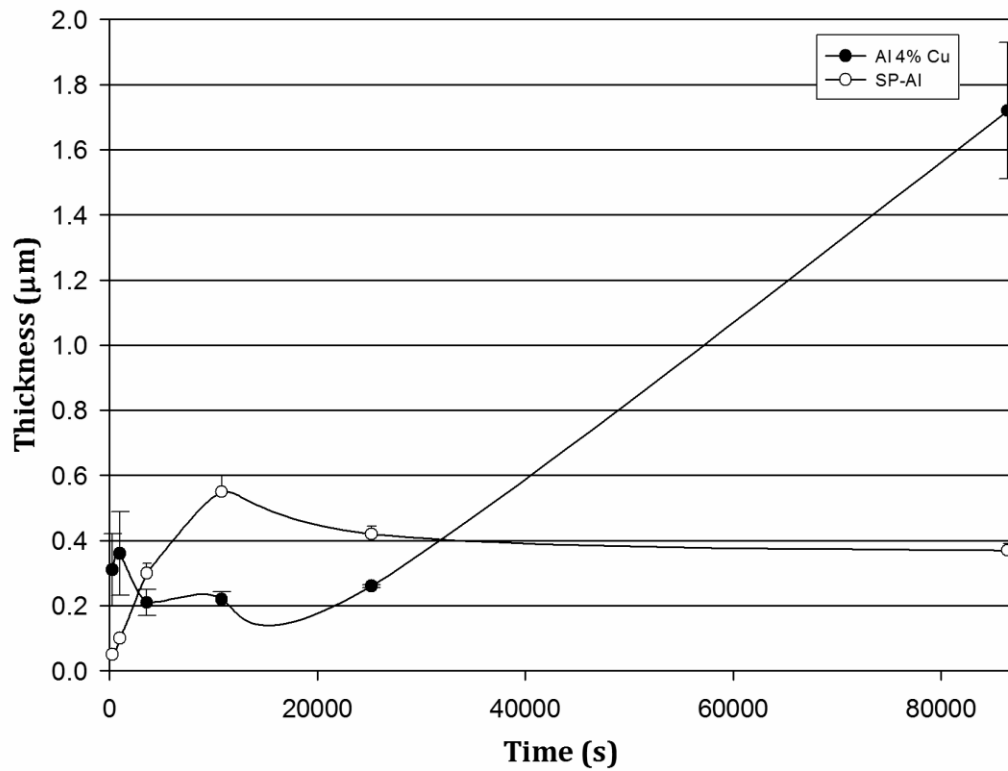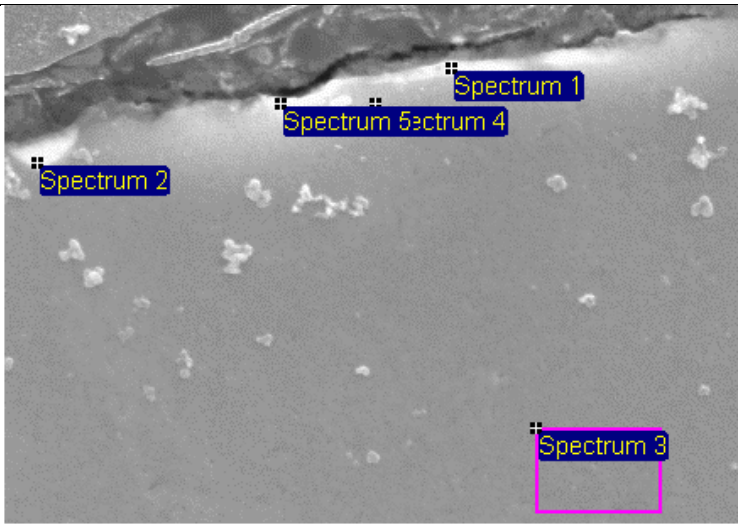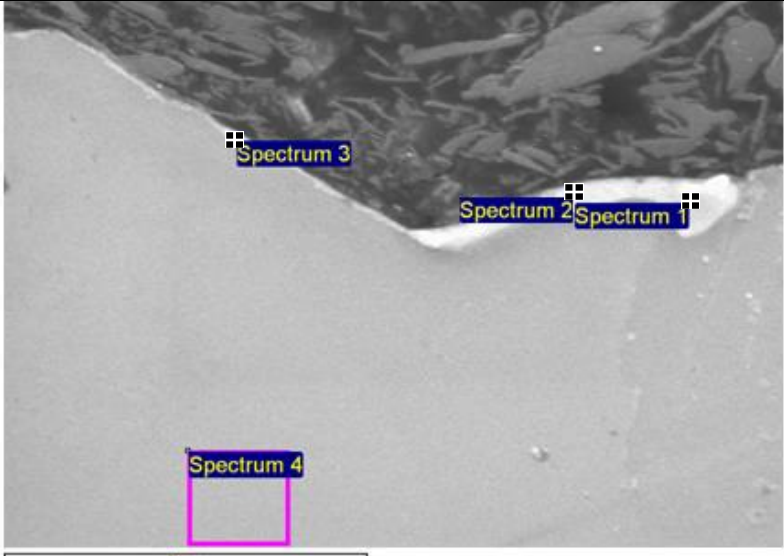
**Figure 63 - Thickness of oxide layer vs. holding time Al 4%Cu samples held at 750 °C, compared with SP-Al for the same time period**

The thickness of the oxide was almost constant over holding times up to 7 hours. This suggests that the layer formed was stable and possibly impermeable layer, e.g. γ-alumina. The increase in thickness at 24 hours could be due to a different oxide layer forming at this time that was less protective than those formed at shorter times. The EDX spectra in Figure 64 show the elements present in the surface and subsurface regions of all samples.

**Figure 64 - EDX spectra for the Al-4%Cu samples melted at 750 °C**

| Sample | Analysis |
|---|---|
| 1<br><br>750 ºC 5 min hold<br><br>Oxide layer ≈ 0.31 μm |  |

Spectrum 1

| Element | Weight % |
|---|---|
| O | 20.14 |
| Al | 60.20 |
| Cu | 19.66 |

Spectrum 2

| Element | Weight % |
|---|---|
| O | 6.72 |
| Al | 56.61 |
| Cu | 36.68 |

Spectrum 3

| Element | Weight % |
|---|---|
| O | 0.00 |
| Al | 95.44 |
| Cu | 4.56 |

Spectrum 4

| Element | Weight % |
|---|---|
| O | 4.85 |
| Al | 91.55 |
| Cu | 3.60 |

Spectrum 5

| Element | Weight % |
|---|---|
| O | 23.22 |
| Al | 76.78 |
| Cu | 0.00 |

| Sample | Analysis |
|---|---|
| 2<br><br>750 ºC 17 min hold<br><br>Oxide layer ≈ 0.36 μm |  |

Spectrum 1

| Element | Weight % |
|---|---|
| O | 1.26 |
| Al | 43.91 |
| Cu | 54.82 |

Spectrum 2

| Element | Weight % |
|---|---|
| O | 3.94 |
| Al | 51.84 |
| Cu | 44.21 |

Spectrum 3

| Element | Weight % |
|---|---|
| O | 7.34 |
| Al | 82.73 |
| Cu | 9.93 |

Spectrum 4

| Element | Weight % |
|---|---|
| O | 0.00 |
| Al | 96.23 |
| Cu | 3.77 |

| | |
|---|---|
| 3<br><br>750 °C 1 hour hold<br><br>Oxide layer ≈ 0.21 μm |  |

Spectrum 1

| Element | Weight % |
|---------|----------|
| O | 35.40 |
| Al | 62.87 |
| Cu | 1.73 |

Spectrum 2

| Element | Weight % |
|---------|----------|
| O | 30.99 |
| Al | 67.24 |
| Cu | 1.77 |

Spectrum 3

| Element | Weight % |
|---------|----------|
| O | 33.11 |
| Al | 63.93 |
| Cu | 2.96 |

Spectrum 4

| Element | Weight % |
|---------|----------|
| O | 0.00 |
| Al | 94.39 |
| Cu | 5.61 |

Spectrum 5

| Element | Weight % |
|---------|----------|
| O | 23.84 |
| Al | 73.71 |
| Cu | 2.45 |

| | |
|---|---|
| 4<br><br>750 °C 3 hour hold<br><br>Oxide layer ≈ 0.22 μm |  |

Spectrum 1

| Element | Weight % |
|---------|----------|
| O | 12.35 |
| Al | 68.26 |
| Cu | 19.39 |

Spectrum 2

| Element | Weight % |
|---------|----------|
| O | 0.00 |
| Al | 97.71 |
| Cu | 2.29 |

**Figure 64 continued - EDX spectra for the Al-4%Cu samples melted at 750 °C**

| | |
|---|---|
| 5<br><br>750 °C 7 hour hold<br><br>Oxide layer ≈ 0.39 μm |  |

Spectrum 1

| Element | Weight % |
|---|---|
| O | 0.00 |
| Al | 94.00 |
| Cu | 6.00 |

Spectrum 2

| Element | Weight % |
|---|---|
| O | 41.45 |
| Al | 43.76 |
| Cu | 14.78 |

Spectrum 3

| Element | Weight % |
|---|---|
| O | 37.46 |
| Al | 45.44 |
| Cu | 17.11 |

Spectrum 4

| Element | Weight % |
|---|---|
| O | 28.72 |
| Al | 64.18 |
| Cu | 7.11 |

Spectrum 5

| Element | Weight % |
|---|---|
| O | 35.17 |
| Al | 51.42 |
| Cu | 13.41 |

Spectrum 6

| Element | Weight % |
|---|---|
| O | 29.65 |
| Al | 55.60 |
| Cu | 14.75 |

| | |
|---|---|
| 6<br><br>750 °C 24 hour hold<br><br>Oxide layer ≈ 1.72 μm |  |

Spectrum 1

| Element | Weight % |
|---|---|
| O | 29.14 |
| Al | 55.00 |
| Cu | 15.86 |

Spectrum 2

| Element | Weight % |
|---|---|
| O | 28.50 |
| Al | 57.29 |
| Cu | 14.21 |

Spectrum 3

| Element | Weight % |
|---|---|
| O | 27.74 |
| Al | 59.04 |
| Cu | 13.22 |

Spectrum 4

| Element | Weight % |
|---|---|
| O | 26.53 |
| Al | 53.07 |
| Cu | 20.40 |

Spectrum 5

| Element | Weight % |
|---|---|
| O | 28.78 |
| Al | 57.59 |
| Cu | 13.64 |

Spectrum 6

| Element | Weight % |
|---|---|
| O | 0.00 |
| Al | 97.07 |
| Cu | 2.93 |

**Figure 64 continued - EDX spectra for the Al-4%Cu samples melted at 750 °C**

The oxide layers in all samples contained a high Cu content. This suggested that the oxides contained a mixture of alumina and Cu, with the possibility of a phase that was a combination of Al, Cu and alumina. The growth of the oxide was clearly inhibited by the presence of the Cu

in the alloy, which seemed to have become incorporated into the layer itself. The results of the XRD can be seen in Figure 65 and Figure 66.
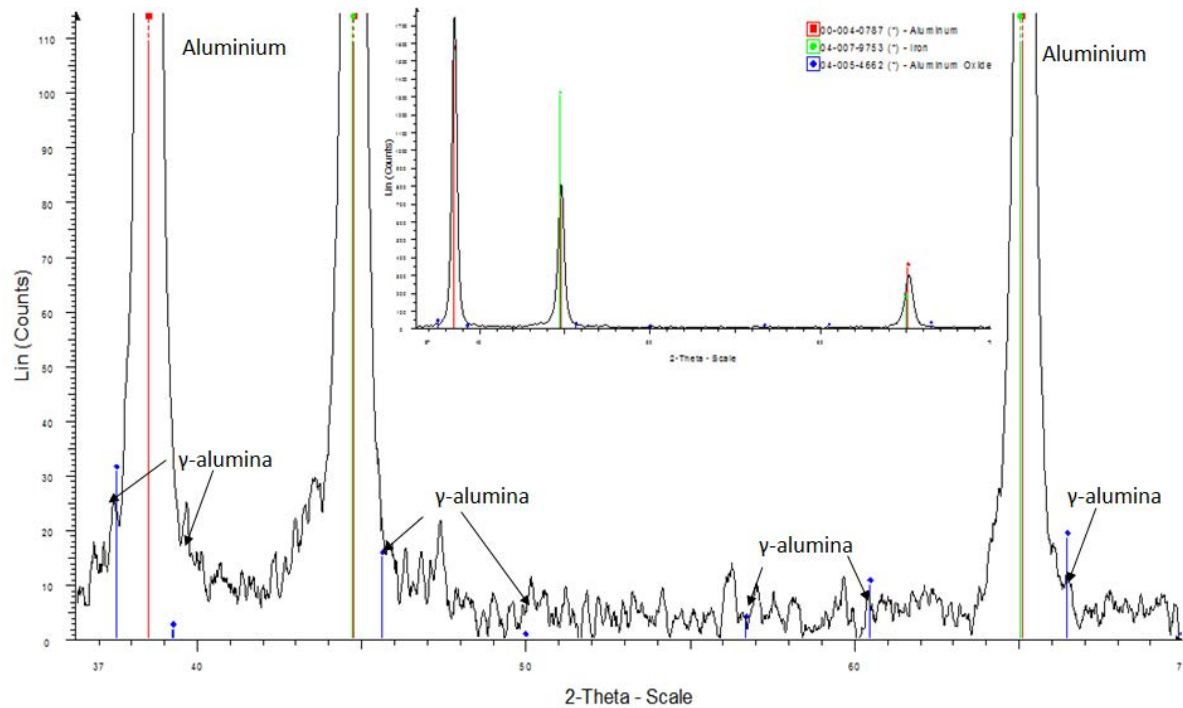


**Figure 65 - The XRD spectra for Al-4%Cu held for 5 minutes at 750 °C (zoomed out spectra inset)**
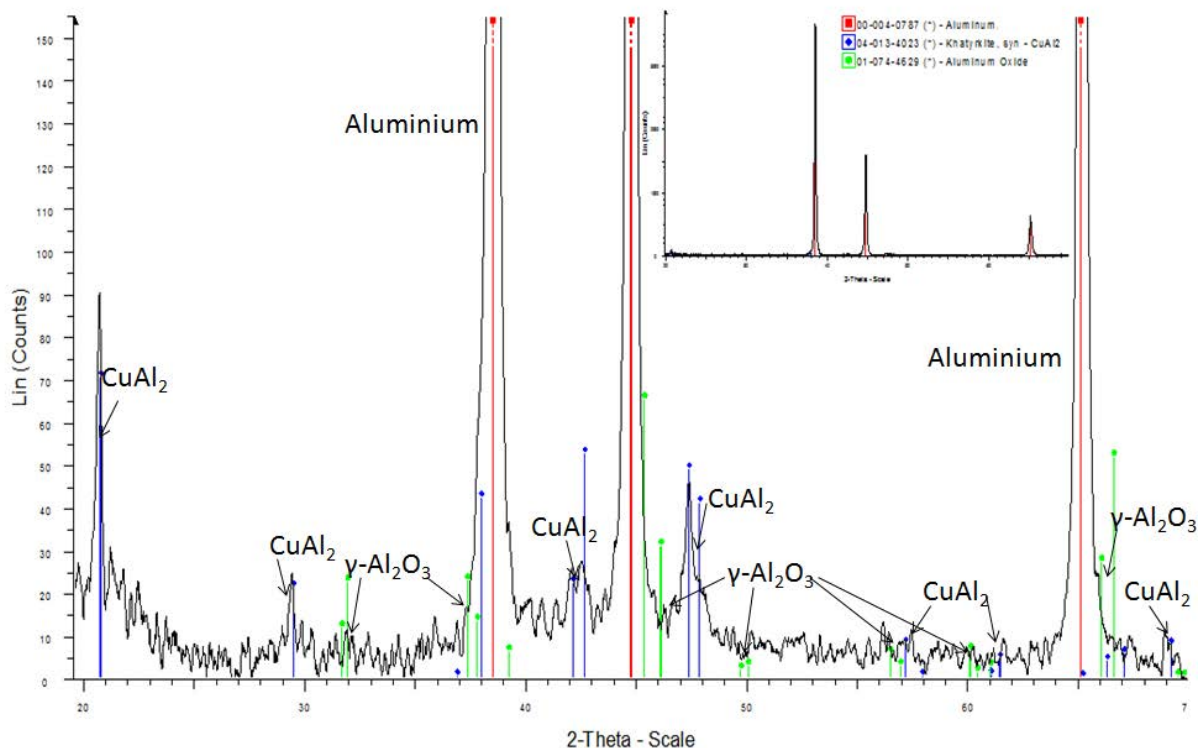


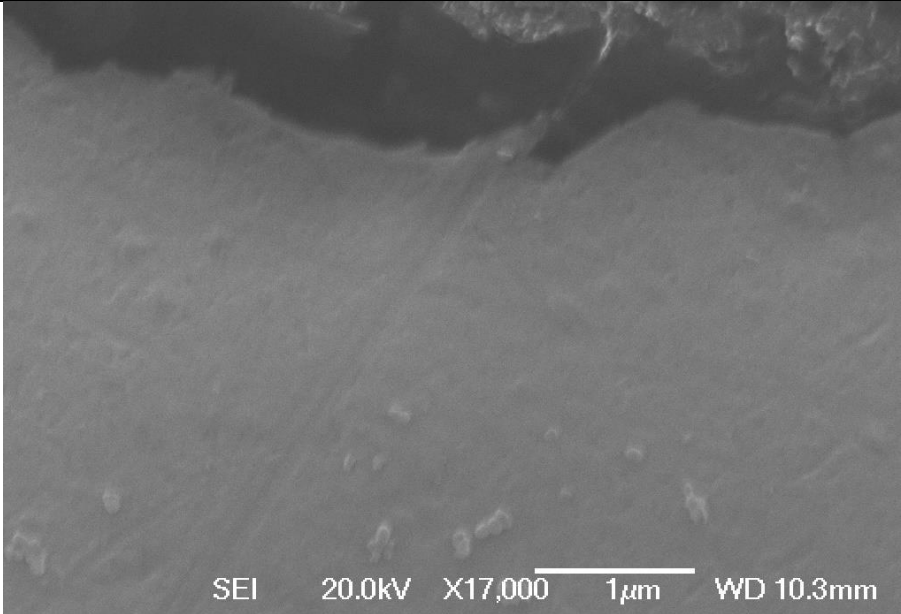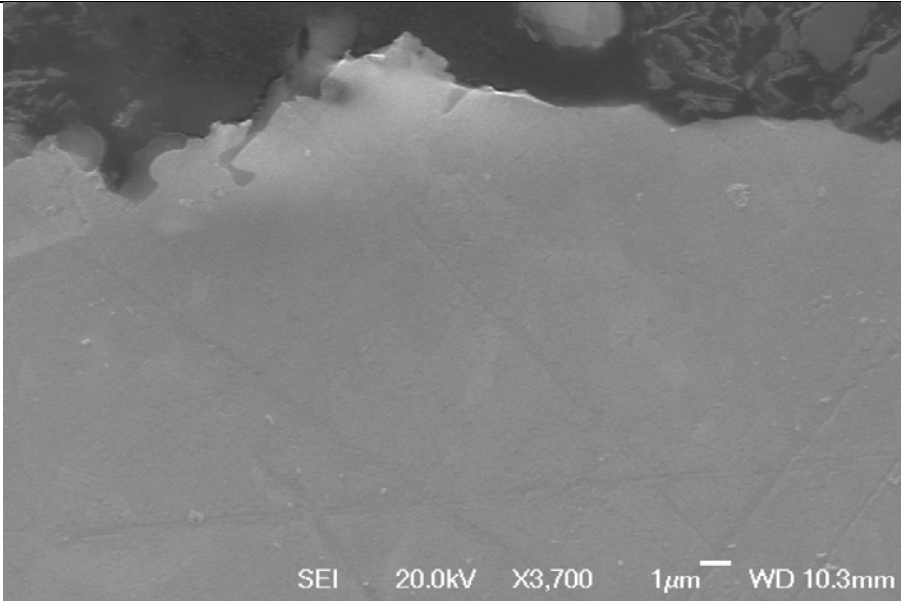**Figure 66 - The XRD spectra for Al-4%Cu held for 24 hours at 750 °C (zoomed out spectra inset)**

XRD shows that a phase CuAl₂ had formed in both samples, at 5 minutes and 24 hours (Figure 65 and Figure 66). From the evidence above, it is impossible to know if the CuAl₂ is forming a

mixed oxide structure with the alumina, present in the oxide by itself, or in a region just below the oxide. However, it is clear that its presence in the metal increases the oxidation. The spectra was very similar for both oxidation times, suggesting that the phases were present throughout the oxidation period. Also, the only crystalline oxide present was γ-alumina. This suggested that the oxide that was initially forming was the amorphous phase, with the γ-alumina forming slowly over the course of oxidation. The stable oxidation period, seen in some of the other oxidation processes (e.g. SP-Al and Al-Si alloy), could have occurred between the 7 hours and 24 hours holding time, but further work at times in between would be needed to ascertain this.

### 3.1.2.5 – Al 1%Fe

SEM images of the Al-1%Fe alloy held at different holding times can be seen in Figure 67.

**Figure 67 - Images of Al-1%Fe melted at 750 °C for different times**

| Sample | Image |
|---|---|
| 1<br><br>750 °C 5 min hold<br><br>Oxide layer ≈ 0.04 μm |  |
| 2<br><br>750 °C 17 min hold<br><br>Oxide layer ≈ 0.14 μm |  |

| | |
|---|---|
| 3<br><br>750 °C 1 hour hold<br><br>Oxide layer ≈ 0.15 μm | SEI    10.0kV   X12,000    1μm    WD 10.2mm |
| 4<br><br>750 °C 3 hour hold<br><br>Oxide layer ≈ 0.27 μm | SEI    10.0kV   X15,000    1μm    WD 10.1mm |
| 5<br><br>750 °C 7 hour hold<br><br>Oxide layer ≈ 0.20 μm | 2μm      Electron Image 1 |

**Figure 67 continued - Images of Al-1%Fe melted at 750 °C for different times**

| 6 |  |
| :---: | :---: |
| 750 ºC 24 hour hold<br><br>Oxide layer ≈ 0.21 μm | |
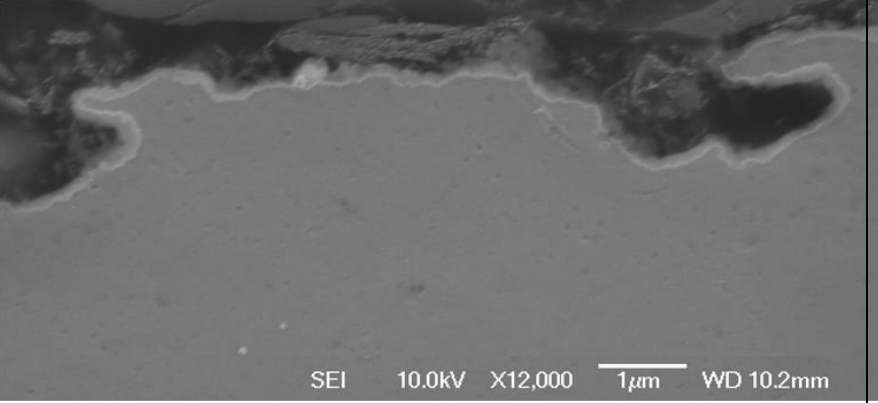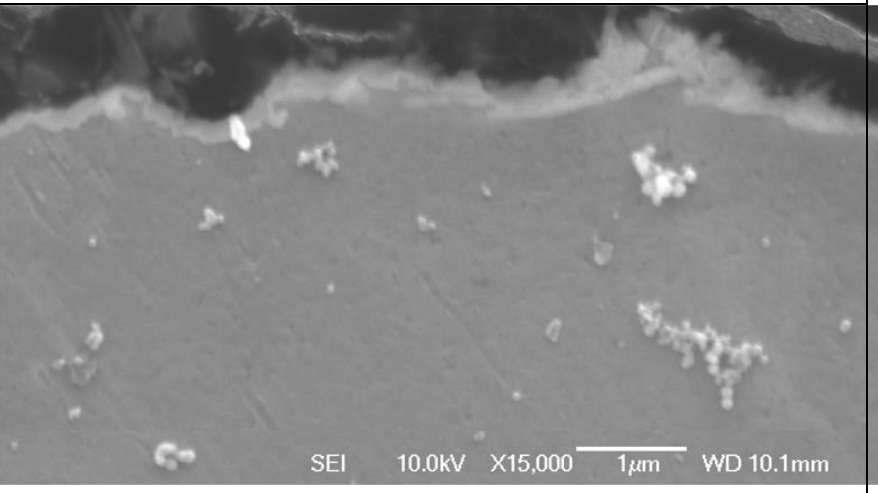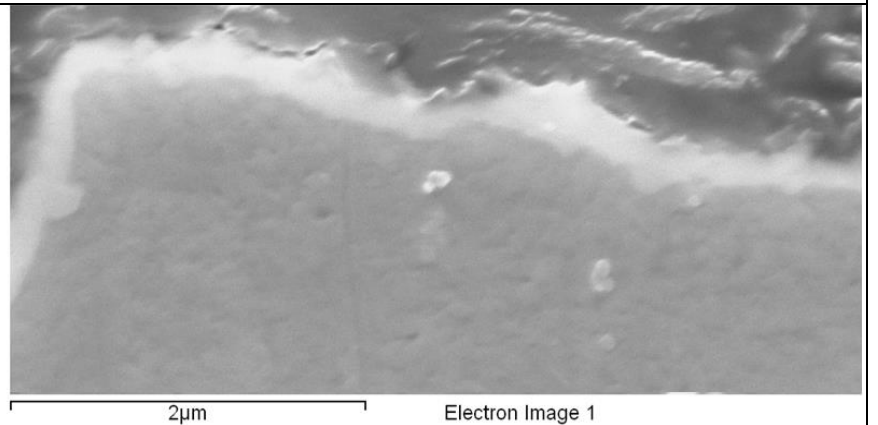
**Figure 67 continued - Images of Al-1%Fe melted at 750 °C for different times**

The oxide thickness for the Al-1%Fe alloy increased with oxidation time, but by a small amount. The thickness growth is summarised in Table 13 and Figure 68, which showed it increased by ~0.23 μm between 5 minutes and 24 hours, and so oxidised at a slower rate than SP-Al over the same time period.

**Table 13 - Thicknesses of oxides for Al-1%Fe melted at 750 °C**

| Melt Conditions | Oxide Thickness |
| :---: | :---: |
| 750ºC 5 min hold | 0.04 μm |
| 750ºC 17 min hold | 0.14 μm |
| 750ºC 1 hour hold | 0.15 μm |
| 750ºC 3 hour hold | 0.27 μm |
| 750ºC 7 hour hold | 0.20 μm |
| 750 ºC 24 hour hold | 0.21 μm |
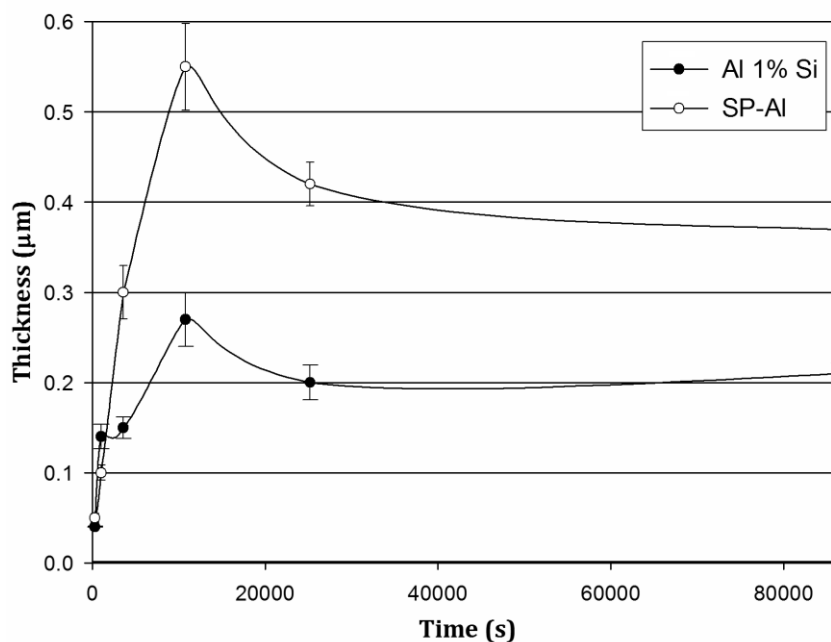
**Figure 68 - Thickness of oxide layer vs. holding time Al 1%Fe samples held at 750 °C, compared to SP-Al**

There was an increase in oxide thickness between 5 minutes and 3 hours. At 7 hours the growth levelled off, suggesting that a stable oxide was present and continuous after this time. There was also a peak present at 3 hours, similar to SP-Al. The EDX analysis can be seen in Figure 69, showing the chemical content of the surface layers.

**Figure 69 - EDX spectra for the Al-1%Fe samples melted at 750 °C**

| Sample | Analysis |
|---|---|
| 1<br><br>750 ºC 5 min hold<br><br>Oxide layer ≈ 0.04 μm |  |

| Spectrum 2 | | Spectrum 3 | | Spectrum 4 | | Spectrum 5 | |
|---|---|---|---|---|---|---|---|
| Element | Weight % | Element | Weight % | Element | Weight % | Element | Weight % |
| O | 6.22 | O | 3.90 | O | 21.40 | O | 23.29 |
| Al | 56.42 | Al | 93.46 | Al | 78.60 | Al | 65.80 |
| Fe | 37.36 | Fe | 2.64 | Fe | 0.00 | Fe | 10.91 |

| Spectrum 6 | | Spectrum 7 | | Spectrum 8 | |
|---|---|---|---|---|---|
| Element | Weight % | Element | Weight % | Element | Weight % |
| O | 29.40 | O | 20.19 | O | 23.76 |
| Al | 70.60 | Al | 68.71 | Al | 76.24 |
| Fe | 0.00 | Fe | 11.10 | Fe | 0.00 |

| 2<br><br>750 ºC 17 min hold<br><br>Oxide layer ≈ 0.14 μm |  |
|---|---|

Spectrum 1

| Element | Weight % |
|---|---|
| O | 5.77 |
| Al | 94.23 |
| Fe | 0.00 |

Spectrum 2

| Element | Weight % |
|---|---|
| O | 13.92 |
| Al | 86.08 |
| Fe | 0.00 |

Spectrum 3

| Element | Weight % |
|---|---|
| O | 6.35 |
| Al | 93.65 |
| Fe | 0.00 |

Spectrum 4

| Element | Weight % |
|---|---|
| O | 1.72 |
| Al | 98.28 |
| Fe | 0.00 |

| 3<br><br>750 ºC 1 hour hold<br><br>Oxide layer ≈ 0.15 μm |  |
|---|---|

Spectrum 1

| Element | Weight % |
|---|---|
| O | 0.00 |
| Al | 100.00 |
| Fe | 0.00 |

Spectrum 2

| Element | Weight % |
|---|---|
| O | 15.99 |
| Al | 59.77 |
| Fe | 24.24 |

Spectrum 3

| Element | Weight % |
|---|---|
| O | 27.83 |
| Al | 72.17 |
| Fe | 0.00 |

Spectrum 4

| Element | Weight % |
|---|---|
| O | 11.03 |
| Al | 88.97 |
| Fe | 0.00 |

Spectrum 5

| Element | Weight % |
|---|---|
| O | 2.72 |
| Al | 97.28 |
| Fe | 0.00 |

**Figure 69 continued - EDX spectra for the Al-1%Fe samples melted at 750 °C**

| 4

750 ºC 3 hour hold

Oxide layer ≈ 0.27 μm |



| Spectrum 1 | | | Point 1 | | | Point 2 | | |
|---|---|---|---|---|---|---|---|---|
| Element | Weight % | | Element | Weight % | | Element | Weight % | |
| O | 0.00 | | O | 28.74 | | O | 41.68 | |
| Al | 100.00 | | Al | 71.26 | | Al | 58.32 | |
| Fe | 0.00 | | Fe | 0.00 | | Fe | 0.00 | |

| Point 3 | | | Point 4 | | | Point 5 | | |
|---|---|---|---|---|---|---|---|---|
| Element | Weight % | | Element | Weight % | | Element | Weight % | |
| O | 30.48 | | O | 10.20 | | O | 9.30 | |
| Al | 59.35 | | Al | 70.06 | | Al | 90.70 | |
| Fe | 10.17 | | Fe | 19.74 | | Fe | 0.00 | |

| Point 6 | | | Point 7 | | | Point 8 | | |
|---|---|---|---|---|---|---|---|---|
| Element | Weight % | | Element | Weight % | | Element | Weight % | |
| O | 9.38 | | O | 5.02 | | O | 2.55 | |
| Al | 90.62 | | Al | 94.98 | | Al | 97.45 | |
| Fe | 0.00 | | Fe | 0.00 | | Fe | 0.00 | |

| 5

750 ºC 7 hour hold

Oxide layer ≈ 0.20 μm |



| Spectrum 1 | | Spectrum 2 | | Spectrum 3 | | Spectrum 4 | |
|---|---|---|---|---|---|---|---|
| Element | Weight % | Element | Weight % | Element | Weight % | Element | Weight % |
| O | 41.61 | O | 34.10 | O | 20.43 | O | 34.49 |
| Al | 58.39 | Al | 65.90 | Al | 79.57 | Al | 65.51 |
| Fe | 0.00 | Fe | 0.00 | Fe | 0.00 | Fe | 0.00 |

**Figure 69 continued - EDX spectra for the Al-1%Fe samples melted at 750 °C**

| 6<br><br>750 °C 24 hour hold<br><br>Oxide layer ≈ 0.21 μm |  |

Figure 69 continued - EDX spectra for the Al-1%Fe samples melted at 750 °C

The EDX shows that the oxide contained only Al and O. The presence of Fe did not occur within the oxide itself but appeared in the subsurface regions. There appeared to be a eutectic region in some samples (see 24 hour sample, spectrum 5 in Figure 69), which when in the surface region, increased the Fe content there. This suggested that Fe in Al slows the oxidation. Fe was detected in the regions just beneath the oxide, suggesting that its presence there somehow reduced the oxide thickness of the alloy (Mondolfo 1976).

**Figure 70 - The XRD spectra for Al-1%Fe held for 5 minutes at 750 °C (zoomed out spectra inset)**
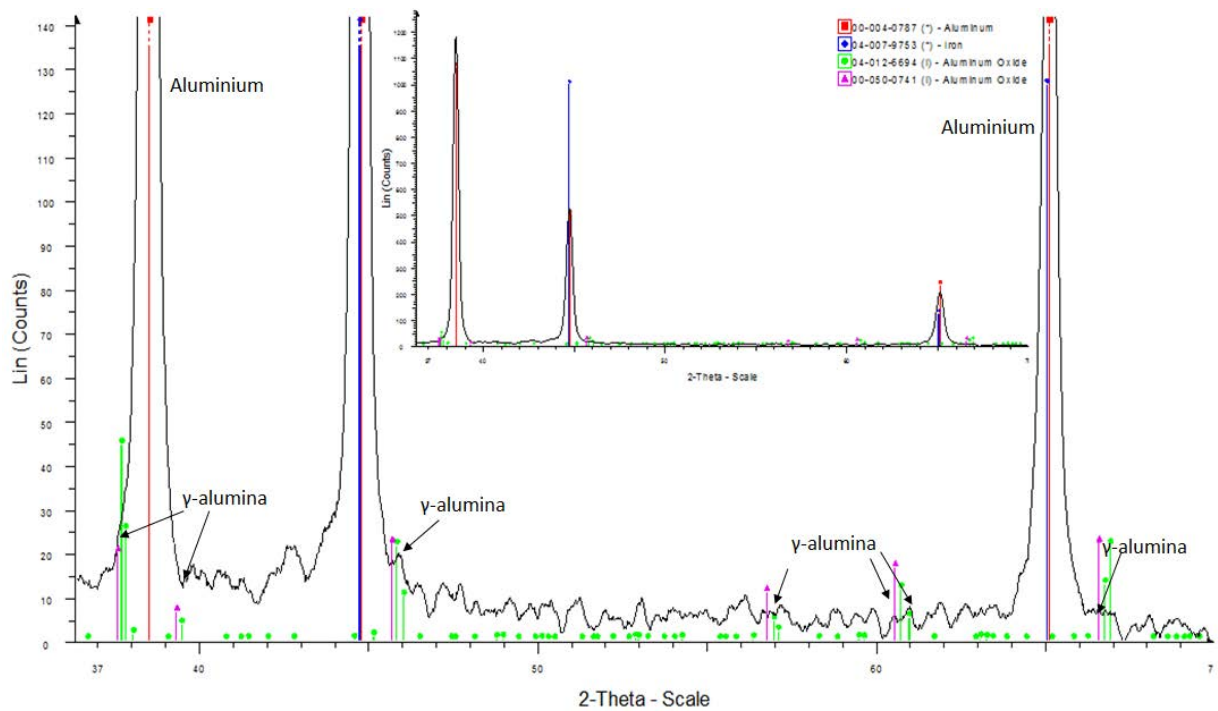


**Figure 71 - The XRD spectra for Al-1%Fe held for 24 hours at 750 °C (zoomed out spectra inset)**

XRD also suggested that the oxide was γ-alumina and that a different phase had not formed. γ-alumina was present at both times suggesting that the oxide was present at the 5 minute holding time, and grew from there, becoming a protective oxide after 3 hours oxidation. It seemed that the Fe present in the alloy was suppressing the oxidation of the alloy, as the thickness is much smaller across the oxidation time (0.21 μm compared to 0.37 μm in SP-Al). A thin layer of FeO (undetected during XRD) may have formed a passivating layer in the subsurface oxide region,

which may explain the small pickup of Fe in EDX analysis. It may have also been the formation of an undetected eutectic phase, seen in the 24 hour sample, which may have stopped diffusion of ions that would cause oxidation.

### 3.1.2.6 – Al 0.3%Sr

SEM images of the Al-0.3%Sr alloy held at different holding times can be seen in Figure 72.

**Figure 72 - Images of Al-0.3%Sr melted at 750 °C for different times**

| Sample | Image |
|---|---|
| 1<br><br>750 ºC 5 min hold<br><br>Oxide layer – too small to measure |  |
| 2<br><br>750 ºC 17 min hold<br><br>Oxide layer – too small to measure |  |

| 3 750 ºC 1 hour hold Oxide layer ≈ 0.42 µm |  |
| 4 750 ºC 3 hour hold Oxide layer ≈ 0.49 µm |  |
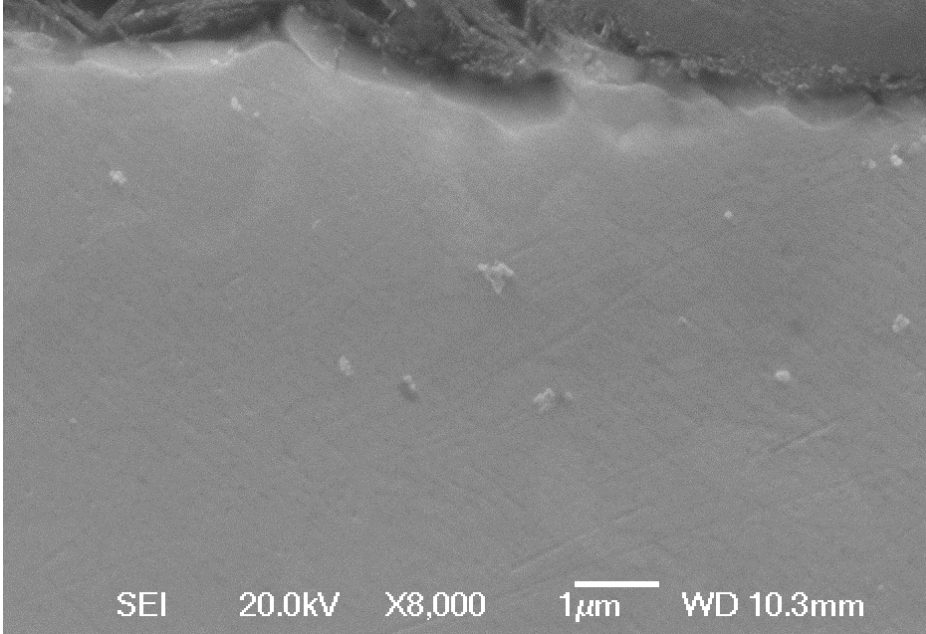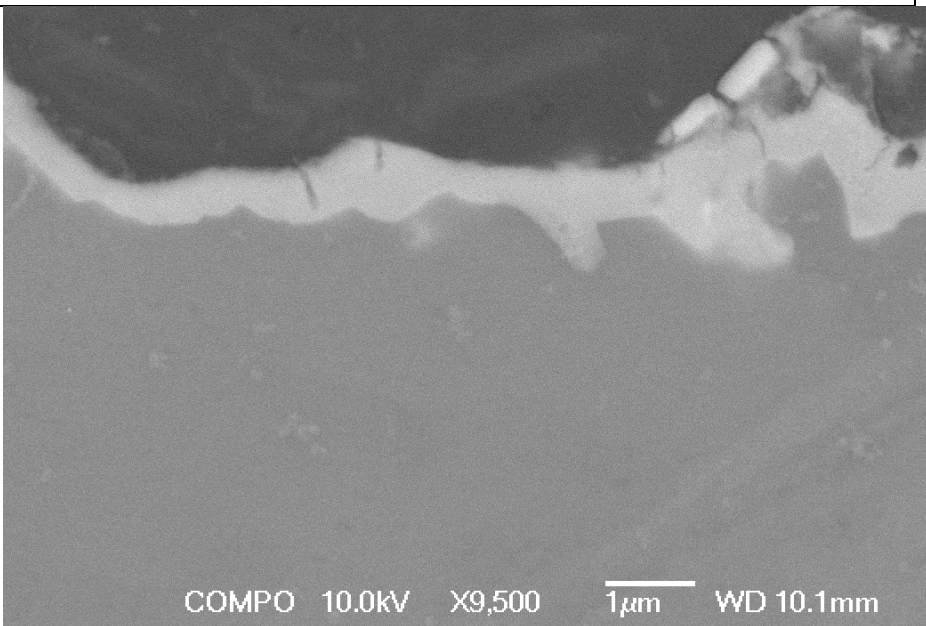
**Figure 72 continued - Images of Al-0.3%Sr melted at 750 °C for different times**
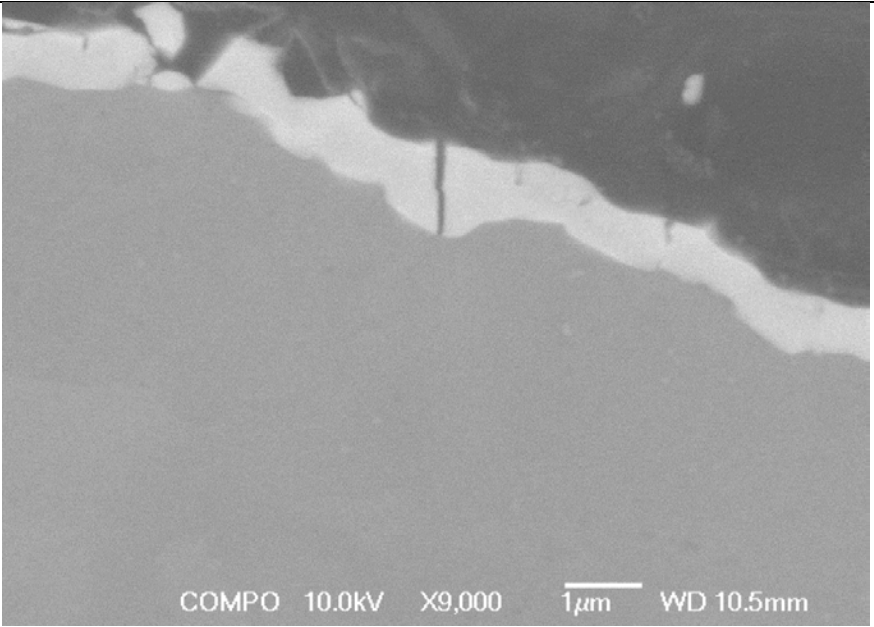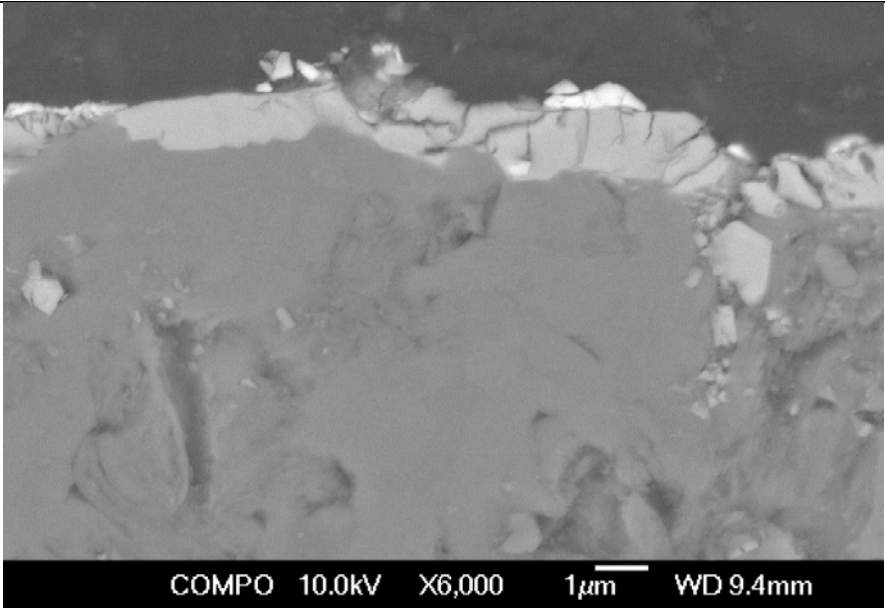
| | |
|---|---|
| 5<br><br>750 °C 7 hour hold<br><br>Oxide layer ≈ 0.64 μm | <br>COMPO 10.0kV X9,000 1μm WD 10.5mm |
| 6<br><br>750 °C 24 hour hold<br><br>Oxide layer ≈ 1.1 μm | <br>COMPO 10.0kV X6,000 1μm WD 9.4mm |

**Figure 72 continued - Images of Al-0.3%Sr melted at 750 °C for different times**

The oxide growth and thickness for the Al-0.3%Sr alloy is summarised in Table 14 and Figure 73. The oxide layer grew over the total oxidation period, by ~1.1 μm, between 5 minutes and 7 hours. The initial oxide was very thin and appeared to be discontinuous, but the oxide was more uniform and continuous after 1 hour oxidation.

113
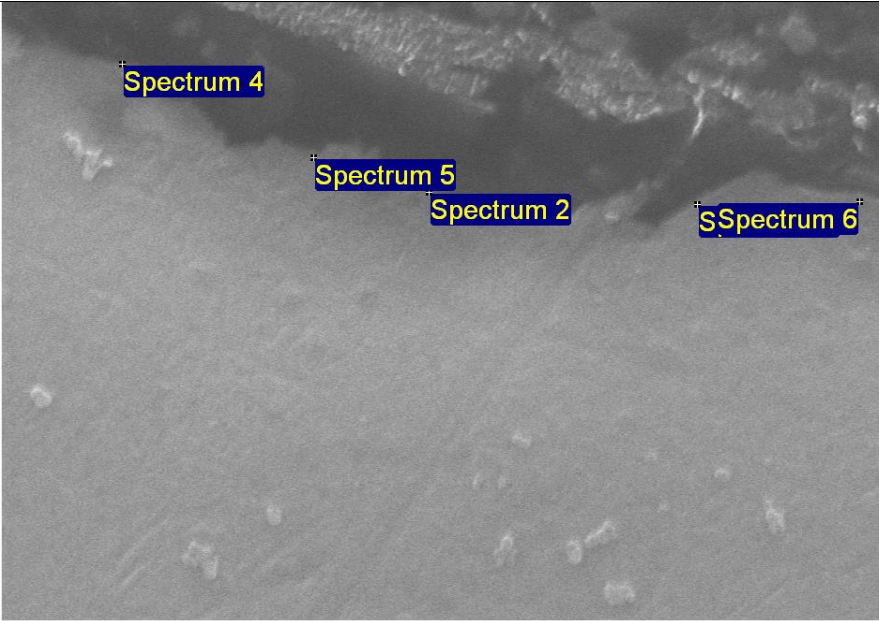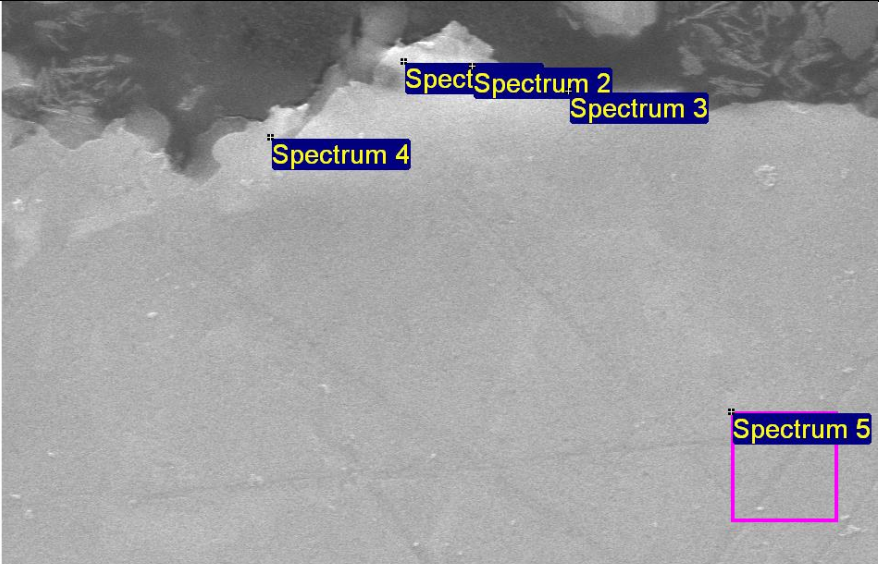
**Table 14 - Thicknesses of oxides for Al-0.3%Sr melted at 750 °C**

| Melt Conditions | Oxide Thickness |
|---|---|
| 750°C 5 min hold | negligible |
| 750°C 17 min hold | negligible |
| 750°C 1 hour hold | 0.42 μm |
| 750°C 3 hour hold | 0.49 μm |
| 750°C 7 hour hold | 0.64 μm |
| 750 °C 24 hour hold | 1.1 μm |
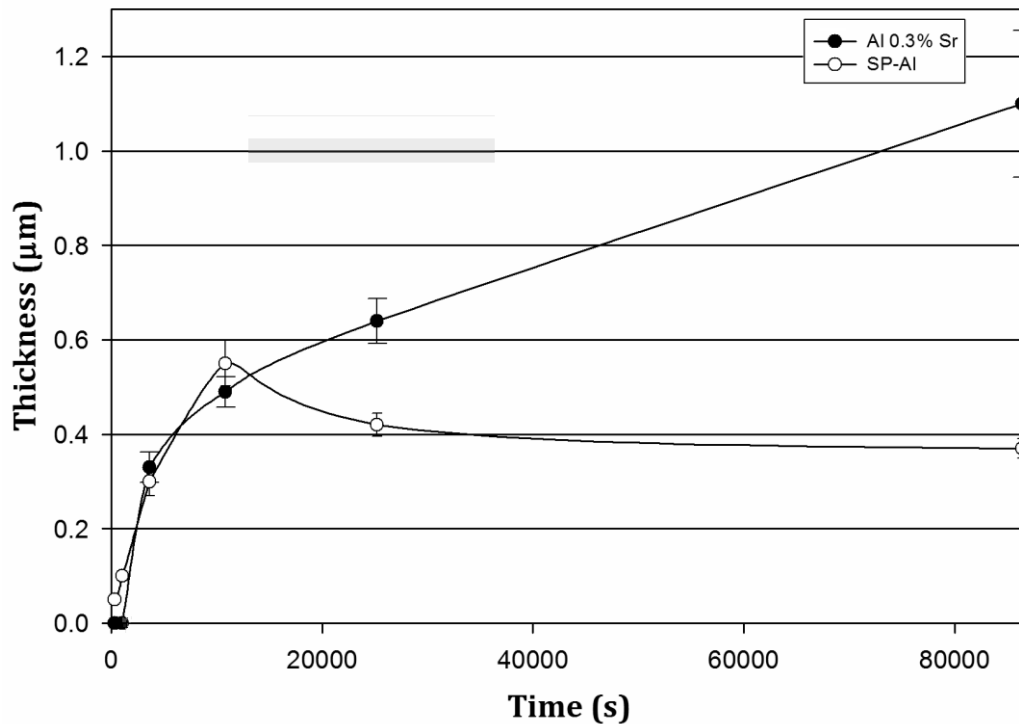


**Figure 73 - Thickness of oxide layer vs. holding time Al 0.3%Sr samples held at 750 °C**

The growth of the oxide thickness suggested that a continuous oxide film formed after 1 hour, and that this slowly grew up to the 24 hour oxidation time. The oxide growth rate followed a similar pattern to SP-Al, but with thinner oxide layers to begin with, but forming a thicker oxide after 24 hours. This implied that the Sr has an effect on how quickly the oxide grew. The initial oxidation rate between 5 minutes and 3 hours was $4.6 \times 10^{-5}$ μm/s, similar to $5.2 \times 10^{-5}$ μm/s for SP-Al and $8.1 \times 10^{-6}$ μm/s, much faster than the apparent reduction in growth rate of $-2.4 \times 10^{-6}$ μm/s for SP-Al. The Sr content of the layers can be seen in the EDX analysis in Figure 74.

**Figure 74 - EDX spectra for the Al-0.3%Sr samples melted at 750 °C**

| Sample | Analysis |
|---|---|
| 1<br><br>750 ºC 5 min hold<br><br>Oxide layer – too small to measure | <br>3µm     Electron Image 1 |

Spectrum 2

| Element | Weight % |
|---|---|
| O | 32.10 |
| Al | 61.29 |
| Sr | 6.61 |

Spectrum 3

| Element | Weight % |
|---|---|
| O | 36.14 |
| Al | 56.92 |
| Sr | 6.94 |

Spectrum 4

| Element | Weight % |
|---|---|
| O | 38.45 |
| Al | 61.55 |
| Sr | 0.00 |

Spectrum 5

| Element | Weight % |
|---|---|
| O | 29.92 |
| Al | 64.67 |
| Sr | 5.42 |

Spectrum 6

| Element | Weight % |
|---|---|
| O | 38.68 |
| Al | 50.27 |
| Sr | 11.05 |

| Sample | Analysis |
|---|---|
| 2<br><br>750 ºC 17 min hold<br><br>Oxide layer – too small to measure | <br>10µm     Electron Image 1 |

Spectrum 1

| Element | Weight % |
|---|---|
| O | 13.17 |
| Al | 86.83 |
| Sr | 0.00 |

Spectrum 2

| Element | Weight % |
|---|---|
| O | 10.13 |
| Al | 89.87 |
| Sr | 0.00 |

Spectrum 3

| Element | Weight % |
|---|---|
| O | 9.19 |
| Al | 90.81 |
| Sr | 0.00 |

Spectrum 4

| Element | Weight % |
|---|---|
| O | 25.93 |
| Al | 66.50 |
| Sr | 7.57 |

Spectrum 5

| Element | Weight % |
|---|---|
| O | 0.00 |
| Al | 100.00 |
| Sr | 0.00 |

**3**

**750 ºC 1 hour hold**

**Oxide layer ≈ 0.42 μm**



7µm    Electron Image 1

| Spectrum 2 | | | Spectrum 3 | | | Spectrum 4 | | |
|---|---|---|---|---|---|---|---|---|
| Element | Weight % | | Element | Weight % | | Element | Weight % | |
| O | 0.00 | | O | 2.77 | | O | 4.79 | |
| Al | 100.00 | | Al | 93.61 | | Al | 87.76 | |
| Sr | 0.00 | | Sr | 3.62 | | Sr | 7.45 | |

| Spectrum 5 | | | Spectrum 6 | | | Spectrum 7 | | |
|---|---|---|---|---|---|---|---|---|
| Element | Weight % | | Element | Weight % | | Element | Weight % | |
| O | 12.28 | | O | 2.62 | | O | 2.59 | |
| Al | 70.82 | | Al | 92.89 | | Al | 95.25 | |
| Sr | 16.90 | | Sr | 4.49 | | Sr | 2.16 | |

**4**

**750 ºC 3 hour hold**

**Oxide layer ≈ 0.49 μm**



6µm    Electron Image 1

| Spectrum 1 | | Spectrum 2 | | Spectrum 3 | | Spectrum 4 | |
|---|---|---|---|---|---|---|---|
| Element | Weight % | Element | Weight % | Element | Weight % | Element | Weight % |
| O | 0.00 | O | 28.99 | O | 36.29 | O | 38.91 |
| Al | 100.00 | Al | 27.81 | Al | 33.79 | Al | 9.46 |
| Sr | 0.00 | Sr | 43.20 | Sr | 29.92 | Sr | 51.64 |

| Spectrum 5 | | Spectrum 6 | | Spectrum 7 | | Spectrum 8 | |
|---|---|---|---|---|---|---|---|
| Element | Weight % | Element | Weight % | Element | Weight % | Element | Weight % |
| O | 27.62 | O | 26.36 | O | 26.73 | O | 28.63 |
| Al | 33.23 | Al | 33.85 | Al | 36.96 | Al | 28.36 |
| Sr | 39.15 | Sr | 39.80 | Sr | 36.30 | Sr | 43.01 |

**Figure 74 continued - EDX spectra for the Al-0.3%Sr samples melted at 750 °C**

| 5 |  |
|---|---|
| 750 ºC 7 hour hold<br><br>Oxide layer ≈ 0.64 μm | |

Spectrum 1
| Element | Weight % |
|---|---|
| O | 0.00 |
| Al | 100.00 |
| Sr | 0.00 |

Spectrum 2
| Element | Weight % |
|---|---|
| O | 24.55 |
| Al | 34.74 |
| Sr | 40.71 |

Spectrum 3
| Element | Weight % |
|---|---|
| O | 27.50 |
| Al | 28.03 |
| Sr | 44.47 |

Spectrum 4
| Element | Weight % |
|---|---|
| O | 28.48 |
| Al | 30.15 |
| Sr | 41.37 |

Spectrum 5
| Element | Weight % |
|---|---|
| O | 26.02 |
| Al | 34.44 |
| Sr | 39.53 |

Spectrum 6
| Element | Weight % |
|---|---|
| O | 30.97 |
| Al | 26.78 |
| Sr | 42.25 |

Spectrum 7
| Element | Weight % |
|---|---|
| O | 25.12 |
| Al | 35.74 |
| Sr | 39.14 |

Spectrum 8
| Element | Weight % |
|---|---|
| O | 7.86 |
| Al | 80.68 |
| Sr | 11.46 |

| 6 |  |
|---|---|
| 750 ºC 24 hour hold<br><br>Oxide layer ≈ 1.1 μm | |

Point 1
| Element | Weight % |
|---|---|
| O | 17.69 |
| Al | 28.56 |
| Sr | 53.75 |

Point 2
| Element | Weight % |
|---|---|
| O | 12.47 |
| Al | 29.91 |
| Sr | 57.62 |

Point 3
| Element | Weight % |
|---|---|
| O | 9.96 |
| Al | 42.58 |
| Sr | 47.46 |

Point 4
| Element | Weight % |
|---|---|
| O | 1.18 |
| Al | 90.91 |
| Sr | 7.91 |

Point 5
| Element | Weight % |
|---|---|
| O | 0.00 |
| Al | 100.00 |
| Sr | 0.00 |

Point 6
| Element | Weight % |
|---|---|
| O | 0.00 |
| Al | 100.00 |
| Sr | 0.00 |

Point 7
| Element | Weight % |
|---|---|
| O | 0.00 |
| Al | 100.00 |
| Sr | 0.00 |

Point 8
| Element | Weight % |
|---|---|
| O | 0.00 |
| Al | 100.00 |
| Sr | 0.00 |

**Figure 74 continued - EDX spectra for the Al-0.3%Sr samples melted at 750 °C**
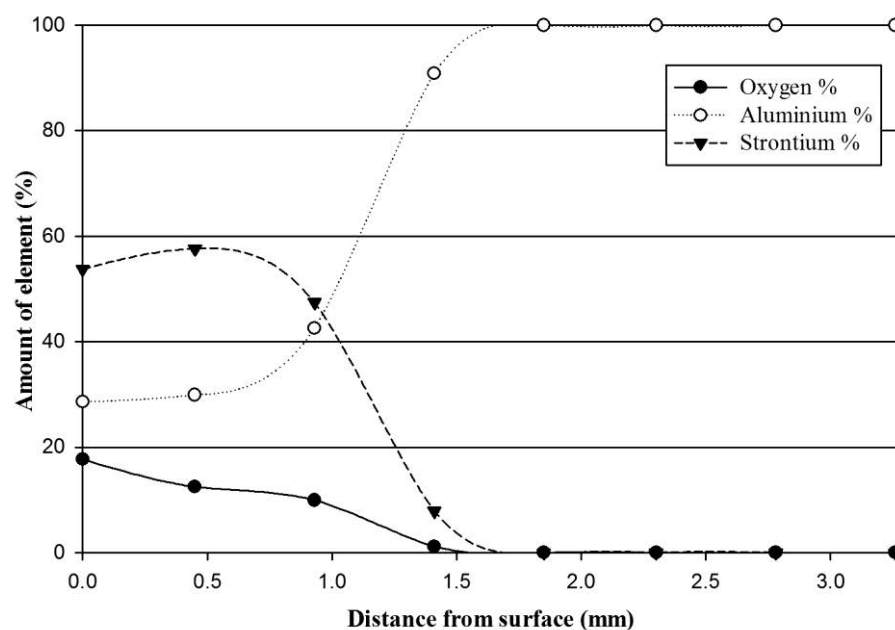
**Figure 75 - Amount of elements vs. distance from the oxide surface, of Al-0.3%Sr held for 24 hours**

The EDS results in Figure 74 show that oxygen was present in the surface layer over the full 24 hour period for the Al-0.3%Sr, suggesting the presence of an oxide on the surface throughout the experimental period. There was also Sr present in the layers, suggesting that Sr had an influence on the growth of the oxide layer. There was little Sr present in the area below the oxide layer, suggesting that there was diffusion of Sr from the alloy to the oxide, as shown in Figure 75. The XRD spectra of the 5 minute and 24 hour samples can be seen in Figure 76 and Figure 77.
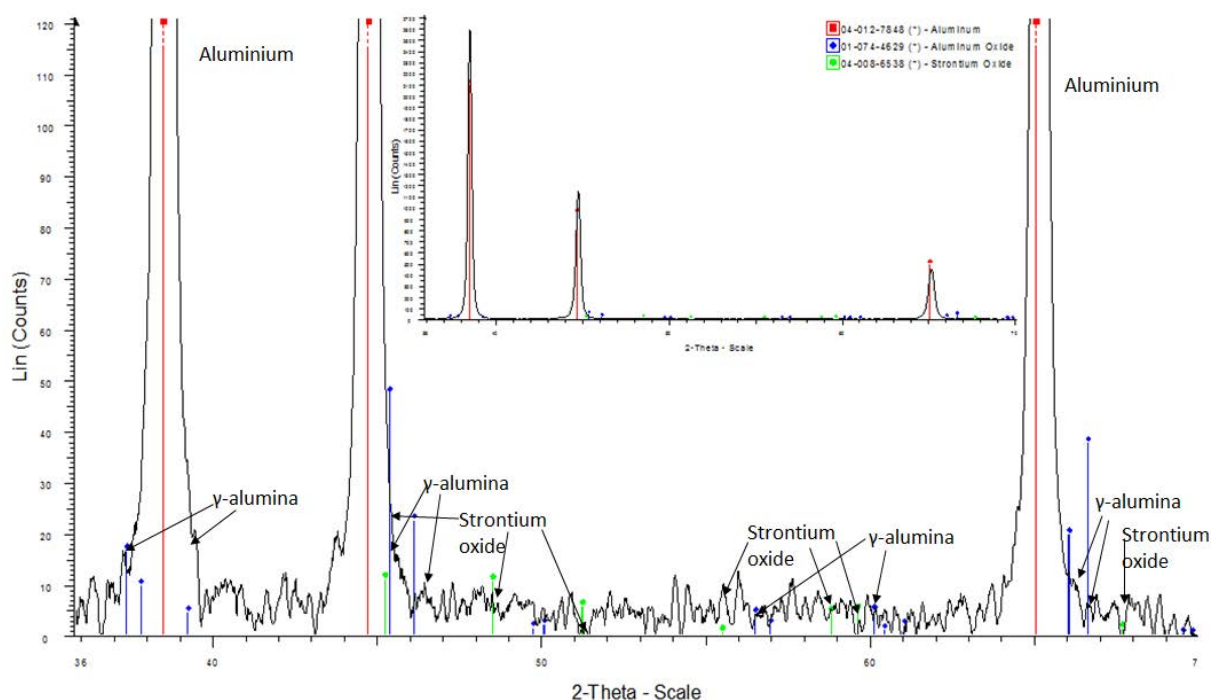


**Figure 76 - The XRD spectra for Al-0.3%Sr held for 5 minutes at 750 °C (zoomed out spectra inset)**
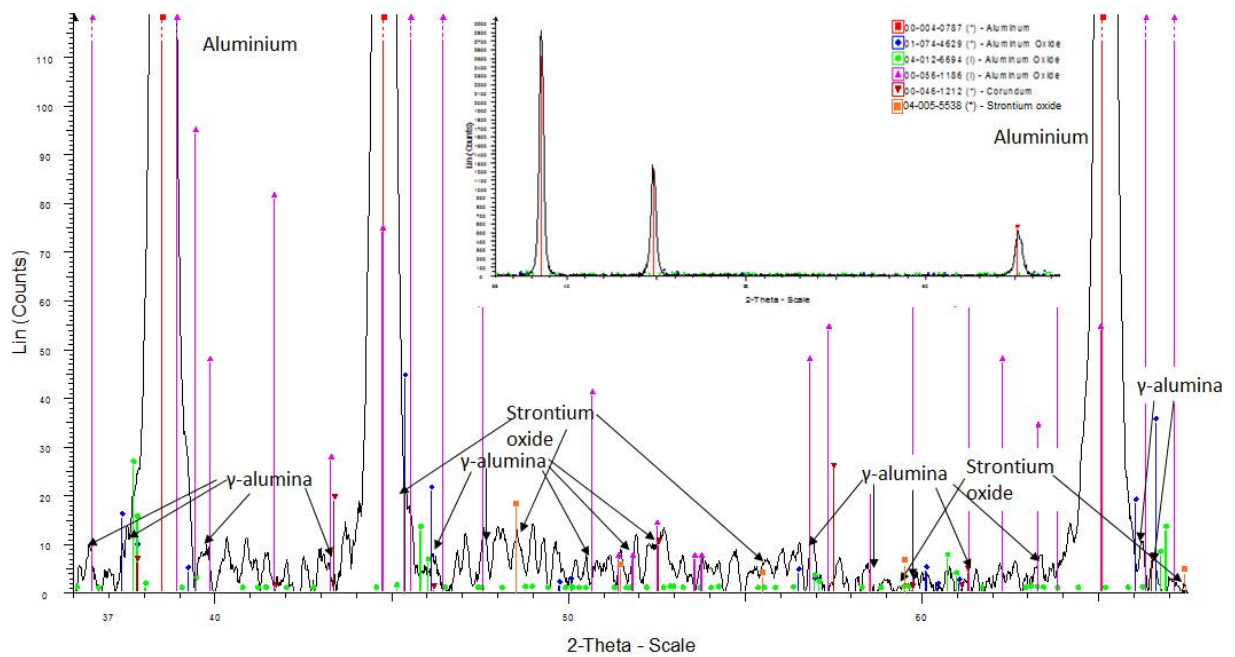
**Figure 77 - The XRD spectra for Al-0.3%Sr held for 24 hours at 750 °C (zoomed out spectra inset)**

The XRD results in Figure 76 and Figure 77 show that γ-alumina and SrO were present in the oxide layers for all holding times. The α-alumina was not present, but as breakaway oxidation had not occurred, as seen in Figure 73, this was unlikely anyway. A separate oxide of SrO had also formed. It is likely that the presence of SrO increased the oxidation rate, as it is non-passivating oxide (0.61 Pilling Bedworth ratio).

### 3.1.2.7 – Al 0.25%Ti

SEM images of the Al-0.25%Ti alloy held at different holding times can be seen in Figure 78.

**Figure 78 - Images of Al-0.25%Ti melted at 750 °C for different times**

| Sample | Image |
|---|---|
| 750 ºC 5 min hold<br><br>Oxide layer ≈ 0.05 μm |  |

| | |
|---|---|
| 750 °C 1 hour hold<br><br>Oxide layer ≈ 0.1 μm |  |
| 750 °C 24 hour hold<br><br>Oxide layer ≈ 0.17 μm |  |
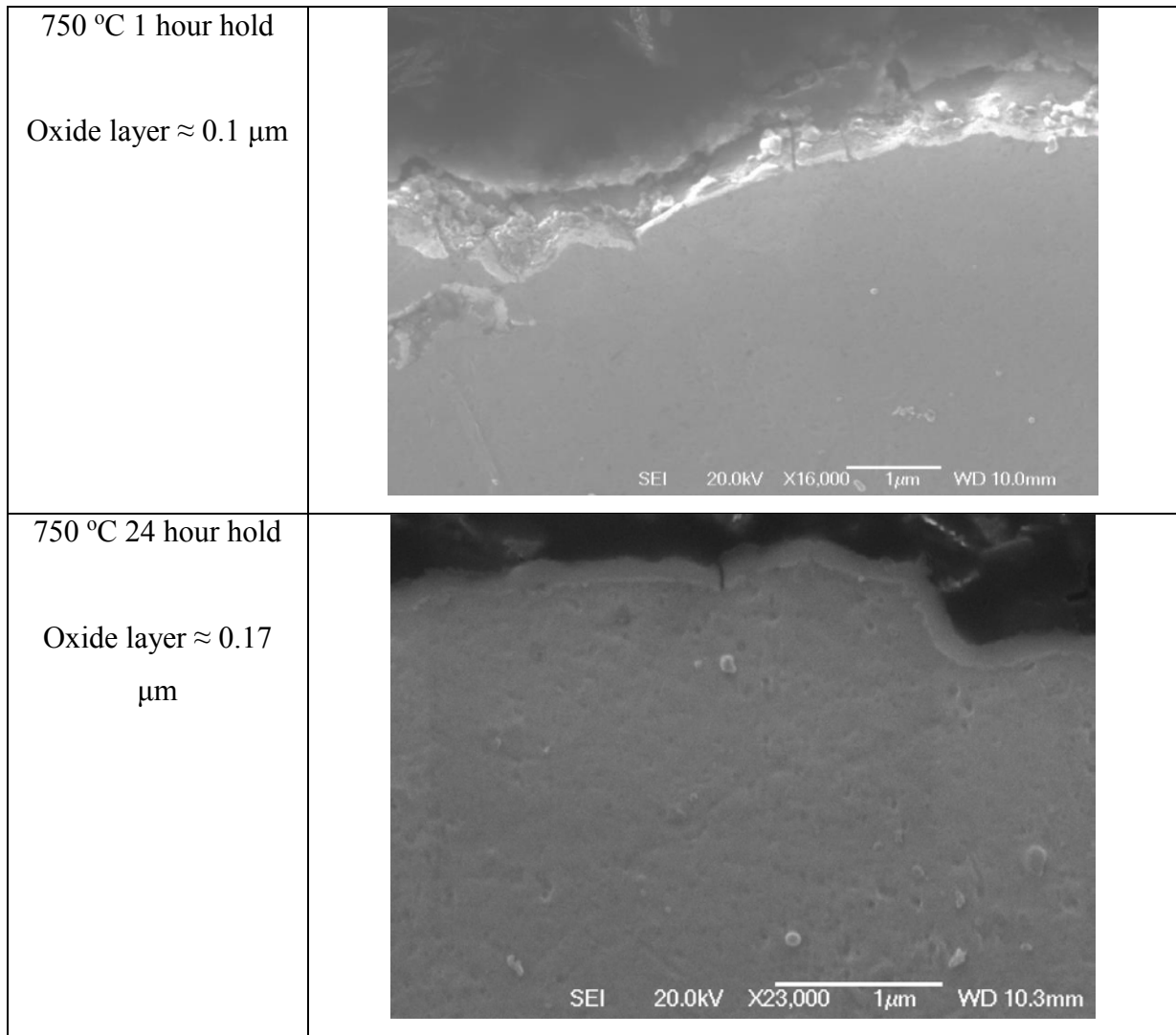
**Figure 78 - Images of Al-0.25%Ti melted at 750 °C for different times**

The oxide thickness increased by ~0.11 μm over the 24 hour oxidation period. The oxide layers were thinner than those formed in SP-Al, and it seems that Ti reduced the rate of oxidation more than any of the other alloying additions. The summary of the thickness changes can be seen in Table 15 and Figure 79.

**Table 15 - Thicknesses of oxides for Al-0.25%Ti melted at 750 °C**

| Melt Conditions | Oxide Thickness |
|---|---|
| 750°C 5 min hold | 0.06 μm |
| 750°C 1 hour hold | 0.10 μm |
| 750°C 24 hour hold | 0.17 μm |
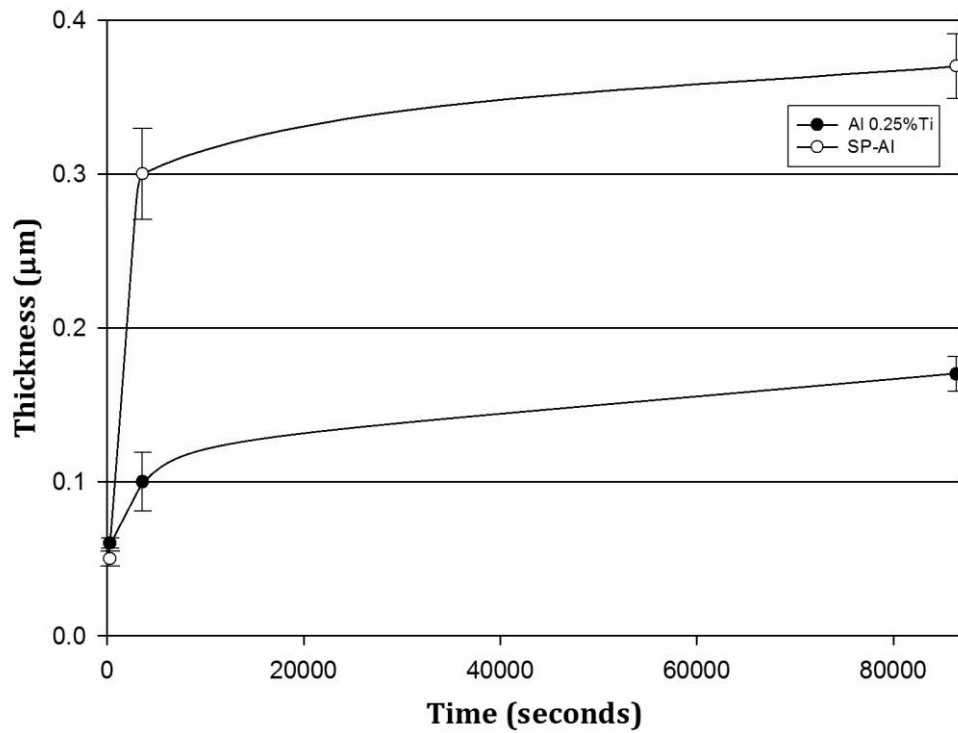
**Figure 79 - Thickness of oxide layer vs. holding time Al 0.25%Ti samples held at 750 °C, compared to SP-Al**

The oxidation seemed to follow a similar pattern to the SP-Al, but with thinner films formed. Between 5 minutes and 1 hour the oxide increased by ~0.04 μm, compared to 0.25 μm for SP-Al, and by ~0.07 μm between 1 hour and 24 hours, the same amount as SP-Al increased by. The oxide formed after 24 hours was 0.2 μm thinner than the same for SP-Al. There was an initial large increase in thickness at a rate of $1.2 \times 10^{-5}$ μm/s, followed by a slower, steadier increase in thickness at a rate of $8.5 \times 10^{-7}$ μm/s. That suggested a stable oxide being present at the 24 hour oxidation time. Elemental analysis of the surface layer regions can be seen in the EDX analysis of Figure 80.

**Figure 80 - EDX spectra for the Al-0.25%Ti samples melted at 750 °C**

| Sample | Analysis |
|--------|----------|
| AT1<br><br>750 ºC 5 min hold<br><br>Oxide layer ≈ 0.06 μm |  |

Spectrum 1

| Element | Weight % |
|---------|----------|
| O | 0.00 |
| Al | 100.00 |
| Ti | 0.00 |

Spectrum 2

| Element | Weight % |
|---------|----------|
| O | 7.89 |
| Al | 92.11 |
| Ti | 0.00 |

Spectrum 3

| Element | Weight % |
|---------|----------|
| O | 10.17 |
| Al | 89.83 |
| Ti | 0.00 |

Spectrum 4

| Element | Weight % |
|---------|----------|
| O | 8.96 |
| Al | 91.04 |
| Ti | 0.00 |

Spectrum 5

| Element | Weight % |
|---------|----------|
| O | 0.00 |
| Al | 100.00 |
| Ti | 0.00 |

AT3

750 ºC 1 hour hold

Oxide layer ≈ 0.10 μm



Spectrum 1

| Element | Weight % |
|---------|----------|
| O | 0.00 |
| Al | 100.00 |
| Ti | 0.00 |

Spectrum 2

| Element | Weight % |
|---------|----------|
| O | 46.11 |
| Al | 53.89 |
| Ti | 0.00 |

Spectrum 3

| Element | Weight % |
|---------|----------|
| O | 31.38 |
| Al | 68.62 |
| Ti | 0.00 |

Spectrum 4

| Element | Weight % |
|---------|----------|
| O | 3.90 |
| Al | 96.10 |
| Ti | 0.00 |

Spectrum 5

| Element | Weight % |
|---------|----------|
| O | 38.88 |
| Al | 61.12 |
| Ti | 0.00 |

Spectrum 6

| Element | Weight % |
|---------|----------|
| O | 41.25 |
| Al | 58.75 |
| Ti | 0.00 |

Spectrum 7

| Element | Weight % |
|---------|----------|
| O | 17.85 |
| Al | 82.15 |
| Ti | 0.00 |

| AT6<br><br>750 °C 24 hour hold<br><br>Oxide layer ≈ 0.17 μm | (SEM image with Spectrum 1–5 labels, 2μm scale, Electron Image 1) |

Spectrum 1

| Element | Weight % |
|---------|----------|
| O | 24.25 |
| Al | 75.75 |
| Ti | 0.00 |

Spectrum 2

| Element | Weight % |
|---------|----------|
| O | 25.28 |
| Al | 74.72 |
| Ti | 0.00 |

Spectrum 3

| Element | Weight % |
|---------|----------|
| O | 27.04 |
| Al | 72.96 |
| Ti | 0.00 |

Spectrum 4

| Element | Weight % |
|---------|----------|
| O | 27.03 |
| Al | 72.97 |
| Ti | 0.00 |

Spectrum 5

| Element | Weight % |
|---------|----------|
| O | 0.00 |
| Al | 100.00 |
| Ti | 0.00 |

**Figure 80 continued - DX spectra for the Al-0.25%Ti samples melted at 750 °C**

It can be seen in Figure 80 that the oxide layers contained no Ti, suggesting that only alumina was present in the oxide, with no secondary oxides forming. However, the presence of the Ti had a large influence on the growth rate of the oxide, suppressing the oxide growth by a significant factor. XRD analysis was undertaken to determine the structure of the layer and sub-layer region and the results can be seen in Figure 81 and Figure 82.
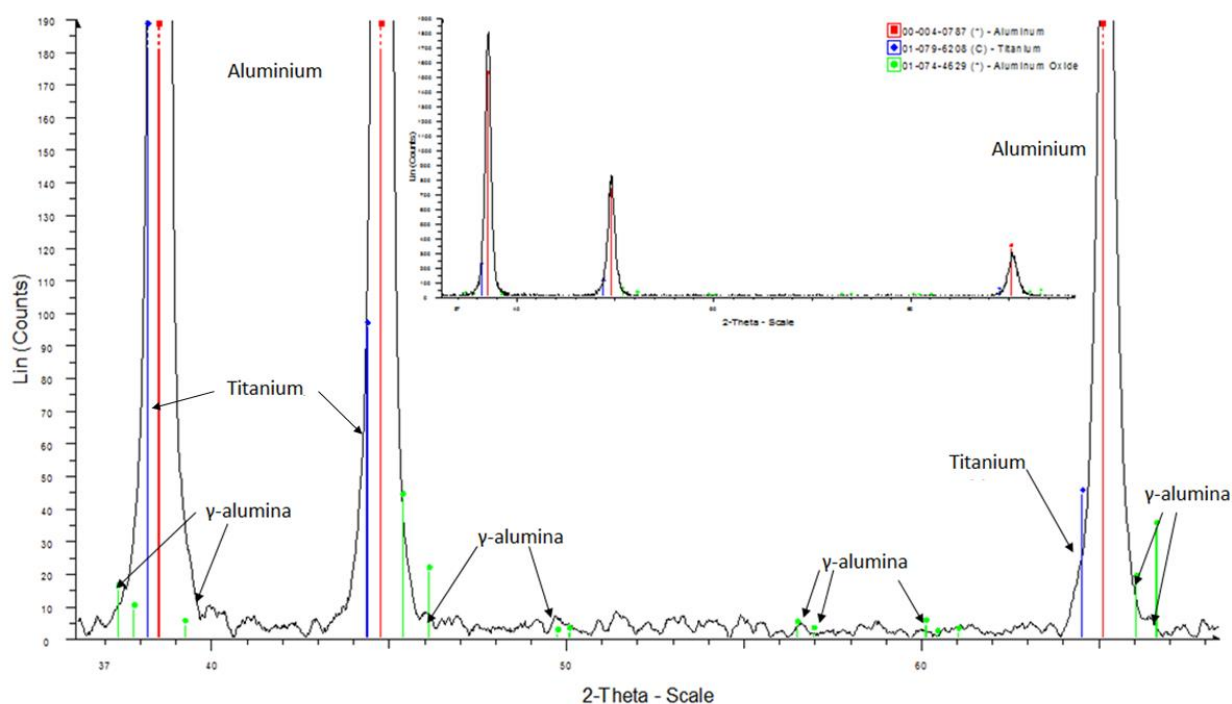


**Figure 81 - The XRD spectra for Al-0.25%Ti held for 5 minutes at 750 °C (zoomed out spectra inset)**
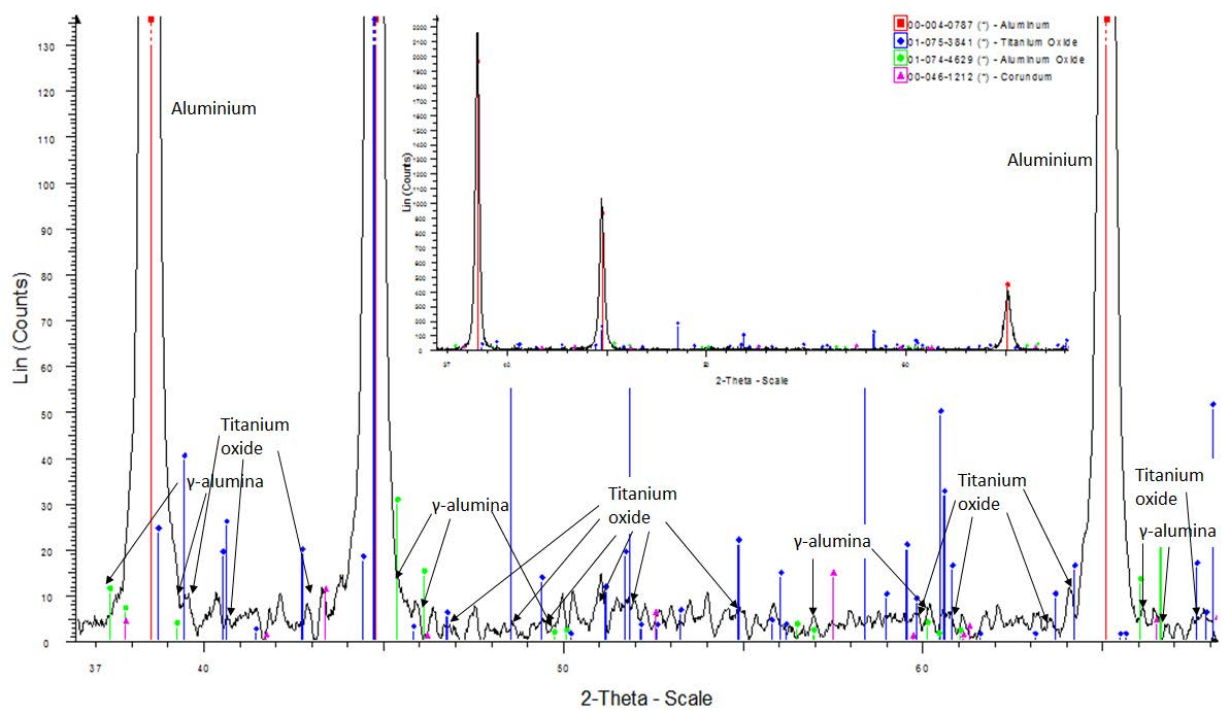
**Figure 82 - The XRD spectra for Al-0.25%Ti held for 24 hours at 750 °C (zoomed out spectra inset)**

There are signals for γ-alumina in both spectra, suggesting that it is the only aluminium oxide present. There is a signal for Ti in the 5 minute sample, but $TiO_2$ is detected at 24 hours. There was no Ti picked up within the oxide layers by EDX, so the presence of Ti may have had an effect within the bulk, perhaps hindering diffusion and so slowing down the oxidation mechanism. The presence of $TiO_2$ in the 24 hour sample suggests that the oxygen has reacted with the Ti in the alloy. This may suppress oxidation better than Ti by itself, and so the combination of $TiO_2$ and continuous γ-alumina prove to have good resistance to oxidation.3.1.3. – Summary of Oxidation Results

The addition of different elements to SP-Al affected the oxidation rate in different ways. The presence of Mg within the alloys of Al-4%Mg and Al-7%Si-0.3%Mg increased the overall rate of oxidation from $3.7 \times 10^{-6}$ μm/s to $2.2 \times 10^{-5}$ μm/s (between 5 minutes and 1 hour) and $1.1 \times 10^{-5}$ μm/s respectively. This was evident in the increase of the final oxide thicknesses of 0.37 μm, 1.56 μm and total oxidation of the sample for SP-Al, Al-7%Si-0.3%Mg and Al-4%Mg respectively. The formation of the non-passivated oxide layer of MgO was most likely to be the reason for this. Addition of Cu also increased the oxidation rate to $1.63 \times 10^{-5}$ μm/s with an oxide thickness of 1.72 μm after 24 hours. This was likely due to the effect of the $CuAl_2$ phase that formed within the oxide. The oxidation rate was also increased by the addition of Sr in the Al-0.3%Sr alloy, which increased the oxidation rate to $1.27 \times 10^{-5}$ μm/s. The oxide layer of a thickness 1.1 μm contained SrO, a non-passivating oxide, which likely increased the rate. The addition of Si did little to change the oxidation rate ($3.1 \times 10^{-6}$ μm/s). The addition of Fe and Ti reduced the oxidation rate by reducing diffusion of oxygen through the oxide layer. The

124

oxidation rates were 1.97 x 10$^{-6}$ μm/s for Al-Ti and 1.27 x 10$^{-6}$ μm/s for Al-Ti, and the oxide thicknesses were 0.21 μm and 0.17 μm respectively. The Al-Ti alloy formed $TiO_2$ after 24 hours, a protective oxide, and this would have slowed the oxidation of the alloy.

## 3.2 - Aluminium and Molybdenum

An accidental contamination of a superpure aluminium sample by molybdenum powder occurred, revealing a unique appearance (for a sample held at 750 °C for 7 hours in air – seen in Figure 83). The oxide layer in the Mo contaminated SP-Al sample was ~3.4 μm, compared to a thickness of ~0.42 μm in SP-Al sample. EDX analysis on the layer indicated a high level of Mo present within the surface oxide, typically 60-70 wt.% (~10 wt.% $O_2$, ~20-30 wt.% Al). There appeared to be different phases of oxide, but it was not possible to determine their structure. This led to the idea that Mo may have an effect on the oxide layer and grain refinement, which led to further investigation.
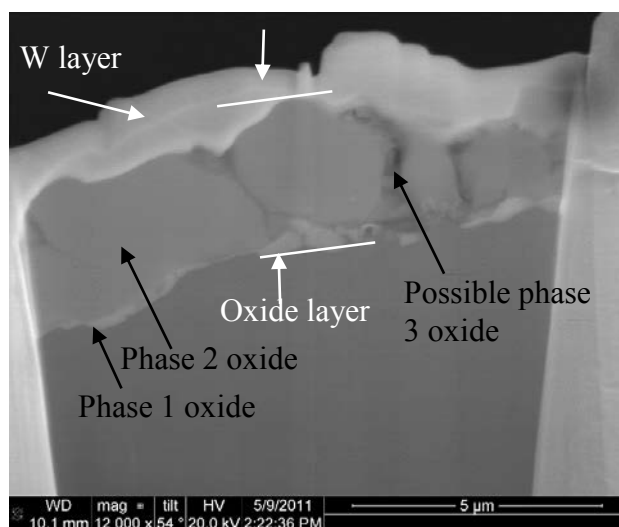


**Figure 83 - SP-Al held for 7 hours at 750 °C, with accidental Mo contamination (courtsey of Dr K Kim)**

3.2.1 - Al with Mo Powder Additions

The thickness of the oxide layers can be seen in Table 16. It can be seen that the oxide thickness was greater in samples with additions of Mo powder, with breakaway oxidation appearing to occur much sooner; between 5 and 17 minutes for Mo samples, compared to between 3 and 7 hours for SP-Al. These samples are referred to as 'Al + Mo powder'.

**Table 16 - Oxide thickness of Superpure Al and samples with Mo powder additions**

| Composition | Oxide thickness of alloy (μm) | | | | | |
|---|---|---|---|---|---|---|
| | 5 min | 17 min | 1 hour | 3 hour | 7 hour | 24 hours |
| Superpure Al | 0.05 | 0.1 | 0.30 | 0.53 | 0.42 | 0.37 |
| Al + 3g Mo powder | 0.34 | 1.93 | 4.21 | 5.00 | 1000 | 1000 |

The presence of molybdenum powder on the surface of a molten SP-Al charge increases its oxidation rate by almost 1000 μm. Figure 84 shows the change in oxide thicknesses with holding time of the samples. It can be seen that the oxide thickness for the samples with the Mo

powder additions was much larger than those without, with almost a tenfold increase in thickness.
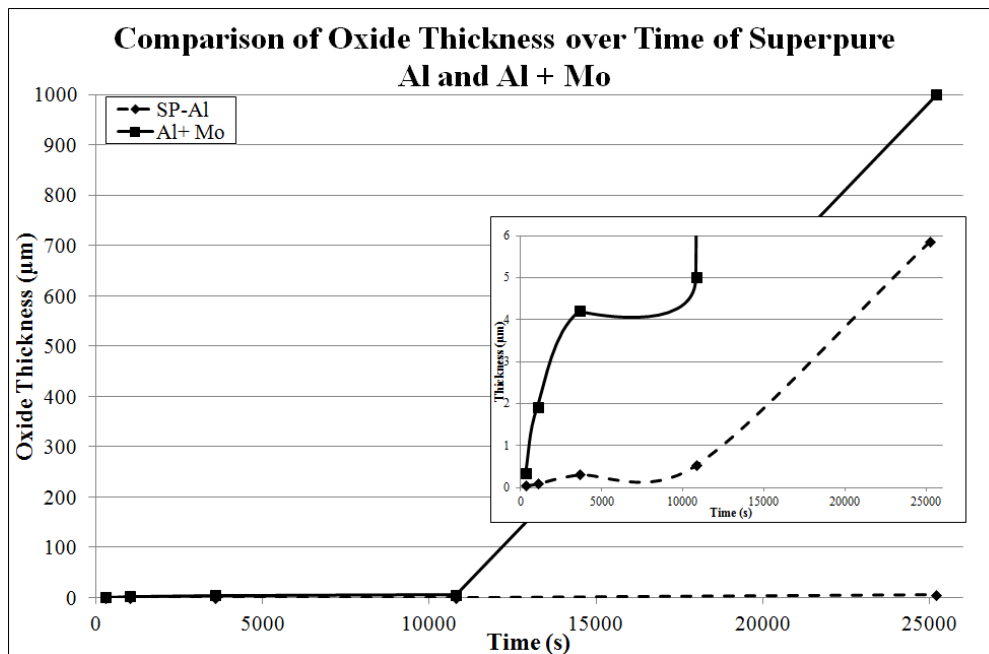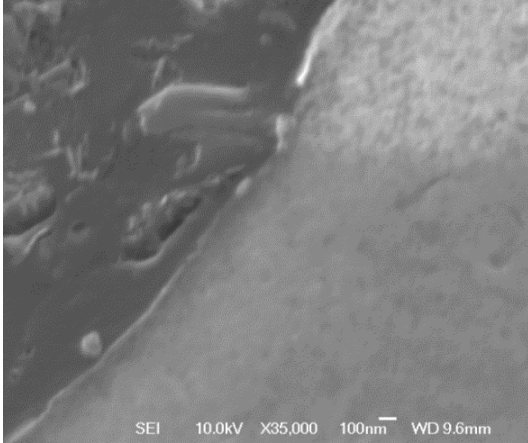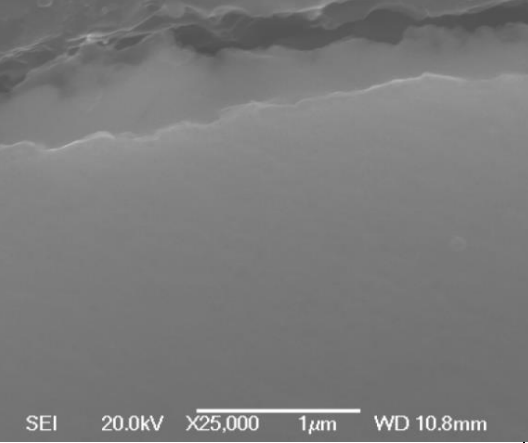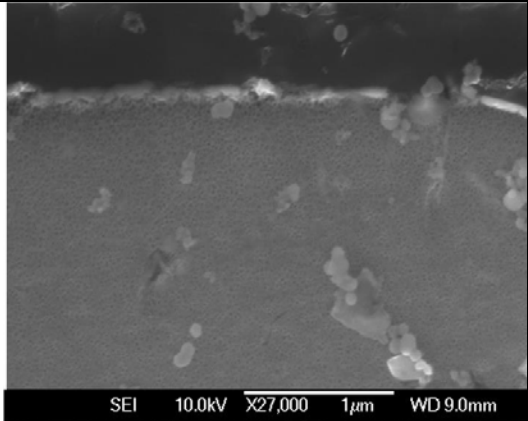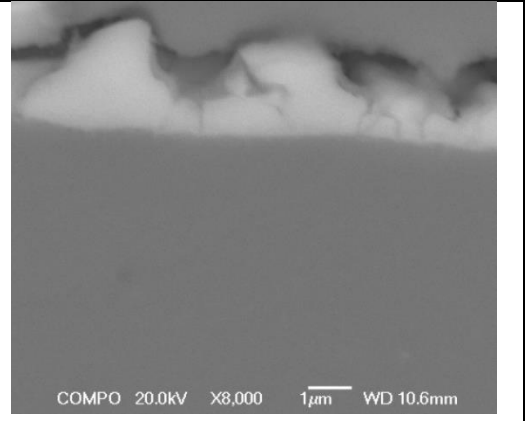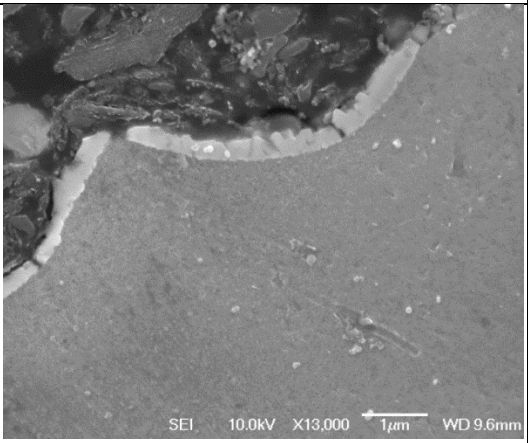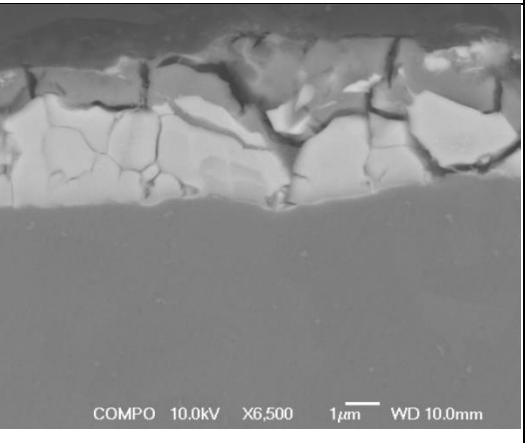


**Figure 84 - Graph of Oxide Thickness of SP-Al samples and Al + 3g Mo samples. Inset graph is a zoom in on the thicknesses up to 6 μm**

Figure 85 shows cross sections of the oxides on samples of SP-Al and with Mo powder additions. It can be seen that the oxide thickness was greater on the samples with the Mo powder additions, increasing from 0.05 μm on SP-Al to 0.34 μm for Al + 3g Mo at 5 minutes. The thickness increased to over 1000 μm after 24 hours, compared to 0.37 μm for SP-Al and the oxidation rate between 5 minutes and 3 hours was $4.4 \times 10^{-4}$ μm/s for Al + Mo powder, much faster than the overall rate of $3.7 \times 10^{-6}$ μm/s for SP-Al. After holding for 7 hours the oxide on the SP-Al sample was uniform whereas that on the Al + Mo sample was not, with a very porous, uneven oxide. This and the larger thickness suggest a different oxide and oxidation sequence may be occurring on the sample.

127

**Figure 85 - Comparison of oxide layers for superpure aluminium only and samples with molybdenum powder additions**

| Time step | SP-Al | Al + Mo |
|---|---|---|
| 5 minutes | <br>~0.045 μm | <br>~0.34 μm |
| 17 minutes | <br>~0.085 μm | <br>~1.925 μm |
| 1 hour | <br>~0.305 μm | <br>~4.208 μm |

| 3 hours | ~0.525 µm | ~5.01 µm |
| 7 hours | ~0.42 µm | ~1000 µm |
| 24 hours | ~0.37 µm | ~1000 µm |
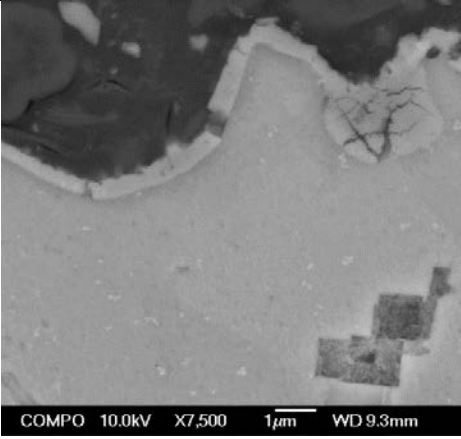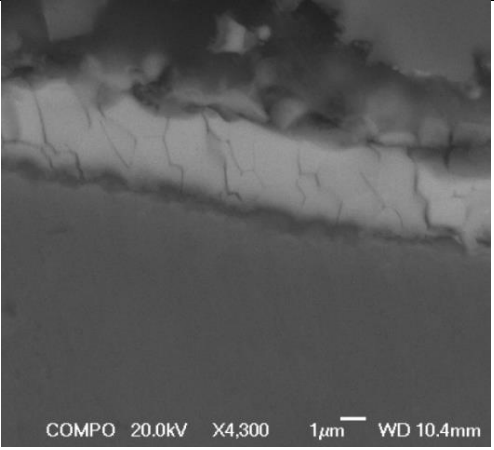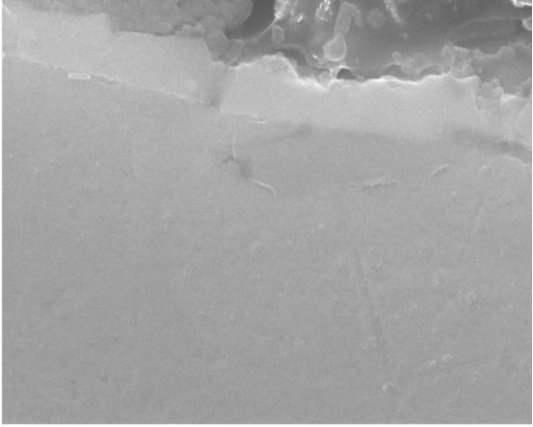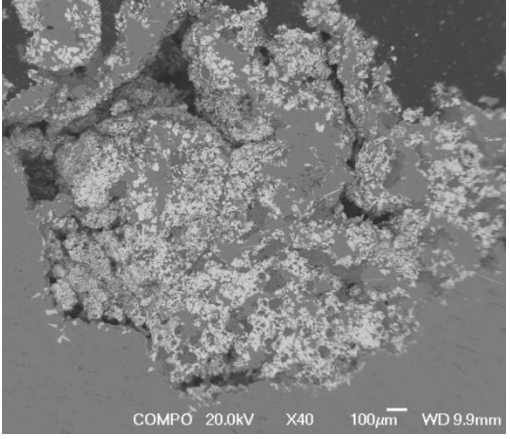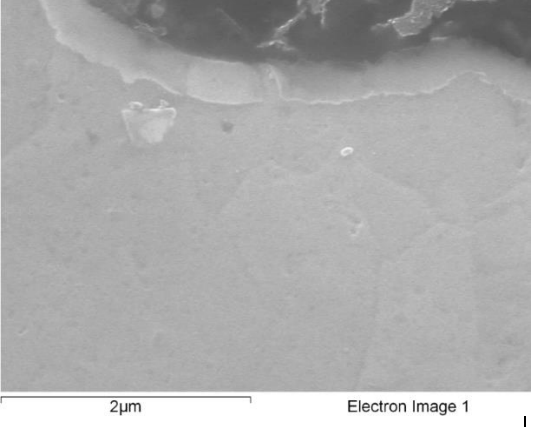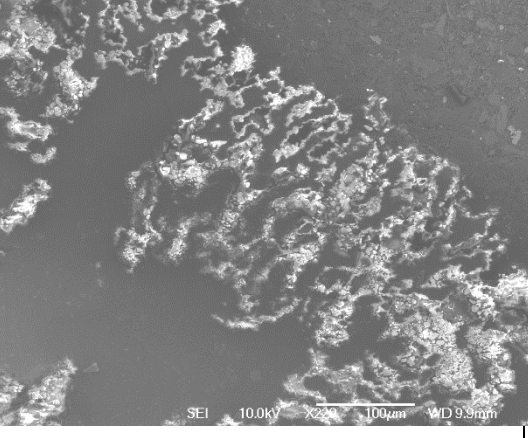
**Figure 85 continued - Comparison of oxide layers for superpure aluminium only and samples with molybdenum powder additions**

The oxides on the SP-Al samples were continuous and appeared to be of one phase. From the images in Figure 85 the oxides on the Al + 3g Mo samples appear to have different phases present, as the backscattered images show two phases present within the layer, which can be seen in the 1 hour sample of Al + 3g Mo powder in Figure 85.

The XRD analysis for the Al + 3g Mo powder samples can be seen in Figure 86, Figure 87 and Figure 88. The sample held at 5 minutes, Figure 86, appeared to contain different oxides. Molybdenum oxide ($MoO_3$), γ-alumina and possibly α-alumina were indicated. The sample held for 1 hour seemed to contain a different form of molybdenum oxide, $MoO_2$, which has a similar structure to $MoO_3$ (monoclinic). XRD of the sample held for 24 hours shows that Al was present along with $MoO_3$, Aluminium Molybdenum Oxide ($Al_2(MoO_4)_3$), γ-Alumina and α-Alumina. The layer grew from 0.34 μm to over 1000 μm in thickness. The presence of Mo increased the oxide thickness, possibly by forming separate oxides. It also seems that an oxide of $Al_2(MoO_4)_3$ formed at longer holding times. It appeared to be a mixed oxide, but it formed as a result of longer holding times; up to 24 hours. Its structure is orthorhombic, suggesting that it formed as a result of Mo becoming incorporated into the γ-alumina, as it is close in structure to the structure of γ-alumina (tetragonal).
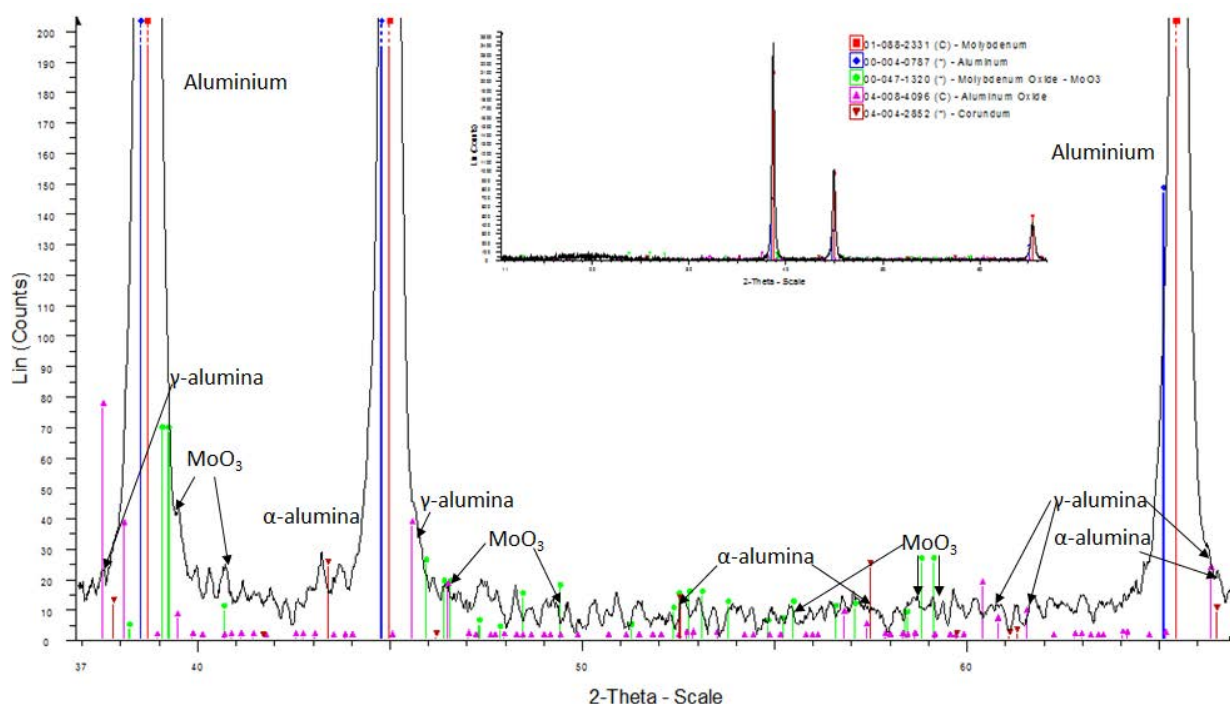


**Figure 86 - The XRD spectra for Al + Mo held for 5 minutes at 750 °C**
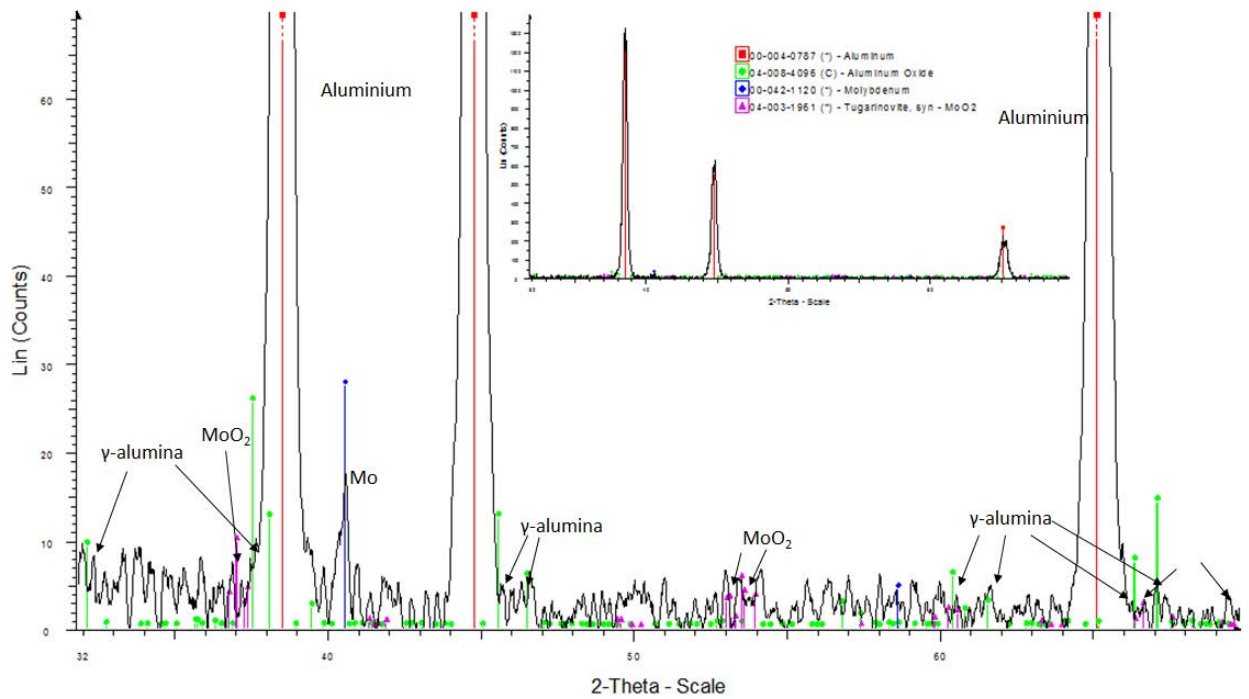
**Figure 87 - The XRD spectrum for Al + Mo held for 1 hour at 750 °C**
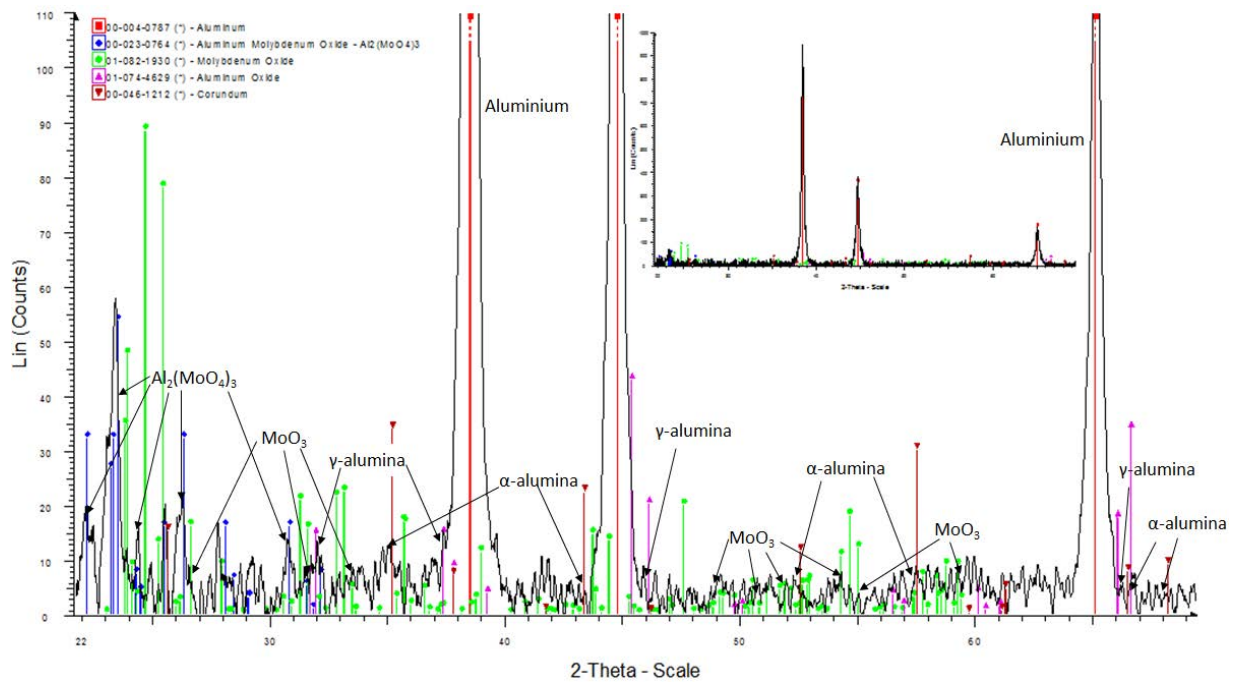


**Figure 88- The XRD spectrum for Al + Mo held for 24 hours at 750 °C**

The XRD data also indicated that α-alumina formed. This could explain why the oxide is much thicker, as the formation of the α-alumina has an associated volume decrease of 24% (Impey et al 1988), causing the oxide to crack and expose the liquid aluminium to air. It also could have been due to the changing structure of the Mo-oxides, which would have associated volume changes and crack the oxide, exposing liquid Al to air and increasing the oxidation rate.

131

## 3.2.2 - Al -1% Mo Alloy

An Al-1%Mo alloy was melted at 750 °C and held for different holding times. The cross sections of the samples were observed using SEM and, compared with the Mo-free metal, can be seen in Figure 89.

**Figure 89 - Comparison of oxide layers for SP-Al and Al-1%Mo alloy**
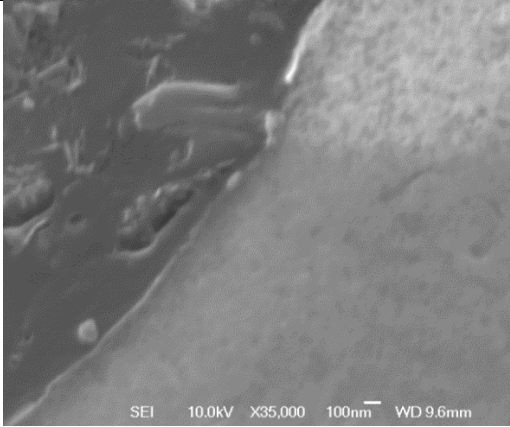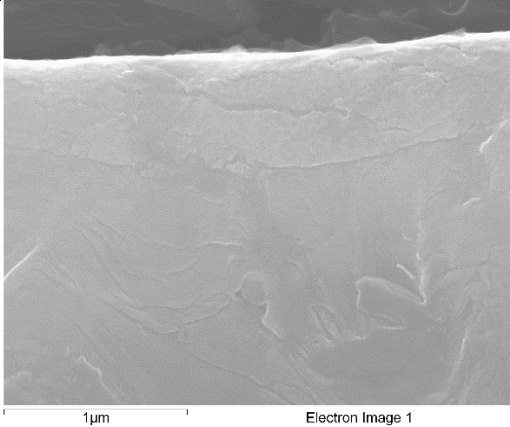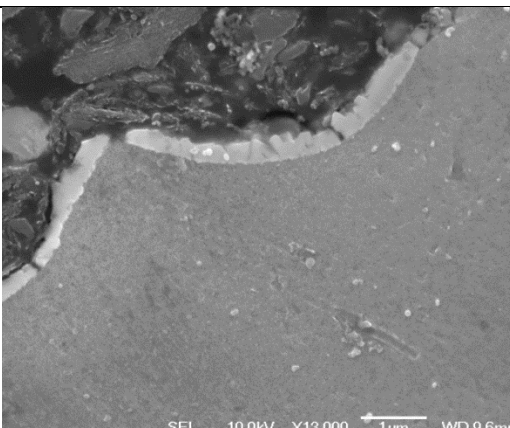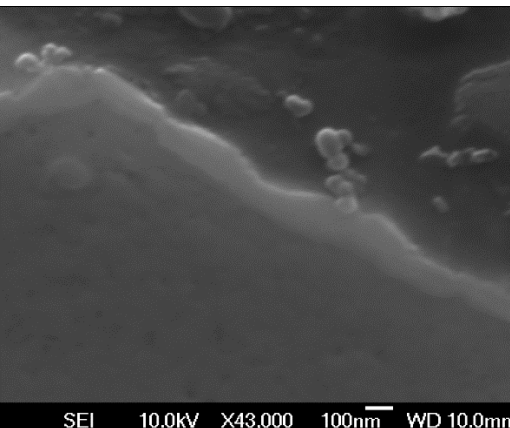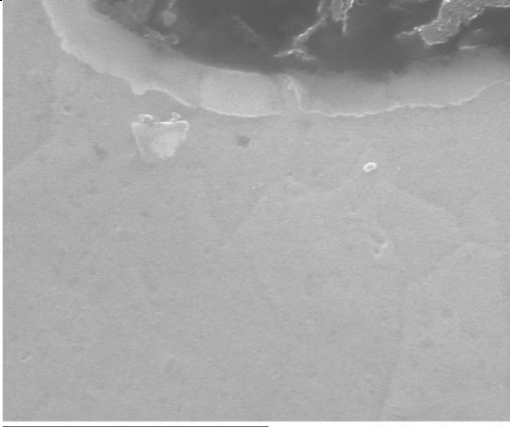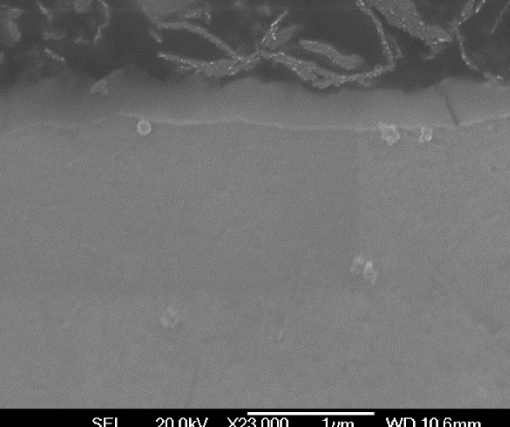
| Time step | SP-Al | Al-1%Mo |
|---|---|---|
| 5 minutes | \n~0.045 µm | \nNegligible thickness |
| 1 hour | \n~0.305 µm | \n~0. 12 µm |
| 24 hours | \n~0.37 µm | \n~0.35 µm |

**Figure 89 conitnued - Comparison of oxide layers for SP-Al and Al-1%Mo alloy**

The thickness of the oxides on the SP-Al and Al-1%Mo samples were very similar across the different holding times. The oxide thickness was increased by ~0.33 μm in the SP-Al over the holding times up to 24 hours and ~0.3 μm for Al-%Mo (summarised in Table 17). The appearances of the oxides are also very similar, with a continuous oxide.

**Table 17 - Oxide thickness of SP-Al with and without 1% Mo addition**

|  | Oxide thickness of alloy (μm) | | |
| --- | --- | --- | --- |
| **Alloy Composition** | **5 min** | **1 hour** | **24 hour** |
| SP-Al | 0.05 | 0.30 | 0.37 |
| Al-1%Mo | negligible | 0.12 | 0.35 |
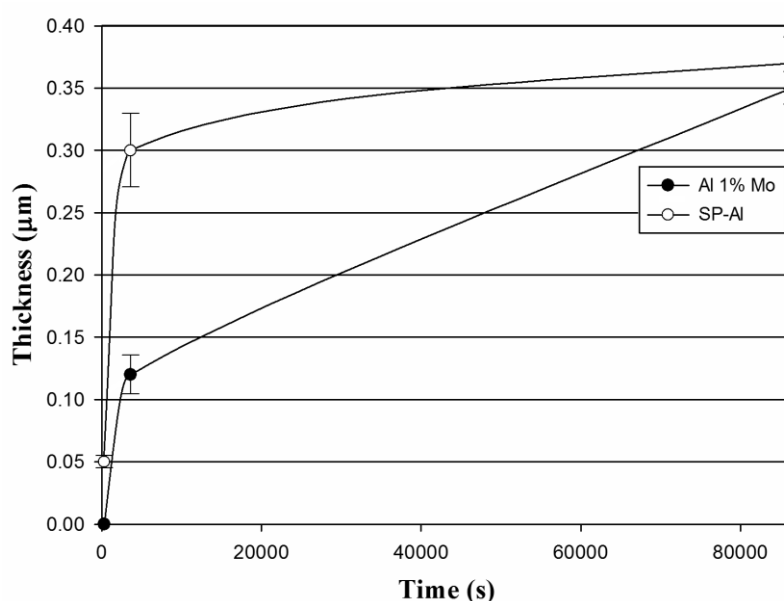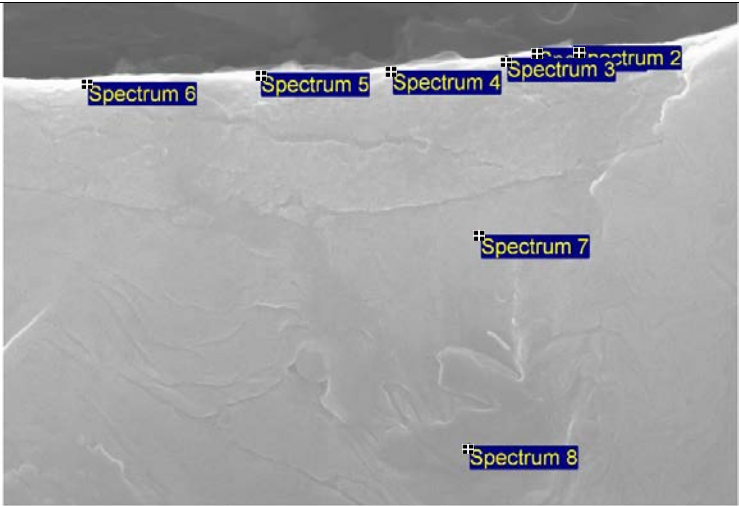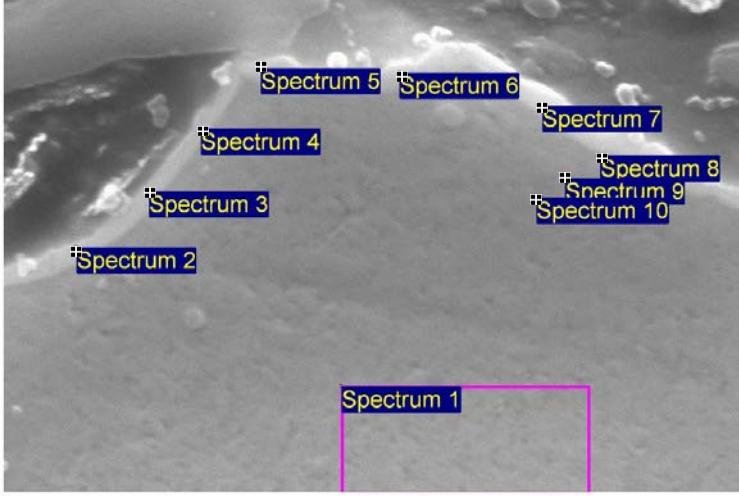


**Figure 90 - Thickness of oxide layer vs. holding time Al 1%Mo samples held at 750 °C, compared to SP-Al**

The initial rate of oxidation for Al l% Mo was slower than that for SP-Al, $3.6 \times 10^{-5}$ μm/s and $7.6 \times 10^{-5}$ μm/s between 5 minutes and 1 hour respectively, but then it grew at a faster rate, $1.7 \times 10^{-6}$ μm/s for Al 1%Mo and $8.45 \times 10^{-7}$ μm/s. The oxide thickness after 24 hours (0.35 μm) was very similar to that of SP-Al (0.37 μm), which suggested that Mo, when present as an alloying addition, had little effect on growth of the oxide. The EDX analysis is shown in Figure 91.

**Figure 91 - EDX analysis of Al-1%Mo samples**

| Sample | Image |
|---|---|
| 750 ºC 5 min hold<br><br>Layer thickness ≈ negligible | <br>1µm    Electron Image 1<br><br>**Spectrum 1**<br>O 4.99, Al 95.01, Mo 0.00<br>**Spectrum 2**<br>O 7.14, Al 92.86, Mo 0.00<br>**Spectrum 3**<br>O 7.96, Al 92.04, Mo 0.00<br>**Spectrum 4**<br>O 6.53, Al 93.47, Mo 0.00<br><br>**Spectrum 5**<br>O 8.86, Al 91.14, Mo 0.00<br>**Spectrum 6**<br>O 6.28, Al 93.72, Mo 0.00<br>**Spectrum 7**<br>O 0.00, Al 100.00, Mo 0.00<br>**Spectrum 8**<br>O 0.00, Al 100.00, Mo 0.00 |

Sample: 750 ºC 5 min hold — Layer thickness ≈ negligible



1µm — Electron Image 1

| Spectrum 1 | | Spectrum 2 | | Spectrum 3 | | Spectrum 4 | |
|---|---|---|---|---|---|---|---|
| Element | Weight % | Element | Weight % | Element | Weight % | Element | Weight % |
| O | 4.99 | O | 7.14 | O | 7.96 | O | 6.53 |
| Al | 95.01 | Al | 92.86 | Al | 92.04 | Al | 93.47 |
| Mo | 0.00 | Mo | 0.00 | Mo | 0.00 | Mo | 0.00 |

| Spectrum 5 | | Spectrum 6 | | Spectrum 7 | | Spectrum 8 | |
|---|---|---|---|---|---|---|---|
| Element | Weight % | Element | Weight % | Element | Weight % | Element | Weight % |
| O | 8.86 | O | 6.28 | O | 0.00 | O | 0.00 |
| Al | 91.14 | Al | 93.72 | Al | 100.00 | Al | 100.00 |
| Mo | 0.00 | Mo | 0.00 | Mo | 0.00 | Mo | 0.00 |

Sample: 750 ºC 1 hour hold — Layer thickness ≈ 0.12 µm



2µm — Electron Image 1

| Spectrum 1 | | Spectrum 2 | | Spectrum 3 | | Spectrum 4 | |
|---|---|---|---|---|---|---|---|
| Element | Weight % | Element | Weight % | Element | Weight % | Element | Weight % |
| O | 0.00 | O | 9.67 | O | 10.86 | O | 12.13 |
| Al | 100.00 | Al | 90.33 | Al | 89.14 | Al | 84.62 |
| Mo | 0.00 | Mo | 0.00 | Mo | 0.00 | Mo | 3.25 |

| Spectrum 5 | | Spectrum 6 | | Spectrum 7 | | Spectrum 8 | |
|---|---|---|---|---|---|---|---|
| Element | Weight % | Element | Weight % | Element | Weight % | Element | Weight % |
| O | 9.58 | O | 6.56 | O | 16.12 | O | 12.95 |
| Al | 85.68 | Al | 89.34 | Al | 79.76 | Al | 82.61 |
| Mo | 4.74 | Mo | 4.10 | Mo | 4.12 | Mo | 4.44 |

| Spectrum 9 | | Spectrum 10 | |
|---|---|---|---|
| Element | Weight % | Element | Weight % |
| O | 3.17 | O | 1.38 |
| Al | 96.83 | Al | 98.62 |
| Mo | 0.00 | Mo | 0.00 |

| 750 °C 24 hour hold<br><br>Layer thickness ≈ 0.35 μm |  |
| --- | --- |

| Point 1 | | Point 2 | | Point 3 | | Point 4 | |
| --- | --- | --- | --- | --- | --- | --- | --- |
| Element | Weight % | Element | Weight % | Element | Weight % | Element | Weight % |
| O | 24.66 | O | 21.98 | O | 17.30 | O | 6.64 |
| Al | 75.34 | Al | 78.02 | Al | 82.70 | Al | 93.36 |
| Mo | 0.00 | Mo | 0.00 | Mo | 0.00 | Mo | 0.00 |

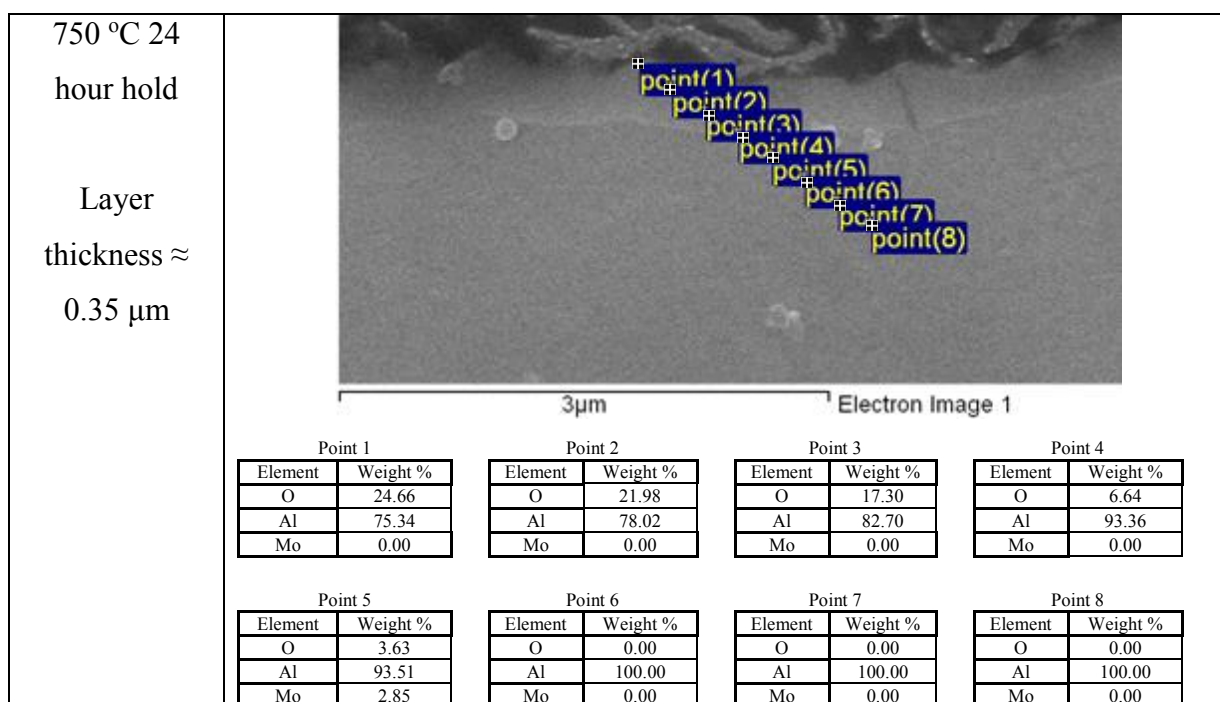| Point 5 | | Point 6 | | Point 7 | | Point 8 | |
| --- | --- | --- | --- | --- | --- | --- | --- |
| Element | Weight % | Element | Weight % | Element | Weight % | Element | Weight % |
| O | 3.63 | O | 0.00 | O | 0.00 | O | 0.00 |
| Al | 93.51 | Al | 100.00 | Al | 100.00 | Al | 100.00 |
| Mo | 2.85 | Mo | 0.00 | Mo | 0.00 | Mo | 0.00 |

**Figure 91 - EDX analysis of Al-1%Mo samples**

The EDX analysis in Figure 91 indicated that Mo was not prevalent in the oxide layer. This suggested that the Mo was not present in the oxide layer, but may have been present in the near oxide region. The presence of Mo did not appear to have much of an effect on the oxidation of the alloy, with only a 0.02 μm difference in thickness after 24 hours, compared to SP-Al. The fact that Mo was not present in the oxide layer was not unexpected, as the growth of the oxide appeared to be unaffected suggesting that the oxide layer was the same for both samples. The XRD for the samples held for 5 minutes and 1 hour are shown in Figure 92 and Figure 93.
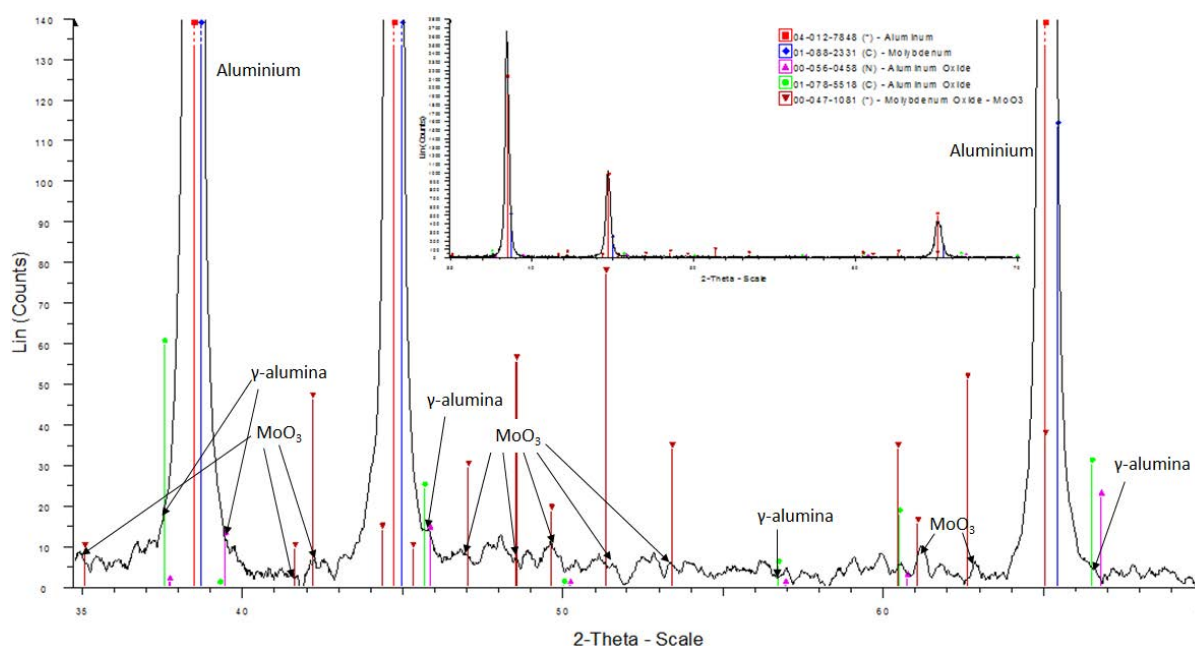


**Figure 92 - XRD data from the Al-1%Mo samples at 5 minutes (zoomed out spectra inset)**
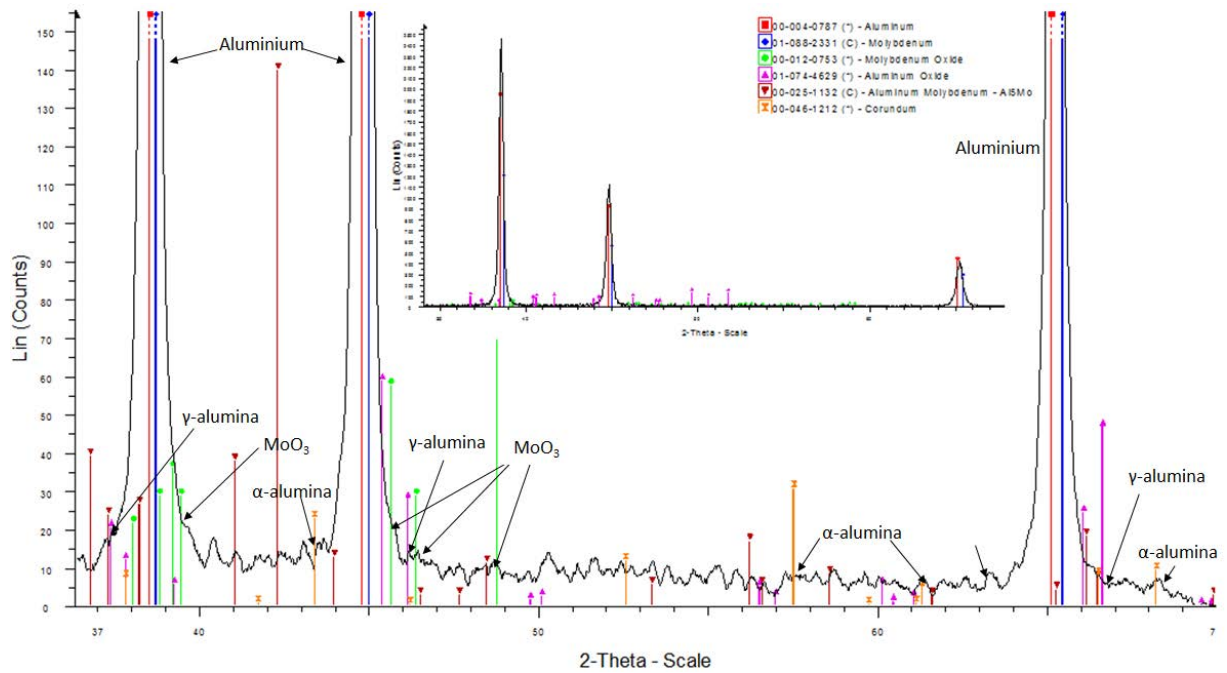
**Figure 93 - XRD data from the Al-1%Mo samples at 24 hours (zoomed out spectra inset)**

The XRD results for the 5 minute sample showed that the oxide contained γ-alumina and $MoO_3$ (Figure 92) with traces of α-alumina being found after 24 hours (Figure 93). This and the EDX results in Figure 91 suggested the $MoO_3$ formed below the layer of γ-alumina, as there was no Mo detected in the EDX. The $MoO_3$ may have formed when α-alumina gave rise to liquid metal becoming exposed due to its volume decrease and the Mo in the alloy reacting with air.

3.2.3 - Al-7%-Si-0.3%Mg-1%Mo Alloy

Al-7%Si-0.3%Mg-1%Mo Al-7%Si-0.3%Mgalloy was melted at 750 °C and held for different holding times. The cross sections of the samples were observed using SEM and compared with the Mo-free Al-7%Si-0.3%Mg alloy is shown in Figure 94.

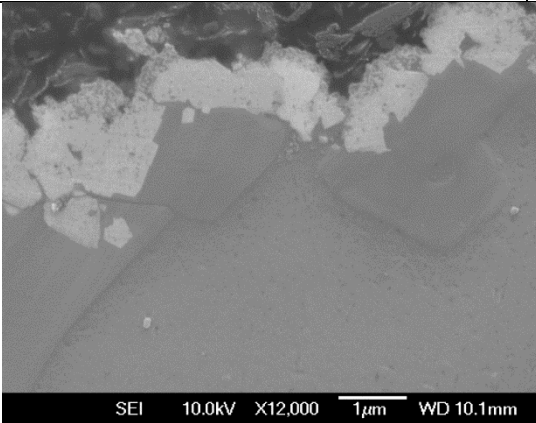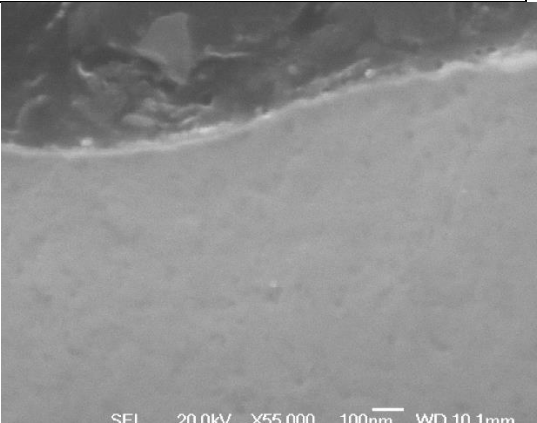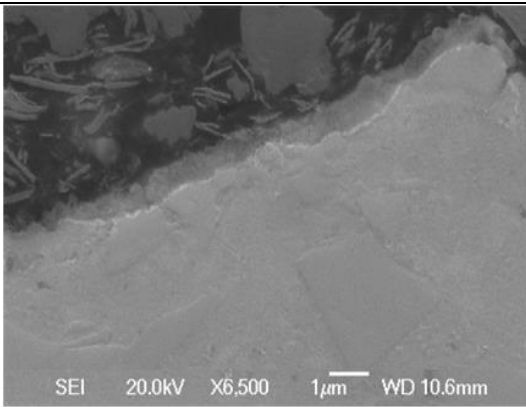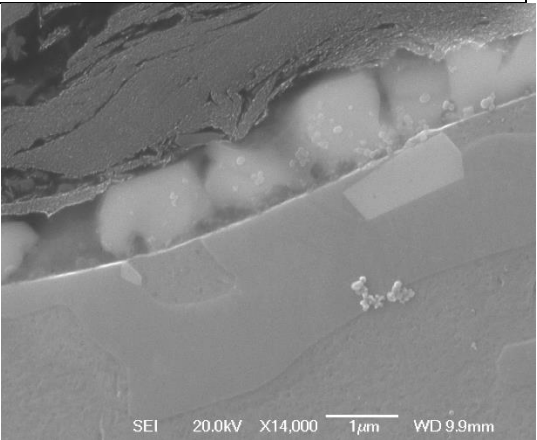**Figure 94 - Comparison of oxide layers for Al-7%Si-0.3%Mg and Al-7%Si-0.3%Mg-1%Mo alloys**
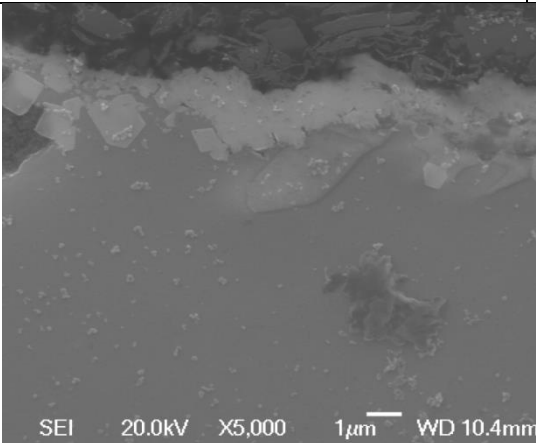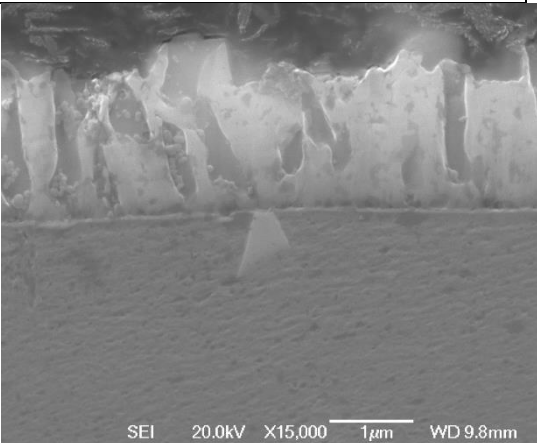
| Time step | Al-7%-Si-0.3%Mg | Al-7%-Si-0.3%Mg-1%Mo |
|---|---|---|
| 5 minutes | ~0.65 μm | ~0.03 μm |
| 1 hour | ~0.67 μm | ~1.1 μm |
| 24 hours | ~1.56 μm | ~1.8 μm |

**Figure 94 - Comparison of oxide layers for Al-7%Si-0.3%Mg and Al-7%Si-0.3%Mg-1%Mo alloys**

The presence of 1wt. % Mo as an alloying addition in Al-7%Si-0.3%Mg gave a change in the growth of the oxide. The oxide thickness at 24 hours was 1.56 μm in Al-7%Si-0.3%Mg and 1.8 μm in Al-7%Si-0.3%Mg-1% Mo, an increase of 1.77 μm (see Table 18 and Figure 95). The appearance of the oxides was also different, as seen in Figure 94, with the oxide with 1% Mo

137

addition having a multi-phase appearance. It had a similar appearance to the original contaminated sample, shown in Figure 83.

**Table 18 - Oxide thickness of Al-7%Si-0.3%Mg with and without 1% Mo addition**

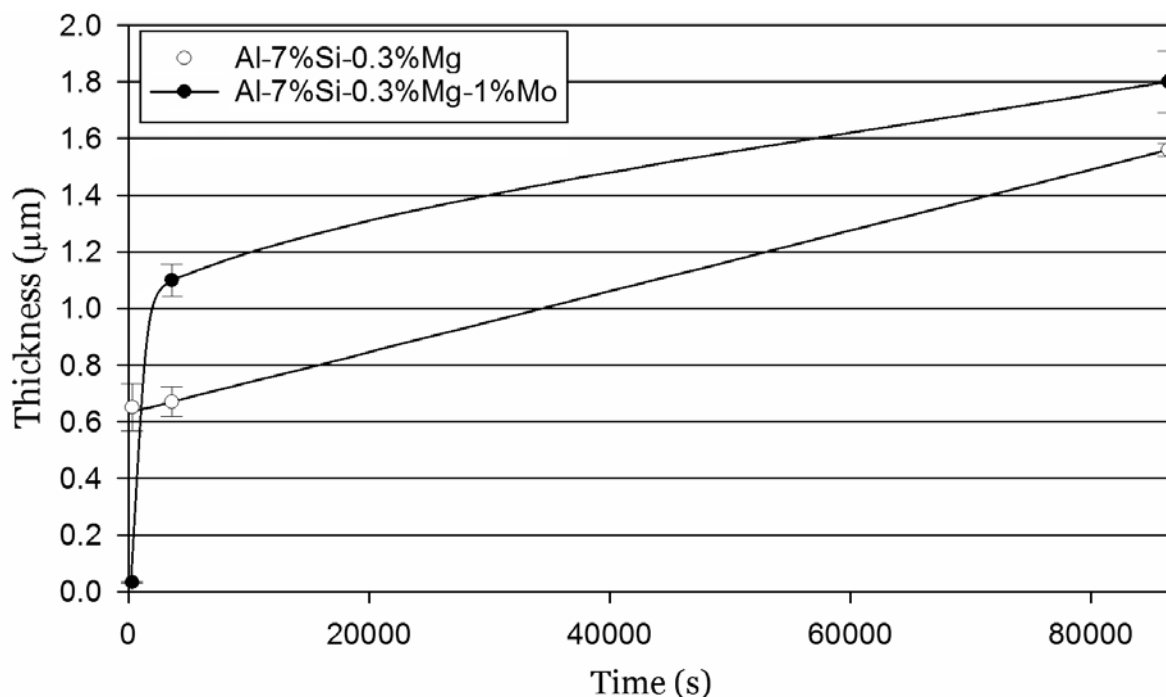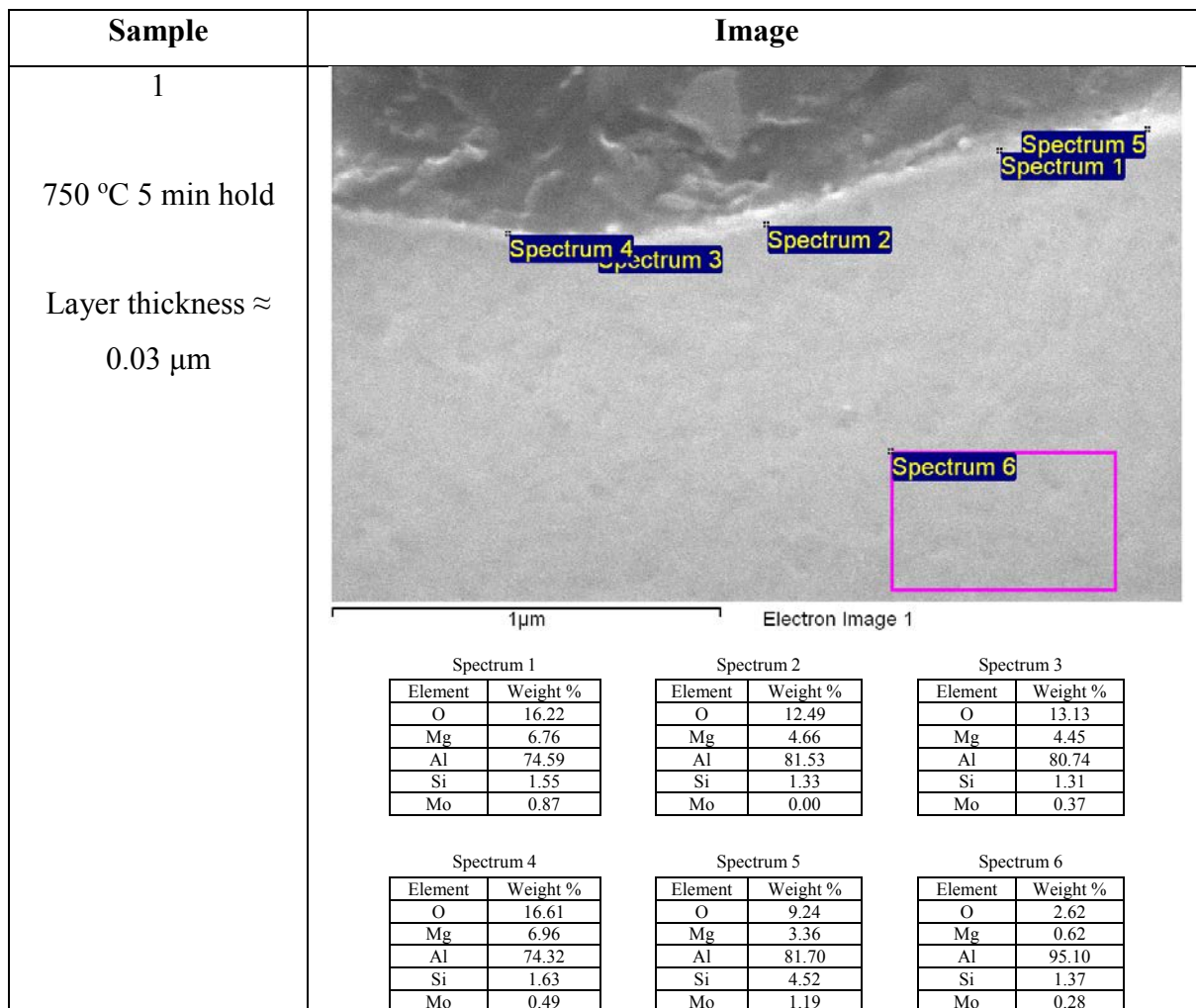| Alloy Composition | Oxide thickness of alloy (µm) | | |
|---|---|---|---|
| | 5 min | 1 hour | 24 hour |
| Al-7%-Si-0.3%Mg | 0.65 | 0.67 | 1.56 |
| Al-7%-Si-0.3%Mg-1%Mo | 0.03 | 1.1 | 1.8 |



**Figure 95 - Thickness of oxide layer vs. holding time Al-7%Si-0.3%Mg-1%Mo samples held at 750 °C**
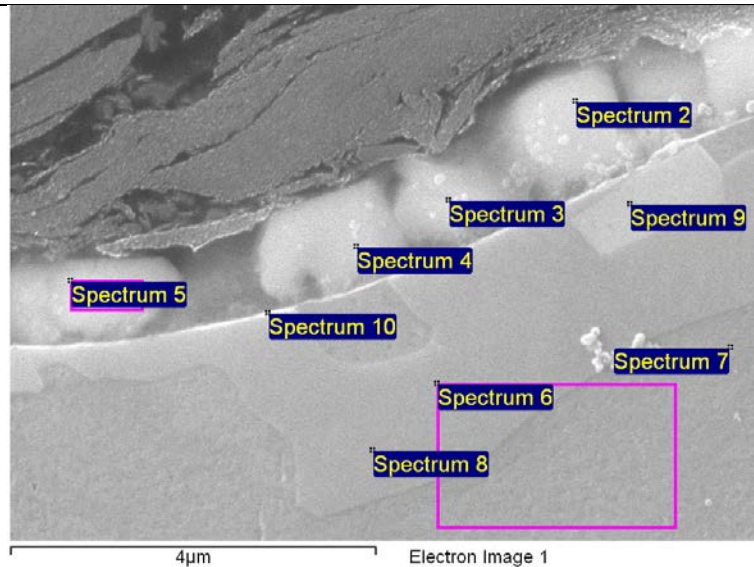
The rate of thickness growth increased over time. There was an initial fast increase in the oxide thickness for the sample containing 1%Mo, shown in Figure 95. This suggested that a stable oxide formed after 1 hour, which would have slowed the oxidation rate, and that it was a protective oxide for the total oxidation period. The initial oxidation rate between 5 minutes and 1 hour was $3.2 \times 10^{-4}$ µm/s, which then slowed to $8.5 \times 10^{-6}$ µm/s between 1 hour and 24 hours. EDX was carried out to determine the composition of the layers present in the alloys, and can be seen in Figure 96.

138

**Figure 96 - EDX analysis of Al-7%Si-0.3%Mg-1%Mo samples**

| Sample | Image |
|---|---|
| 1<br><br>750 °C 5 min hold<br><br>Layer thickness ≈<br><br>0.03 μm |  |

Spectrum 1

| Element | Weight % |
|---|---|
| O | 16.22 |
| Mg | 6.76 |
| Al | 74.59 |
| Si | 1.55 |
| Mo | 0.87 |

Spectrum 2

| Element | Weight % |
|---|---|
| O | 12.49 |
| Mg | 4.66 |
| Al | 81.53 |
| Si | 1.33 |
| Mo | 0.00 |

Spectrum 3

| Element | Weight % |
|---|---|
| O | 13.13 |
| Mg | 4.45 |
| Al | 80.74 |
| Si | 1.31 |
| Mo | 0.37 |

Spectrum 4

| Element | Weight % |
|---|---|
| O | 16.61 |
| Mg | 6.96 |
| Al | 74.32 |
| Si | 1.63 |
| Mo | 0.49 |

Spectrum 5

| Element | Weight % |
|---|---|
| O | 9.24 |
| Mg | 3.36 |
| Al | 81.70 |
| Si | 4.52 |
| Mo | 1.19 |

Spectrum 6

| Element | Weight % |
|---|---|
| O | 2.62 |
| Mg | 0.62 |
| Al | 95.10 |
| Si | 1.37 |
| Mo | 0.28 |

| | 2 |
|---|---|
| | 750 °C 1 hour hold |
| | Layer thickness ≈ 1.1 μm |



4μm — Electron Image 1

**Spectrum 2**

| Element | Weight % |
|---|---|
| O | 29.09 |
| Mg | 10.75 |
| Al | 13.87 |
| Si | 8.10 |
| Mo | 38.19 |

**Spectrum 3**

| Element | Weight % |
|---|---|
| O | 23.91 |
| Mg | 7.68 |
| Al | 26.14 |
| Si | 14.00 |
| Mo | 28.27 |

**Spectrum 4**

| Element | Weight % |
|---|---|
| O | 23.48 |
| Mg | 6.99 |
| Al | 27.96 |
| Si | 14.88 |
| Mo | 26.69 |

**Spectrum 5**

| Element | Weight % |
|---|---|
| O | 24.31 |
| Mg | 8.19 |
| Al | 32.82 |
| Si | 7.22 |
| Mo | 27.46 |

**Spectrum 6**

| Element | Weight % |
|---|---|
| O | 0.39 |
| Mg | 0.06 |
| Al | 76.91 |
| Si | 22.26 |
| Mo | 0.38 |

**Spectrum 7**

| Element | Weight % |
|---|---|
| O | 0.95 |
| Mg | 0.29 |
| Al | 79.32 |
| Si | 18.76 |
| Mo | 0.68 |

**Spectrum 8**

| Element | Weight % |
|---|---|
| O | 0.80 |
| Mg | 0.26 |
| Al | 43.43 |
| Si | 54.73 |
| Mo | 0.79 |

**Spectrum 9**

| Element | Weight % |
|---|---|
| O | 13.62 |
| Mg | 3.36 |
| Al | 35.52 |
| Si | 40.19 |
| Mo | 7.31 |

**Spectrum 10**

| Element | Weight % |
|---|---|
| O | 7.96 |
| Mg | 3.01 |
| Al | 29.92 |
| Si | 49.28 |
| Mo | 9.82 |

**Figure 96 - EDX analysis of Al-7%Si-0.3%Mg-1%Mo samples**

| 3

750 °C 24 hour hold

Layer thickness ≈

1.8 μm | 

4μm    Electron Image 1 |

Spectrum 1

| Element | Weight % |
|---------|----------|
| O | 25.43 |
| Mg | 30.48 |
| Al | 24.83 |
| Si | 0.42 |
| Mo | 18.84 |

Spectrum 2

| Element | Weight % |
|---------|----------|
| O | 33.11 |
| Mg | 24.76 |
| Al | 14.33 |
| Si | 0.30 |
| Mo | 27.50 |

Spectrum 3

| Element | Weight % |
|---------|----------|
| O | 26.86 |
| Mg | 34.74 |
| Al | 22.41 |
| Si | 0.33 |
| Mo | 15.67 |

Spectrum 4

| Element | Weight % |
|---------|----------|
| O | 32.33 |
| Mg | 24.60 |
| Al | 8.00 |
| Si | 0.35 |
| Mo | 34.73 |

Spectrum 5

| Element | Weight % |
|---------|----------|
| O | 24.00 |
| Mg | 23.49 |
| Al | 40.64 |
| Si | 0.31 |
| Mo | 11.57 |

**Figure 96 - EDX analysis of Al-7%Si-0.3%Mg-1%Mo samples**

The EDX spectra in Figure 96 show that Mo was present in the oxide layers of all samples. The layers appeared to have different phases in the 24 hour sample, but it was difficult to determine the difference between them. The presence of Mo in the alloys appears to increase the growth of the oxide. The percentage of Mo decreased further away from the oxide layer, as the Mo percentage was less in spectra 6-10 (0.4-9.8% Mo) of sample 2 (Figure 96) than the spectra on the oxide layer (up to 38% Mo), and was higher than that in the alloy itself (1% Mo). The Mo levels were up to 34wt. % in the oxide layer, suggesting that the Mo migrated to the oxide, where it may have increased the rate. The Mg levels were also high within the oxide layers, so this could have also been a contributing factor to the different phases. XRD analysis was undertaken to ascertain the structure of the oxide and can be seen in Figure 97, Figure 98 and Figure 99.
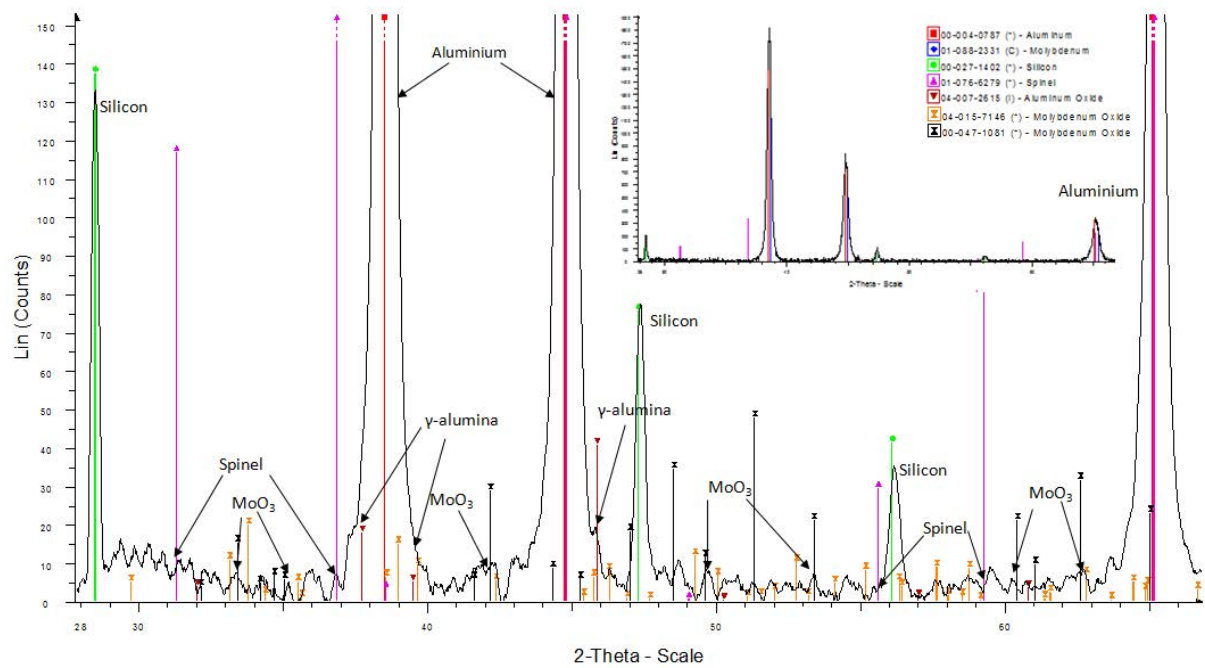
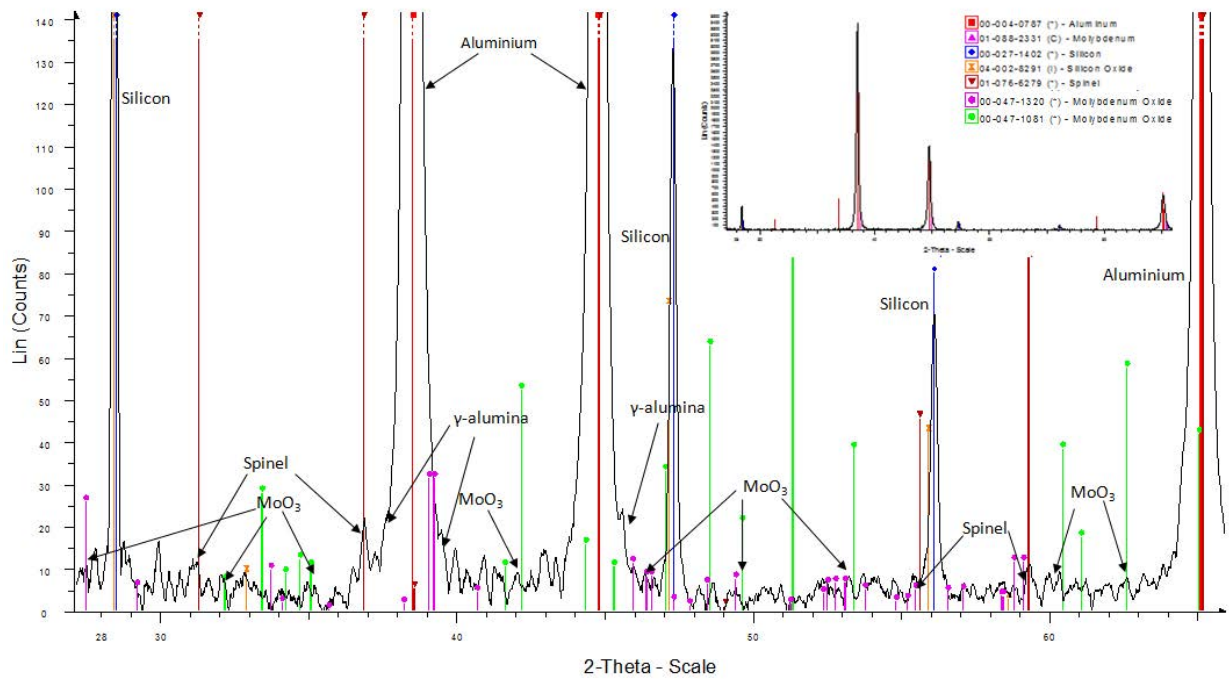**Figure 97 - XRD data from the Al-7%-Si-0.3%Mg-1%Mo samples at 5 minutes (zoomed out spectra inset)**



**Figure 98 - XRD data from the Al-7%-Si-0.3%Mg-1%Mo samples at 1 hour (zoomed out spectra inset)**
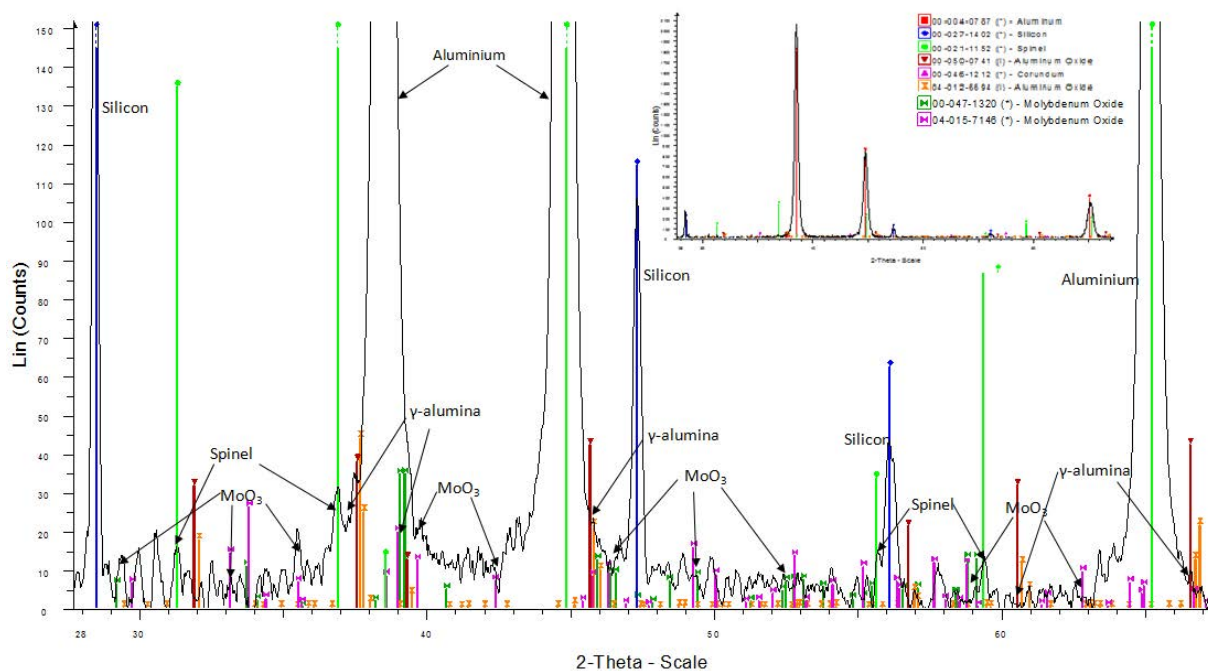
142

**Figure 99 - XRD data from the Al-7%-Si-0.3%Mg-1%Mo samples at 24 hours (zoomed out spectra inset)**

The XRD of the oxides can be seen in Figure 97, Figure 98 and Figure 99. There was an increase in the spinel signal over oxidation time; there were also signals for γ-alumina. The $MoO_3$ oxide was detected at all oxidation times. It could be that the different oxide phases were spinel, γ-alumina and $MoO_3$ within the layers.
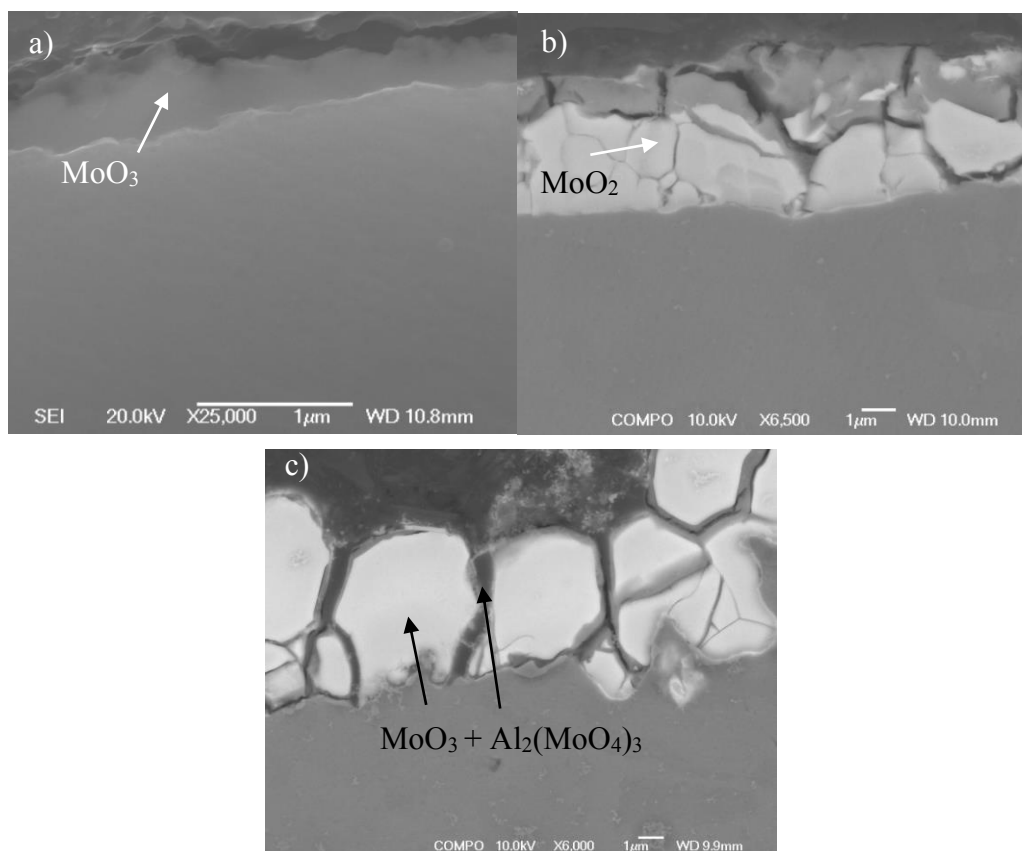


**Figure 100 - Images of Al + 3g Mo powder a) 5 mins b) 1 hour c) 24 hours (close up of 24 hour Al +Mo powder sample from Figure 85). Possible different phases are marked**

The effect of Mo additions on the oxidation of Al was different depending on the alloy. When Mo was added as a powder to the surface of liquid Al, the final oxide thickness increased from 0.37 μm to 1000 μm, and the Mo oxide changed from $MoO_3$ at 5 minutes, to $MoO_2$ at 1 hour to $Al_2(MoO_4)_3$ after 24 hours (structures seen in Figure 100). This change in oxide structure is likely to have led to deformation and cracking of the oxide, which in turn led to a higher level of oxidation (cracks shown in Figure 100b and c). The effect of 1%Mo additions to SP-Al only changed the oxide thickness by 0.07 μm to give a final thickness of 0.35 μm after 24 hours, compared to 0.37 μm for SP-Al. $MoO_3$ formed alongside γ-alumina at all times, with traces of α-alumina at 24 hours, similar to those found on SP-Al. It seemed that Mo additions had no significant effect on the oxidation of this alloy. When 1% Mo was added to Al-7%Si-0.3%Mg alloy, the thickness increased to 1.8 μm, compared to 1.56 μm for un-alloyed Al-7%Si-0.3%Mg. The oxide was made up of γ-alumina, spinel and $MoO_3$. It seemed that the presence of Mo in this alloy led to the formation of a multiphase oxide.
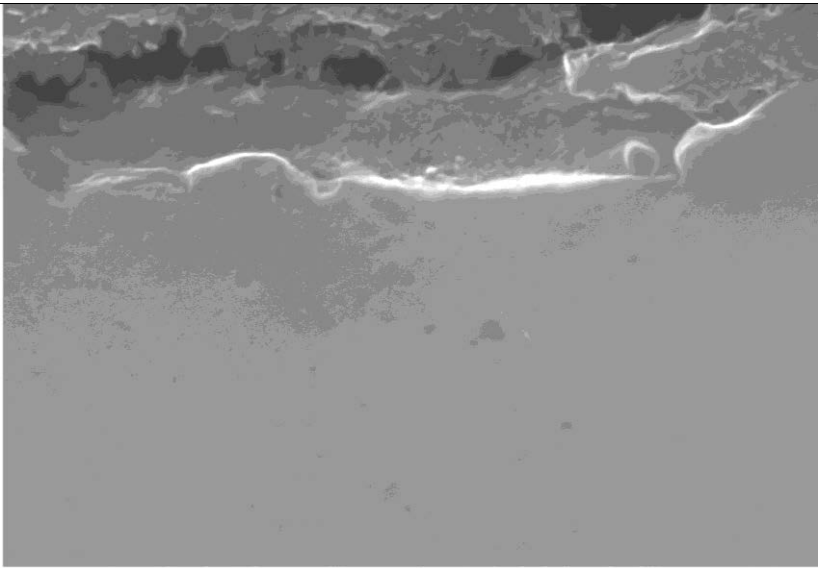
## 3.3 – Nitrogen Atmosphere

It has been reported that the air in a double oxide film defect forms different reaction products depending on time (Raeiszadeh 2005). It was noted that initially the oxygen reacted to form oxides, but when all the oxygen in the defect has been used up, the remaining nitrogen reacts with the liquid metal to form nitrides. Therefore, work was undertaken to determine the species that would form if the metals were melted and held at 750 °C in a nitrogen atmosphere.

### 3.3.1 – Superpure Al

Cross sections of samples observed in the SEM held for increasing time at 750 °C in a nitrogen atmosphere (99.998% min. purity) can be seen in Figure 101. Oxygen free nitrogen was used for all experiments.

**Figure 101 - Images from the 750 °C holds at different times for superpure Al in $N_2$ atmosphere, the thickness of the layer is also noted**

| Sample | Image |
|---|---|
| 1<br><br>750 ºC 5 min hold<br><br>Layer thickness ≈ 0.03 µm | <br>1µm Electron Image 1 |

| 2  750 °C 1 hour hold  Layer thickness ≈ 0.27 μm |  |
|---|---|
| 3  750 °C 24 hour hold  Layer thickness ≈ 1.37 μm  Average height of feathers ≈ 3.72 μm |  |
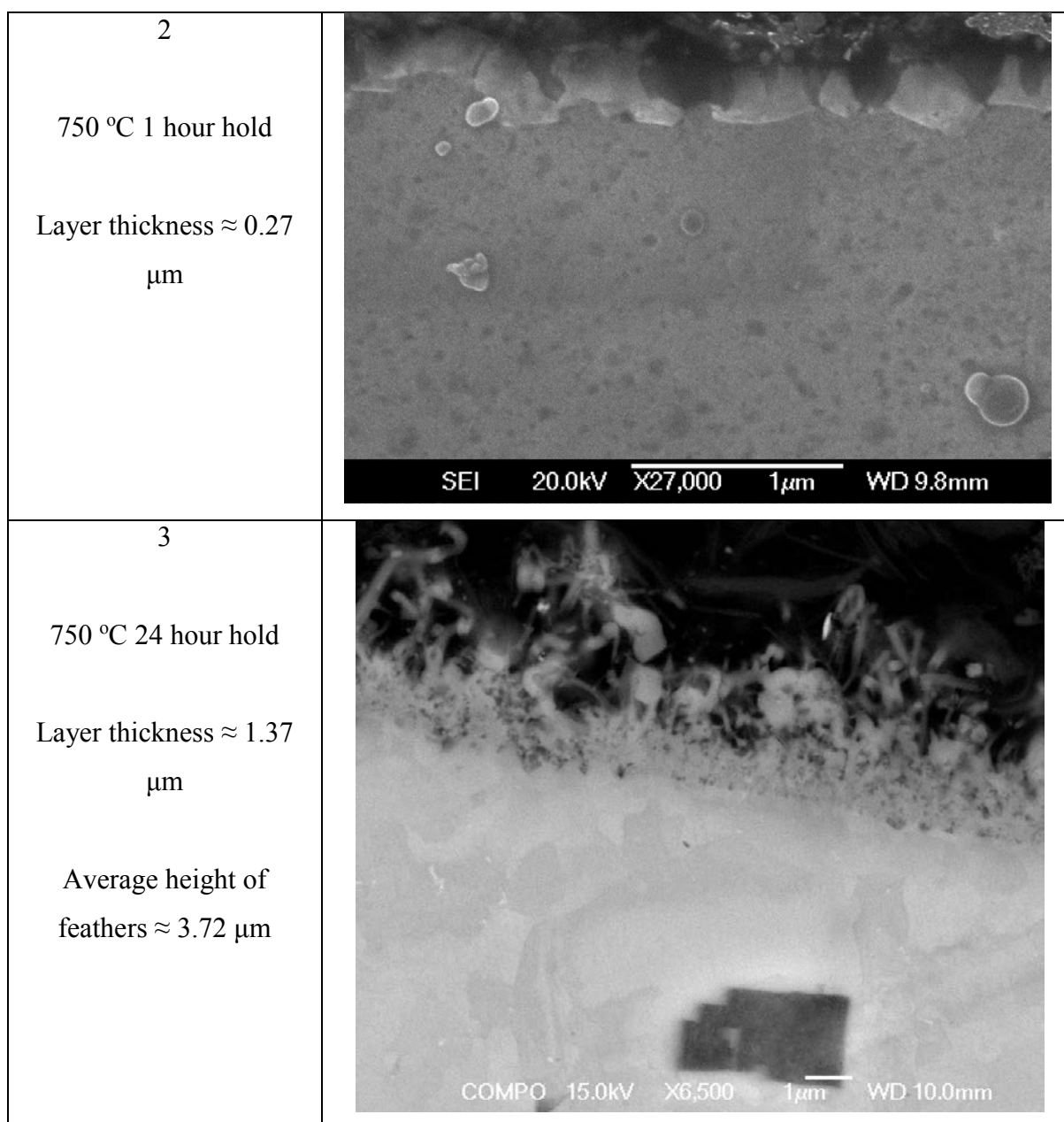
**Figure 101 continued - Images from the 750 °C holds at different times for superpure Al in N₂ atmosphere, the thickness of the layer is also noted**

The thickness of the layers increased with holding time, as shown in Figure 101. The layer started very thin, with a thickness of ~0.03 μm after 5 minutes, increasing to 0.27 μm at 1 hour, and then 1.37 μm at 24 hours. The appearance of the layer in the 24 hours sample was feather-like, which reached an average height of 3.72 μm above the surface film. The thickness of the layers is summarised in Table 19.

**Table 19 - Summary of layer thicknesses for superpure Al held at 750 °C in nitrogen atmosphere**

| Holding time (s) | Layer thickness (μm) |
|---|---|
| 300 | 0.03 |
| 3600 | 0.27 |
| 86 400 | 1.37 |
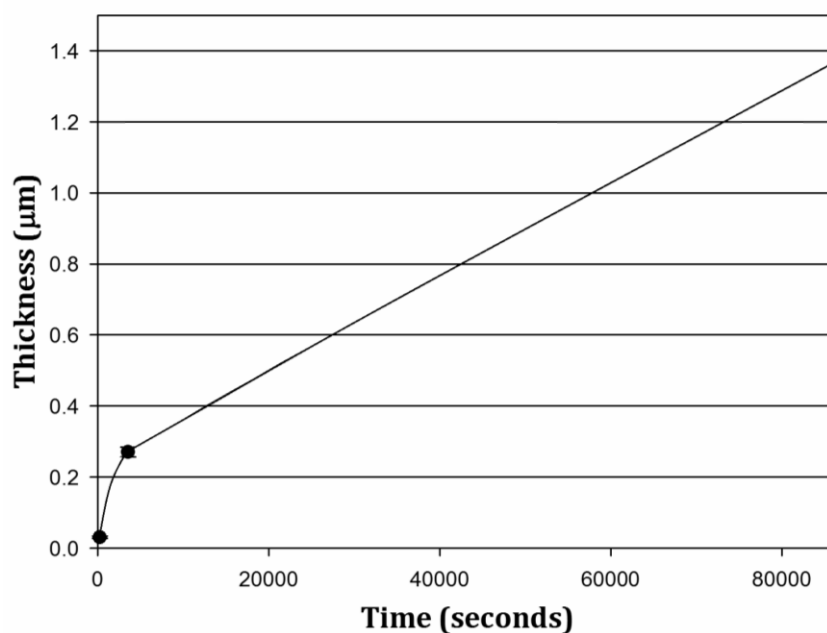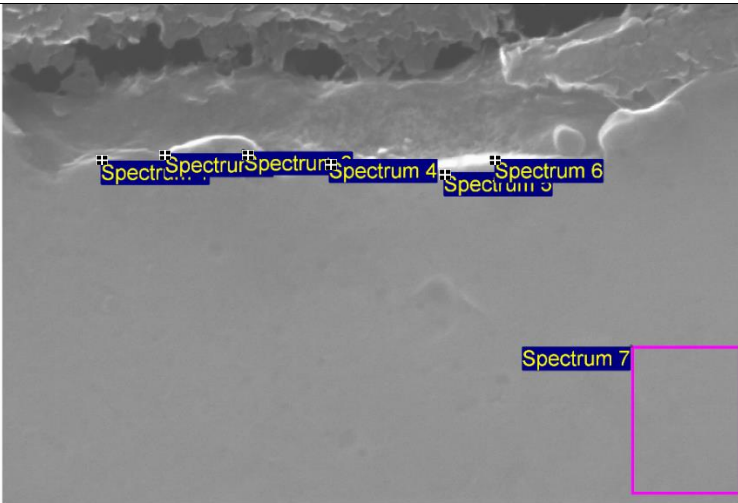
**Figure 102 - Thickness of the layer vs. holding time for superpure Al samples held at 750 °C in N₂**

The rate of layer growth appeared to be faster between 5 minutes and 1 hour, at ~7.27 x 10$^{-5}$ $\mu$m s$^{-1}$. The rate slows and levels off between 1 hour and 24 hours, to ~1.33 x 10$^{-5}$ $\mu$m s$^{-1}$. This suggests that the layer that formed became more protective over time. To ascertain the composition of the layers EDX was carried out on the samples, shown in Figure 103.

**Figure 103 - EDX analysis of superpure Al samples**

| Sample | Image |
|---|---|
| 1<br><br>750 ºC 5 min hold<br><br>Layer thickness ≈ 0.03 $\mu$m |  |

| Spectrum 1 | | Spectrum 2 | | Spectrum 3 | | Spectrum 4 | |
|---|---|---|---|---|---|---|---|
| Element | Weight % | Element | Weight % | Element | Weight % | Element | Weight % |
| N | 0.00 | N | 0.00 | N | 0.00 | N | 0.00 |
| O | 15.95 | O | 13.28 | O | 12.60 | O | 4.28 |
| Al | 84.05 | Al | 86.72 | Al | 87.40 | Al | 95.72 |

| Spectrum 5 | | Spectrum 6 | | Spectrum 7 | |
|---|---|---|---|---|---|
| Element | Weight % | Element | Weight % | Element | Weight % |
| N | 0.00 | N | 0.00 | N | 0.00 |
| O | 5.27 | O | 4.25 | O | 0.00 |
| Al | 94.73 | Al | 95.75 | Al | 100.00 |

147

| | |
|---|---|
| 2<br><br>750 ºC 1 hour<br>hold<br><br>Layer thickness<br>≈ 0.27 μm | <br>2μm   Electron Image 1 |

| Spectrum 1 | | Spectrum 2 | | Spectrum 3 | | Spectrum 4 | |
|---|---|---|---|---|---|---|---|
| Element | Weight % | Element | Weight % | Element | Weight % | Element | Weight % |
| N | 0.00 | N | 0.00 | N | 0.00 | N | 0.00 |
| O | 5.00 | O | 4.53 | O | 0.00 | O | 0.00 |
| Al | 95.00 | Al | 95.47 | Al | 100.00 | Al | 100.00 |

| Spectrum 5 | | Spectrum 6 | | Spectrum 7 | | Spectrum 8 | |
|---|---|---|---|---|---|---|---|
| Element | Weight % | Element | Weight % | Element | Weight % | Element | Weight % |
| N | 0.00 | N | 0.00 | N | 0.00 | N | 0.00 |
| O | 0.00 | O | 0.00 | O | 0.00 | O | 0.00 |
| Al | 100.00 | Al | 100.00 | Al | 100.00 | Al | 100.00 |

| | |
|---|---|
| 3<br><br>750 ºC 24 hour<br>hold<br><br>Layer thickness<br>≈ 1.37 μm | <br>9μm   Electron Image 1 |

| Spectrum 1 | | Spectrum 2 | | Spectrum 3 | |
|---|---|---|---|---|---|
| Element | Weight % | Element | Weight % | Element | Weight % |
| O | 0.00 | O | 1.25 | O | 24.19 |
| Al | 100.00 | Al | 98.75 | Al | 75.81 |
| N | 0.00 | N | 0.00 | N | 0.00 |

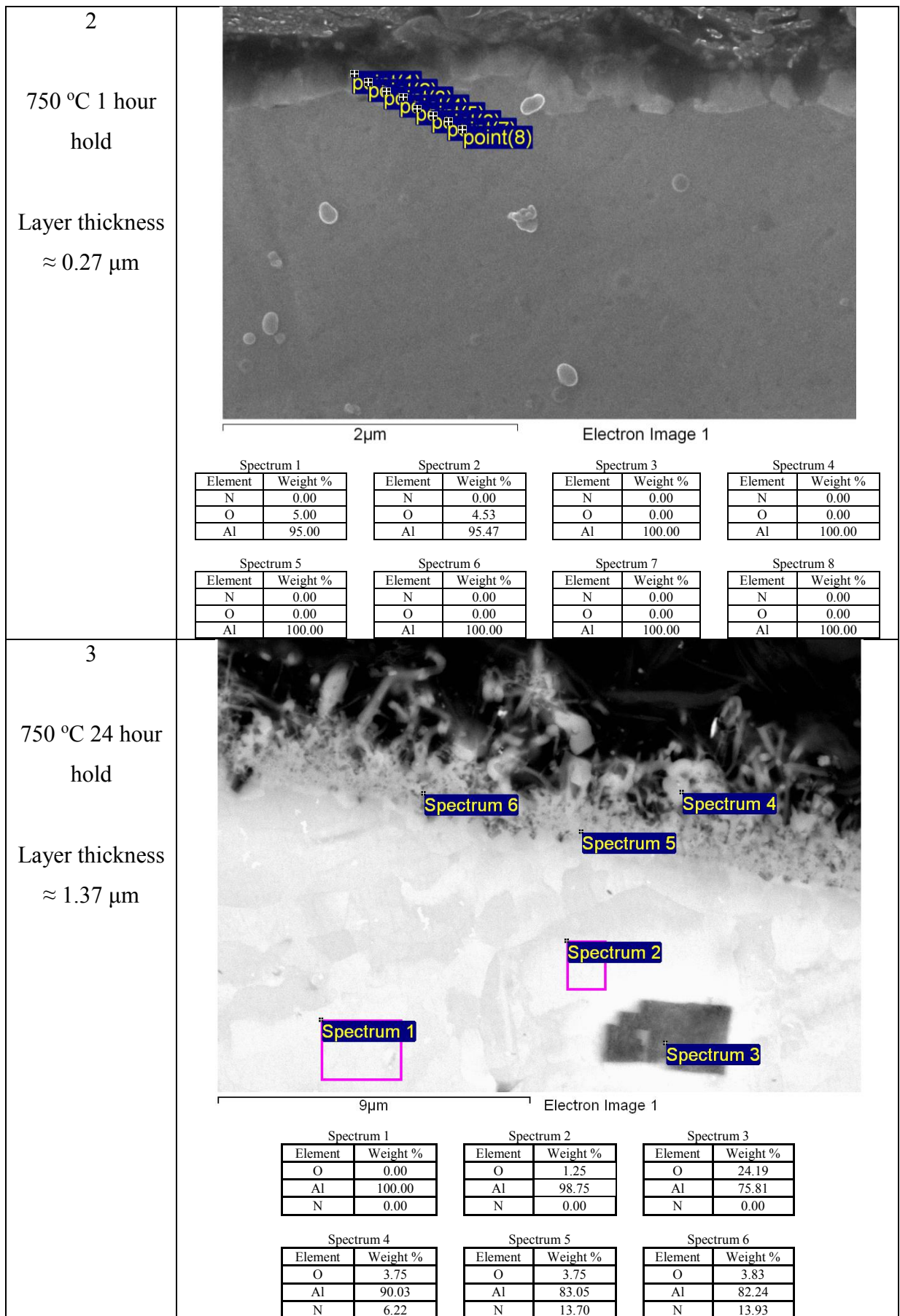| Spectrum 4 | | Spectrum 5 | | Spectrum 6 | |
|---|---|---|---|---|---|
| Element | Weight % | Element | Weight % | Element | Weight % |
| O | 3.75 | O | 3.75 | O | 3.83 |
| Al | 90.03 | Al | 83.05 | Al | 82.24 |
| N | 6.22 | N | 13.70 | N | 13.93 |

**Figure 103 continued - EDX analysis of superpure Al samples in N₂**

It can be seen in Figure 103 that the layer on the 24 hour sample contained nitrogen within the layer, seen in sample 3. This could mean that a nitride may have formed during the holding times up to 24 hours. The feather-like film on the 24 hours sample had the highest concentration of nitrogen, suggesting that this feature was a nitride. Nitrogen was not detected at lower holding times. This could be due to the fact that the SEM struggles to detect low levels of nitrogen. The levels of oxygen present in the cell, likely still present after purging with hyydrogen, even when very low, preferentially react with the liquid Al (Raeiszadeh 2005). XRD analysis was untaken to determine the crystal structure of the layers and can be seen in Figure 104 and Figure 105.
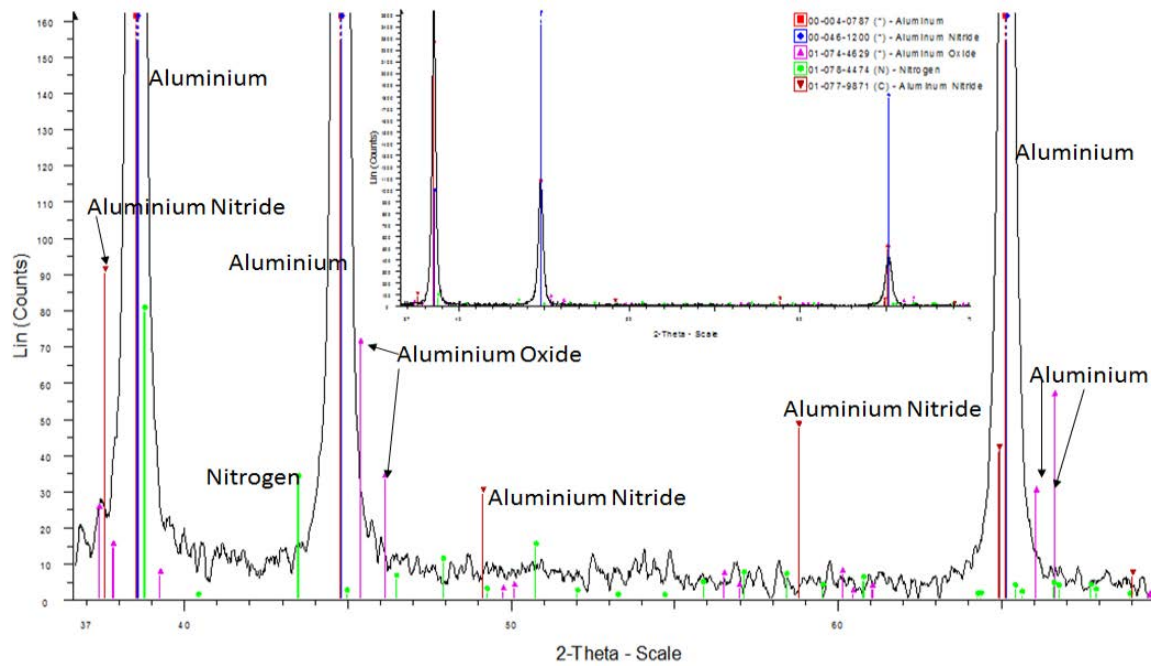


**Figure 104 - The XRD spectra for SP-Al held for 5 minutes at 750 °C in N2 (zoomed out spectra inset)**
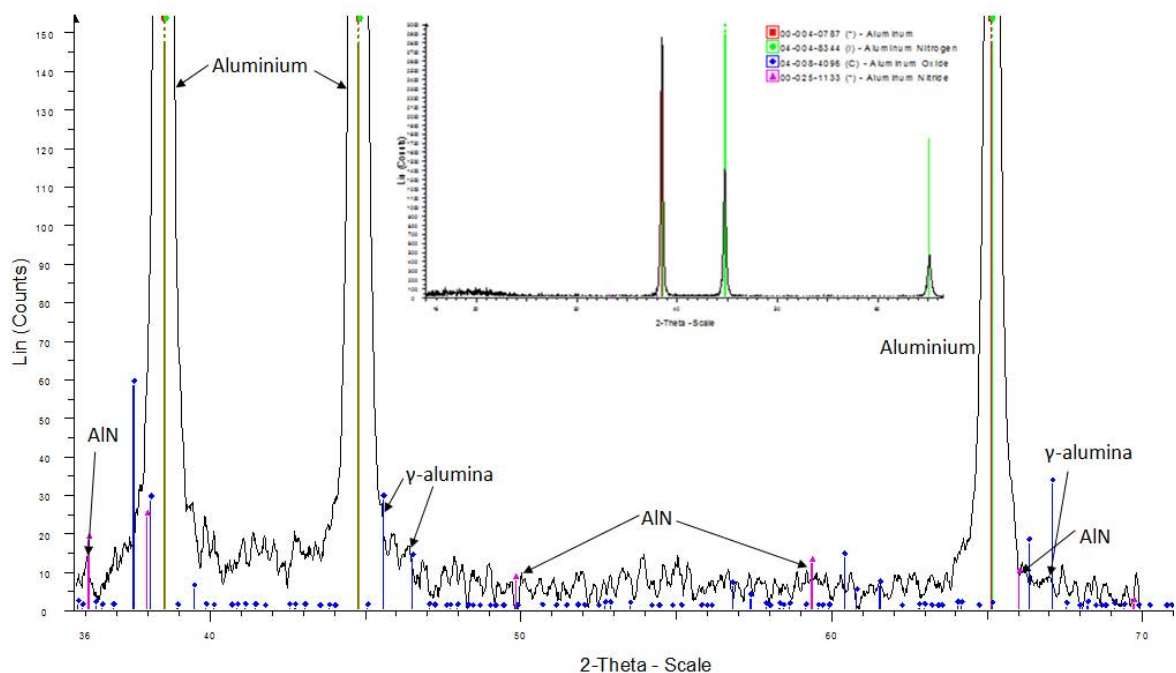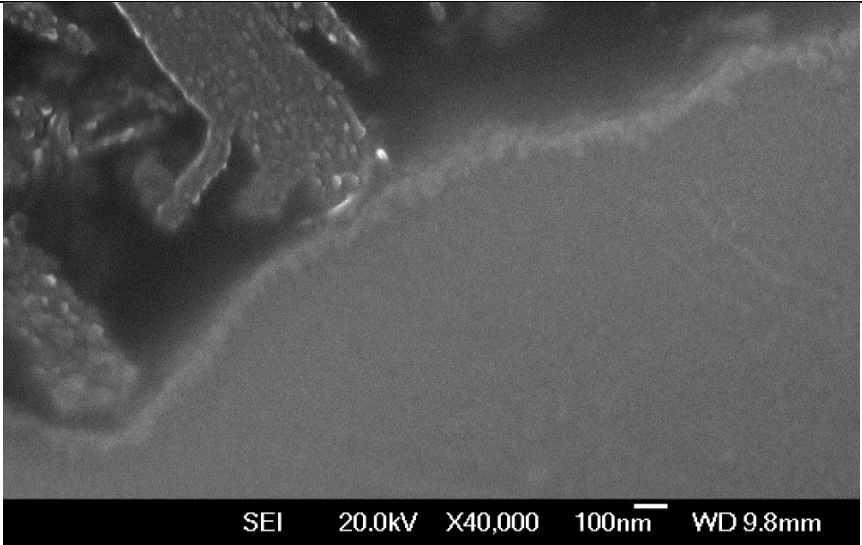


**Figure 105 - The XRD spectra for SP-Al held for 24 hours at 750 °C in N2 (zoomed out spectra inset)**

149

The XRD spectra in Figure 104 and Figure 105 have signals for γ-alumina at both holding times. This suggests that alumina was formed initially, possibly in the solid state before the experiment began or with any remaining oxygen present in the cell after purging. Signals for AlN were also present in both samples, leading to the conclusion that the alumina detected is likely to have formed early in the experiment rather than later on. The signals for AlN were weak, suggesting that the amount present was low in the surface region. The thickness of the layers and the presence of $N_2$ from the EDX analysis suggest this was the case. EDX struggles to detect $N_2$ in low levels, so the fact it was picked up in levels of up to 13.9 wt.% suggests a layer of nitride, with AlN being the likely layer on SP-Al.

3.3.2 – Al-4 wt. % Mg

Al-4%Mg alloy was exposed to nitrogen for different holding times. SEM images from the cross-sections of the samples can be seen in Figure 106.

**Figure 106 - Images from the 750 °C holds at different times for Al-4%Mg in N2 atmosphere, the thickness of the layer is also noted**

| Sample | Image |
|---|---|
| 750 °C 5 min hold<br><br>Layer thickness ≈<br><br>0.06 μm |  |

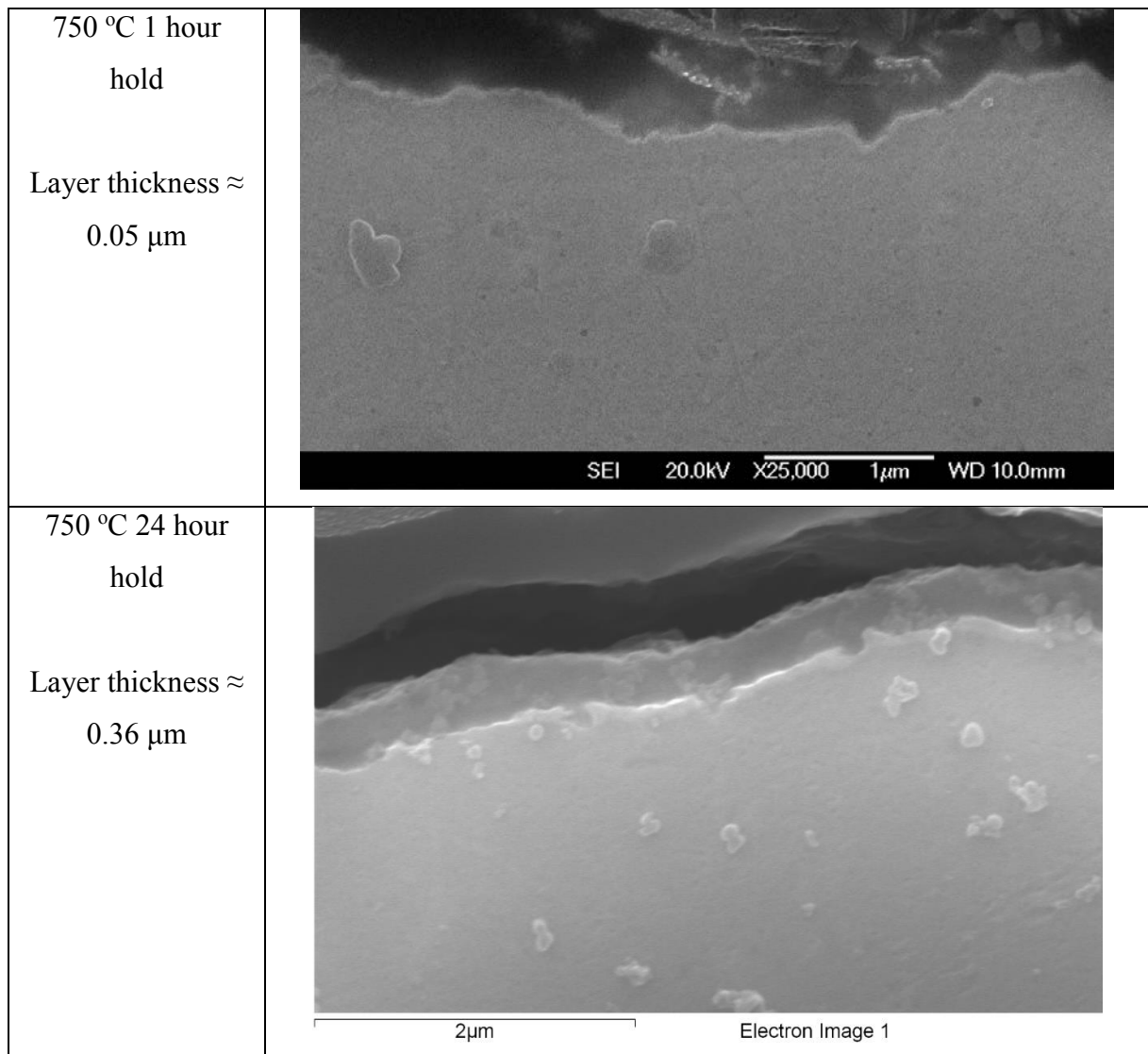| 750 ºC 1 hour hold<br><br>Layer thickness ≈ 0.05 μm |  |
|---|---|
| 750 ºC 24 hour hold<br><br>Layer thickness ≈ 0.36 μm |  |

**Figure 106 continued -  Images from the 750 °C holds at different times for Al-4%Mg in N2 atmosphere, the thickness of the layer is also noted**

The layers, seen in Figure 106, increased in thickness over time. The layer thickness changed very little between 5 minutes and 1 hour, only by ~0.01 μm. The layer then increased by ~0.3 μm from ~0.05 μm at 1 hour and ~0.36 μm at 24 hours. The thickness and growth details are shown in Table 20 and Figure 107.

**Table 20 - Summary of layer thicknesses for Al-4%Mg held at 750 °C in nitrogen atmosphere**

| Holding time (s) | Layer thickness (μm) |
|---|---|
| 300 | 0.06 |
| 3600 | 0.05 |
| 86 400 | 0.36 |
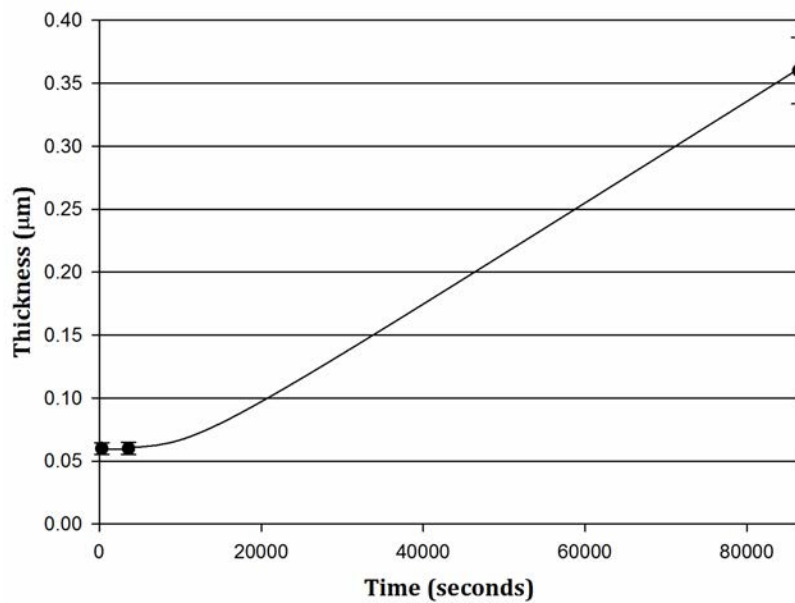
**Figure 107 - Thickness of the layer vs. holding time for Al-4%Mg samples held at 750 °C in N2**

The layer thickness after 24 hours, ~0.36 μm, was less than that for SP-Al, ~0.37 μm. The initial growth rate was negligible, as the thickness did not increase between 5 minutes and 1 hour. Between 1 and 24 hours, the rate increased to ~$3.6 \times 10^{-6}$ μm s$^{-1}$. EDX spectra used to determine the composition of the layers can be seen in Figure 108.

**Figure 108 - EDX analysis of Al-4%Mg samples in N2**

| Sample | Image |
|---|---|
| 1<br><br>750 °C 5 min hold<br><br>Layer thickness ≈ 0.06 μm |  |

Spectrum 1

| Element | Weight % |
|---|---|
| N | 0.00 |
| O | 2.99 |
| Mg | 4.4 |
| Al | 92.61 |

Spectrum 2

| Element | Weight % |
|---|---|
| N | 0.00 |
| O | 4.55 |
| Mg | 6.17 |
| Al | 89.28 |

Spectrum 3

| Element | Weight % |
|---|---|
| N | 0.00 |
| O | 4.14 |
| Mg | 5.53 |
| Al | 90.33 |

Spectrum 4

| Element | Weight % |
|---|---|
| N | 0.00 |
| O | 2.56 |
| Mg | 5.08 |
| Al | 92.36 |

Spectrum 5

| Element | Weight % |
|---|---|
| N | 0.00 |
| O | 0.00 |
| Mg | 4.19 |
| Al | 95.81 |

Spectrum 6

| Element | Weight % |
|---|---|
| N | 0.00 |
| O | 0.00 |
| Mg | 3.82 |
| Al | 96.18 |

| 2 |  |
|---|---|
| 750 °C 1 hour hold | |
| Layer thickness ≈ 0.05 μm | |

| Spectrum 1 | | Spectrum 2 | | Spectrum 3 | | Spectrum 4 | |
|---|---|---|---|---|---|---|---|
| Element | Weight % | Element | Weight % | Element | Weight % | Element | Weight % |
| N | 0.00 | N | 0.00 | N | 0.00 | N | 0.00 |
| O | 2.36 | O | 1.94 | O | 2.53 | O | 1.88 |
| Mg | 4.32 | Mg | 3.99 | Mg | 4.09 | Mg | 4.05 |
| Al | 93.32 | Al | 94.07 | Al | 93.38 | Al | 94.07 |

| Spectrum 5 | | Spectrum 6 | | Spectrum 7 | |
|---|---|---|---|---|---|
| Element | Weight % | Element | Weight % | Element | Weight % |
| N | 0.00 | N | 0.00 | N | 0.00 |
| O | 2.89 | O | 2.62 | O | 0.00 |
| Mg | 4.36 | Mg | 4.33 | Mg | 3.74 |
| Al | 92.76 | Al | 93.06 | Al | 96.26 |

| 3 |  |
|---|---|
| 750 °C 24 hour hold | |
| Layer thickness ≈ 0.36 μm | |

| Spectrum 1 | | Spectrum 2 | | Spectrum 3 | | Spectrum 4 | |
|---|---|---|---|---|---|---|---|
| Element | Weight % | Element | Weight % | Element | Weight % | Element | Weight % |
| N | 0.00 | N | 0.00 | N | 0.00 | N | 0.00 |
| O | 24.57 | O | 19.29 | O | 19.17 | O | 16.40 |
| Mg | 5.03 | Mg | 5.77 | Mg | 5.96 | Mg | 6.26 |
| Al | 70.40 | Al | 74.94 | Al | 74.87 | Al | 77.34 |

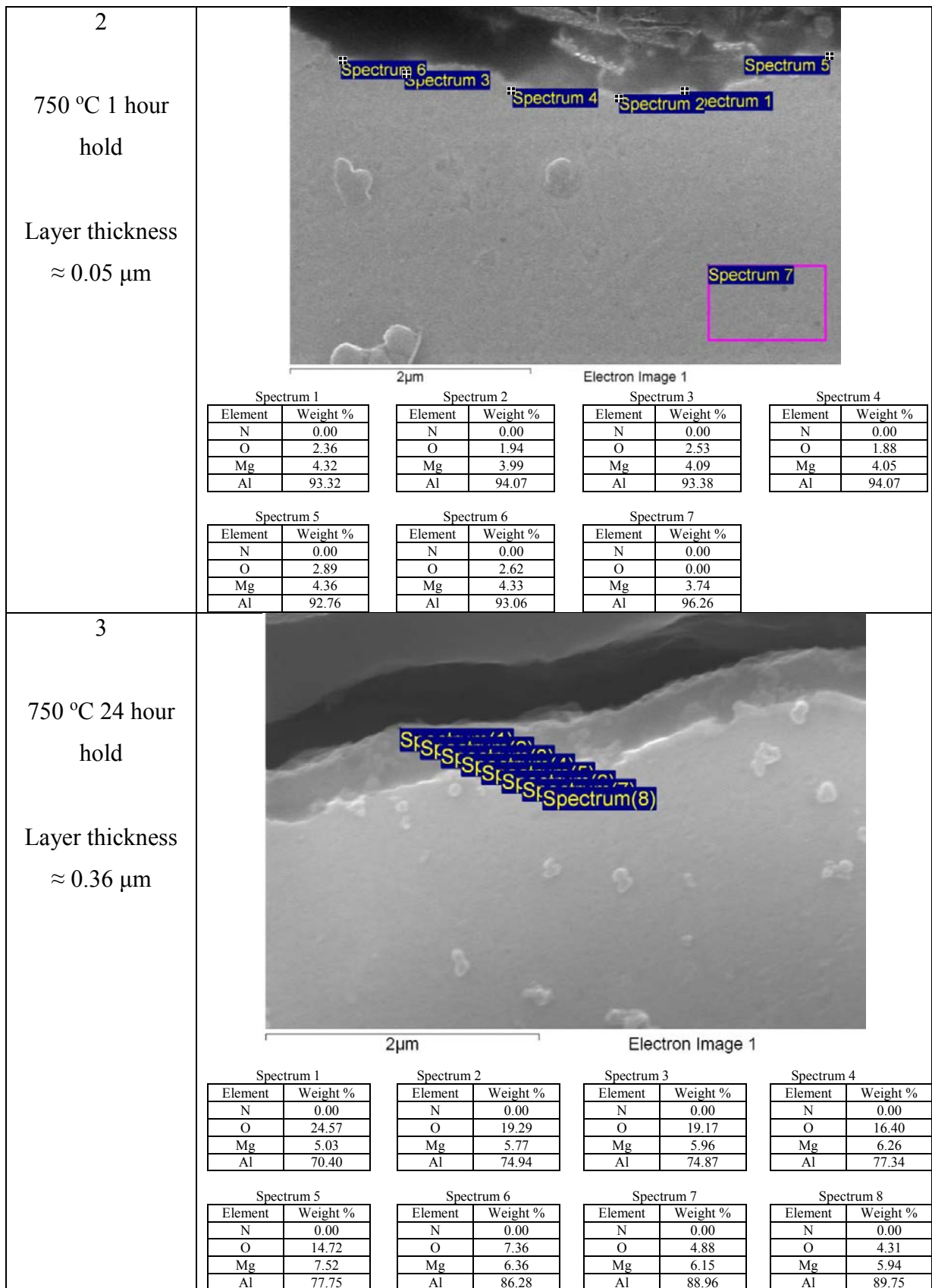| Spectrum 5 | | Spectrum 6 | | Spectrum 7 | | Spectrum 8 | |
|---|---|---|---|---|---|---|---|
| Element | Weight % | Element | Weight % | Element | Weight % | Element | Weight % |
| N | 0.00 | N | 0.00 | N | 0.00 | N | 0.00 |
| O | 14.72 | O | 7.36 | O | 4.88 | O | 4.31 |
| Mg | 7.52 | Mg | 6.36 | Mg | 6.15 | Mg | 5.94 |
| Al | 77.75 | Al | 86.28 | Al | 88.96 | Al | 89.75 |

**Figure 108 continued - EDX analysis of Al-4%Mg samples in N$_2$**

The EDX analysis seen in Figure 108 shows the composition of the layers. There were no signals for nitrogen within the layers. EDX struggles to pick up nitrogen at low levels, so it may

have contributed to this (The author was informed that WDX could not be used accurately on surface regions, so a more accurate result was not achieved). The levels of Mg in the layers were generally similar to those in the alloy itself (~4 wt. %) in both the 5 minute and 1 hour samples (Figure 108 sample 1 and 2, respectively), suggesting that migration of Mg did not occur to a great level. The oxygen levels were also very low in these samples, but as the layers were thin, this was not unexpected. The 24 hour sample (Figure 108 sample 3) the Mg levels were slightly higher overall (~5-7 wt. %), as were the oxygen levels. This suggests that Mg migrated to the surface as the liquid alloy reacted with residual oxygen present in the cell to form MgO or spinel. The XRD spectra for these samples can be seen in Figure 109 and Figure 110.
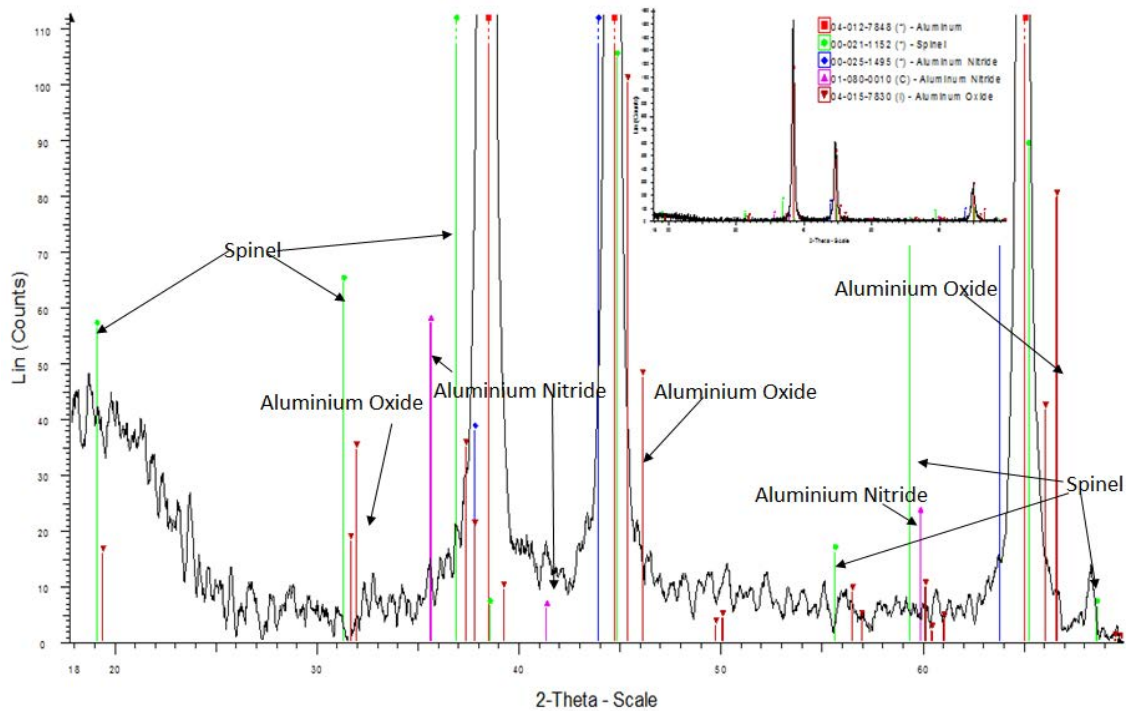


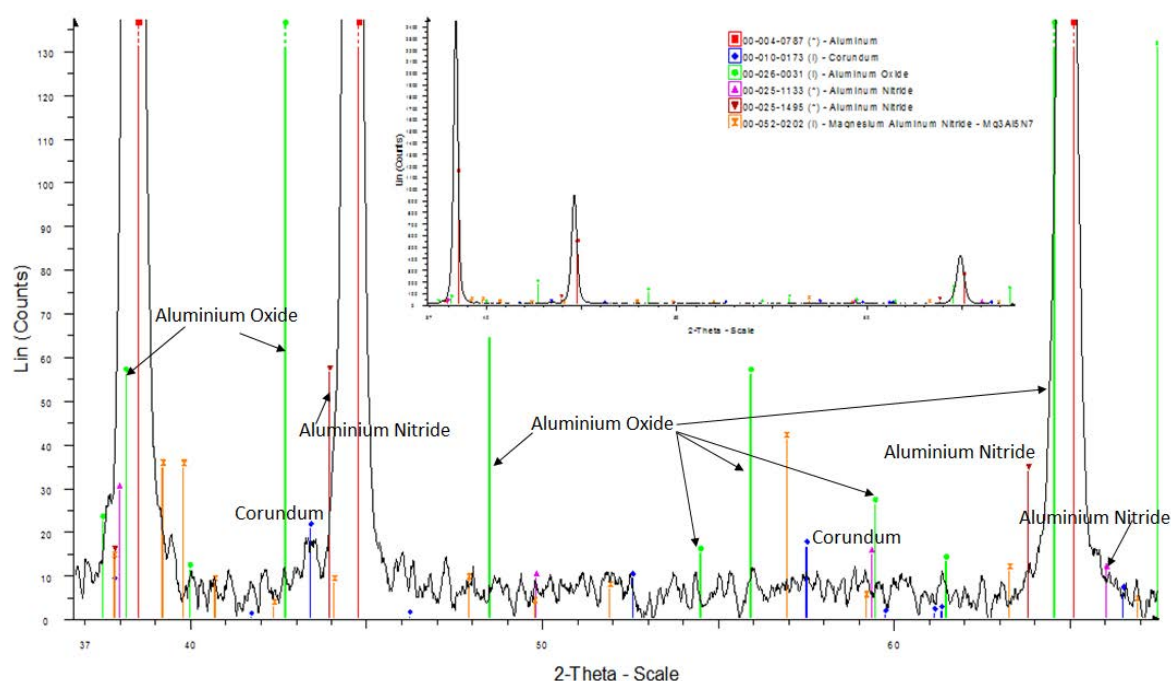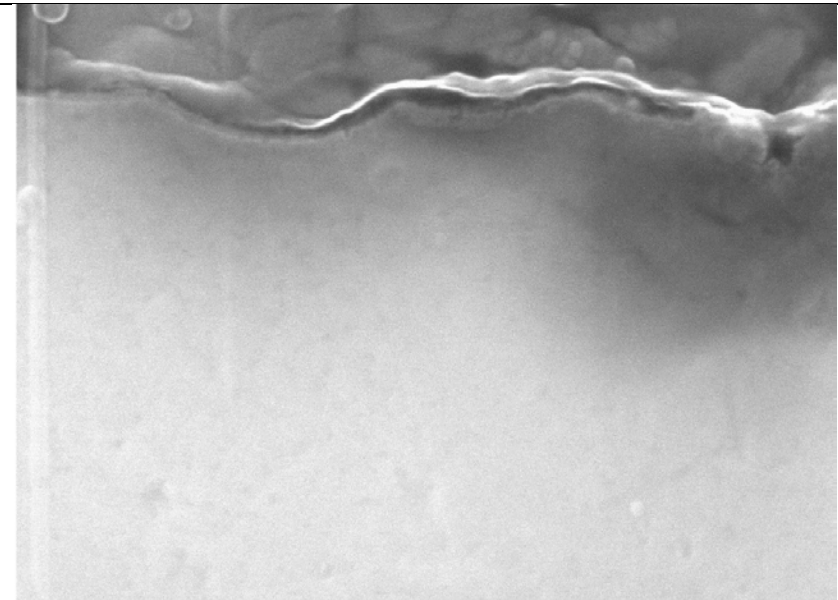**Figure 109 - The XRD spectra for Al-4%Mg held for 5 minutes at 750 °C in N2 (zoomed out spectra inset)**
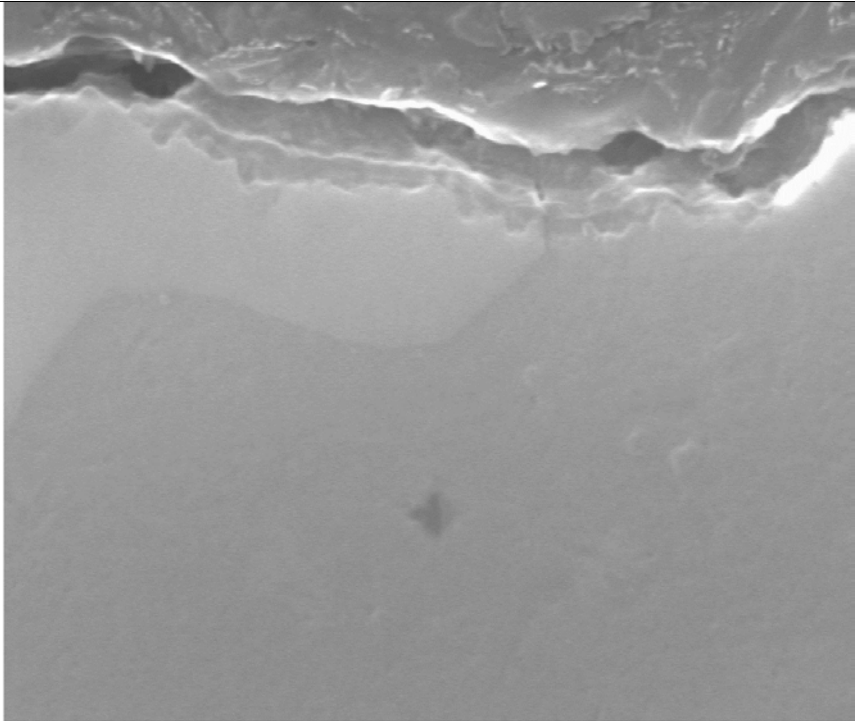
**Figure 110 - The XRD spectra for Al-4%Mg held for 24 hours at 750 °C in N2 (zoomed out spectra inset)**

The XRD spectra in Figure 109 and Figure 110 both had small signals for AlN. This suggested that the layers of AlN were very thin, as seen in the SEM images for Al-4%Mg in Figure 106, which may be why the EDX detector struggled to detect them. Alumina, in the gamma form, was detected in both samples and α-alumina was detected in the 24 hour sample. The initial growth of oxide was very slow, as seen in the SEM images in Figure 106. But even though the layer on the 24 hour sample was thinner than that for SP-Al, α-alumina formed. Under normal atmospheric conditions, i.e. in air, Mg increases the oxidation rate by forming a porous oxide of MgO (Agema & Fray 1989). There was not any indication that MgO formed in these samples, but spinel did form in the 5 minute sample (Figure 109), so it may have been this that encouraged the formation of α-alumina whilst growing a relatively thin layer.

3.3.2 – Al-7 wt. % Si-0.3 wt. % Mg

Cross sections of Al-7%-0.3%MgAl-7%Si-0.3%Mg observed by SEM can be seen in Figure 110, which includes the measurements for average layer thickness.

**Figure 111 - Images from the 750 °C holds at different times for Al-7%Si -0.3%Mg in N2 atmosphere, the thickness of the layer is also noted**

| Sample | Image |
|---|---|
| 1<br><br>750 ºC 5 min hold<br><br>Layer thickness ≈ 0.03 µm | <br>1µm   Electron Image 1 |
| 2<br><br>750 ºC 1 hour hold<br><br>Layer thickness ≈ 0.15 µm | <br>2µm   Electron Image 1 |

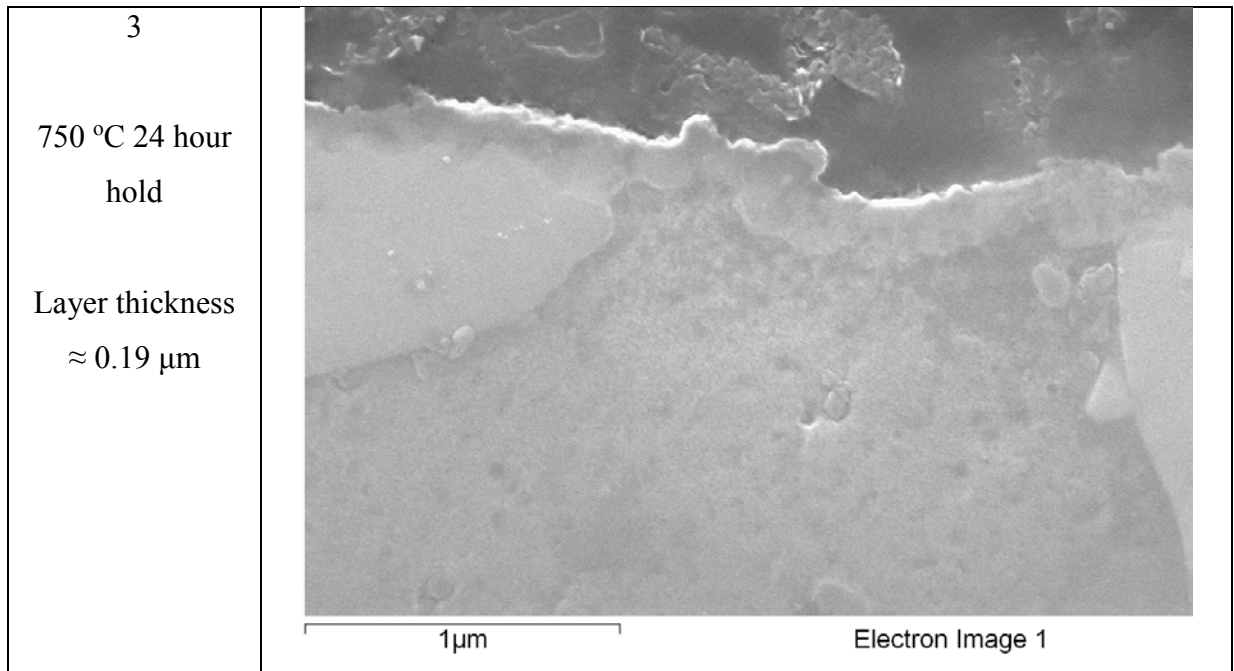| 3  750 °C 24 hour hold  Layer thickness ≈ 0.19 μm |  |
|---|---|

1μm                    Electron Image 1

**Figure 111 continued - Images from the 750 °C holds at different times for Al-7%Si -0.3%Mg in N2 atmosphere, the thickness of the layer is also noted**

The layer thickness in the Al-7%Si-0.3%Mg alloy increased by ~0.16 μm over 24 hours in $N_2$. The changes are summarised in Table 21 and Figure 112. The layer initially grew by ~0.12 μm, from 0.03 μm at 5 minutes (Figure 111, sample 1) to ~0.15 μm at 1 hour (sample 2). The growth increased by only ~0.04 μm during the longer holding time, from ~0.15 μm at 1 hour to ~0.19 μm at 24 hours (sample 3). The layers were much thinner than those of SP-Al, being thinner by ~1.18 μm after 24 hours.

**Table 21 - Summary of layer thicknesses for Al-7%Si-0.3%Mg held at 750 °C in nitrogen atmosphere**

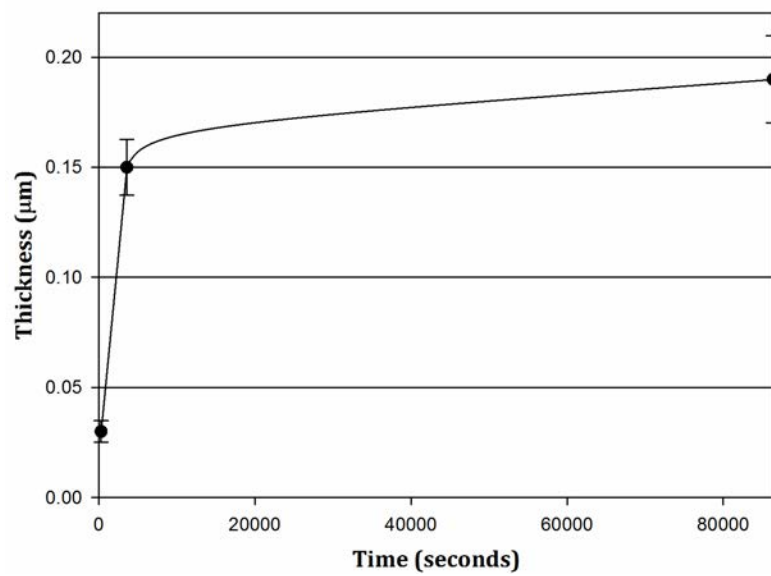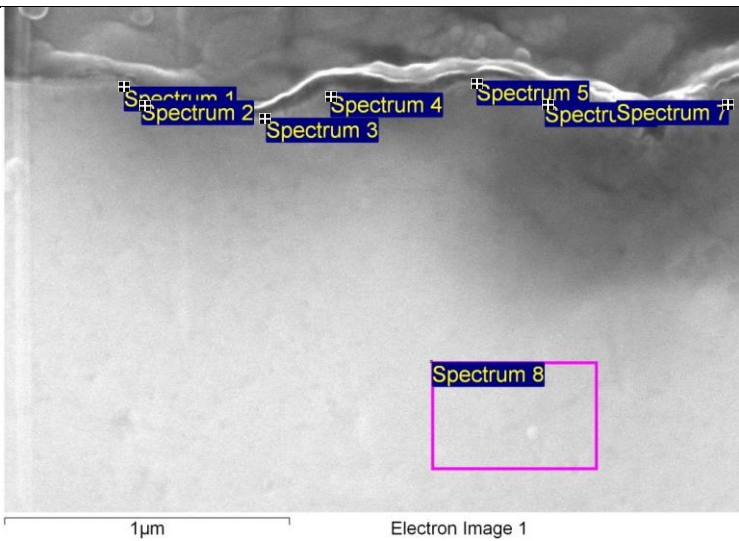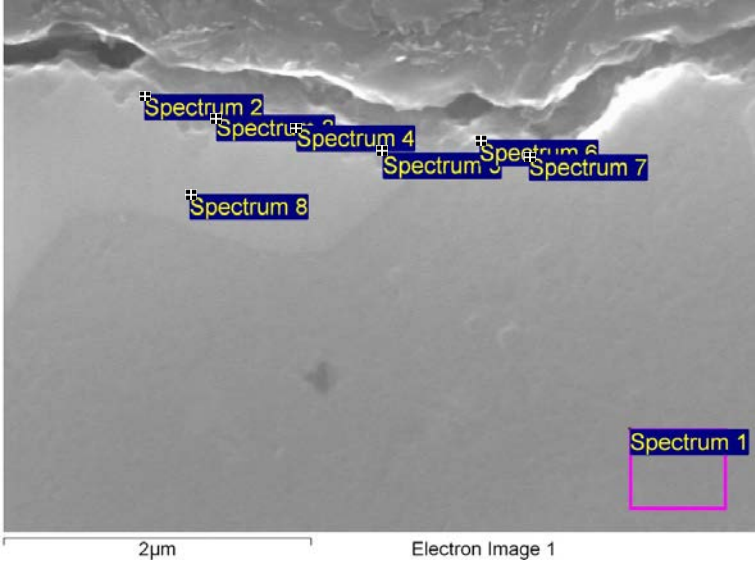| Holding time (s) | Layer thickness (μm) |
|---|---|
| 300 | 0.03 |
| 3600 | 0.15 |
| 86 400 | 0.19 |

**Figure 112 - Thickness of the layer vs. holding time for Al-7%Si-0.3%Mg samples held at 750 °C in N2**

The initial growth rate of the layer between 5 minutes and 24 hours was faster than that between 1 hour and 24 hours. The initial growth occurred at a rate of ~3.6 x $10^{-5}$ $\mu$m s$^{-1}$. The growth rate between 1 and 24 hours was ~4.8 x $10^{-7}$ $\mu$m s$^{-1}$. EDX analysis for the samples can be seen in Figure 112.

**Figure 113 - EDX analysis of Al-7%Si-0.3%Mg samples in N2**

| Sample | Image |
|---|---|

### 750 ºC 5 min hold

### Layer thickness ≈ 0.03 μm



Electron Image 1 (1μm)

| Spectrum 1 | | Spectrum 2 | | Spectrum 3 | | Spectrum 4 | |
|---|---|---|---|---|---|---|---|
| Element | Weight % | Element | Weight % | Element | Weight % | Element | Weight % |
| N | 0.00 | N | 0.00 | N | 0.00 | N | 0.00 |
| O | 16.44 | O | 10.39 | O | 11.10 | O | 14.90 |
| Mg | 4.91 | Mg | 4.42 | Mg | 4.03 | Mg | 7.15 |
| Al | 78.65 | Al | 81.46 | Al | 82.67 | Al | 74.73 |
| Si | 0.00 | Si | 3.73 | Si | 2.20 | Si | 3.22 |

| Spectrum 5 | | Spectrum 6 | | Spectrum 7 | | Spectrum 8 | |
|---|---|---|---|---|---|---|---|
| Element | Weight % | Element | Weight % | Element | Weight % | Element | Weight % |
| N | 0.00 | N | 0.00 | N | 0.00 | N | 0.00 |
| O | 14.43 | O | 14.47 | O | 19.47 | O | 2.39 |
| Mg | 4.06 | Mg | 4.67 | Mg | 5.30 | Mg | 1.00 |
| Al | 76.72 | Al | 80.86 | Al | 75.23 | Al | 94.56 |
| Si | 4.78 | Si | 0.00 | Si | 0.00 | Si | 2.05 |

### 750 ºC 1 hour hold

### Layer thickness ≈ 0.15 μm



Electron Image 1 (2μm)

| Spectrum 1 | | Spectrum 2 | | Spectrum 3 | | Spectrum 4 | |
|---|---|---|---|---|---|---|---|
| Element | Weight % | Element | Weight % | Element | Weight % | Element | Weight % |
| N | 0.00 | N | 0.00 | N | 0.00 | N | 0.00 |
| O | 0.00 | O | 5.30 | O | 3.99 | O | 2.50 |
| Mg | 0.32 | Mg | 0.75 | Mg | 0.38 | Mg | 0.52 |
| Al | 93.74 | Al | 44.44 | Al | 46.55 | Al | 53.45 |
| Si | 5.95 | Si | 49.50 | Si | 49.08 | Si | 43.53 |

| Spectrum 5 | | Spectrum 6 | | Spectrum 7 | | Spectrum 8 | |
|---|---|---|---|---|---|---|---|
| Element | Weight % | Element | Weight % | Element | Weight % | Element | Weight % |
| N | 0.00 | N | 0.00 | N | 0.00 | N | 0.00 |
| O | 2.66 | O | 3.02 | O | 2.71 | O | 1.54 |
| Mg | 0.35 | Mg | 0.81 | Mg | 0.32 | Mg | 0.40 |
| Al | 82.90 | Al | 88.66 | Al | 88.08 | Al | 78.92 |
| Si | 14.10 | Si | 7.51 | Si | 8.89 | Si | 19.15 |

| 750 °C 24 hour hold<br><br>Layer thickness ≈ 0.19 μm |  |
| --- | --- |

Figure 113 continued - EDX analysis of Al-7%Si-0.3%Mg samples in N2

The EDX analysis results are shown in Figure 113. It was noted that there was no signal for $N_2$ in any sample, but this could be due to the fact that EDX detectors struggle to pick up $N_2$ in low levels. There was only 0.3wt.% Mg present in the Al-7%Si-0.3%Mg alloy, but the EDX results suggested that higher levels were present (typically 4-5wt.% in sample 1 (5 mins), 0.35-0.8 wt.% in sample 2 (1 hour), 1.5-3.5 wt.% in sample 3 (24 hours)). This suggests a migration of Mg from the bulk to the surface during the reaction period, which could have led to the oxidation rate increase. The XRD spectra in Figure 114 and Figure 115 show the crystal structures picked up at the surface and near surface region.
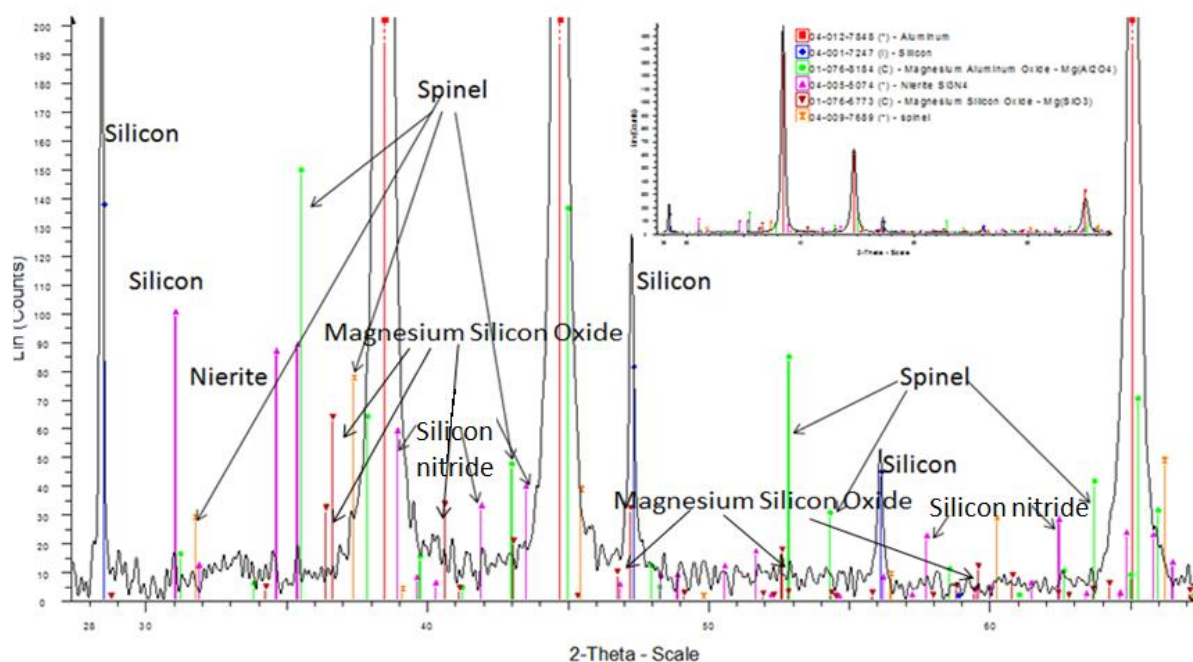
**Figure 114 - The XRD spectra for Al-7%Si-0.3%Mg held for 5 minutes at 750 °C in N2 (zoomed out spectra inset)**
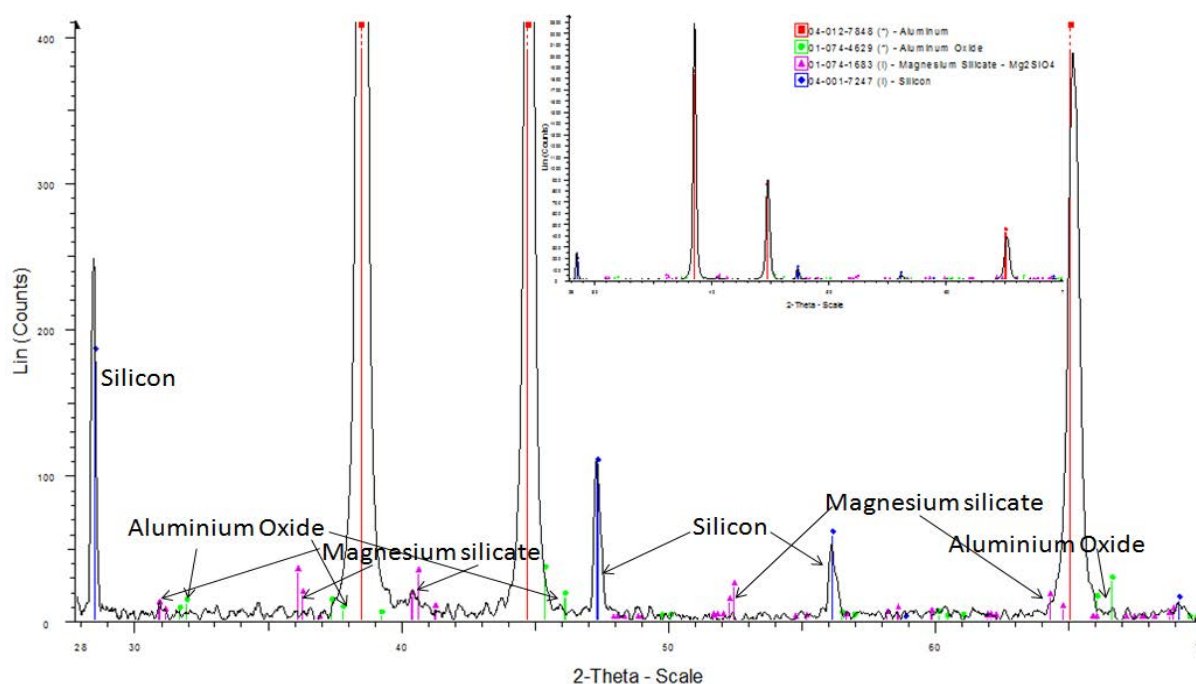


**Figure 115 - The XRD spectra for Al-7%Si-0.3%Mg held for 24 hours at 750 °C in N2 (zoomed out spectra inset)**

The XRD spectra in Figure 114 and Figure 115 suggested the presence of Si and Al, which were expected in this alloy. There was no detection for AlN, but small amounts were detected in the 5 minute sample (Figure 114) of a silicon containing nitride or $Si_3N_4$. This could be why no AlN was detected, as it may be that the nitrogen reacted preferentially with the silicon. The level of nitride does not appear to have increased, as it was not detected in the 24 hour sample (Figure 115), suggesting that as the rest of the layer grew, it did not. There was no sign of

161

alumina in the 5 minute sample, suggesting it was very small (high levels of oxygen (10-15%) were picked up in the EDX results (Figure 113, sample 1)), which seemed likely as the layer was ~0.03 μm at this time. There are signals for γ-alumina in the 24 hour sample. In both cases there were signals for oxides containing Al and Si, Magnesium silicon oxide ($Mg(SiO_3)$) in the 5 minute sample (Figure 114) and Magnesium silicate ($Mg_2SiO_4$) in the 24 hour sample (Figure 115). It seemed likely that the growth of the layer was due to the growth of γ-alumina and the oxides containing Mg and Si rather than any nitride growth, but the presence of nitrogen may have suppressed the growth overall as there would have been little residual oxygen for the liquid metal to react with.

The effect of a nitrogen atmosphere, was that the growth of oxides was suppressed, in favour of the formation of nitrides. The SP-Al sample grew a layer containing γ-alumina and AlN, with a final thickness of 1.37 μm, much thicker than the 0.37 μm that grew in air. The thicker layer suggested the higher growth rate of the nitrides compared to the oxide. The AlN had a feather-like structure after 24 hours which reached a height of 3.72 μm above the main nitride layer, which was a different structure to the layer that grew in air. This suggests the formation of a nitride layer is favoured while the formation of oxides is suppressed. The Al-4%Mg alloy did not grow a very thick layer when in the presence of a $N_2$ atmosphere. The layer grew to 0.36 μm, much thinner than the oxide that grew in air whose sample was completely oxidised. There was a small detection of AlN in these samples, and Mg did not appear to react with the nitrogen to form nitrides. The Al-7%Si-0.3%Mg alloy also had a much thinner layer of 0.19 μm after 24 hours, compared to 1.56 μm in air. No AlN was detected for the samples, but a $Si_3N_4$ was formed suggesting this has a role in suppressing the growth of the film. It was apparent that a nitrogen atmosphere changed the growth of surface layers.

**3.4 – Manufacture of Spinel-containing Copper Layers and their use as Grain Refiners**

The potential grain refinement of oxides has been explored in (Fan et al 2009c). Grain refinement tests were undertaken to determine the potential refinement capabilities of spinel ($MgAl_2O_4$) in commercial purity Al (CP-Al). The results are described in the following chapter.

3.4.1 – Commercial Purity and Spinel Additions

*3.4.1.1 – Microstructure of Commercial Purity Samples*

Samples of CP-Al were cast in to test bars. The bars were cross-sectioned, etched and viewed using optical microscopy. They can be seen in Figure 116.
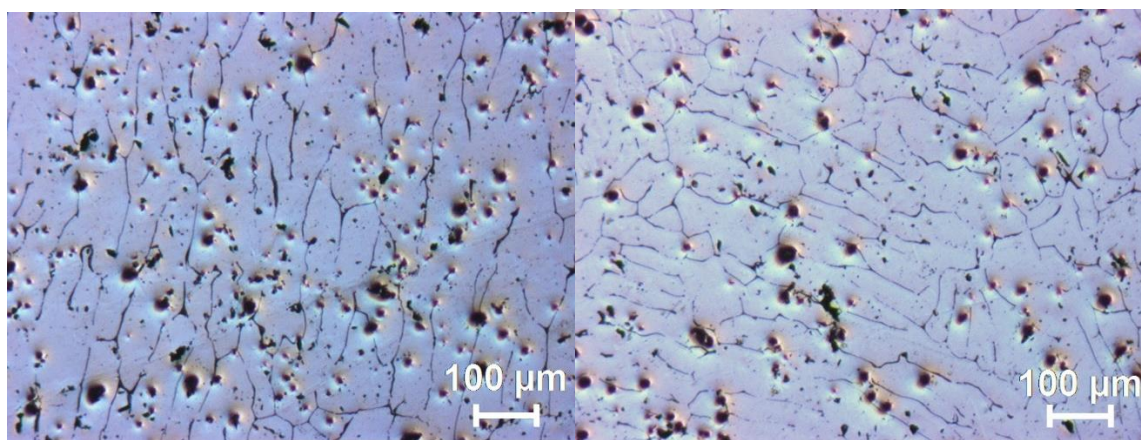


**Figure 116 - Optical micrographs of cast CP-Al samples (black spherical objesct are pores that occurred from the casting process)**

The optical images for sand cast CP-Al samples without can be seen in Figure 116. The appearance of the grains was aligned, with an average grain size of ~47 μm, measured across a series of images. There were pores present on the surface due to turbulence. As the pouring temperature varied by little (<3 °C), this would have had little effect on the grain size.

*3.4.1.2 – Microstructure of CP-Al with Spinel Grain Refiner*

*3.4.1.2.1 – Codeposition Tests*

The codeposition tests were undertaken to determine the optimum method for deposition of spinel in a coating of copper (Cu). The percentage of Mg and Al in the layer was determined by EDX analysis, and was used to calculate the percentage of spinel in the layer. The EDX results can be seen in Table 23. Multiple EDX spectra were observed in multiple locations and the percentages of the spinel were calculated. The levels of Mg + Al make up 55 wt. % of the spinel total and so was calculated using equation (38. The Mg and Al content was taken from EDX results (an example is given in Figure 119) As the spinel used in the experiments was

bought from an external supplier, it was assumed that the levels of Mg and Al directly corresponded to the amount of spinel in the Cu layer (i.e no unreacted Mg).

$$\frac{Mg\ content + Al\ content}{0.55} = \%\ spinel\ in\ layer \tag{38}$$

The initial deposition experiments (section 2.6, Table 4) proved to be poor techniques for optimum deposition of spinel within the layers. There did not appear to be much pickup of spinel particles. Examples of the deposited layers can be seen in Figure 117.
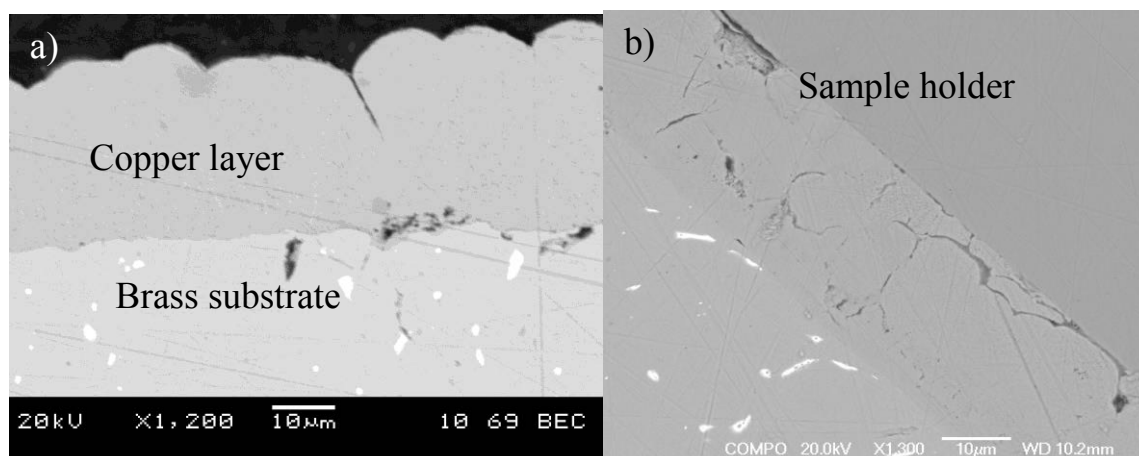


**Figure 117 - SEM images of codeposited layers, no surfactant, 10 g/l spinel a) DC -20mA 500 rpm b) FPR 50 Hz 1000 rpm**

Experiments with higher concentrations of spinel in the solution along with the addition of a surfactant (SDS), as seen in section 2.6 Table 5, were performed. The speed of the pulse reverse was also increased in order to achieve higher percentages of spinel particles in the layer. The experiments had much higher percentages of spinel than the initial experiments, with the optimum pickup of 8% on the sample made at 200 Hz, 1000 rpm after 30 minutes. The calculated spinel levels can be seen in Table 22 and examples of samples in Figure 118.

**Table 22 -  Spinel pickup for secondary electrodeposition experiments**

| Experimental parameters | Rotating electrode speed (rpm) | Spinel pickup (%) |
|---|---|---|
| -20 mA/cm$^2$ , 30 mins | 800 | <1 |
| 50 Hz | 800 | 5 |
| 200 Hz | 800 | 6 |
| 200 Hz | 1000 | 8 |
| 200 Hz | 1200 | 7 |
| 200 Hz, 50 °C | 800 | 4 |
| 50 Hz | 2000 | <1 |
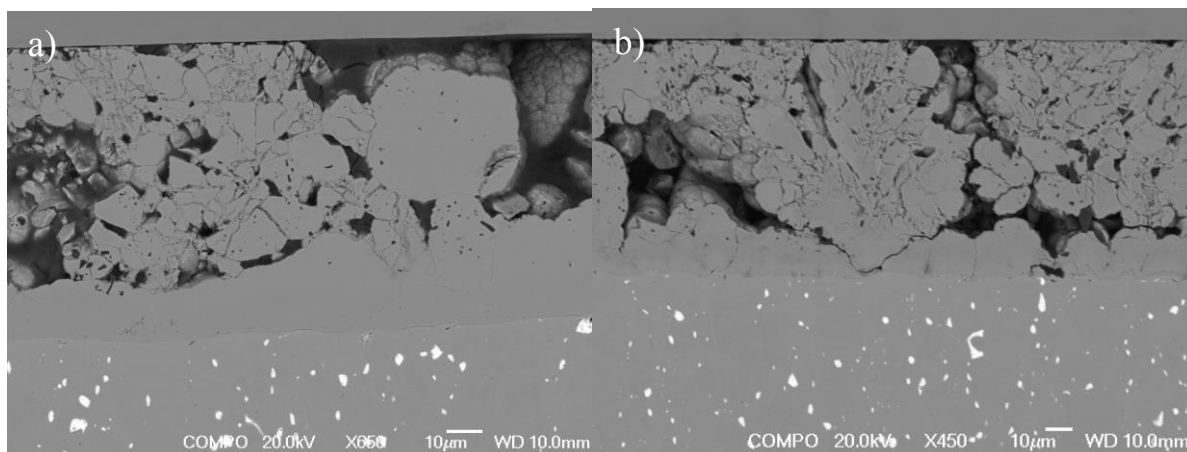
**Figure 118 - SEM images of codeposited layers, 0.4 g/l SDS, 50 g/l spinel a) FPR 200 Hz 800 rpm 50 °C b) FPR 50 Hz 800rpm**

These results were then taken forward to the experimental design so that the variables were the pulse speed and rotation speed. The design aimed to determine the optimum conditions for spinel incorporation. An example of EDX analysis used for spinel calculations can be seen in Figure 119.
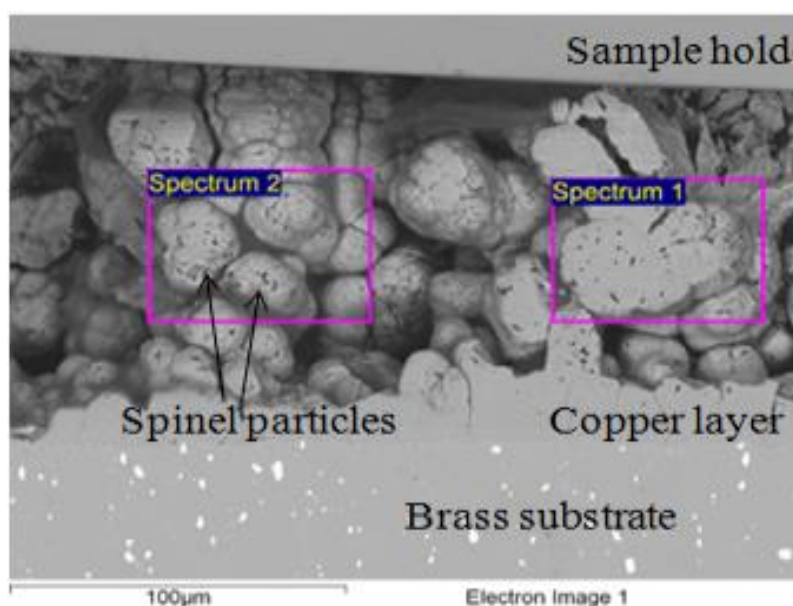


|  | Spectrum 1 | Spectrum 2 |
|---|---|---|
| Element | Weight% | |
| O K | 7.39 | 9.76 |
| Mg K | 0.78 | 1.17 |
| Al K | 1.72 | 2.25 |
| Cu K | 90.11 | 86.81 |

**Figure 119 - Image and EDX analysis of one area of sample 8 (200 Hz, 1000 rpm)**

The levels of Mg + Al were used to calculate the amount present in the layer. The average for the section shown in Figure 119 was 5.35 wt. %. The mean percentage for different areas of each layer was taken and the average for experiment 8 (the best result - 200 Hz, 1000 rpm, as shown in Table 23) was 8.5 wt. %.

165

| Experiment | Method (Hz, rpm) | Spinel pickup (%) |
|---|---|---|
| 1 | 200, 2000 | 6.25 |
| 2 | 125, 1400 | 2.73 |
| 3 | 50, 2000 | 4.5 |
| 4 | 231.66, 1400 | 2.3 |
| 5 | 125, 550 | 1 |
| 6 | 18.9, 1400 | 2 |
| 7 | 125, 2248 | 3 |
| 8 * | 200, 1000 * | 8.5 * |
| 9 | 200, 800 | 6.5 |
| 10 | 50, 800 | 5.5 |
| 11 | 200, 1200 | 7 |

The method used in experiment 8 was used to make 4 samples of copper containing spinel. The codeposition took place for 2 hours in this case, rather than 30 minutes, to provide a thicker coating with more particles. A cross section of a sample made with this method is shown in Figure 120.
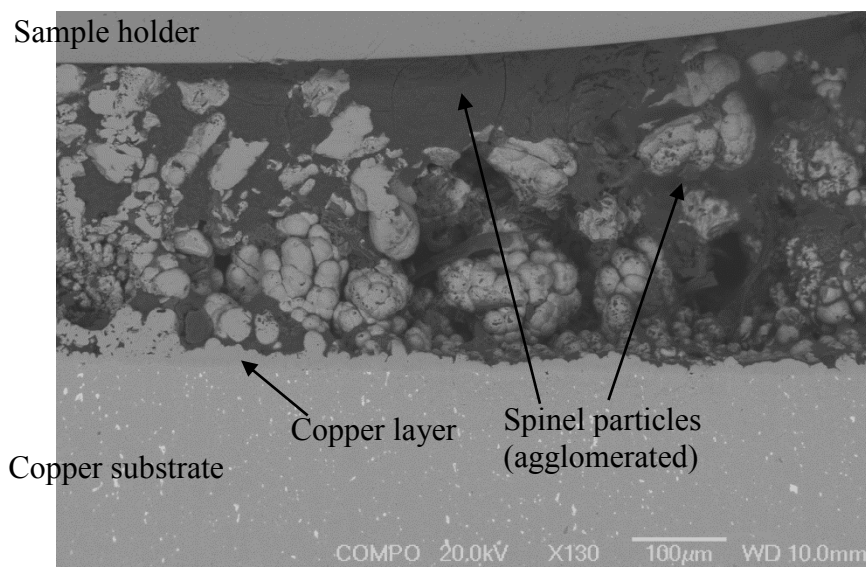


Figure 120 - SEM image of layer using method 8 (200 Hz, 1000 rpm) for 2 hours

The same calculation (38) was used to determine the spinel content of this layer, which was calculated to be ~13.6 wt. %. The mean thickness of the layer was determined to be ~420 μm and was used, along with the diameter of the sample (8 mm cylindrical substrate) and density of copper (8.96 g/cm$^3$, Smithells 1976) to calculate the amount of spinel within a casting of 2 kg (the weight of the casting to be made). This can be seen in the calculations below (Equations (39) to (43)).

$$Area\ of\ disc = \frac{(8 \times 10^{-3})^2}{2} \times \pi = 5.0265 \times 10^{-5} m^2 \tag{39}$$

$$Volume\ of\ layer = area\ of\ disc \times thickness\ of\ layer$$
$$(5.0265 \times 10^{-5})(4.20 \times 10^{-4}) = 2.111 \times 10^{-8} m^3 = 0.0211\ cm^3 \tag{40}$$

$$Mass\ of\ layer = 0.0211 \times 8.96 = 0.189\ g \tag{41}$$

$$Mass\ of\ spinel = 0.189 \times 0.136 = 0.0257\ g \tag{42}$$

$$\frac{0.025}{2000} \times 100 = 0.00125\ (\%) = 12.5\ ppm \tag{43}$$

The amount of spinel in a layer was 12.5 ppm. Four such samples were added to the 2 kg charge of CP-Al to be cast, meaning that the addition level was 50 ppm. This was cast in to a sand mould to form test bars as shown in Figure 37.

*3.4.1.2.2 – Microstructure of Spinel Containing CP-Al samples*

Cross sections (transverse across test bar) were taken, etched and observed using an optical microscope. Some areas did not etch well, so the measurements were taken from locations with a clearer etched microstructure, to ensure the measurement grain boundaries rather than dendrite arms. The images can be seen in Figure 121.
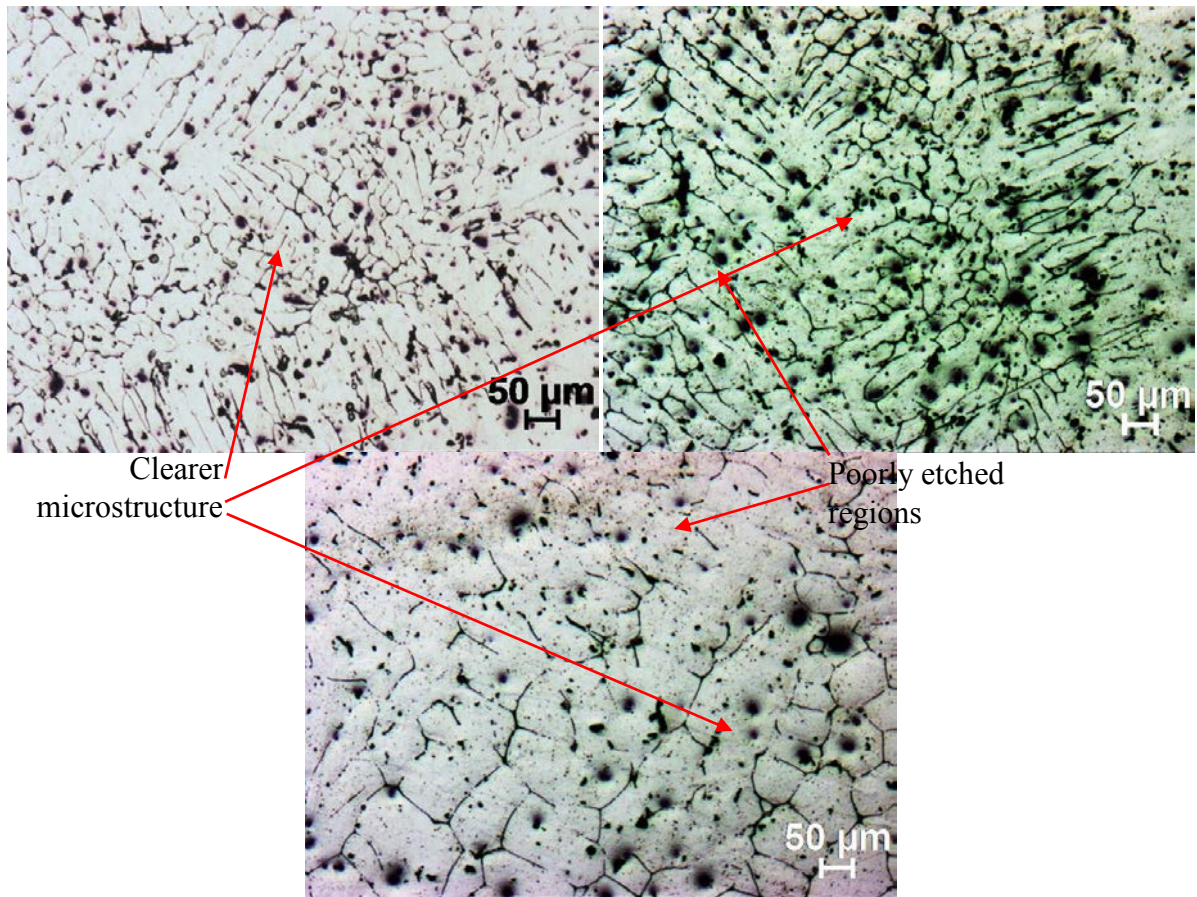
**Figure 121 - Images of CP-Al samples with a spinel grain refiner**

The mean grain size was taken from the images in Figure 121, and found to be ~36 µm. A comparison between the CP-Al and CP-Al with spinel addition can be seen in Table 23 and Table 24.

**Table 24 - Summary of the grain size in sample with and without spinel additions**

| Experiment | Average grain size (µm) | Error (µm) |
|------------|-------------------------|------------|
| CP-Al | 47 | 4.65 |
| CP-Al + spinel | 36 | 3.75 |

The addition of spinel to the melt therefore resulted in a reduction in grain size of ~23%. But it can be seen from Figure 121 that the grains in the spinel sample were smaller in certain areas, they have a more columnar appearance. The smaller grains also appeared to be localised, suggesting that the grain size reduction was not uniform throughout the casting. The addition used was only 50 ppm, lower than the minimum level of 125-150 ppm used in commercial alloys (Cook 1998). The equivalent of 50 ppm was the most that could be made via deposition method during the time taken for manufacture, so industrial levels could not be added. This could be the reason why the grain size reduction was non-uniform. If the addition was greater, perhaps the effect would be more pronounced. The presence of Cu in the brass stub may have

also had an effect.  Sigworth & Kuhn (2007) showed that copper can hinder the grain refining effect of $TiB_2$, but as the levels used here are small (~0.04 wt.%), compared to those in the work (3.5 wt.%) the effect should not have been too great.

3.4.2 - Comparison of Spinel with a Commercial Grain Refiner

A casting of CP-Al with a commercial grain refiner added, 5:1 titanium diboride, was completed. The grain structure of the sample can be seen in Figure 122.
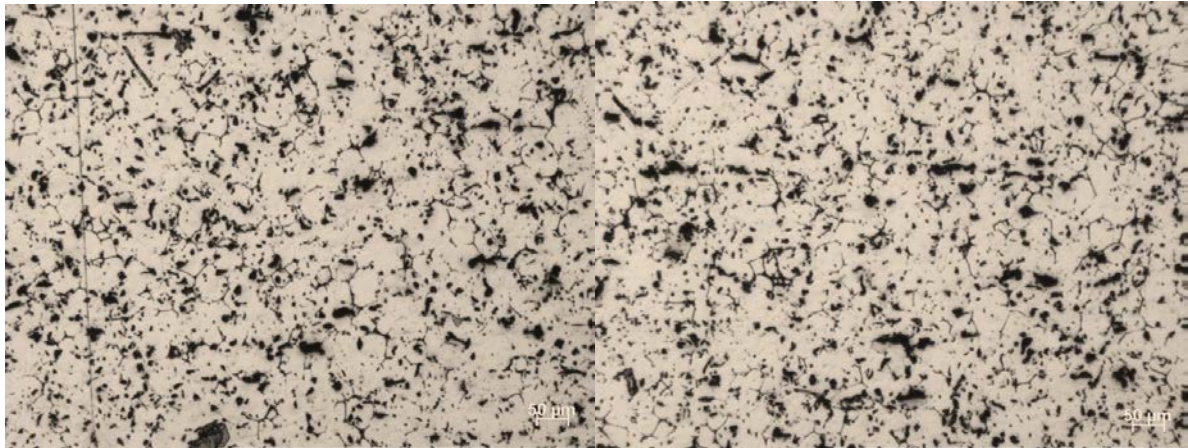


**Figure 122 - Images of CP-Al samples with a standard 5:1 $TiB_2$ grain refiner (containing pores due to casting procedure)**

The mean grain size was taken from the images in Figure 122 and was ~30 μm. A comparison of the grain sizes of CP-Al, CP-Al + spinel and CP-Al + $TiB_2$ can be seen in Table 25.

**Table 25 - Summary of the grain size in sample with and without spinel additions**

| Experiment | Average grain size (μm) | Error (μm) |
|---|---|---|
| CP-Al | 47 | 4.65 |
| CP-Al + spinel | 36 | 3.75 |
| CP-Al + $TiB_2$ | 30 | 4.04 |

The addition of the $TiB_2$ grain refiner led to a grain size of 30 μm, a reduction in grain size of ~36% when compared to CP-Al alone and a reduction of ~17% when compared with CP-Al + spinel.

It can be seen by comparing the images in Figure 116Figure 120, Figure 121 and Figure 122, and the comparison in Table 25, that the addition of a grain refiner improved the grain structure by reducing grain size. The manufacture of the spinel containing copper layer seemed to have had a beneficial effect on the grain size by reducing it by 23%. As the addition was less than the usual level (~50 ppm spinel as opposed to 125-150 ppm Tibor), this may have been the

reason why the effect did not seem to be uniform. A larger addition of spinel may improve the grain refining effect.

# 4 - Discussion

## 4.1 - Effects of Additional Elements on Oxidation of Superpure Aluminium

A comparison of the oxide thicknesses of the different alloys from the experiments is shown in Table 26 and Figure 123.

**Table 26 - A comparison of the oxide thickness for different alloys held for up to 24 hours at 750 °C**

| Oxide thickness (µm) | Holding time | | | | | |
|---|---|---|---|---|---|---|
| | 5 min | 17 min | 1 hour | 3 hour | 7 hour | 24 hours |
| Superpure Al | 0.05 | 0.10 | 0.30 | 0.53 | 0.42 | 0.37 |
| Al 4%Mg | 5.25 | 6.15 | 7.15 | oxidised* | oxidised* | oxidised* |
| Al 7%Si | 0.12 | 0.14 | 0.15 | 0.40 | 0.10 | 0.39 |
| Al 7%Si 0.3%Mg | 0.65 | 0.6 | 0.67 | 0.73 | - | 1.56 |
| Al 4%Cu | 0.31 | 0.36 | 0.21 | 0.22 | 0.26 | 1.72 |
| Al 1%Fe | 0.04 | 0.14 | 0.15 | 0.27 | 0.20 | 0.21 |
| Al 0.3%Sr | neg* | neg* | 0.33 | 0.49 | 0.64 | 1.1 |
| Al 0.25%Ti | 0.06 | - | 0.1 | - | - | 0.17 |
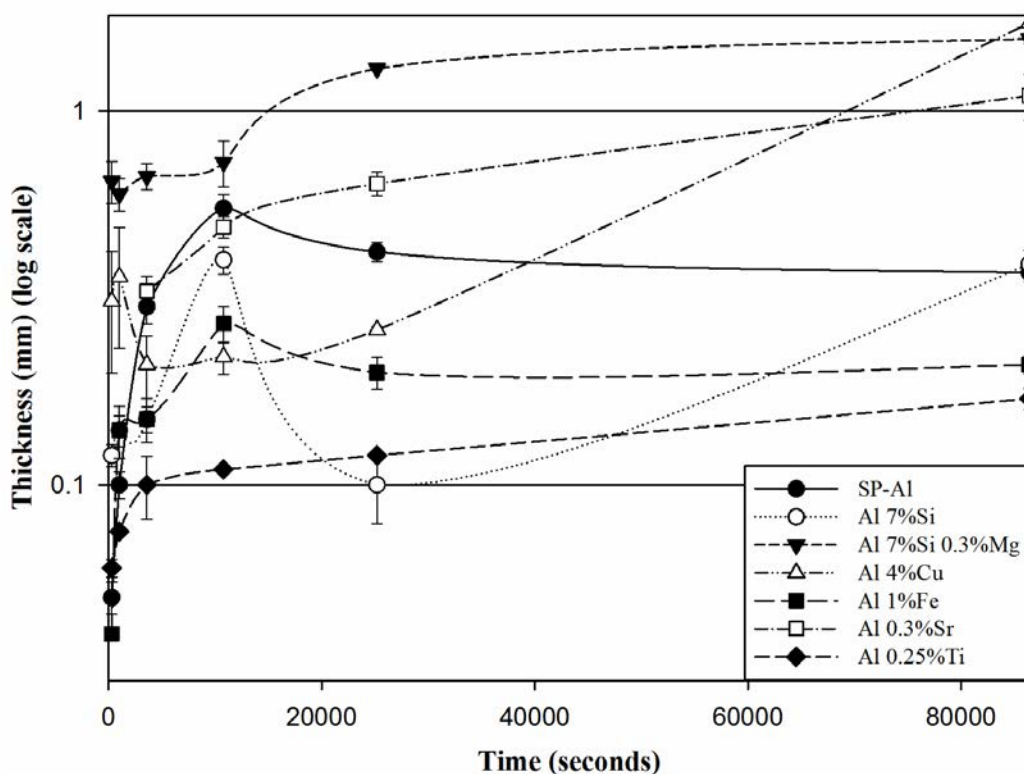


**Figure 123 - Comparison of oxide growth for different alloys held at 750 °C (without Al 4%Mg results – log scale used)**

The XRD results for the SP-Al samples suggested that traces of α-alumina were formed before 24 hours at 750 °C (Figure 44) but after the 5 minute or 1 hour sample (Figure 42 and Figure 43). The growth pattern and the XRD data suggest the formation of γ-alumina from 5 minutes, which slowly grew until 24 hours. It seems that α-alumina formed at some point between 1 hour and 24 hours. Work done by Thiele (1962) suggested that corundum (α-alumina) formed at 1000 minutes (~16.5 hours, see Figure 124), which seems to concur with the results in this work. The experiment that was held for 24 hours (1440 minutes) had traces of α-alumina present. Figure 124 suggests that by this time α-alumina should have been forming for at least 8 hours, leaving a thick oxide on the surface, perhaps thicker than the one present. The work of Thiele (1962) appeared to be similar to the results found in this work, as α-alumina was not found until 24 hours. Perhaps because CP-Al was used by Thiele and SP-Al in this work meant that less α-alumina formed. Thiele demonstrated that samples of different purities and different attempts vary in oxidation rate, shown in Figure 125.
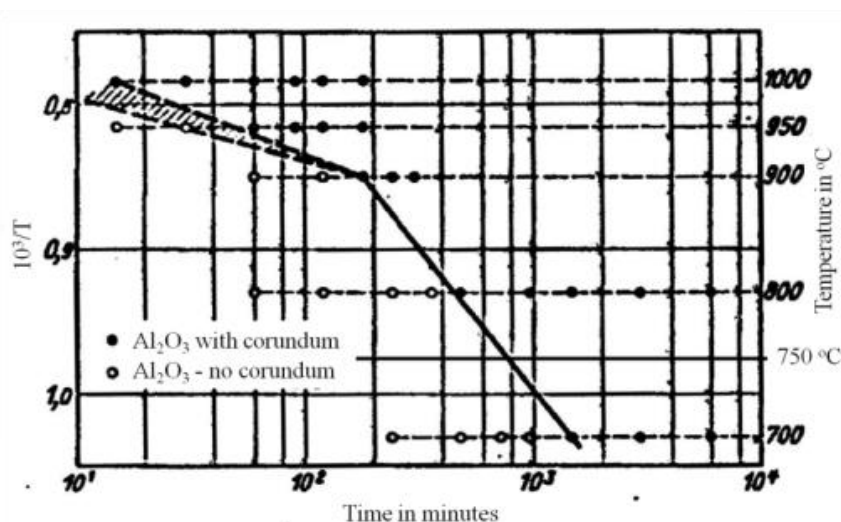


**Figure 124 - Time vs temperature showing the formation of corundum (Thiele 1962)**

172
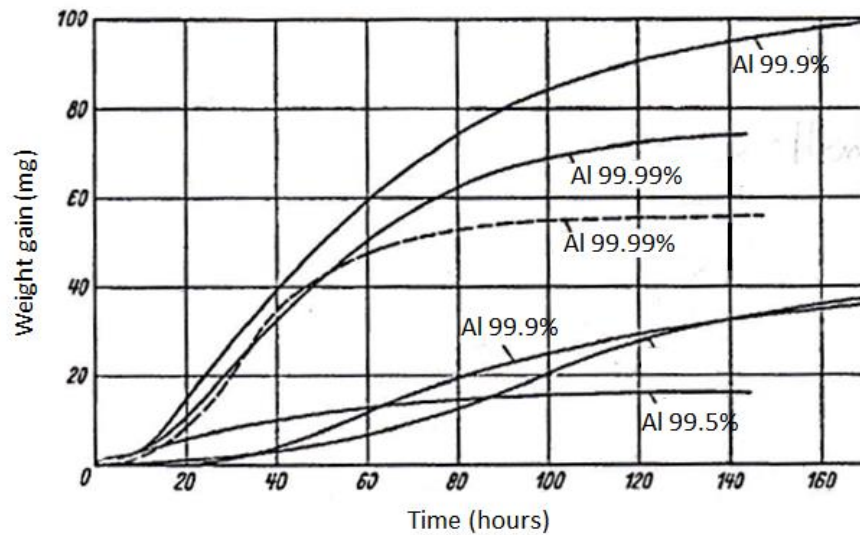
**Figure 125 - Time vs weight gain showing the difference in oxidation for different aluminium purities and samples at 800 °C (Thiele 1962)**

The growth rate of alumina on SP-Al was compared to the known a growth law, the parabolic law and Scully 1990).

$$y^2 = Kt \tag{8}$$

y = thickness

K = constant

t = time

The plot of thickness vs. √time, according to the parabolic growth law of equation (8), can be seen in Figure 126.
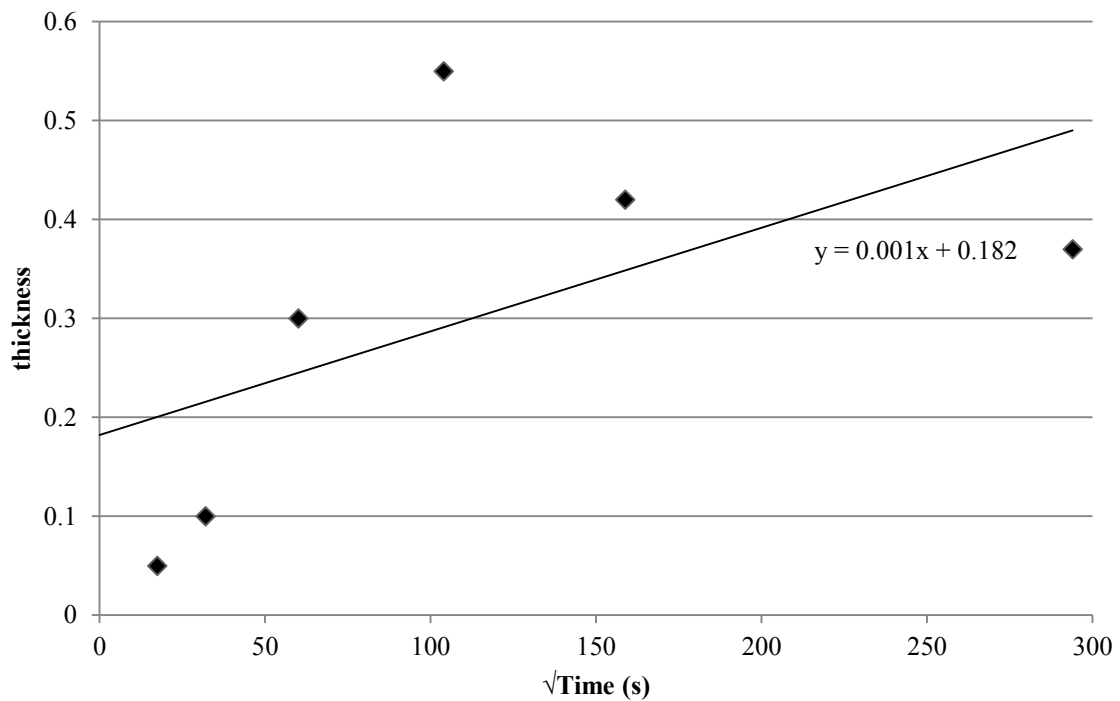
**Figure 126 - Plot of thickness vs. √time for SP-Al samples melted at 750 °C, according to the parabolic growth law**

The straight line plot in Figure 126 suggested that there would be an instantaneous oxide of ~0.18 μm. This is more than the oxide value of 5 minutes (0.05 μm) so it seems that the parabolic growth law was not in force for the entire period of growth. Plus the actual best fit line was not a straight line, but was a curve shape. So the first three results were plotted for the parabolic growth law, which can be seen in Figure 127.
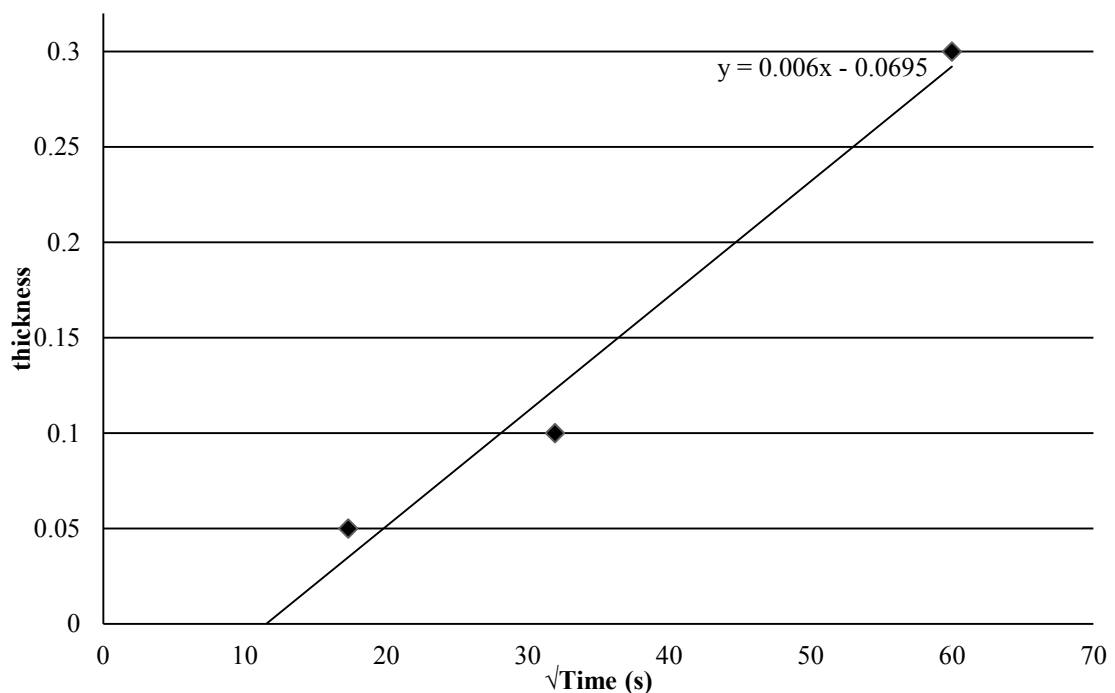


**Figure 127 - Plot of the first three sample holding times of SP-Al samples at 750 °C, according to the parabolic growth law**

The growth of the oxide was calculated to begin at ~10 seconds ($t_0$ = x intercept). This was a more realistic value and it seemed that the parabolic growth law may have been in force during the initial stages of oxidation.

A growth rate was proposed by Pragnell et al (2005), called the hyperbolic growth rate, which stated that oxidation undergoes a transitional state (growth in between $\gamma$ and $\alpha$-alumina). It applies to the entire growth period, rather than just sections of it, as seen with the parabolic law. It was observed that during this transitional period, the oxidation rate begins to slow to almost to zero, seen over long oxidation times. The rate was seen to follow a hyperbolic growth pattern. The alloy used in the literature was Fe 22.3%Cr 5.4Al 1Y steel, so the hyperbolic growth pattern did not become apparent until samples had been held for 70 hours at 925ºC. At higher temperature and holding times, the main oxides were still morphologies of alumina (Pragnell et al 2005). Comparing the growth curves from the literature and from SP-Al, a similarity in their shape can be seen, suggesting that the growth may have followed a hyperbolic growth law.
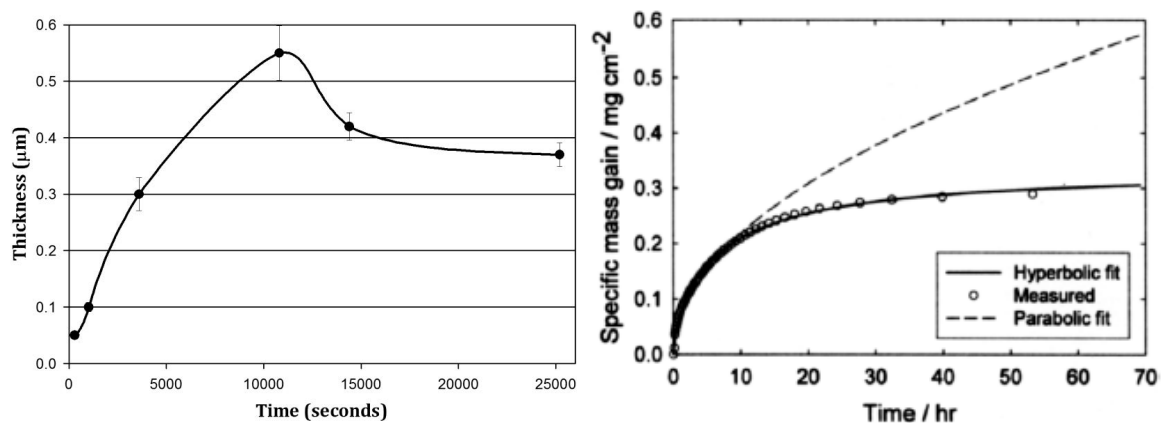


**Figure 128 - Comparison of growth rates a) experimental thickness of oxides on SP-Al b) oxide gain on steel held at 925 ºC (Pragnell et al 2005)**

It can be seen from the oxide thicknesses in Table 26 that different elements had different effects on the thickness of the oxide. When compared to SP-Al, the alloys of Al-4%Mg, Al-7%Si-0.3%Mg, Al-4%Cu and Al-0.3%Sr all had a larger oxide film thickness. The possible causes of the increase in thickness are discussed.

It has been widely reported that Mg increases the oxidation of Al, especially when present in amounts as in the alloy used here (4%Mg) (Agema and Fray 1989, Drouzy and Mascré 1969, Impey et al 1990, Scamans and Butler 1975, Wakefield & Sharp 1991). They described the growth of the oxide as following the pattern of forming MgO within amorphous alumina. When the concentration of Mg starts to fall (due to it reacting with oxygen) formation of spinel is favoured over alumina. The results in this work agreed with this. There was an increase in oxide

175

thickness from 0.37 μm to total oxidation of the sample after 24 hours at 750 °C. XRD suggested that the oxide formed as MgO, spinel and γ-alumina at 5 minutes, with the levels of MgO and spinel increasing at 1 hour and 24 hours (Figure 48, Figure 49 and Figure 50). There was not a strong signal for α-alumina, but was found after 24 hours. This suggested that the increase in thickness was due to the formation of MgO and as the Mg concentration decreased in certain areas, γ-alumina grew and became α-alumina. This was similar to the growth pattern shown in Impey et al (1990), where samples containing up to 5wt. % Mg formed MgO crystals within an amorphous layer of alumina, rather than forming α-alumina. Growth was also more rapid than the growth in SP-Al, which was shown in the work done by Scamans and Butler (1975), who also found that spinel growth occurred faster than growth of alumina. They suggested that it was due to oxygen diffusion increasing inwards and Mg diffusing outwards through the amorphous alumina, which corresponds to the EDX data shown in Figure 47, which was also described in Esposto et al (1994). However, Lea and Molinari (1984) suggested that when an Al-Mg alloy is held for a period of time at elevated temperature (over 200 °C), Mg evaporates from the surface more quickly than it segregates there, leading to depletion of Mg in the surface regions. However, in this work it was found that the Mg content increased towards the upper surface oxide, as was found in the EDX of the Al-Mg sample (Figure 47).

The Al-7%Si-0.3%Mg alloy had a final oxide thickness of ~1.56 μm after 24 hours, compared to ~0.37 μm with SP-Al. The XRD results also indicated that γ-alumina and spinel were present both at 5 minutes and 24 hours, with traces of MgO (Figure 59 and Figure 61). These structures have been noted in the literature for similar alloys. Cao and Campbell (2005) found that the oxides (found at fracture surfaces) formed in a sand casting of Al-11.5Si-0.4Mg were alumina, spinel and MgO, which concurred with the results of this work. The XRD results in Figure 59, Figure 60 and Figure 61 suggested that γ-alumina, spinel and MgO occurred between 5 minutes and 24 hours of oxidation. The oxidation growth also followed a similar pattern to those seen in Partington et al. (1998), as there was an initial slow rate of oxidation that increased at 1 hour and then levelled off after 2-3 hours. However, the increase shown in the literature occurred a little more quickly than in this work, most likely due to the fact that the alloys in Partington et al. were held at higher temperatures (up to 1250 °C) and contained higher levels of Mg (up to 5%) which would increase the rate of oxidation. The increased concentration of Mg at the surface regions most likely occurred due to diffusion of Mg towards the surface and they would have led to reactions with oxygen, forming MgO. It could also be that as the Al is oxidising in the surface regions, the relative Mg concentration increases at the oxide/metal interface as a

result. It seems likely that the porous nature of MgO increased the oxidation rate and therefore resulted in a higher oxide thickness (Drouzy and Mascré 1969).

The Al-4%Cu alloy had a final oxide thickness of 1.72 μm after 24 hours, compared to 0.37 μm in SP-Al after the same time period. It has been noted in the literature that the presence of Cu in Al increases the thickness of the oxide (Brock and Pryor 1973, Saunders and Pryor 1968). The growth of the oxide on an Al-Cu alloy was discussed in Brock and Pryor (1973) and is summarised in Figure 129. It was described that, initially, amorphous oxide grew parabolically by Al ions migrating through it. At temperatures over 525 °C, $Cu^{2+}$ ions reduce the number of cation vacancies as oxygen ions move though these defective regions of the lattice. The ions become more mobile at higher temperatures, and so move through the lattice more easily. The oxygen ions migrate inwards through defective regions in the amorphous lattice at the same time the Al ions move outwards, as discussed in the literature review. Crystalline oxide develops at the metal-oxide interface as a rod-like structure which then grows and causes undulations in the surface oxide (Brock & Pryor 1973). The SEM image shown in Figure 129 has a structure that could have been a result of this growth. It could also explain the $CuAl_2$ peaks that arose in the XRD spectra of the Al-4%Cu sample, held for 24 hours (Figure 66). Other authors stated that Cu had a limited effect on the oxidation of Al; however these works only used alloys of ~1 wt. % Cu, so any effect would be less pronounced (Thiele 1962, Drouzy & Mascré 1969).
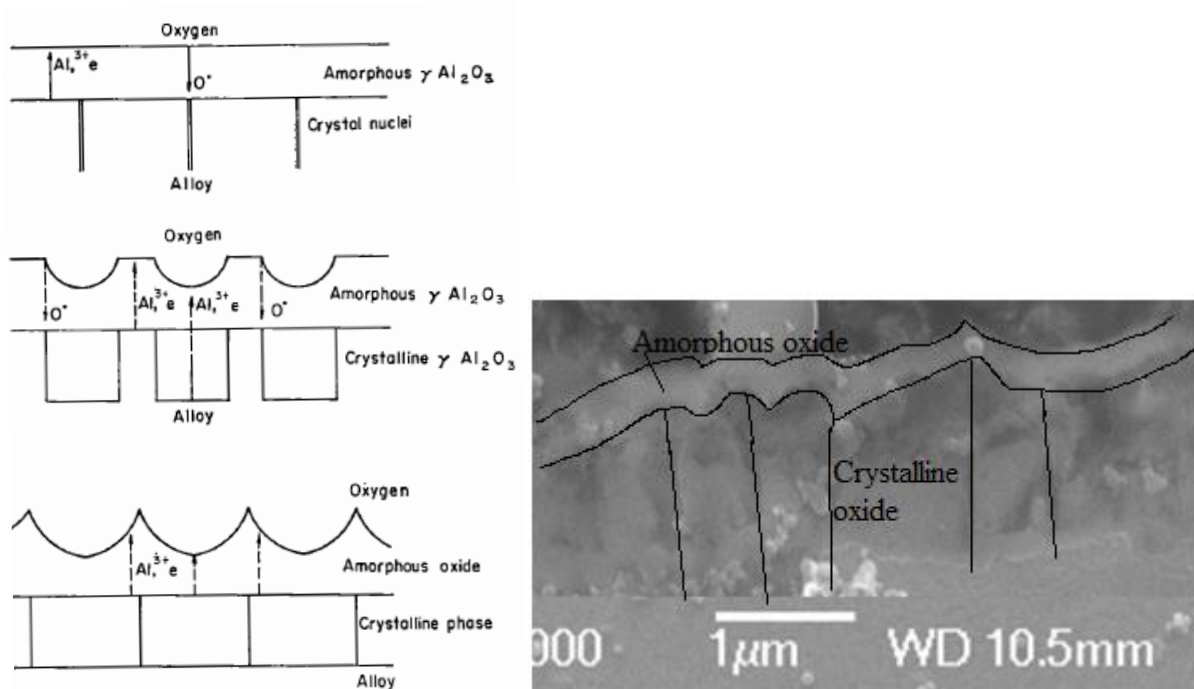


**Figure 129 - Growth of oxides on Al-Cu alloys (Brock & Pryor 1973) compared to the oxide in Cu-4%Cu held for 24 hours at 750 °C**

The alloy Al-0.3%Sr had an oxide thickness of ~1.1 µm after 24 hours at 750 °C. Traces of SrO were detected at both 5 minutes and 24 hours, along with γ-alumina (Figure 76 and Figure 77). This is similar to what was found in Miresmaeili et al (2005), in which A356 alloy (Al-7%Si-0.3%Mg-0.1%Ti) was alloyed with 0.04wt.% Sr. Oxides of γ-alumina, $Al_2O_3.SrO$ mixed oxide and SrO were found to be present in the oxide film. The XRD results in Figure 76 and Figure 77 suggests the presence of γ-alumina and SrO, but it could not be determined if a mixed oxide was present. The mixed oxide mentioned may account for the high levels of Sr that were detected within the oxide layers during EDX analysis (Figure 74) (Miresmaeili et al 2005). This mixed oxide was also found by Liu et al (2003).

The Al-Si alloy had a very similar oxide thickness to SP-Al, ~0.39 µm compared with ~0.37 µm. This was also reported in Thiele (1962), that the addition of 1 wt.% Si had little effect on the thickness of the oxide formed, and this was also seen in this work. There was no presence of Si within the layers after EDX analysis (Figure 53), and Si did not appear to form its own oxide during the experiment, since there was not one seen in the XRD after 24 hours (Figure 55). Little effect was found by Partington et al (1998), who found that 12.5 wt.% Si had little effect on the growth of the oxide.

The alloys of Al 1%Fe and Al 0.25%Ti both had a decreased oxide thickness compared to SP-Al as seen in Table 26.

The alloy of Al-1%Fe had an oxide thickness of ~0.21 µm after 24 hours compared to ~0.37 µm for SP-Al. The XRD spectra showed that only alumina formed during oxidation (Figure 70 and Figure 71). There were a few areas that picked up an Fe presence near the oxide-metal interface (Figure 69, sample 3, 4 and 6). This could have been due to the formation of trace levels of FeO, levels too low to be detected during XRD analysis. It is likely that FeO would be the first Fe oxide to form, with a Gibbs Free Energy of Formation of -414 kJ/mol, then $Fe_3O_4$ at -373 kJ/mol and $Fe_2O_3$ at -195 kJ/mol. If FeO formed, this would be a likely reason for the low oxide thickness (changing by only 0.23 µm over 24 hours), as the Pilling-Bedworth ratio for FeO is 1.72. This means that FeO is a passivating layer, meaning it would be a protective oxide if present with the oxide layer. It could also be that the Fe particles restricted diffusion of Al ions towards the surface, as seem by Hou (2003) and Mennicke et al (1998).

The alloy for Al-0.3%Ti had an increased oxide thickness from 0.06 µm after 5 minutes to 0.17 µm after 24 hours, compared to a thickness of 0.37 µm for SP-Al after 24 hours. The XRD

results found that γ-alumina and $TiO_2$ was present at 24 hours (Figure 82), but no Ti was detected in the oxide layer during EDX analysis (Figure 80).This suggested that the $TiO_2$ was present outside of the main alumina layer. The Pilling Bedworth ratio for $TiO_2$ is 1.2, which means that it is a passivating layer. This means that the presence of $TiO_2$ is protecting the alloy from rapid oxidation.

## 4.2 – Effects of Molybdenum on Oxidation of Aluminium

A comparison of the oxide film thicknesses to the oxidation of the SP-Al and Al-7%Si-0.3%Mg samples can be seen in Table 27 and Figure 130. The samples on to which powder Mo was added had changes in the molybdenum oxide structure from 5 minutes to 24 hours at 750 °C. The XRD results in Figure 93 show that the initial Mo oxide formed at 5 minutes was $MoO_3$, later forming $MoO_2$ at 1 hour, and then $Al_2(MoO_4)_3$ at 24 hours. There was an increase in the size of the unit cell as these species formed, as it changed from monoclinic for $MoO_3$ and $MoO_2$ (a=3.95 Å, b=3.607 Å, c=7.095 Å and a=5.61 Å, b= 40.5 Å, c=5.62 Å respectively) to orthorhombic for $Al_2(MoO_4)_3$ (a=12.55 Å, b=8.93 Å, c=9.04 Å). The changes in structure and increase in volume would have put strain on the oxide film, causing it to crack and fragment. The fragmentation of the oxide would have led to the liquid metal underneath becoming exposed to air. In turn this would have led to the increase in oxidation rate and oxide thickness as the exposed metal reacted to form more Mo oxide and γ-alumina and α-alumina, suggesting a relationship between holding time of the alloy and the size of the unit cell of the oxide.

**Table 27 - Comparison of oxide thickness of Al with Mo additions to SP-Al and Al-7%Si-0.3%Mg without additions**

| Molybdenum | Holding time | | |
|---|---|---|---|
| Oxide thickness (µm) | 5 min | 1 hour | 24 hours |
| Al + Mo powder | 0.34 | 4.208 | 1000 |
| Superpure Al | 0.05 | 0.3 | 0.37 |
| SP-Al 1%Mo | negligible | 0.12 | 0.35 |
| Al 7%Si 0.3%Mg | 0.65 | 0.67 | 1.56 |
| Al 7%Si 0.3%Mg-1%Mo | 0.32 | 1.1 | 1.8 |

The Al-1%Mo sample grew with an oxide layer of negligible thickness to ~0.35 µm, between 5 minutes and 24 hours. The growth of the oxide was comparable to that for SP-Al, as shown in Figure 130. The final thicknesses were very similar, 0.37 µm and 0.35 µm for SP-Al and Al-1%Mo respectively, giving a difference of ~0.02 µm 24 after hours. The growth was initially lower with the Mo addition, starting with an oxide of unmeasurable thickness growing to 0.12 µm at 1 hour, compared to the oxide of SP-Al that grew from 0.05 µm to 0.3 µm over the same

time period. The oxides formed were γ-alumina, with $MoO_3$ at both oxidation times, and α-alumina at 24 hours, seen in the XRD results (Figure 93). This growth was very different to the growth on the samples with the Mo powder additions.

The thickness difference between the Al-1%Mo and the Mo powder samples were 0.34 μm, 4.1 μm and 999.5 μm for the 5 minute, 1 hour and 24 hour samples respectively. The difference in oxide growth was very large, and this is likely due to the fact that the Mo oxides would form easily from the powder on the liquid metal surface, as the large surface area of the particles would encourage reaction with oxygen. It could also be that the powder on the surface would, firstly, react with oxygen and this may have hindered the passage of oxygen to the liquid Al underneath. Mo does not melt until over 2000 °C, but it does dissolve in Al (Mondolfo 1976). The surface region would have been rich in dissolved Mo, and this region may have prevented diffusion of oxygen to the liquid Al beneath. The Gibbs Free Energy of Formation for $MoO_3$ is -314 kJ/mol, compared to -907 kJ/mol for alumina. This means that, when present in an alloy, alumina would form preferentially to Mo oxide, and it is likely that the Al-1%Mo formed alumina more readily. However, according to the EDX data in Figure 91, there was Mo build up in areas of the surface, which would have reacted with oxygen to form $MoO_3$, which is the likely reason $MoO_3$ was detected in the XRD analysis shown in Figure 93.
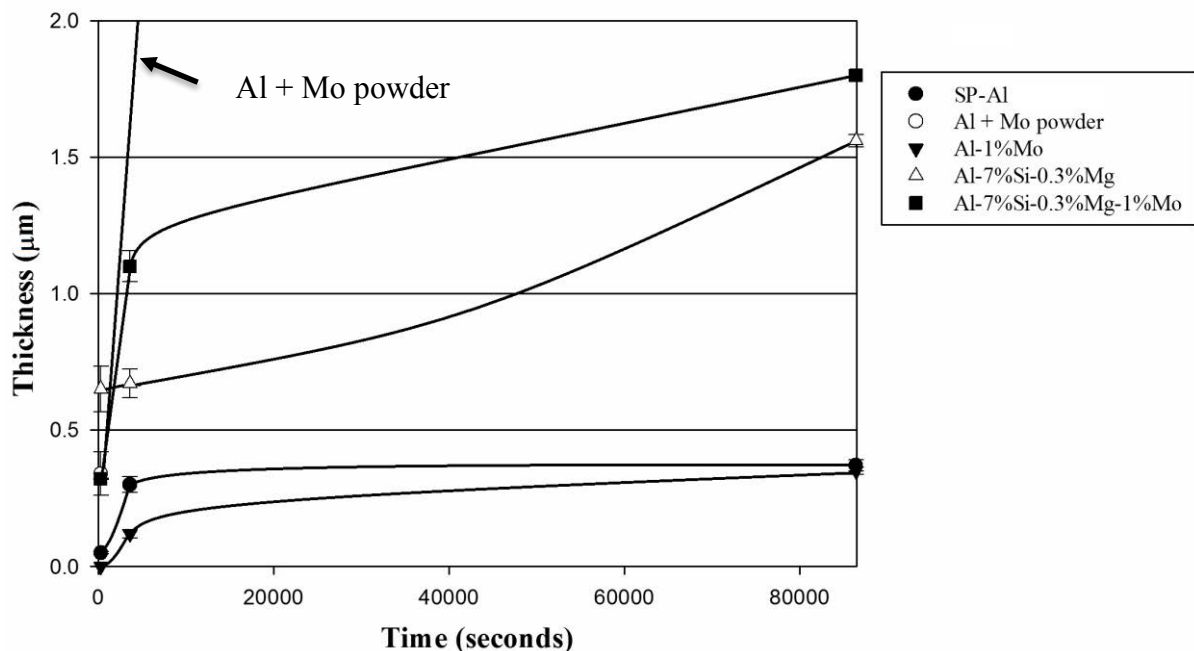


**Figure 130 - Comparison of growth patterns for samples with and without Mo additions**

Al-7%Si-0.3%Mg-1%Mo alloy formed an oxide of $MoO_3$ on all samples, as shown in Figure 96. The oxide layer grew from 0.32 μm after 5 minutes, to 1.1 μm after 1 hour and 1.8 μm after 24 hours. This is to be compared with 0.65 μm 0.67 μm and 1.56 μm for the same times for the Al-7%Si-0.3%Mg alloy. There appeared to be an initial fast growth rate between 5 minutes and

1 hour, 2.3 x 10$^{-4}$ μm/s for Al-7%Si-0.3%Mg-1%Mo, compared to 3.0 x 10$^{-6}$ μm/s for Al-7%Si-0.3%Mg with no addition. Comparing the data for Al-7%Si-0.3%Mg in Figure 123 and Figure 130, the period of slow oxidation occurred after 1 hour of oxidation, whereas it occurred between 5 minutes and 1 hour for Al-7%Si-0.3%Mg -1%Mo. The oxides detected using XRD analysis were MoO$_3$, spinel and traces of γ-alumina (Figure 99) and the SEM image of the 1 hour and 24 hour sample appeared to show different phases making up the oxide (Figure 94, sample 2 and 3, Al-7%Si-0.3%Mg-1%Mo). The XRD results suggested that spinel and MoO$_3$ may have been present in the oxide. The appearance of this sample was similar to the sample seen in Figure 83, the sample with accidental Mo contamination. It may be that MoO$_3$ in the oxide layer was present in one of the phases shown in the SEM images.

## 4.3 - Effect of Nitrogen Atmosphere on Al and Selected Alloys

A summary of the layer thicknesses on samples held in a nitrogen atmosphere at 750 °C are shown in Table 28.

**Table 28 - Layer thickness of samples held in N2 at 750 °C**

| | | Holding time | | |
|---|---|---|---|---|
| | **Alloy** | **5 min** | **1 hour** | **24 hours** |
| **Oxide thickness (μm)** | Superpure Al | 0.03 | 0.27 | 1.37 |
| | Al 4%Mg | 0.06 | 0.06 | 0.05 |
| | Al 7%Si 0.3%Mg | 0.03 | 0.15 | 0.16 |

The layer formed on SP-Al after 24 hours in N$_2$ was a combination of γ-alumina and AlN, as shown in the XRD spectrum, see Figure 105. AlN has been found on samples in other works. Other authors (Gerrard & Griffiths 2014, Saravanan et al 2001, Zheng & Reddy 2004) found that if Al is kept molten in nitrogen, it reacts to form AlN. If oxygen is present, Al will preferentially react with it but react with nitrogen when there is none left. The Gibbs Free Energy for the reaction of Al with oxygen is lower than that for nitrogen (-680 kJmol$^{-1}$ and -211 kJmol$^{-1}$ – Raeiszadeh 2005). The appearance of the top surface of the layer that formed on Al can be seen in Figure 131(a), from Gerrard & Griffiths (2014), (b) from Raeiszadeh (2005) and (c) from the sample held for 24 hours in this work.
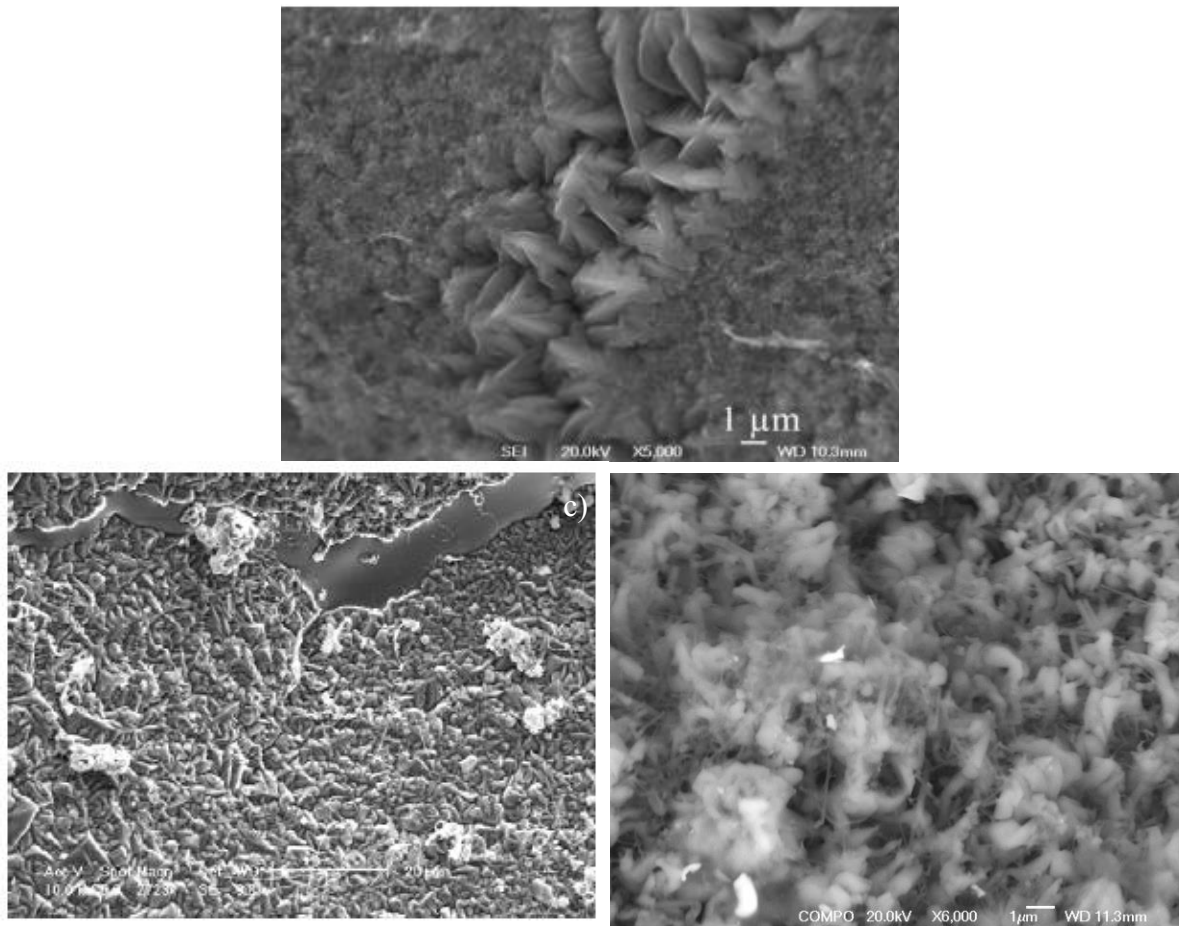
**Figure 131 - Top suface SEM images of AlN on samples melted in N₂ a) sample from Gerrard & Griffths (2014) b) from Raeiszadeh 2005 c) samples from SP-Al held for 24 hours**

There was a feather-like appearance to the layer, which appeared to be AlN and there were similarities with images of AlN found in previous work (Gerrard and Griffiths 2014, Raeiszadeh 2005). The layers found in the literature also had a feather like appearance, as shown in Figure 131. The layer was very different to the oxide formed on the SP-Al in air. The thickness was ~1.37 μm, and a 3.72 μm height of the feathered layer when melted in nitrogen for 24 hours, compared to ~0.37 μm in air. The formation of nitrides has been reported to increase the rate of layer growth. Saravanan et al (2001) observed that local heating from the reaction of Al with nitrogen led to a reduction in surface tension of the layer making it more likely to crack and expose liquid to the atmosphere. Gerrard & Griffiths (2014) suggested that the AlN was a permeable layer and it was observed that hydrogen was absorbed more quickly into molten Al when the samples were previously melted in a nitrogen atmosphere. The formation of permeable AlN may have led to the increase in layer thickness between 1 hour and 24 hours, from ~0.27 μm to ~3.5 μm.

The thickness of Al-4%Mg did not change much over 24 hours, being in the region of ~0.05-0.06 μm. It can be seen from the XRD data in Figure 109 and Figure 110 that γ-alumina and

spinel were formed, with some traces of AlN. This suggests that unlike its reaction with air, Mg did not readily react with nitrogen. This is because the Gibbs Free Energy for the formation of AlN is -423 kJ/mol, compared to -257 kJ/mol for $Mg_3N_2$, making the formation of AlN more favourable. This was the most likely reason for the lack of growth of layers, as once most of the residual oxygen had reacted; the growth of the layer was effectively stopped. This was very different to the reaction in air, which had through thickness oxidation at 24 hours, meaning a nitrogen atmosphere was very effective at reducing oxidation of the alloy.

The layer on the Al-7%Si-0.3%Mg alloy only grew to ~0.16 μm after 24 hours. Compared to the samples in air, which grew to ~1.56 μm after 24 hours, this was a much thinner layer. This was probably due to the fact that Mg does not seem to react with nitrogen. The XRD (Figure 114 and Figure 115) detected silicon nitride present in the samples, which has a Pilling-Bedworth ratio of 1.23, suggesting that it was a passivating layer, protecting the sample from any further growth of the layer.

## 4.4 - Effects of Alloying Additions on Double Oxide Film Defects

Double oxide film defects are common defects that occur in Al castings. They are formed when the surface of the molten Al folds during turbulent flow of the surface, as demonstrated in Figure 132. These defects are detrimental to the mechanical properties of the casting and so any attempt to reduce their size can be regarded as beneficial. Closure of double oxide film defects would reduce their potential detriment of the mechanical properties, as the defect would be smaller in size and cause less of a stress concentration in a component. A thicker oxide in the defect would only be useful in bifilm if it enabled gaseous flow through it, and therefore assist crack closure (Campbell 2003). Therefore the oxides and nitrides formed in this work were judged on their potential to reduce the size of double oxide film defects.
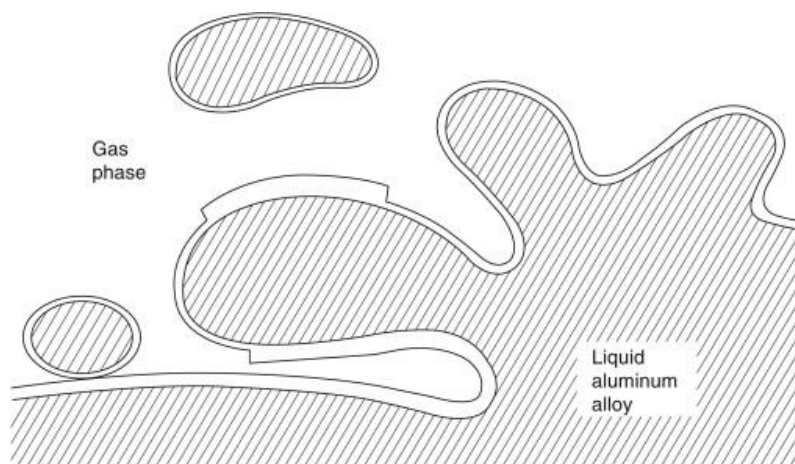


**Figure 132 - Schematic of an entrainment event that results in a double oxide film defect (Campbell 2003)**

183

The layers more likely to assist in defect closure are those that allow the gases trapped within the defect to move through them, to react with the surrounding melt, leading to a reduction of the volume of the defect and subsequent defect closure. Therefore a non-protective layer is favoured. This would discount the oxides that formed on the alloys of Al-1%Fe and Al-0.25%Ti in air, as these oxides grew less than those formed on SP-Al, suggesting that they were more protective oxides. The layers formed on SP-Al appeared to be protective, but traces of the non-protective α-alumina were found after 24 hours during XRD analysis (Figure 44). This α-alumina tends to be less protective due to the volume decrease that occurs (Impey et al 1988), leading to breaks in the oxide. These breaks lead to an increase in oxidation rate and could also lead to crack closure as the air in the crack reacts with the newly exposed liquid metal. The SP-Al melted under a nitrogen atmosphere formed AlN on its surface, which was a thick layer of ~3.5 μm after 24 hours. This layer would allow good mobility of defect gases and allow for closure of the defect. The Pilling-Bedworth ratio for AlN is 1.28, suggesting that it is a passivating nitride, that forms a protective layer. It could be that the reduction in surface tension (as seen by Saravanan et al 2001) that caused the layer to crack and become exposed to the atmosphere, subsequently leading to more growth of the nitride. This has been shown by Gerrard and Griffiths (2014), who showed that hydrogen was more able to diffuse into CP-Al samples that were previously heated in nitrogen. There were also cracks in the AlN surface, as shown in Figure 131a. The hydrogen diffused more easily through AlN than alumina, resulting in more hydrogen porosity. This suggests that oxygen and nitrogen could more easily diffuse through AlN resulting in a reduction in the size of a defect. Plus the reaction with the gases present within the defect would lead to a small growth in the layer thickness and reduction in defect size. However, it is unlikely that a casting of SP-Al would be made commercially, or the melt would be held for 24 hours to form these species.

The porous MgO formed on the Al-4%Mg alloy would likely enable the closure of an oxide film defect, as it allows for the passage of gases through the oxide. It has also been found that Mg did not seem to react with nitrogen. The Gibbs Free Energy of Formation for AlN is -423 kJ/mol compared to -257 kJ/mol for magnesium nitride ($Mg_3N_2$), so AlN would form preferentially. The oxygen in an entrained defect reacts with the liquid metal first, followed by the nitrogen, once oxygen has been mostly consumed in the reaction (Raeiszadeh 2005). If the Al-Mg alloy contained a double oxide film defect, closure would occur as long as the oxygen is reacting with the metal. But if all the oxygen reacted before the defect had fully closed, crack closure would stop, due to the fact the metal would not react with nitrogen. The amount of Mg would affect the rate of defect closure. This was seen in Raeiszadeh (2005) where a bubble of

air was trapped in liquid aluminium alloys and observed to determine the rate at which it reduced in size. Al-5%Mg had a faster bubble contraction rate due to the fact that the oxidation reaction led to a thick oxide forming, which suggests that the MgO formed on the Al-4%Mg alloys from this work would have some degree of defect closure. An alloy of Al-0.1%Mg reacted at first to form MgO, but this slowed once the Mg had reacted, so the reduction time of the bubble was no greater than for CP-Al. Many industrial fluxes contain Mg, and are used to react with any surface oxides on the surface of a liquid Al alloy, so they can be removed as a solid layer. They could reduce the growth of the underlying oxide by preventing oxidation of the layers underneath the formed solid layer. Any oxide formed can be removed before casting as part of the flux layer (Davis 1993).

The oxidation of the Al-7%Si-0.3%Mg alloy led to a greater oxide film thickness, as seen in Table 26, suggesting that the oxide would allow for gases to escape the defect more easily. The samples formed $\gamma$-alumina and spinel, with traces of MgO at 24 hours. The more reactive nature of this alloy, when compared with SP-Al, could lead to growth of the oxide within the double oxide film defect, and the possibility of defect closure. However, there was no reaction with nitrogen detected during XRD analysis Figure 114 and Figure 115. Reactions of elements in the alloy with oxygen (Gibbs Free Energies at 727 °C, MgO = -985 kJ/mol, spinel = -939 kJ/mol, $Al_2O_3$ = -907 kJ/mol, $SiO_2$ = -730 kJ/mol) are more favourable than reactions with nitrogen (AlN = -423 kJ/mol, $Mg_3N_2$ = -257 kJ/mol, $Si_3N_4$ = -206.61 kJ/mol). If the oxygen in the defect were to be depleted due to reaction, the liquid alloy would not readily react with the nitrogen left in the defect, slowing down closure.

The Al-4%Cu alloy had an increased oxide thickness of 1.72 $\mu$m compared to 0.37 $\mu$m for SP-Al after 24 hours. The XRD of the oxide that formed was estimated to be $\gamma$-alumina with Cu in interstitial sites within the oxide. As $\gamma$-alumina is a protective oxide it would not enable the easy diffusion of gases from the defect. The Cu ions present in the amorphous alumina layer increase the cation vacancies allowing the transport of oxygen through it to form the crystalline oxide, as shown in Figure 129 (Brock & Pryor 1973). It seems likely that the reduction of a double oxide film defect could occur during this period when the oxygen ions within the defect can be mobile and the crystalline oxide is growing. But when the crystalline oxide becomes protective, the ions would be immobile and reduction would cease.

The Sr present in Al alloys has been shown to increase the tendency of Al alloys to form hydrogen pores, as SrO forms a more permeable oxide layer than $Al_2O_3$ (Pilling Bedworth ratios

of 0.61 and 1.28 respectively (Liu et al 2003)). The mobility of hydrogen in liquid Al is known and it has been proposed that hydrogen diffuses into the double oxide film defects present in liquid castings to inflate them (Campbell 2003). The SrO present on samples in this work would form preferentially to alumina in a defect, with the Gibb Free Energy of formation being -982 kJ/mol compared to -905 kJ/mol for alumina. A mixed oxide $Al_2SrO_3$ also formed on the surface (Figure 76 and Figure 77). The permeability of SrO would mean that gases present in a double oxide film defect would be able to react with liquid metal beneath the oxide layer, potentially leading to closure of the defect as the gases react and the internal volume of the defect decreases.

The oxides on the Al + Mo powder, when present at the surface, grew from $MoO_3$ at 5 minutes, to contain $MoO_2$ at 1 hour and $Al_2(MoO_4)_3$ at 24 hours. The formation of these different phases comes with an increase in the unit cell size, the volume of $MoO_2$ is 21% larger than $MoO_3$ and $Al_2(MoO_4)_3$ is 87% larger than $MoO_2$. This increase would cause cracks in the oxide layer inside a double oxide film defect and cause it to fragment. This would lead to an increase in the oxidation rate due to more liquid Al being exposed to the atmosphere in the defect. In turn, this would lead to an increase in the thickness of the oxide layers within the defect, and internal gases would be able to leave the defect.

The oxide present on the alloys containing 1%Mo formed $MoO_3$ on their surfaces. The oxides on the Al-7%Si-0.3%Mg-1%Mo alloys contained $MoO_3$, along with spinel and traces of γ-alumina (Figure 99). The oxides that formed on the Al-7%Si-0.3%Mg alloy may lead to defect closure by reacting with the gases and causing a reduction in defect size. The gases in the defect would also be consumed during the reaction. The oxides formed in the Al-1%Mo alloy were γ-alumina and $MoO_3$ and would behave in a similar way to those on Al-7%Si-0.3%Mg-1%Mo. The presence of Mo seemed to increase the amount of oxide formed, suggesting that the oxides formed in a defect in this alloy may further reduce the volume of the defect, due to the oxide growing more quickly, and consuming the gases within.

### 4.5 - Oxide Species as Potential Nuclei for Solidification

It is known that for a species to be a good nucleation site for solidification of a liquid metal there should be little difference in structure and lattice size, so as to give as little strain on the lattice as possible. Other variables can have an effect on nucleation, such as surface defects, wettability of the particles and the possible formation of peritectic phases. However the lattice mismatch plays a key role in nucleation and grain refinement and is the main focus here.

186

Ideally, the mismatch between the two species should be less than ±20% (Turnbull and Vonnegut 1952).

$$\delta = \frac{d_\beta - d_\alpha}{d_\alpha} \qquad (44)$$

$\delta$ = Lattice mismatch
$d_\alpha$, $d_\beta$ = interplanar spacings

(from Porter et al. 2009)

The lattice parameters and lattice mismatch of oxides, nitrides and other species that formed in the experiments are summarised in Table 29. The lattice mismatch was calculated from the formula in equation (44). It should be noted that temperature will have an effect on the lattice parameter, generally increasing with temperature. The lattice mismatch also increases with temperature, but the difference between a typical FCC lattice and an Al lattice was modelled to increase to -10% from upto -3% in a liquid and solid structure respectively (Men & Fan 2011).

Table 29 - Lattice parameters of formed oxides and their calculated disregistry with Al, when multiple parameters are given those, used for calculations are underlined (data taken from Miresmaeili et al 2005, Mondolfo 1973, Lin et al 2011 and from XRD data)

| Species/Oxide | Structure | Lattice parameter (nm) | Lattice mismatch with Al (%) | Potential grain refiner |
|---|---|---|---|---|
| Al | Cubic | a= 0.4049 | 0 | - |
| $\gamma$-alumina | Cubic | a = 0.7859 | 94.07 (= 5.93) | Yes |
| $\alpha$-alumina | Rhombohedral | a = 0.513, 55 ° | 26.68 | No |
| | Hexagonal | a = 0.476, c = 1.299 | 17.54 | Yes |
| MgO | Cubic | a= 0.4211 | 3.99 | Yes |
| Spinel | Cubic | a = 0.808 | 99.53 (= 0.47) | Yes |
| | Sub-lattice | a= 0.404 | 0.24 | Yes |
| Cu Al$_2$ | Tetragonal | a = 0.6066, c = 0.4874 | 20.36 | Maybe |
| CuAl$_2$O$_4$ | Cubic | a = 0.8045 | 98.66 (= 1.34) | Yes |
| AlCuO$_2$ | Rhombohedral | a=0.5896, 28 ° | 45.59 | No |
| | Hexagonal | a = 0.2870, c = 1.698 | 29.13 | No |
| SrO | Tetragonal | a = 0.35, c = 0.6616 | 13.57 | Yes |
| AlN | Hexagonal | a = 0.31, c = 0.496 | 22.48 | Maybe |
| Mg$_3$N$_2$ | Cubic | a=0.997 | 146.23 | No |
| MoO$_3$ | Monoclinic | a = 0.395, b = 0.3607, c = 0.7095 | 2.46 | Yes |
| MoO$_2$ | Monoclinic | a = 0.561, b = 0.405, c = 0.562 | 0.24 | Yes |
| Al$_2$(MoO$_4$)$_3$ | Orthorhombic | a = 1.255, b = 0.893, c = 0.904 | 120.52 | No |
| TiAl$_3$ | Tetragonal | a = 0.3851, c = 0.8608 | 4.90 | Yes |
| TiB$_2$ | Hexagonal | a = 0.302, c = 0.322 | 20.29 | Maybe |

The species most likely to act as nucleation sites were those with a lattice mismatch of ±20% or less. The standard grain refiner, $TiB_2$, reacts to form $TiAl_3$, which initiates nucleation in Al (Marcanto and Mondolfo 1971). $TiAl_3$ had a lattice mismatch of 4.9%, as shown in Table 29. This was a low mismatch value, and the structure was tetragonal, a stretched form of the cubic structure of Al. The grain refining ability of $TiB_2$ has been well documented (McCartney 1989, Johnsson et al. 1993), and these calculations seemed to confirm this, as well as the grain refining effect seen in comparing Figure 116 and Figure 122. $TiB_2$ itself has a lattice mismatch of 20.29%, suggesting it would not be an effective refiner. This illustrates why grain refiner amounts should not be too large, as any unreacted $TiB_2$ would not refine as effectively as $TiAl_3$ (which forms when $TiB_2$ reacts in Al). There was a reduction in average grain size of 36% when 125 ppm of $TiB_2$ grain refiner was added to CP-Al (shown in Table 25). Other species formed also appeared to have the potential to nucleate solidification (even more than that for $TiAl_3$) as follows.

The oxides of $MoO_2$ and $MoO_3$ that formed on the Al + Mo powder samples, and were found in the Al-1%Mo and Al-7%Si-0.3%Mg-1%Mo, had lattice mismatches of 0.24% and 2.46% respectively, (shown in Table 29), and both had a monoclinic structure, a similar structure to the cubic Al structure. This suggests oxides formed with molybdenum have the possibility to act as grain refiners. This agrees with statements made by Mondolfo (1976), who suggested that Mo in Al alloys improved their mechanical properties. However, as the lattice is not cubic and there is a larger mismatch with some of the other planes (38% for $MoO_2$ and 75% for $MoO_3$); it could be that nucleation would favour the plane with lowest mismatch, as seen in Kelton and Greer (2010) in $TiB_2$. This is opposed to the mixed oxide of $Al_2(MoO_4)_3$ that formed, which had a mismatch of 120.52 %, and an orthorhombic structure. The large mismatch suggested that this oxide would make a poor grain refiner, as it would place too much strain on the lattice for it to be effective.

The lattice mismatch between spinel and Al was 99.53%, as seen in Table 29. This is equivalent to a mismatch of -0.47%. This very low mismatch plus the similarity in the cubic structures of spinel and Al, means that spinel would act as an effective grain refiner. Lin et al. (2011) observed that spinel also had a sub-lattice structure, within its regular lattice, which is common to complex lattices such as spinel. The mismatch between Al and the secondary structure was 2.4%, suggesting that this would also be an effective grain refiner. The grain refining effect was seen in the tests done with spinel particles in CP-Al. When comparing a CP-Al casting and a

CP-Al casting containing 50 ppm of spinel particles (Figure 116 and Figure 121), a reduction in the average grain size of 23% was seen for the samples containing the spinel particles. The small lattice mismatch could be a reason for this reduction in grain size.

The mixed oxide of $CuAl_2O_4$ had a lattice mismatch with Al of 98.66%, or -1.34%. Its cubic structure also matched the crystal structure of Al. The low mismatch of the size and structure of the $CuAl_2O_4$ means that it has good potential to initiate solidification in Al alloys.

Another species that had a low lattice and structure mismatch was MgO. The calculation in Table 29 shows that the lattice mismatch between MgO and Al was 3.99% and the structures are both cubic. This means that MgO could be a good potential nucleation site for the solidification of Al. The potential of MgO was discussed in Fan et al (2009c) where an Al-Mg alloy was melt conditioned, and it was proposed that fragmented oxides initiated a grain refining effect (alumina phase was not specified in Fan 2009c, only 'oxides' or 'oxide films' are mentioned in relation to Al alloys).

The oxide SrO that formed on the Al-0.3%Sr alloy had a lattice mismatch of 13.57% and the structure is a tetragonal structure, as seen in Table 29. This gave an acceptable match with the cubic structure of Al, so it would act as a grain refiner but perhaps not as effectively as oxides with lower mismatches. But as the structure is tetragonal, the lattice parameter in the c direction is different, giving a mismatch of 64%. This could mean that the nucleation would only occur on the one face of the oxide with the smallest mismatch.

The 24 hour SP-Al sample had γ-alumina and traces of α-alumina in the XRD spectrum (Figure 44). The lattice mismatch between γ-alumina and Al was 94.07, equivalent to a mismatch of -5.93%. This mismatch is low, and the cubic structures are similar, suggesting that γ-alumina would act as a good nucleation point. The lattice mismatch between α-alumina and Al was calculated to be 17.54%, which was an acceptable mismatch for nucleation. However, the structure is hexagonal, which is quite different to the cubic structure of Al. The difference in structure may cause a strain in the lattice which is unfavourable for nucleation. Fan et al (2009c) suggested that alumina may nucleate solidification in Al-Mg alloys after melt conditioning. However, the mismatch in structure suggests it was likely to be another species, e.g. MgO or spinel.

There were two species that were just over the 20% minimum mismatch, which were $CuAl_2$ (from the Al-4%Cu alloy), with a mismatch of 20.36% and a tetragonal structure, and AlN (from SP-Al in $N_2$) with a mismatch of 22.48% and a hexagonal structure. The mismatch between $CuAl_2$ was only just over the recommended mismatch size and the structure was similar to the cubic Al structure, so this may work as a grain refiner if no other nucleation sites were present. The AlN structure has a larger mismatch in lattice parameter and structure, making it unlikely to be an effective grain refiner.

Other species, e.g. $Mg_3N_2$ and the $AlCuO_2$ mixed oxide, had larger mismatches, over 25%, as seen in Table 29. This would cause strain in the lattice meaning there would be ineffective grain refinement with these species.

There are many species that formed in the oxidation work that could act as possible nucleation centres for Al and its alloys. Fan et al (2009a, b, c) suggested that oxides formed during castings can act as grain refiners once a melt has been melt conditioned. It appears that this could be the case, with oxides such as $MoO_3$, MgO and spinel being particularly potent, due to their low lattice mismatches and similar crystal structures to Al.

**4.6 – Codeposition of Spinel Particles in Copper Layers**

A series of experiments were undertaken to determine an efficient method for depositing spinel particles in a copper layer, in order to manufacture master alloys for use as grain refiners.

It is apparent that the addition of surfactants is important to achieve a good particle pickup. Samples with and without SDS were made and it was found that the particle pickup without SDS has a very low pickup, if anything at all. The samples containing SDS had much higher pickups (up to 8%), which confirms what has been said in the literature by Weston et al (2011) who suggested that surfactants play an important role in attracting particles to the layer. This can be seen by comparing the images in Figure 117b and Figure 118b, with the latter having a much higher pickup than the former for similar experimental parameters.

It was also shown that pulse reverse methods attracted far more particles than the DC methods, with up to 8% spinel in FPR and less than 1% in DC methods. The anodic stage of the pulse method helped to attract the particles to the layer, which are then embedded during the cathodic stage (when the copper is deposited).

190
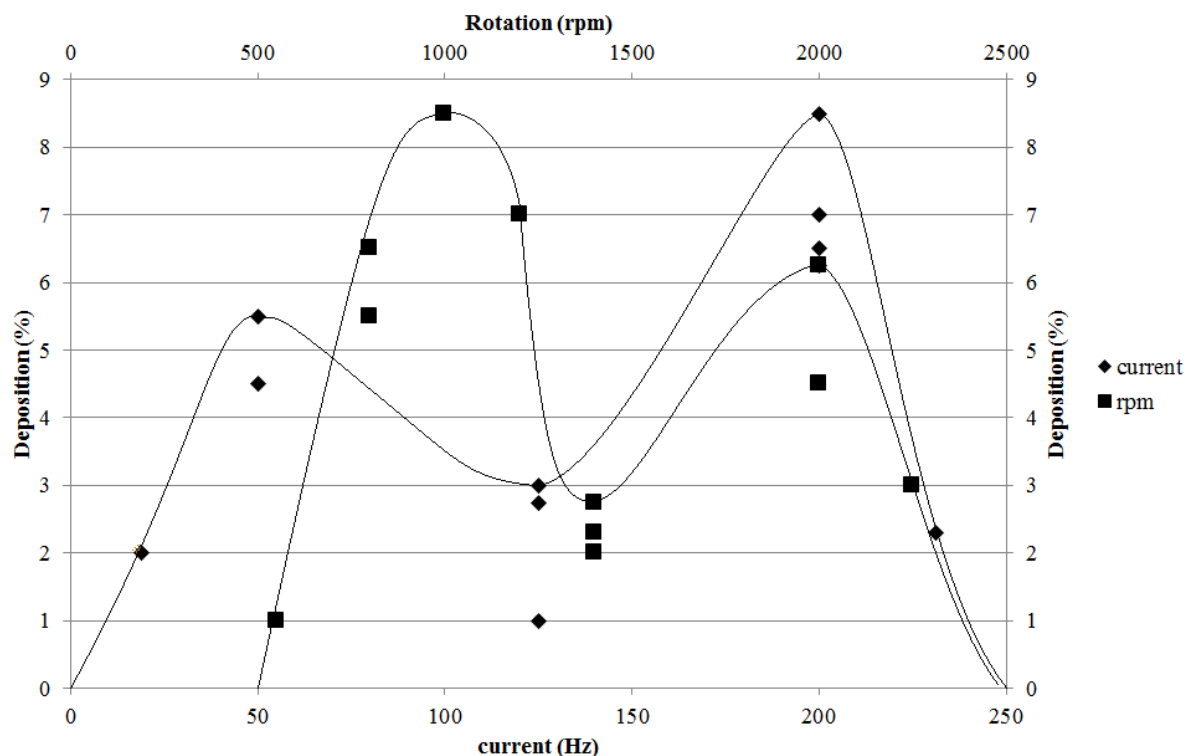
**Figure 133 - Effects of pulse reverse current and rotation speed on the deposition of spinel particles**

The effect of the frequency of the pulse reverse current is shown in Figure 133. There was not a single point at which the deposition rate was high. The deposition was high at the 50 Hz (up to 5.5%) and 200 Hz (up to 8.5%) and lower towards the highest and lowest currents (231 Hz and 18.9 Hz). There was also a dip in deposition rates at 125 Hz with deposition of 1-3% at this frequency. The pattern gave a pseudo bi-modal distribution of data.

The rotation speed of the electrode had a similar pseudo bi-modal distribution of results. The peaks in deposition occurred at 1000 rpm (8.5%) and 2000 rpm (6.25%) and the deposition began to lower at the slowest and fastest rotation speeds of 550 rpm (1% spinel) and 2248 rpm (3% spinel). There was also a dip in deposition rate at 1400 rpm, with a deposition range 2-2.73% spinel pickup.

## 5 - Conclusions

1.  Superpure aluminium was melted and held at 750 °C at varying intervals from 5 minutes to 24 hours in air. The oxide layer thickness for SP-Al grew from 0.05 μm to 0.37 μm over the total oxidation period. XRD detected that γ-alumina was present at all oxidation times and α-alumina was detected after 24 hours

2.  The oxide on Al 4wt. % Mg grew from 5.25 μm at 5 minutes to 7.15 μm at 1 hour in air. After 3 hours holding at 750 °C the sample was completely oxidised. The oxide was composed of MgO, spinel and traces of γ and α-alumina.

3.  The oxide on Al 7wt. % Si in air did not grow differently to SP-Al. The initial oxide at 5 minutes was 0.12 μm which grew to 0.39 μm after 24 hours. The oxide detected was γ-alumina, with Si present within the solution and as $SiO_2$.

4.  Al-7%wt. %Si-0.3wt.Mg had its oxide thickness grow from 0.65 μm to 1.56 μm from 5 minutes and 24 hours in air. The oxides detected were γ-alumina, spinel and MgO with Si present in solid solution and $SiO_2$. The presence of 0.3% Mg seemed to increase the oxide thickness by 1.19 μm in comparison with air.

5.  The Al 4wt. % Cu alloy developed a $CuAl_2$ phase in the surface oxide, the presence of which seemed to accelerate its growth. The oxide thickness grew from 0.31 μm to 1.72 μm over a 24 hour period in air, with γ-alumina being detected as the only oxide phase.

6.  The oxide on Al 0.3 wt. % Sr alloy was initially too thin to measure, but grew to 1.1 μm after 24 hours in air. The oxides detected were γ-alumina and SrO, a permeable oxide whose presence increased the oxidation rate.

7.  The alloys of Al 1 wt. % Fe and Al 0.25 wt. % Ti had a reduced oxide thickness in air. The oxide thickness of the Al-Fe alloy increased from 0.04 μm to 0.21 μm over 24 hours, with the oxides found being γ-alumina. The oxide thickness of the Al-Ti alloy increased from 0.06 μm to 0.17 μm over 24 hours, with γ-alumina and $TiO_2$ being detected. The presence of these elements led to passivation of the oxide and little growth.

8.  Aluminium melted with additions of Molybdenum developed different oxides in air. Samples with Mo powder added to the surface formed oxides of $MoO_3$, $MoO_2$ and $Al_2(MoO_4)_3$, at 5

minutes, 1 hour and 24 hours respectively. The growth of this oxide was accompanied by an increase in unit cell volume (as $MoO_2$ is 21% larger than $MoO_3$ and $Al_2(MoO_4)_3$ is 87% larger than $MoO_2$). This led to cracks in the layer and increase of oxidation rate. The oxide grew in thickness from 0.34 μm to over 1000 μm over 24 hours.

9. An alloy of Al 1 wt.% Mo oxidised to give an oxide containing $MoO_3$ and γ-alumina in air. Initially this was too thin to measure, and grew to 0.35 μm after 24 hours. The addition of Mo in the alloy did not seem to greatly change the oxide thickness of Al.

10. The alloy Al-7%wt.%Si-0.3wt.%Mg-1%Mo had an oxide thickness that increased from 0.32 μm to 1.8 μm between 5 minutes and 24 hours in air. The oxides present were $MoO_3$, spinel and γ-alumina. The presence of $MoO_3$ seemed to increase the oxidation rate of the alloy.

11. Al and its alloys were also melted in a nitrogen atmosphere. SP-Al reacted with nitrogen to form a feather-like layer of AlN after 24 hours. The layer increased from 0.03 μm at 5 minutes to 1.37 μm at 24 hours. The height of the AlN feathers reached an average of 3.72 μm. The porous nature of the layer was the likely reason for its increase in thickness.

12. The Al 4 wt. % Mg alloy did not grow as thick a layer in nitrogen as in air. The layer grew as AlN, γ-alumina and traces of α-alumina, changing in thickness only by 0.01 μm over 24 hours. The formation of $Mg_3N_4$ was thermodynamically unfavourable compared to AlN, and it was likely that the increased Mg content near the surface slowed the formation of AlN.

13. The thickness of the surface layer on an alloy of Al-7%wt.%Si-0.3wt %Mg grew from 0.03 μm to 0.16 μm over 24 hours in nitrogen. The layer contained AlN, Si and $Si_3N_4$, with a trace of γ-alumina at 24 hours. The nitrogen atmosphere seemed to suppress the growth of the layer, and the growth of AlN seemed to be suppressed by the presence of $Si_3N_4$, as it was much thinner than the 1.37 μm layer for SP-Al under the same conditions.

14. The reduction of double oxide film defects occurs by passage of gases from the defect, either by diffusion through an oxide layer or reaction to form a thicker one, in order to reduce the gaseous volume within. Alloys with layers most likely to assist volume reduction if the interior gases inside the defect were SP-Al (γ-alumina and α-alumina), Al-Mg (MgO, spinel), Al-Cu ($CuAl_2O_4$ and Cu enabled oxygen to diffuse more easily through γ-alumina), Al-Sr (SrO) and Al-Mo ($MoO_3$).

15. Lattice parameters of the oxides, nitrides and other species formed were compared with that of Al, to ascertain their grain refining potential. Those with most potential (a lattice mismatch of less than 20%) were, in descending order of effectiveness, $MoO_2$, spinel (its secondary lattice), $MoO_3$, MgO, SrO and α-alumina.

16. The grain refining effect of spinel was compared with CP-Al (no refiner added) and TiBor refined CP-Al. The addition of ~50 ppm spinel led to a reduction in grain size of 23%, compared to the 36% reduction in grain size that resulted from the addition of 125 ppm TiBor to CP-Al, showing spinel could be a suitable grain refiner.

17. Electro-codeposition experiments were carried out in order to incorporate spinel particles into a copper layer. The optimum technique was a fast pulse reverse mechanism with a frequency of 200Hz and a rotation speed of the electrode of 1000 rpm for 30 minutes. This gave a spinel pickup of 8.5% in a layer of copper. There was a bi-modal distribution of the effects of pulse frequency and electrode rotation speed on the deposition of spinel in the layer.

## 6 - References

(Agema & Fray 1989) Agema KS & Fray DJ, 1989, *Preliminary Investigations on the Deformation Behaviour of an Oxide Scale on Molten Aluminium*, Department of Materials Science and Metallurgy, University of Cambridge

(Beck et al 1967) Beck AF, Heine MA, Caule EJ & Pryor MJ, 1967, *The Kinetics of Oxidation of Al in Oxygen at High Temperature*, Corrosion Science, vol. 7, no. 1, p 1-22

(Bergsmark et al 1989) Bergsmark E, Simensen CJ & Kofstad C, 1989, *The Oxidation of Molten Aluminium*, Materials Science and Engineering A, no. 120, p 91-95

(Blackburn & Gulbransen 1960) Blackburn PE & Gulbransen EA, Dec 1960, *Aluminium Reactions with Water Vapour, Dry Oxygen, Moist Oxygen and Moist Hydrogen between 500º and 625º*, Journal of the Electrochemical Society, vol. 107, no. 12, p 944-950

(Brock & Pryor 1973) Brock AJ & Pryor, 1973, *The Kinetics of the Oxidation of Aluminum-Copper Alloys in Oxygen at High Temperature*, Corrosion Science, vol. 13, p199-227

(Cambridge 2014)  taken from http://www.doitpoms.ac.uk/tlplib/ellingham_diagrams/images/Ellingham_1.jpg (correct 28/8/14)

(Campbell 2003) Campbell J, 2003, *Castings (2nd Edition)*, Butterworth-Heinemann, Oxford UK

(Cao & Campbell 2005) Cao X & Campbell J, 2005, *Oxide Inclusion Defects in Al-Si-Mg Cast Alloys*, Canadian Metallurgical Quarterly, vol. 44, no. 4, p 435-448

(Cashion et al 2002) Cashion SP, Ricketts NJ & Hayes PC, 2002, *The Mechanisms of Protection of Molten Magnesium by Cover Gas Mixtures Containing Sulphur Hexafluoride*, Journal of Light Metals, vol. 2, p 43-47

(Celis & Roos 1977) Celis JP & Roos JR, Oct. 1977, *Kinetics of the Deposition of Alumina Particles from Copper Sulfate Plating Baths*, Journal of the Electrochemical Society, vol. 124, no. 10, p 1508-1511

(Celis et al 1987) Celis JP, Roos JR & Buelens C, June 1987, *A Mathematical Model for the Electrolytic Codeposition of Particles with a Metallic Matrix*, Journal of The Electrochemical Society, vol. 134, no. 6, p 1402-1408

(Chandrasekar & Pushpavanam 2008) Chandrasekar MS & Pushpavanam M, 2008, *Pulse and Pulse Reverse Plating – Conceptual, Advantages and Applications*, Electrochemica Acta, vol. 53, p 3313-3312

(Cibula 1952) Cibula A, Dec 1952, *Grain Refinement and its Effects in Non-Ferrous Casting Alloys*, Foundry Trade Journal, vol. 93, p 695

(Cochran et al 1977) Cochran CN, Belitskus DL & Kinosz DL, June 1977, *Oxidation of Aluminium-Magnesium Melts in Air, Oxygen, Flue Gas and Carbon Dioxide*, Metallurgical Transactions B, vol. 8B, p 323-332

(Cook 1998) Cook R, 1998, *Grain Refinement of Aluminium-Silicon Foundry Alloys*, LSM Booklets, London & Scandinavian Metallurgical Co. Ltd, Rotherham UK

(Crossley & Mondolfo 1951) Crossley FA & Mondolfo LF, December 1951, *Mechanism of Grain Refinement in Aluminum Alloys*, Transactions of AIME, vol. 191, p 1143

(Davis 1993) Davis JR (edited by), 1993, *ASM Speciality Handbook: Aluminum and Aluminum Alloys*, ASM International, USA

(Delamore & Smith 1971) Delamore GW & Smith RW, June 1971, *The Mechanisms of Grain Refinement in Dilute Aluminum Alloys*, Metallurgical Transactions, vol. 2, p 1733-1738

(Doherty & Davis 1963) Doherty PE & Davis RS, March 1963, *Direct Observation of the Oxidation of Aluminium Single-Crystal Surfaces*, Journal of Applied Physics, vol. 32, no. 1, p 619-628

(Drouzy & Mascré 1969) Drouzy M & Mascré C, 1969, *The Oxidation of Liquid Non-Ferrous Metals in Air or Oxygen*, Metallurgical Reviews, no. 14, p 25-46

(Easton & StJohn 1999) Easton M & StJohn D, June 1999, *Grain Refinement of Aluminium Alloys: Part I. The Nucleant and Solute Paradigms – A Review of the Literature*, Metallurgical and Materials Transactions A, vol. 30A, p 1616-1623

(Emsdiasum 2011) Image taken from
 http://www.emsdiasum.com/microscopy/products/grids/lift_out.aspx - correct 15/6/2011

(Esposto et al 1994) Esposto FJ, Zhang CS, Norton PR & Tismit RS, 1994, *Segregation of Mg to the Surface of an Al-Mg Single Crystal Alloy and its Influence on the Initial Oxidation at Room Temperature*, Surface Science, vol. 302, p 109-120

(Evans 1960) Evans UR, 1960, *The Corrosion and Oxidation of Metals: Scientific Principles and Practical Applications*, Edward Arnold (Publishers) Ltd., London UK

(Fan et al 2009a) Fan Z, Wang Y, Xia M & Arumuganathar S, July 2009, *Enhanced Heterogeneous Nucleation in AZ91D Alloy by Intensive Melt Shearing*, Acta Materialia, no. 57, p 4891–4901

(Fan et al 2009b) Fan Z, Xia M, Zhang H, Liu G, Patel JB, Bian Z, Bayandorian I, Wang Y, Li HT & Scamans GM, 2009, *Melt Conditioning by Advanced Shear Technology (MCAST) for Refining Solidification Microstructures*, International Journal of Cast Metals Research, vol. 22, no. 1-4, p 103

(Fan et al 2009c) Fan Z, Wang Y, Zhang ZF, Xia M, Li1 HT, Xu J, Granasy L & Scamans GM, 2009, *Shear Enhanced Heterogeneous Nucleation in Some Mg- and Al-alloys*, International Journal of Cast Metals Research, vol. 22, no. 1-4, p 318

(Grace & Seybolt 1958) Grace RE & Seybot AU, October 1958, *Selective Oxidation of Al from an Al-Fe Alloy*, vol. 105, no. 10, p 582-585

(German & Munir 1974) German RM & Munir ZA, 1974, *The Correlation Between the Pilling-Bedworth Ratio and the Radius of Curvature of Metallic Substrates with Coherent Thin Oxide Layers*, Oxidation of Metals, vol. 8, no. 3, p 123-129

(Gerrard & Griffiths 2014) Gerrard AJ & Griffiths WD, March 2014, *The Formation of Hydrogen Related Porosity by Double Oxide Film Defects in Al Alloys*, 5th International Shapecasting Symposium, p 269-276

(Greenberg et al 2004) Greenberg R, Haplerin G, Etsion I & Tenne R, Aug 2004, *The Effect of WS2 Nanoparticles on Friction Reduction in Various Lubrication Regimes*, Tribology Letters, vol. 17, no. 2, p 179-186

(Greer et al 2000) Greer AL, Bunn AM, Tronche A, Evans PV & Bristow DJ, 2000, *Modelling of Inoculation of Metallic Melts: Application to Grain Refinement of Aluminium by Al-Ti-B*, Acta Materialia, vol. 48, p 2823-2835

(Guglielmi 1972) Guglielmi N, Aug. 1972, *Kinetics of the Deposition of Inert Particles from Electrolytic Baths*, Journal of the Electrochemical Society, vol. 119, no. 8, p 1009-1012

(Gugowski et al 1987) Gugowski MM, Sigworth GK & Sentner DA, April 1987, *The Role of Boron in the Grain Refinement of Aluminum with Titanium*, Metallurgical Transactions A, vol. 18a, p 603-619

(Guo et al 2006) Guo D, Zhang M Jin Z & Kang R, 2006, *Pulse Plating of Copper-ZrB$_2$ Composite Coatings*, Journal of Materials Science and Technology, vol. 22, no. 4, p 514-518

(Hart 1956) Hart RK, July 1956, *The Oxidation of Aluminium in Dry and Humid Oxygen Atmospheres*, Proceedings of the Royal Society of London A: Mathematical and Physical Sciences, vol. 236, no. 1204, p 68-88

(Hart & Maurin 1970) Hart RK & Maurin JK, April 1970, *The Nucleation and Growth of Oxide Islands on Aluminium*, Surface Science, vol. 20, p 285-303

(Hou 2003) Hou PY, 2003, *Impurity Effects on Alumina Scale Growth*, Journal of the American Ceramic Society, vol. 86, no. 4, p 660-668

(Impey et al 1988) Impey SA, Stephenson DJ & Nicholls JR, Dec 1988, *Mechanism of Scale Growth on Liquid Aluminium*, Materials Science and Technology, vol. 4, p 1126-1132

(Impey et al 1990) Impey S, Stephenson DJ & Nicholls JR, March 1990, *A Study of the Effect of Magnesium Additions on Oxide Growth Morphologies on Liquid Aluminium Alloys*, Microscopy of Oxidation: Proceedings of the First International Conference on the Microscopy of Oxidation, Cambridge UK, p 238-244

(Impey et al 1993) Impey S, Stephenson DJ & Nicholls JR, March 1993, *The Influence of Surface Preparation and Pretreatments on the Oxidation of Liquid Aluminium and Aluminium-Magnesium Alloys*, Microscopy of Oxidation 2: Proceedings of the Second International Conference on the Microscopy of Oxidation, Cambridge UK, p 323-337

(Johnsson 1995) Johnsson M, 1995, *Grain Refinement of Aluminium Studied by Use of a Thermal Analytical Technique*, Thermochimica Acta, vol. 256, p 107-121

(Johnsson et al 1993) Johnsson M, Backerud L & Sigworth GK, Feb 1993, *Study of the Mechanism of Grain Refinement of Aluminum after Additions of Ti and B Containing Master Alloys*, Metallurgical Transactions A, vol. 24A, p 481-491

(Jones & Pearson 1976) Jones GP & Pearson J, June 1976, *Factors Affecting the Grain Refinement of Aluminum Using Titanium and Boron Additives*, Metallurgical Transactions B, bol. 7B, p 223-234

(Kanani 2004) Kanani, Nasser, 2004, *Electroplating: Basic Principles, Processes and Practice*, Elsevier, Oxford UK

(Kelton & Greer 2010) Kelton KF & Greer AL, 2010, *Nucleation in Condensed Matter: Applications in Materials and Biology*, Elsevier, Oxford UK

(Kiusalaas & Bäckerud 1987) Kiusalaas R & Bäckerud L, Sept 1987, *Influence of Production Parameters on Performance of Al-Ti-B Master Alloys*, Solidification Processing 1987 – Proceedings, p 137

(Kooi et al 2002) Kooi BJ, Wouters O, De Hosson J.Th.M, January 2002, *Analysis of Gibbsian Segregation at Heterophase Interfaces using Analytical Transmission Electron Microscopy: A Novel Approach*, Acta Materialia, vol. 50, no. 2, p 223-235

(Lea & Molinari 1984) Lea C & Molinari C, 1984, *Magnesium Diffusion, Surface Segregation and Oxidation in Al-Mg Alloys*, Journal of Materials Science, vol. 19, p2236 - 2352

(Lin et al 2011) Lin Y, Norman AG, McMahon WE, Moutinho HR, Jiang CS & Ptak AJ, 2011, *Effects of Substrate Orientation on Aluminum Growth on MgAl$_2$O$_4$ Spinel using Molecular Beam Epitaxy*, Journal of Crystal Growth, vol. 314, p 298-301

(Liu et al 2003) Liu L, Samuel AM, Samual FH, Doty HW & Valtierra S, March 2003, *Influence of Oxides on Porosity Formation in Sr-Treated Al-Si Casting Alloys*, vol. 38, p 1125-1267

(Low et al 2006) Low CTJ, Wills RGA & Walsh FC, Sept. 2006, *Electrodeposition of Composite Coatings Containing Nanoparticles in a Metal Deposit*, Surface and Coatings Technology, vol. 201, no. 1-2, p 371-383

(Marcanto & Mondolfo 1971) Marcanto JA & Mondolfo LF, Feb 1971, *Grain Refinement in Aluminum Alloyed with Titanium and Boron*, Metallurgical Transactions, vol. 2, p 465-471

(McCartney 1989) McCartney DG, 1989, *Grain Refining of Aluminium and its Alloys Using Inoculants*, International Materials Reviews, vol. 34, no. 5, p 247-260

(Men & Fan 2011) Men H & Fan Z, 2011, *Effects of Lattice Mismatch on Interfacial Structures of Liquid and Solidified Al in Contact with Hetero-phase Substrates: MD Simulations*, Materials Science & Engineering, vol. 27, p 1-6

(Mennicke et al 1998) Mennicke C, Schumann E, Rühle M, Hussey RJ, Sproule GI & Graham MJ, 1998, *The Effect of Yttrium on the Growth Process and Microstructure of α-Al$_2$O$_3$ on FeCrAl*, Oxidation of Metals, vol. 49, no. 5-6, p 455-466

(Miresmaeili et al 2005) Miresmaeili SM, Campbell J, Shabestrari SG & Boutorabi SMA, Sept. 2005, *Precipitation od Sr-Rich Intermetallic Particles and Influence on Pore Formation in Sr-Modified A356 Alloy*, Metallurgical and Materials Transactions A, vol. 36A, p 2341-2349

(Mishra et al 2004) Mishra R, Basu B & Balasubramaniam R, May 2004, *Effect of Grain Size on the Tribological Behavior of Nanocrystalline Nickel*, Materials Science and Engineering A – Structural Materials Properties, Microstructure and Processing, vol.373, no.1-2, p 370-373

(Mohanty & Gruzleski 1995) Mohanty PS & Gruzleski JE, May 1995, *Mechanism of Grain Refinement in Aluminium*, Acta Metallurgica et Materialia, vol. 43, no. 5, p 2001-2012

(Mondolfo 1976) Mondolfo LF, 1976, *Aluminum Alloys: Structure and Properties*, Butterworth & co (Publishers) Ltd., London UK

(Murty et al 2002) Murty BS, Kori SA, Chakraborty M, 2002, *Grain Refinement of Aluminium and its Alloys by Heterogenous Nucleation and Alloying*

(Partington et al 1998) Partington EC, Grieveson P & Terry B, 1998, *Self-sustaining Oxidation of Liquid Aluminium and Its Alloys Containing Magnesium and Silicon*, Journal of Materials Science, vol. 33, p 2247-2455

(Perepezko & LeBeau 1981) Perepezko JH & LeBeau SE, August 1981, *Nucleation of Al During Solidification*, Aluminium Transformation Technology and Its Applications, p 309

(Porter et al 2009) Porter DA, Easterling KE & Sherif MY, 2009, *Phase Transformation in Metals and Alloys*, CRC Press, Taylor & Francis Group, Florida USA

(Pragnell WM et al 2005) Pragnell WM, Evans HE, Naumenko D & Quadakkers WJ, 2005, *Aluminium Depletion in FeCrAlY Steel During Transitions Alumina Formation*, Materials at High Temperatures, vol. 22, no. 3-4, p 561-566

(Prescott & Graham 1992) Prescott R & Graham MJ, 1992, *The Formation of Aluminum Oxide Scales on High-Temperature Alloys*, Oxidation of Metals, vol. 38, no. 3-4, p 233-254

(Quested 2004) Quested TE, November 2004, *Understanding Mechanism of Grain Refinement of Aluminium Alloys by Inoculation*, Materials Science and Technology, vol. 20, p 1357-1369

(Quested & Greer 2004) Quested TE & Greer AL, 2004, *The Effect of the Size Distribution of Inoculant Particles on As-Cast Grain Size in Aluminium Alloys*, vol. 52, p 3859-3868

(Raeiszadeh 2005) Raeiszadeh R, Nov 2005, *A Method to Study the Behaviour of Double Oxide Film Defects in Aluminium Alloys*, PhD Thesis, The University of Birmingham UK

(Rao et al 1996) Rao AA, Murty BS, Chakraborty M, March 1996, *Influence of Chromium and Impurities on the Grain-Refining Behavior of Aluminum*, Metallurgical and Materials Transactions A - Physical Metallurgy and Materials Science, vol. 27, no. 3, p791

(Ritchie et al 1971) Ritchie IM, Sanders JV & Weickhardt PL, 1971, *Oxidation of a Dilute Aluminum Magnesium Alloy*, Oxidation of Metals, vol. 3, no. 1, p 91-101

(Robert & Cupini 1987) Robert MH & Cupini NL, Sept 1987, *Aluminium Grain Refinement by Nb, Zr and Ti Additions and Their Effect on Mechanical and Electrical Properties*, Solidification Processing 1987 – Proceedings, p 153

(Roos et al 1990) Roos JR, Celis JP, Fransaer J & Buelens C, Nov 1990, *The Development of Composite Plating for Advanced Materials*, Journal of Materials, vol. 42, no. 11, p 60-63

(Saravanan et al 2001) Saravanan RA, Molina JM, Narciso J, Garcia-Cordovilla C & Luis E, 2001, *Effects of Nitrogen on the Surface Tension of Pure Aluminium at High Temperatures*, Scripta Materialia, vol. 44, no. 6, p 965-970

(Saunders & Pryor 1968) Saunders SRJ & Pryor MJ, 1968, *The Growth of Aluminum Oxide Films on Copper-Aluminum Alloys*, Journal of the Electrochemical Society, vol. 115, no. 10, p1037-1039

(Scamans & Butler 1975) Scamans GM & Butler EP, Nov 1975, *In Situ Observations of Crystalline Oxide Formation During Aluminium and Aluminium Alloy Oxidation*, Metallurgical Transactions A, vol. 6A, p 2055-2063

(Schmid-Fetzer & Kozlov 2011) Schmid-Fetzer R & Kozlov A, 2011, *Thermodynamic Aspects of Grain Growth Restriction in Multicomponent Alloy Solidification*, Acta Materialia, vol. 59, p 6133-6144

(Scully 1990) Scully JC, 1990, *Fundamentals of Corrosion (3rd Edition)*, Pergamon Press PLC, Oxford UK

(Shackelford 2005) Shackelford JF, 2005, *Materials Science for Engineers (6th Edition)*, Pearson Education Inc., New Jersey, USA

(Shimizu et al 1998) Shimizu K, Brown GM, Kobayashi K, Skeldon P, Thompson GE & Wood GC, 1998, *The Early Stages of High Temperature Oxidation of an Al-0.5wt%Mg Alloy*, Corrosion Science, vol. 40, no. 4/5, p 557-575

(Sigworth & Kuhn 2007) Sigworth GK & Kuhn TA, 2007, *Grain Refinement of Aluminum Casting Alloys*, AFS Transactions, vol. 115, p 177-188

(Sleppy 1961) Sleppy WC, Dec 1961, *Oxidation of Molten High Purity Aluminium in Dry Oxygen*, Journal of the Electrochemical Society, vol. 108, no. 12, p 1097, 1102

(Smithells 1976) Smithells CJ, 1976, *Metals Reference Book*, Butterworth & Co., London UK

(Steinbach & Ferkel 2001) Steinbach J & Ferkel H, 2001, *Nanostructured Ni-Al$_2$O$_3$ Films Prepared by DC and Pulsed DC Electroplating*, Scripta Materialia, vol. 44, no. 8-9, p 1813-1816

(Thiele 1962) Thiele W, 1962, *Oxidation of Melts of Aluminium and Aluminium Alloys*, Aluminium, vol. 38, p 707-715 and p 780-786

(Thiemig et al 2007) Thiemig D, Lange R & Bund A, 2007, *Influence of Pulse Plating Parameters on the Electrocodeposition of Matrix Metal Nanocomposites*, Electrochemica Acta, vol. 52, p 7362-7371

(Turnbull & Vonnegut 1952) Turnbull D & Vonnegut B, June 1952, *Nucleation Catalysis*, Industrial and Engineering Chemistry, vol. 44, no. 6, p 1292-1298

(Wakefield & Sharp 1991) Wakefield GR & Sharp RM, 1991, *The Composition of Oxides Formed on Al-Mg Alloys*, Applied Surface Science, vol. 51, p 95-102

(Weston et al 2011) Weston DP, Zhu YQ, Zhang D, Miller C, Kingerley DG, Carpenter C, Harris SJ, Weston NJ, 2011, *Co-electrodeposition of Inorganic Fullerene (IF-WS$_2$) Nano-*

*particles with Cobalt from a Gluconate Bath with Anionic and Cationic Surfactants*, Electrochimica Acta, vol. 56, p 6837-6846

(Xu & Gao 2000) Xu C & Gao W, 2000, *Pilling-Bedworth Ratio for Oxidation of Alloys*, Materials Research Innovation, vol. 3, p 231-235

(Zheng & Reddy 2004) Zheng Q & Reddy RG, 2004, *Mechanism of In Situ Formation of AlN in Al melt Using Nitrogen Gas*, Journal of Materials Science, vol. 39, 141-149

## Appendix 1 – XRF Analysis of Alloys Made

All results have been normalised

**Al 4%Mg**

| Formula | Concentration | Stat. error |
|---------|---------------|-------------|
| Al | 95.31% | 0.48% |
| Mg | 4.34% | 1.63% |
| Si | 0.17% | 20.90% |
| S | 0.03% | 30.20% |
| Ca | 0.03% | 27.20% |
| Fe | 0.02% | 19.10% |
| V | 0.01% | 30.50% |

**Al-7%Si**

| Formula | Concentration | Stat. error |
|---------|---------------|-------------|
| Al | 92.75% | 0.46% |
| Si | 7.09% | 3.15% |
| Ca | 0.04% | 24.30% |
| S | 0.03% | 30.60% |
| Ni | 0.02% | 12.10% |
| Mo | 39 PPM | 18.00% |

**Al 4%Cu**

| Formula | Concentration | Stat. error |
|---------|---------------|-------------|
| Al | 95.61% | 0.48% |
| Cu | 4.10% | 0.62% |
| Ce | 0.04% | 31.40% |
| Ca | 0.03% | 27.50% |

**Al 1%Fe**

| Formula | Concentration | Stat. error |
|---------|---------------|-------------|
| Al | 97.20% | 0.45% |
| Si | 1.64% | 6.69% |
| Fe | 0.97% | 1.94% |
| Cl | 0.09% | 23.20% |
| Ni | 0.01% | 19.30% |

**Al 0.3%Sr**

| Formula | Concentration | Stat. error |
|---------|---------------|-------------|
| Al | 87.96% | 0.47% |
| Si | 10.96% | 2.46% |
| Mo | 1.17% | 0.45% |

| | | |
|---|---|---|
| Mg | 0.28% | 10.80% |
| Ti | 0.10% | 12.10% |
| Fe | 0.08% | 7.43% |

**Al-1%Mo**

| Formula | Concentration | Stat. error |
|---|---|---|
| Al | 98.58% | 0.26% |
| Mo | 0.77% | 0.32% |
| Si | 0.56% | 6.70% |
| S | 0.03% | 15.00% |
| Fe | 0.02% | 12.60% |
| Ti | 87 PPM | 24.30% |

**Al-7%Si-0.3%Mg 1% Mo**

| Formula | Concentration | Stat. error |
|---|---|---|
| Al | 87.40% | 0.47% |
| Si | 10.89% | 2.46% |
| Mo | 1.16% | 0.45% |
| Mg | 0.28% | 10.80% |
| Ti | 0.10% | 12.10% |
| Fe | 0.08% | 7.43% |

**SP-A**
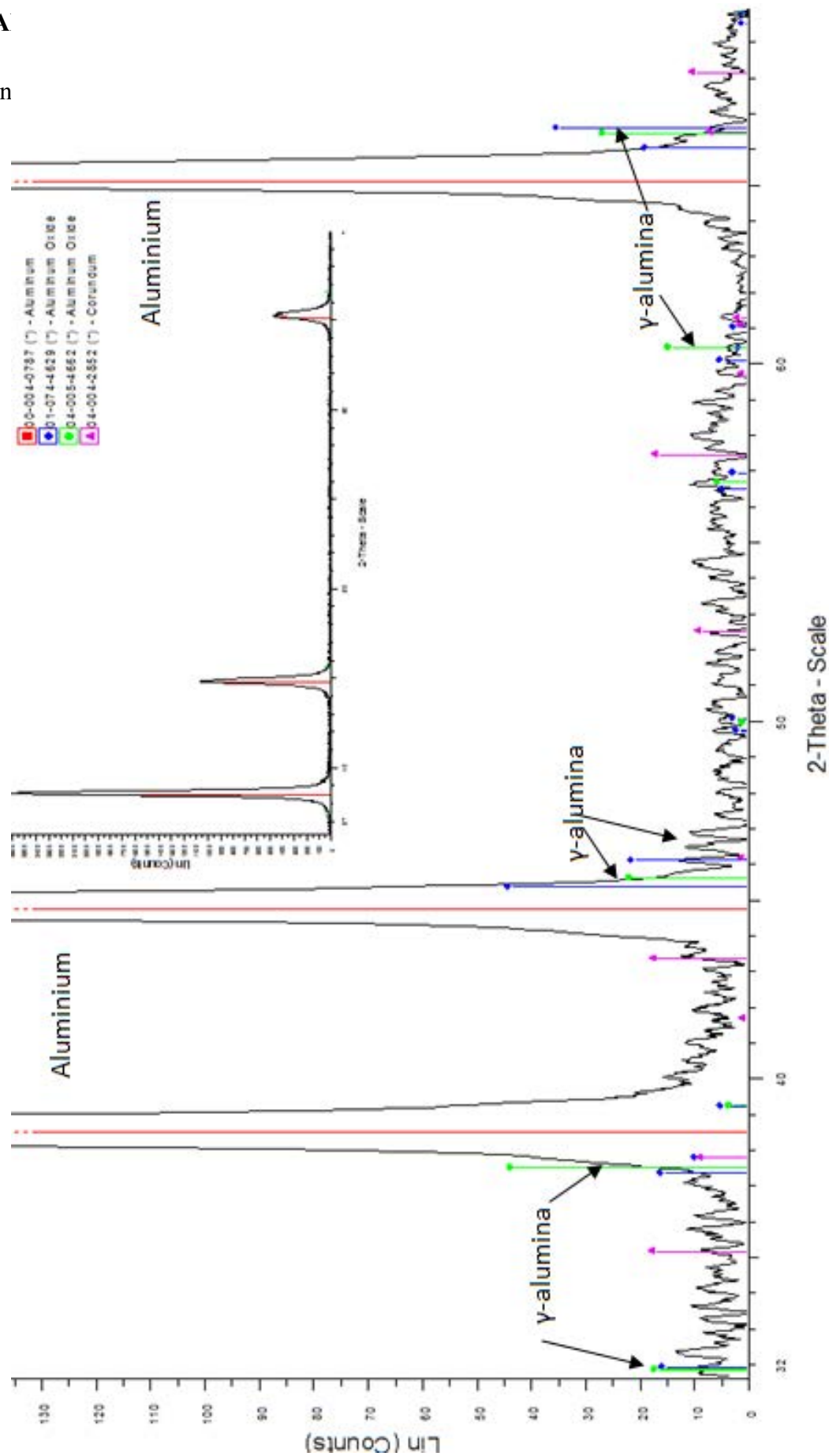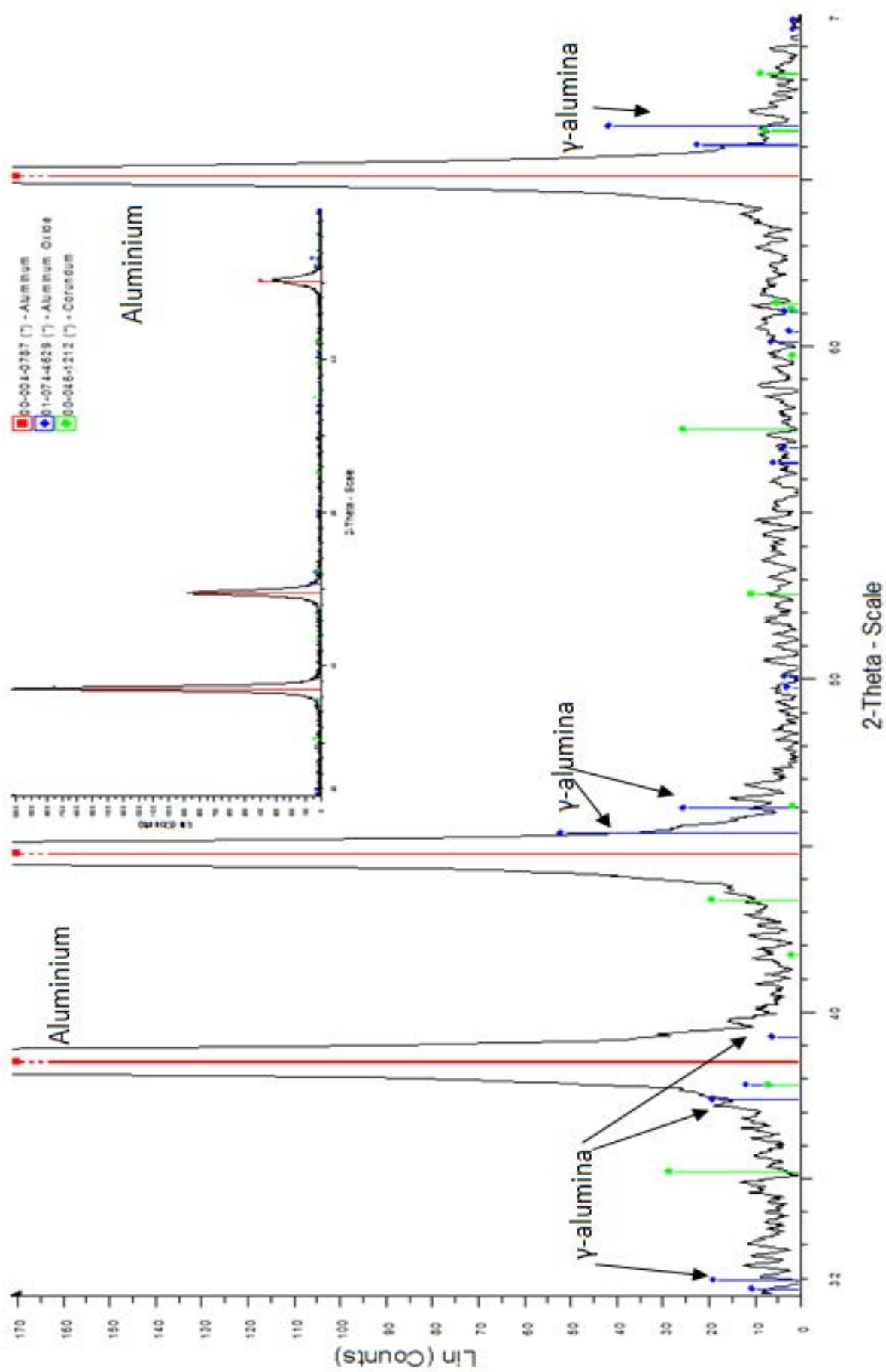
5 min

1 hour

24 hours
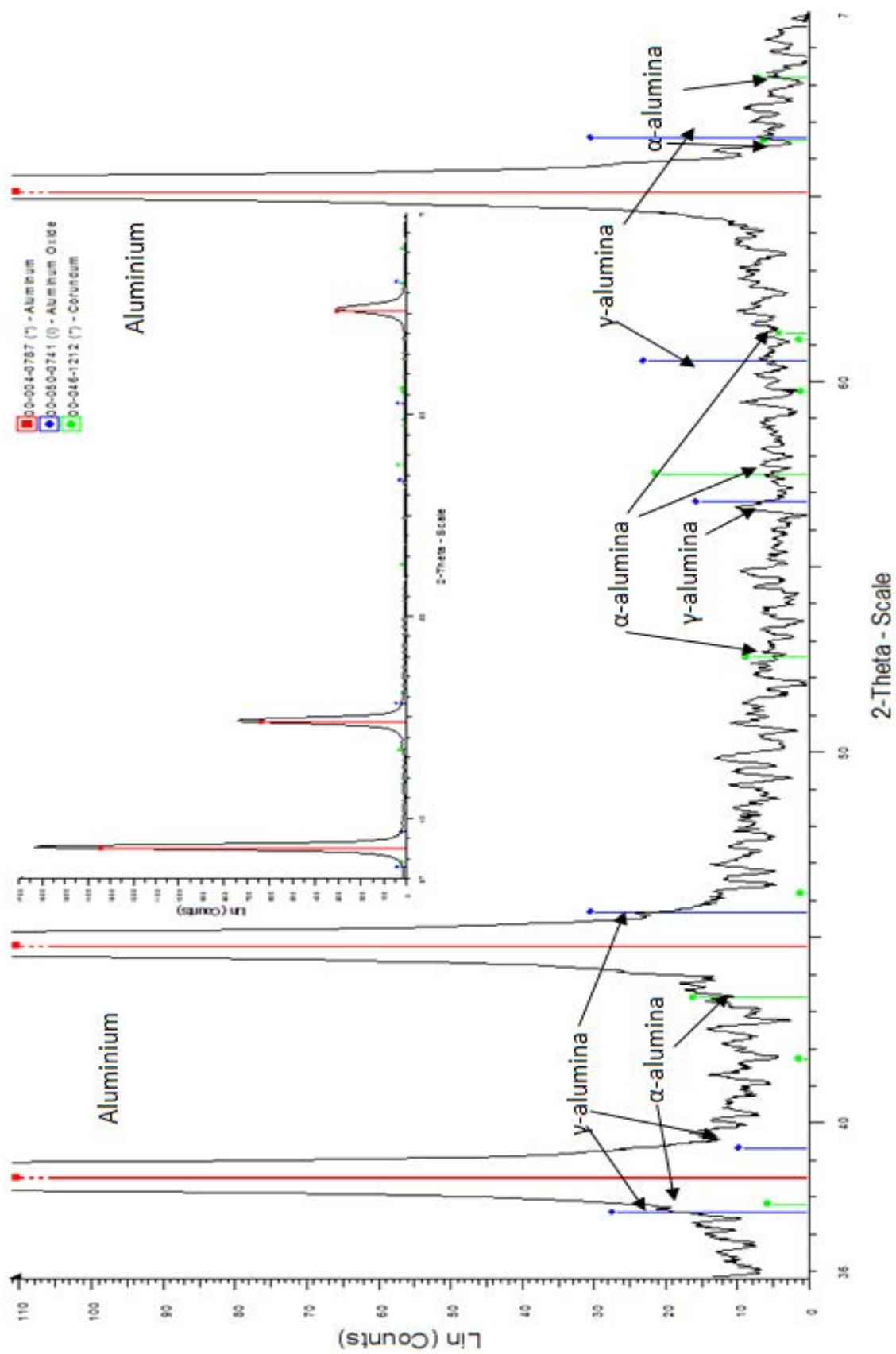
**Al-Mg**

5 minu
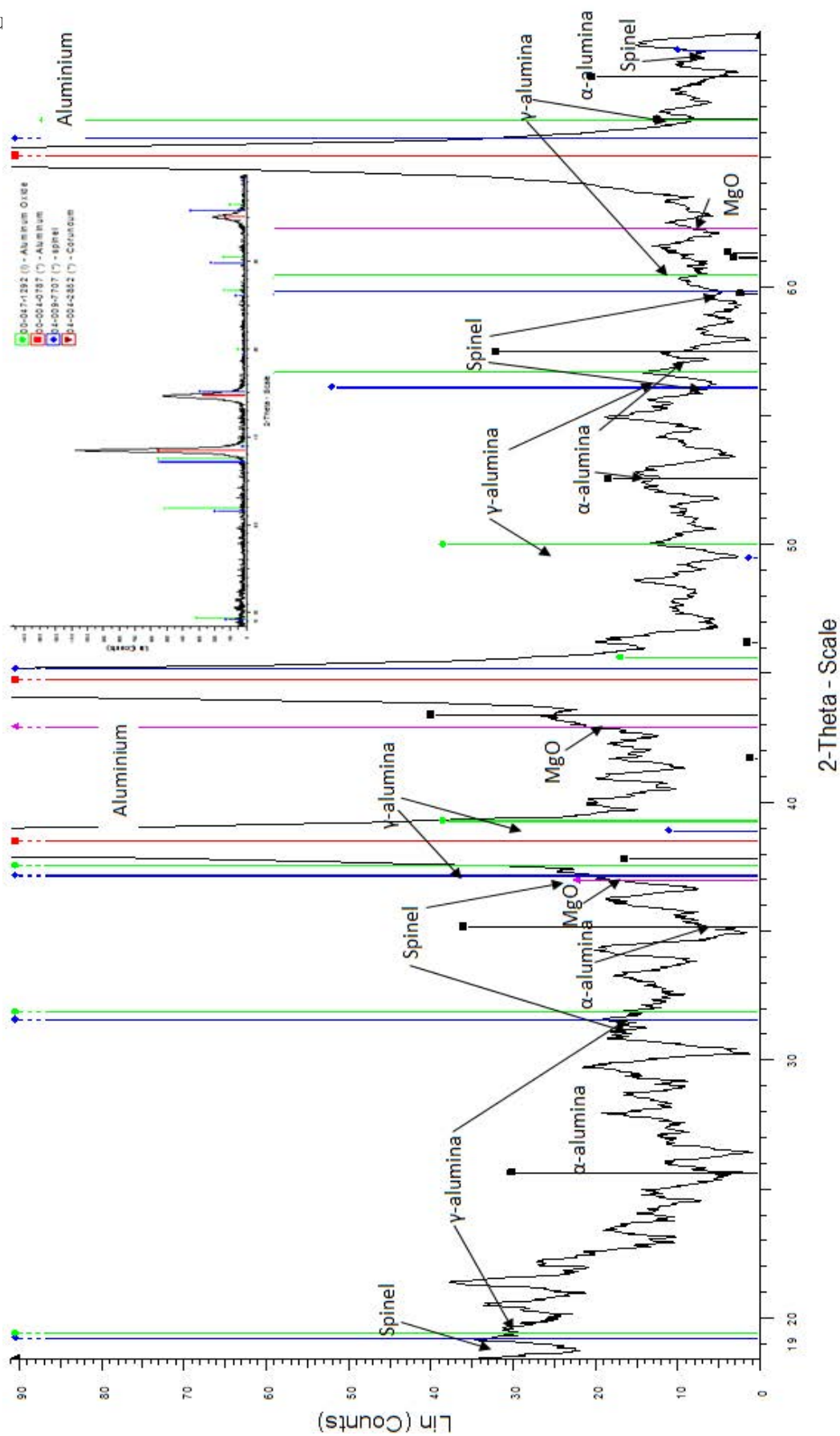
1 hour
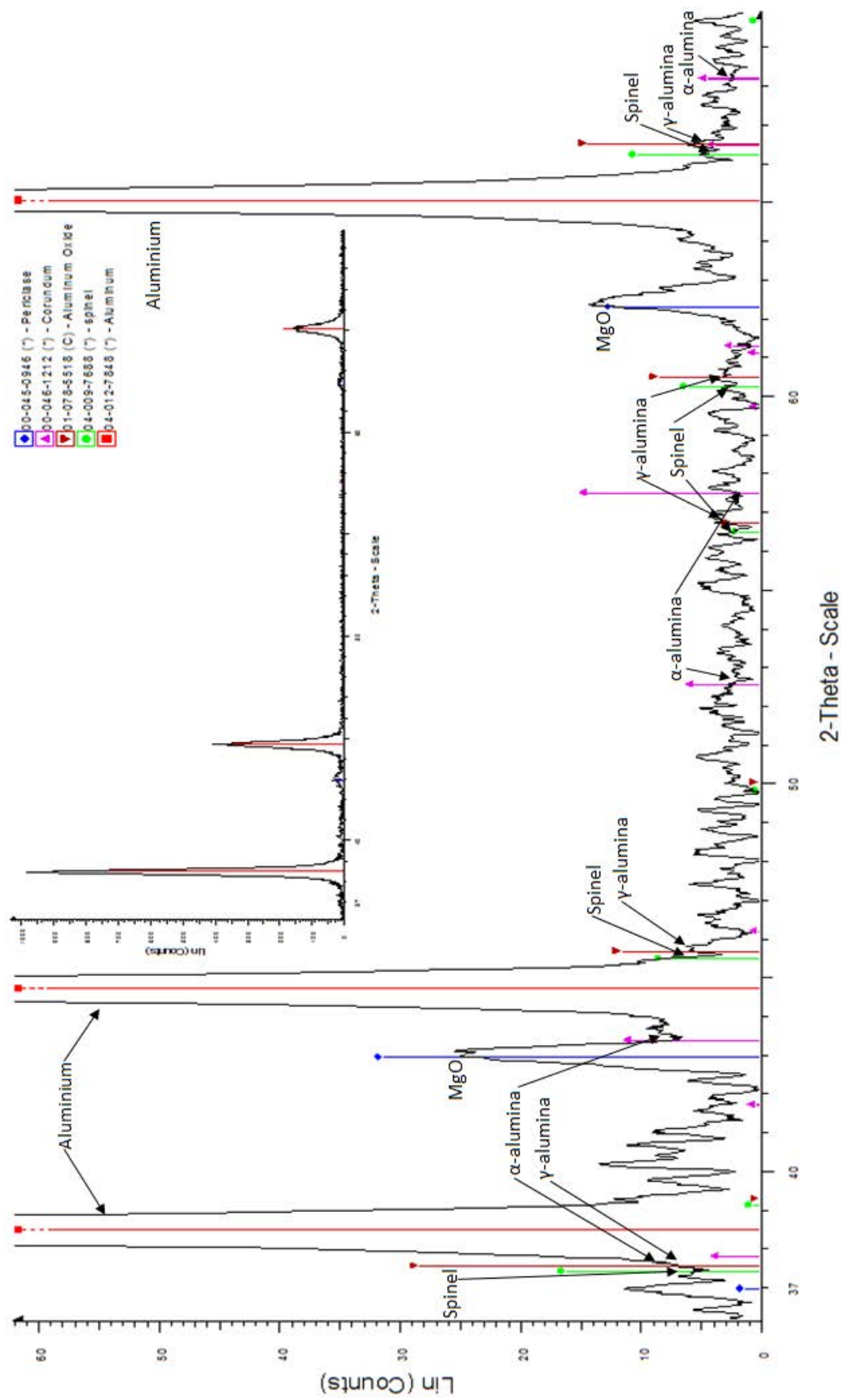
24 hours
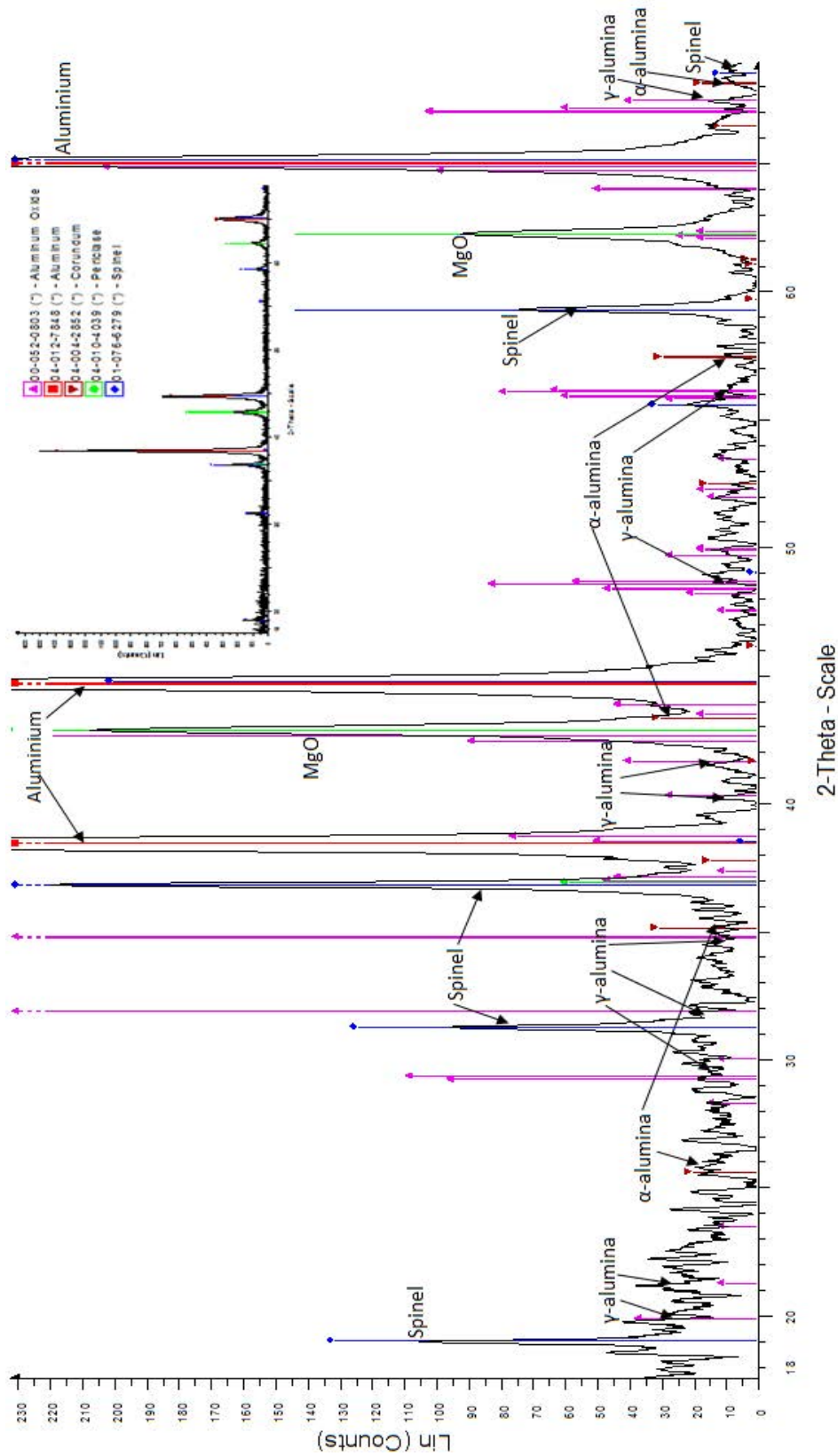
**Al-Si**

5 minutes
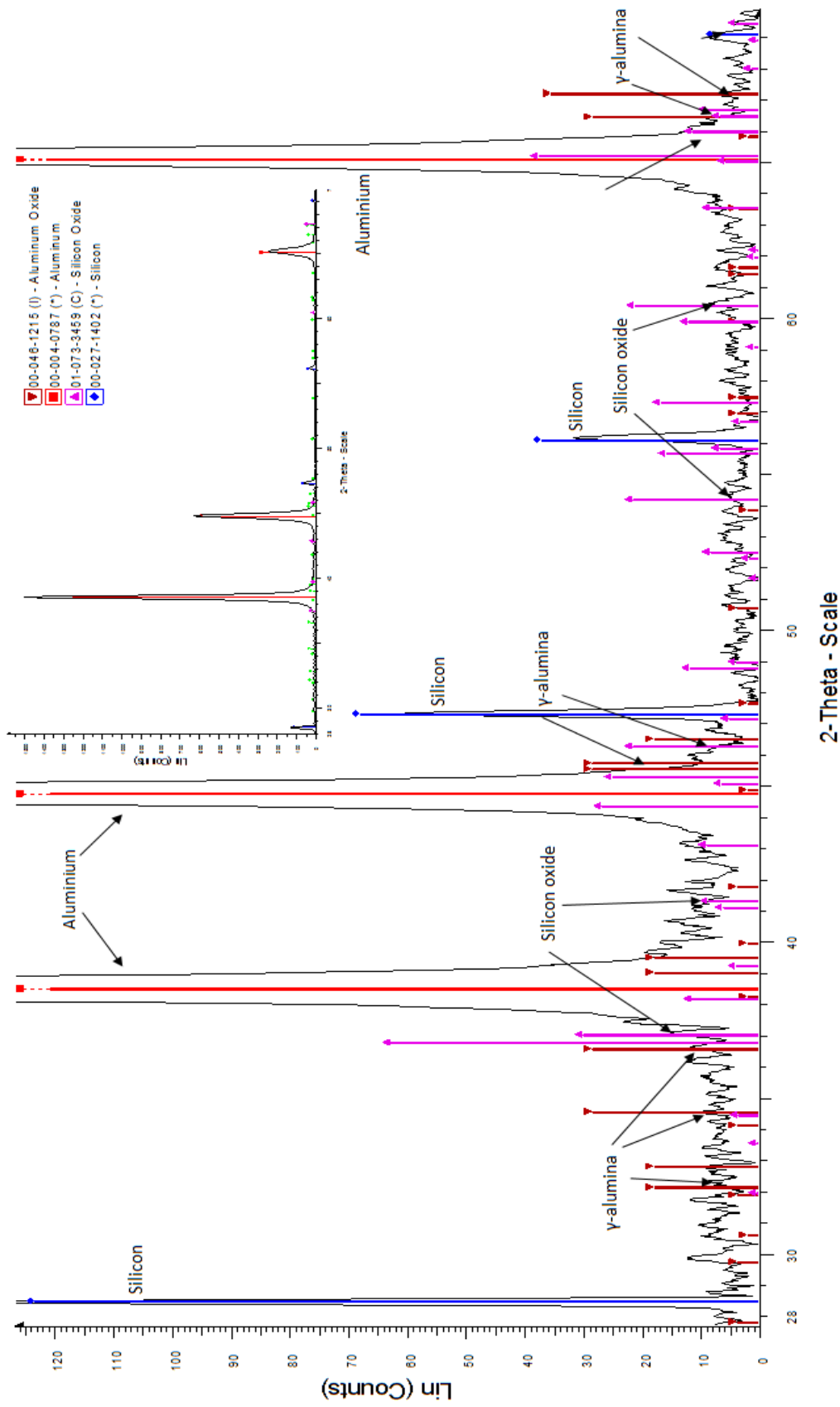
24 hours
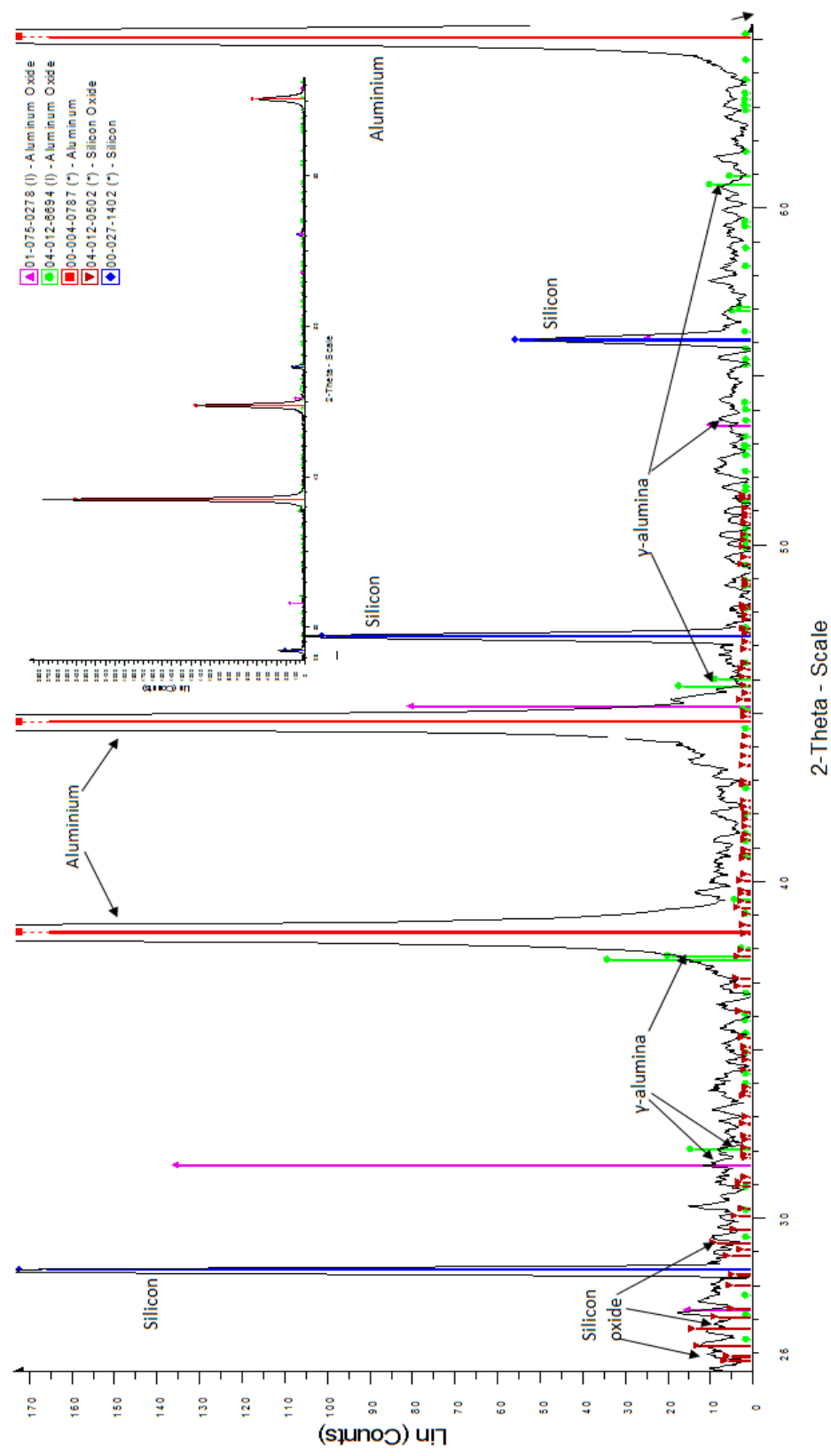
**Al-Si-Mg**

5 minutes

1 hour

24 hours



215

**Al-Cu**
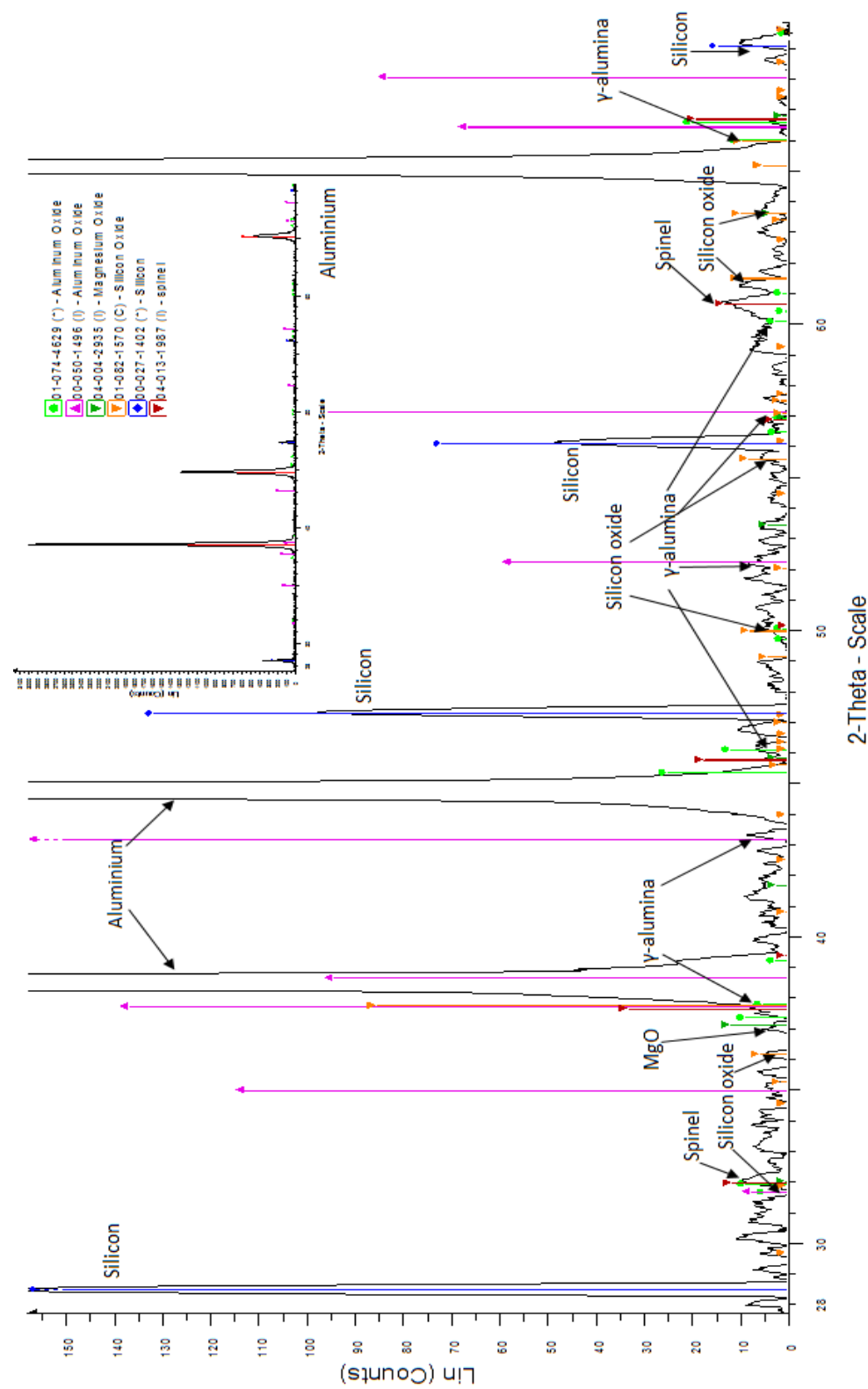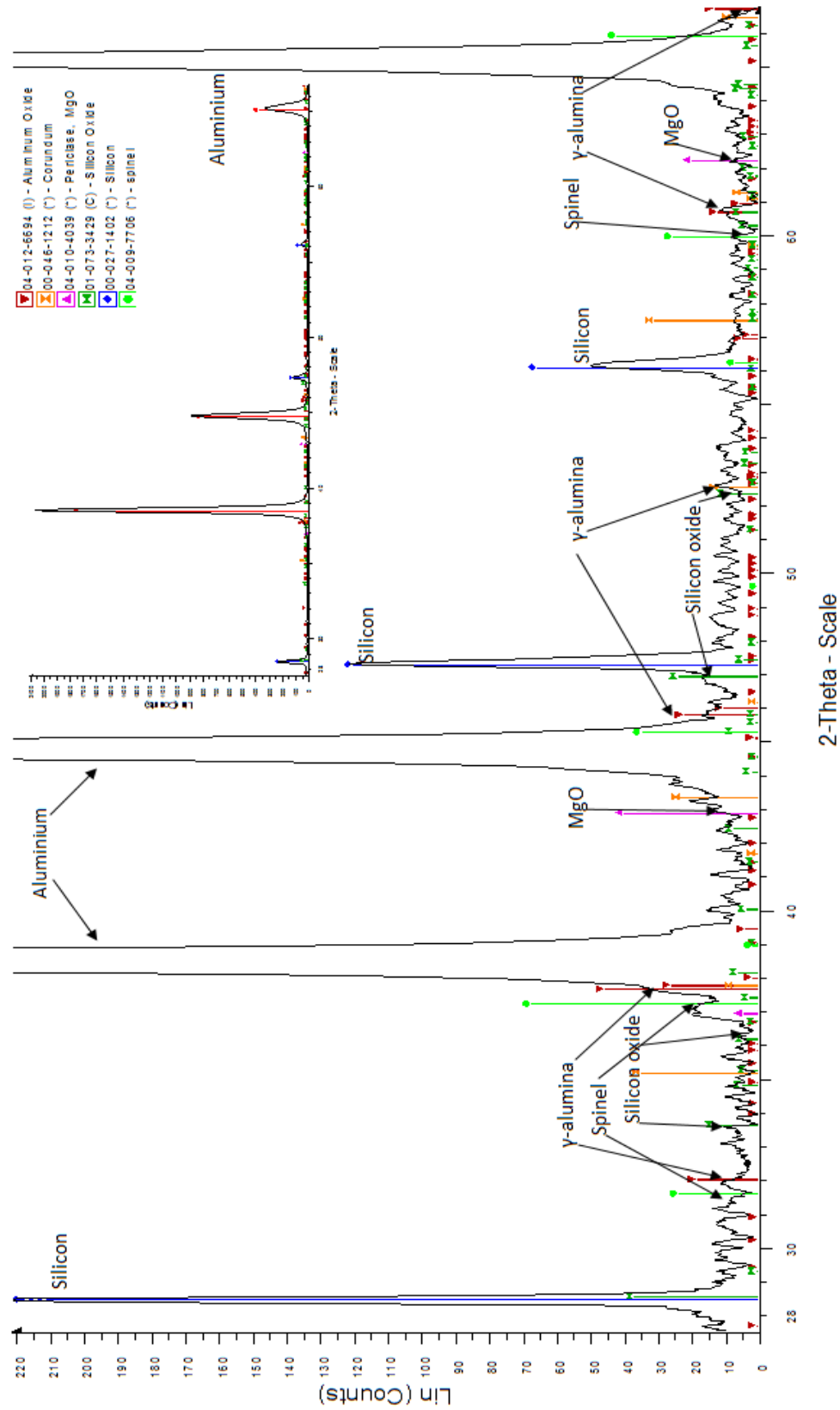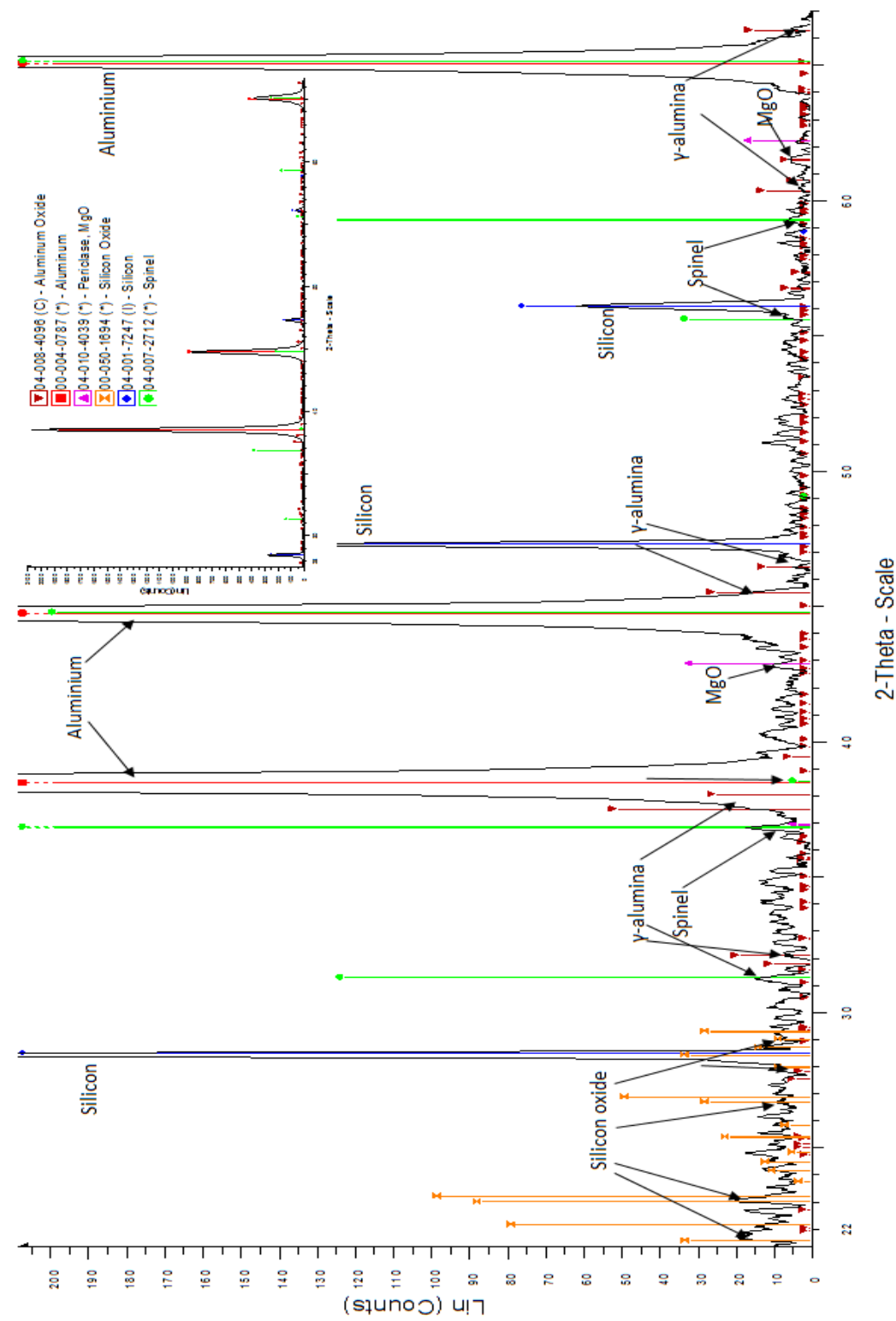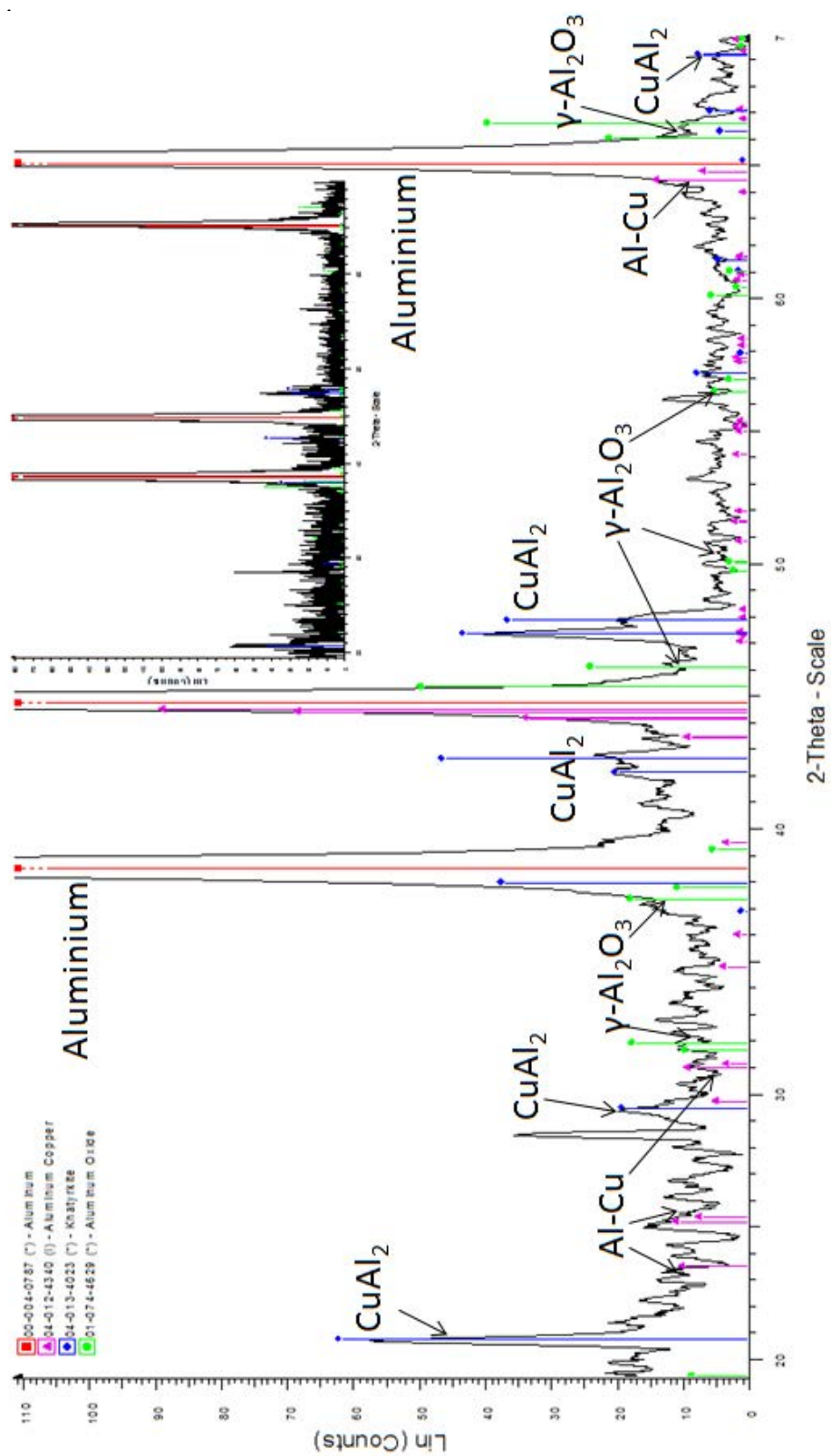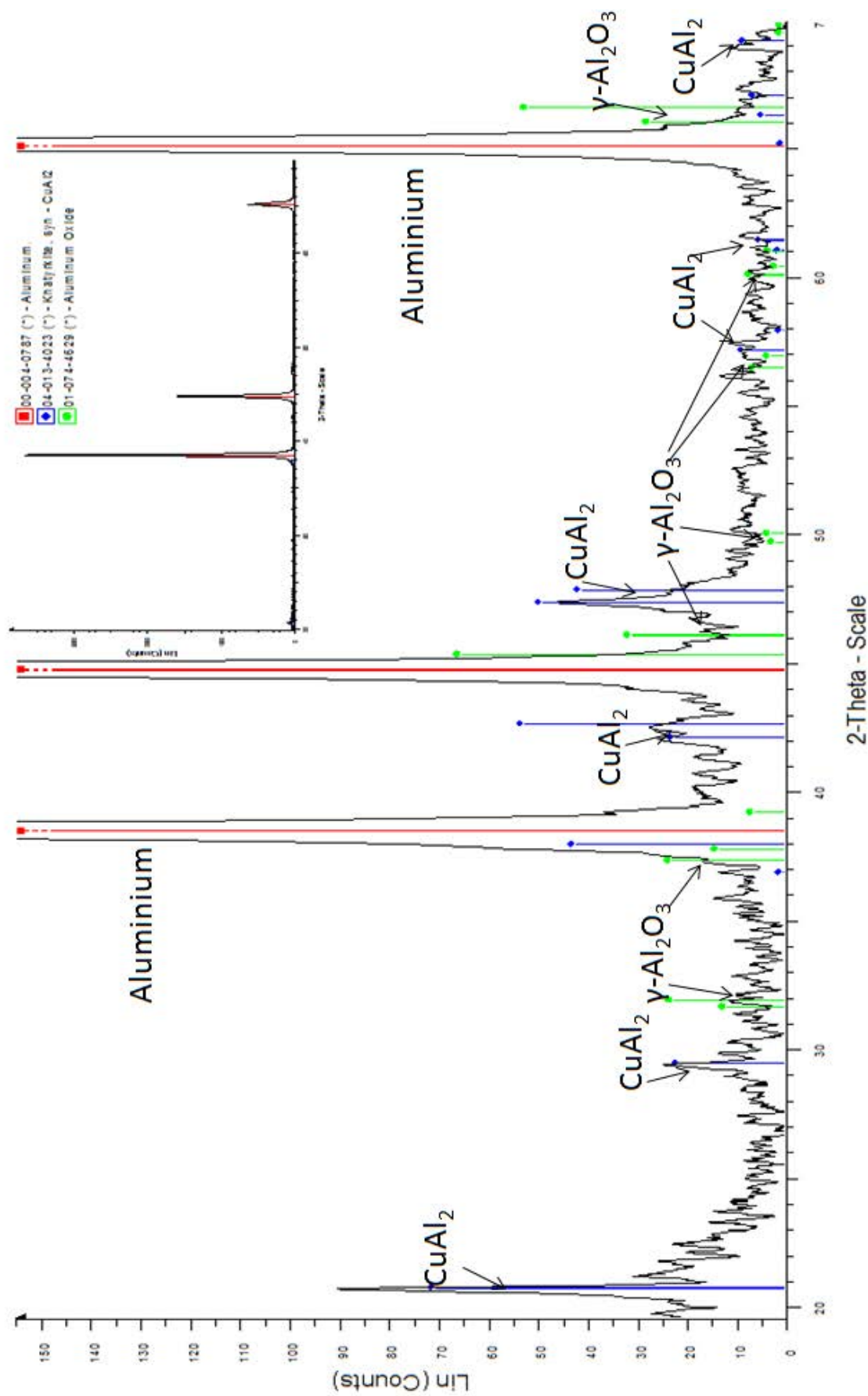
24 hours

**Al-Fe**

5 minutes
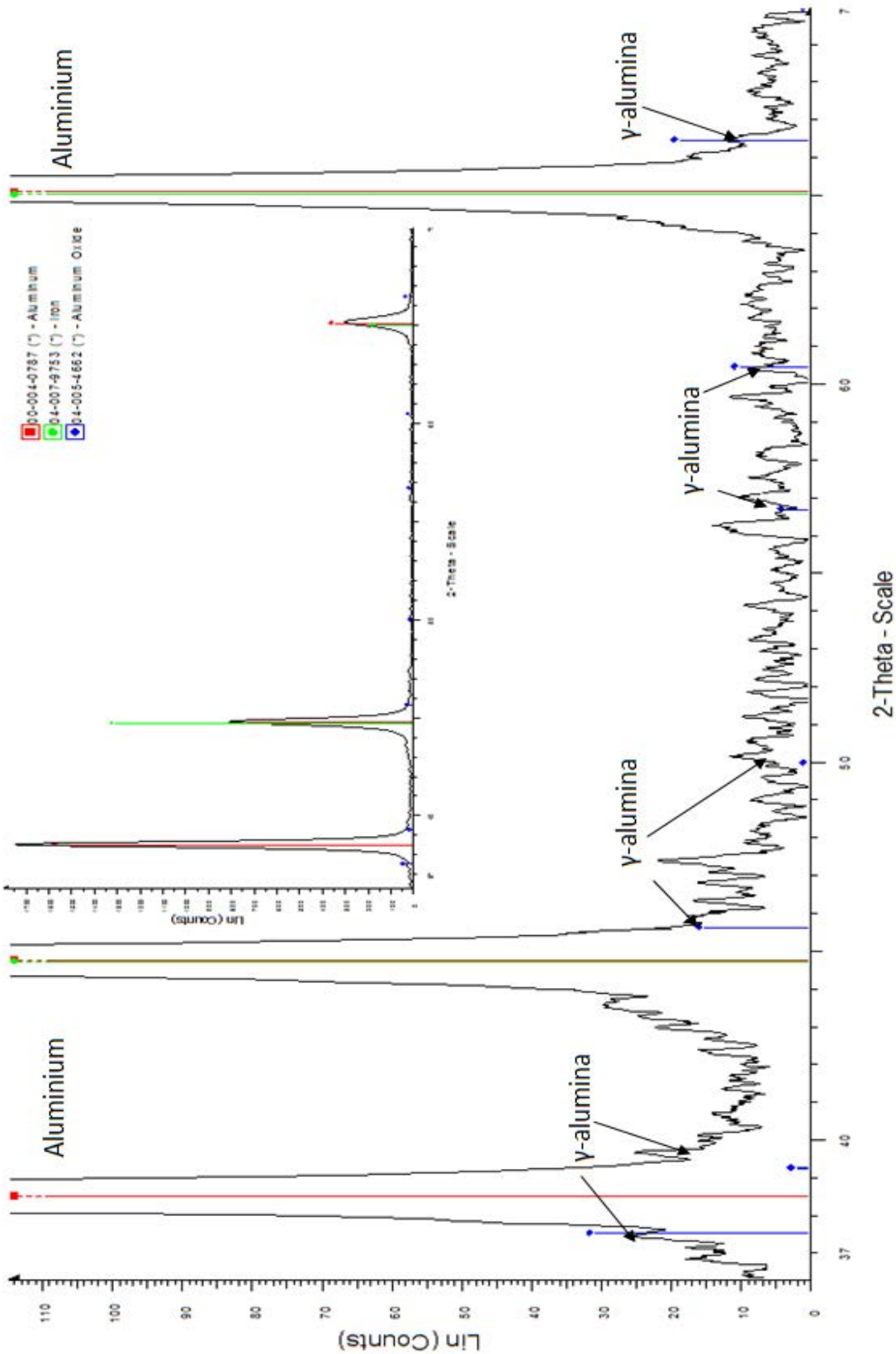
24 hours
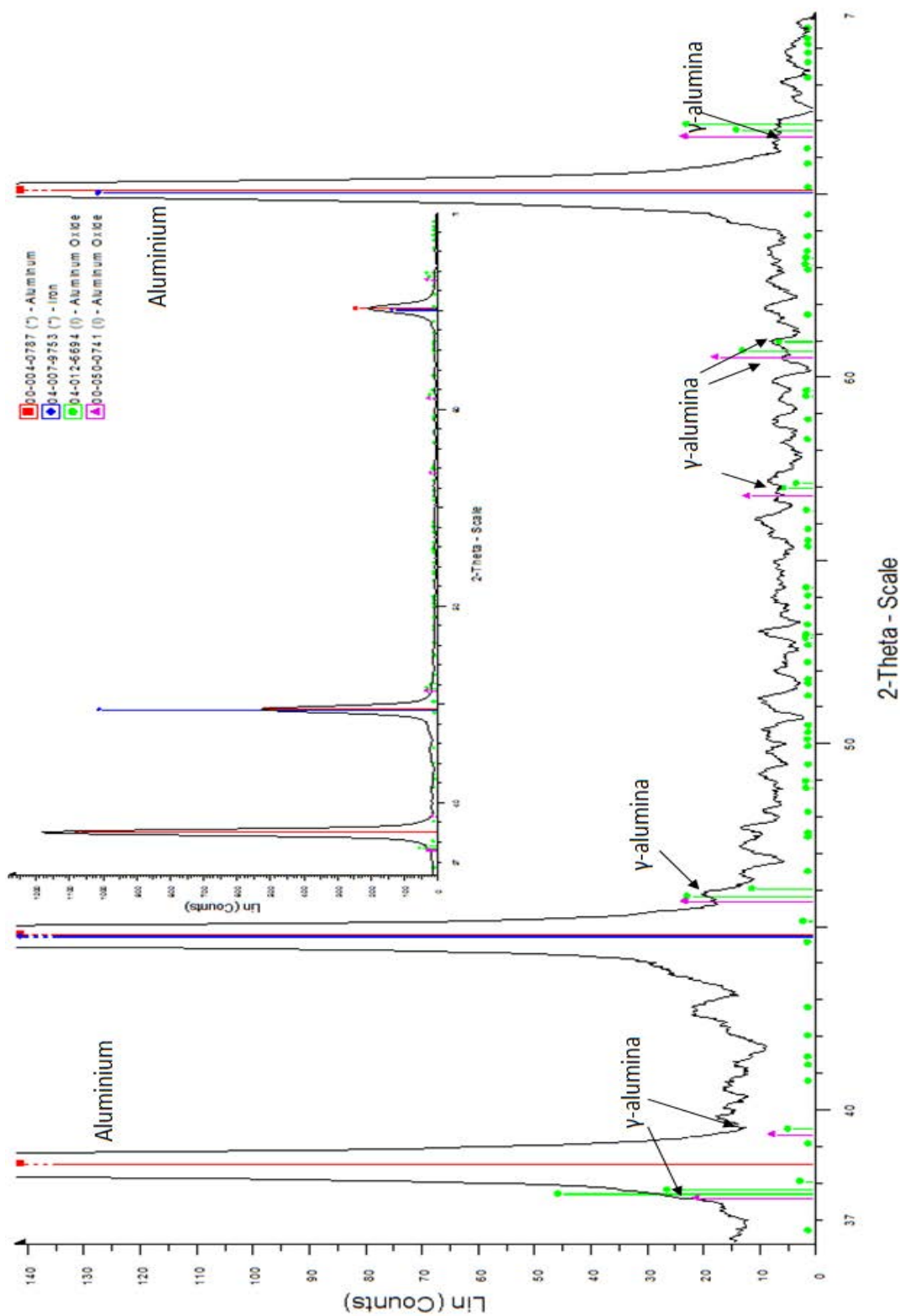
**Al-Sr**

5 minutes

24 hours

**Al-Ti**
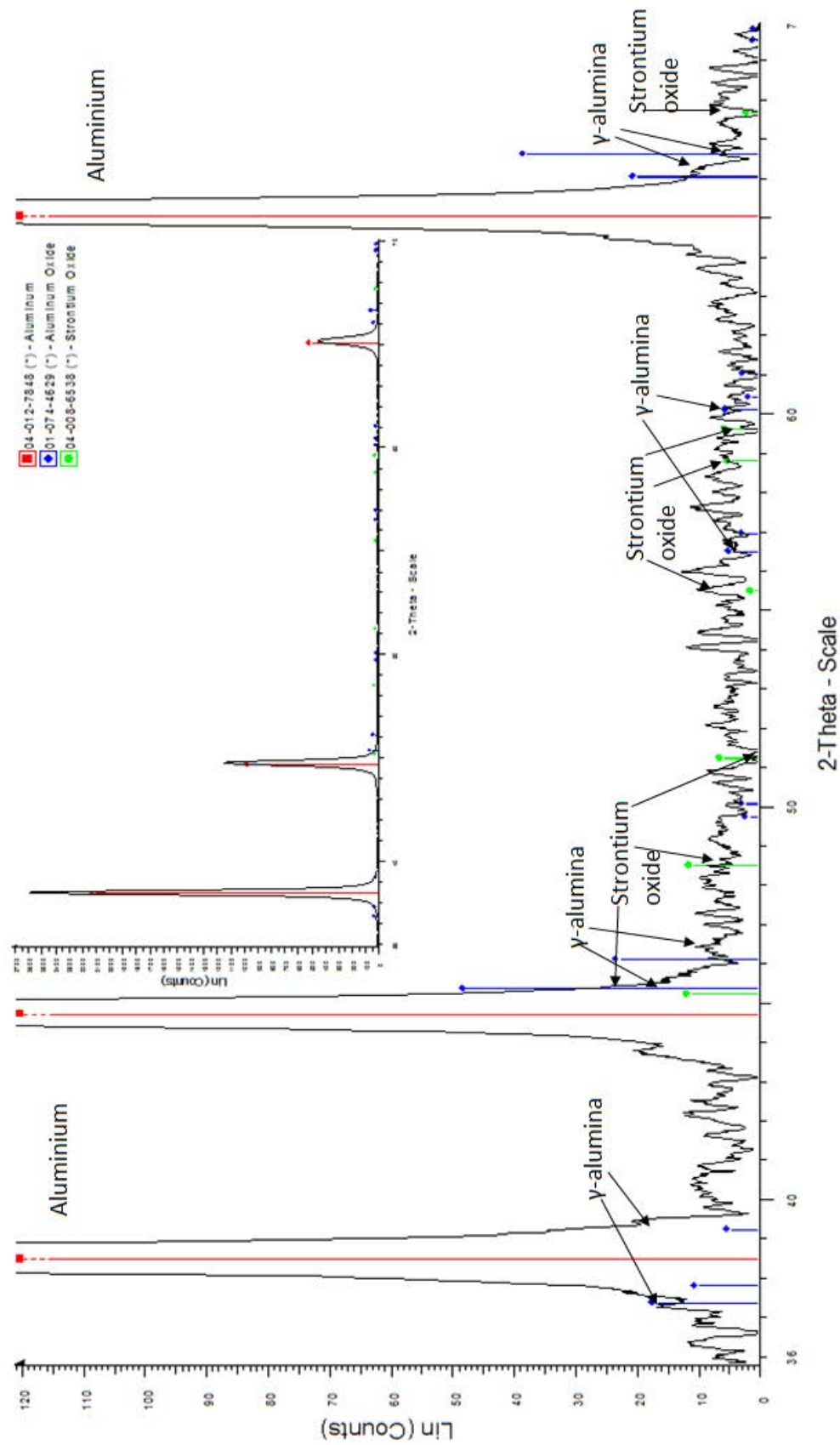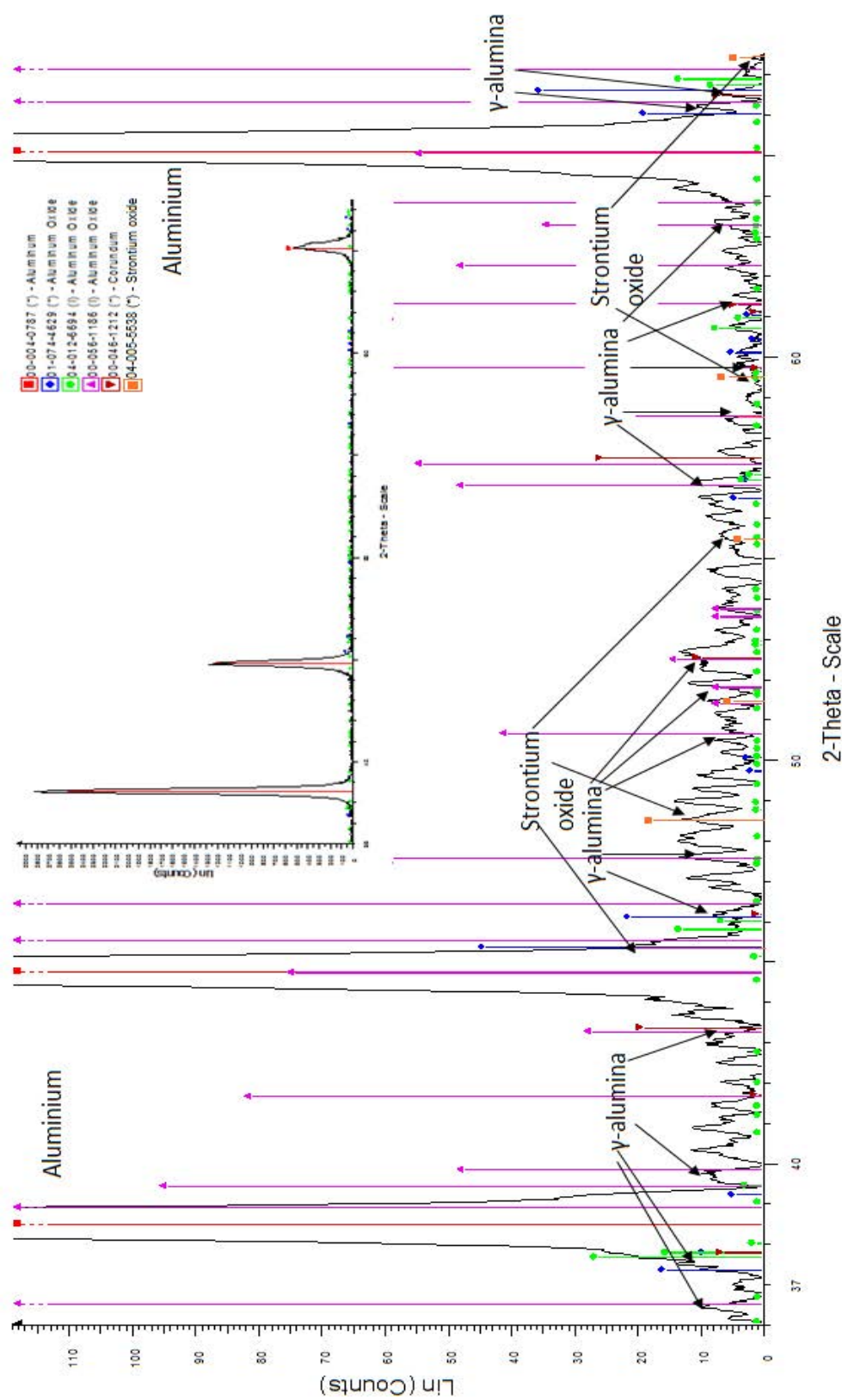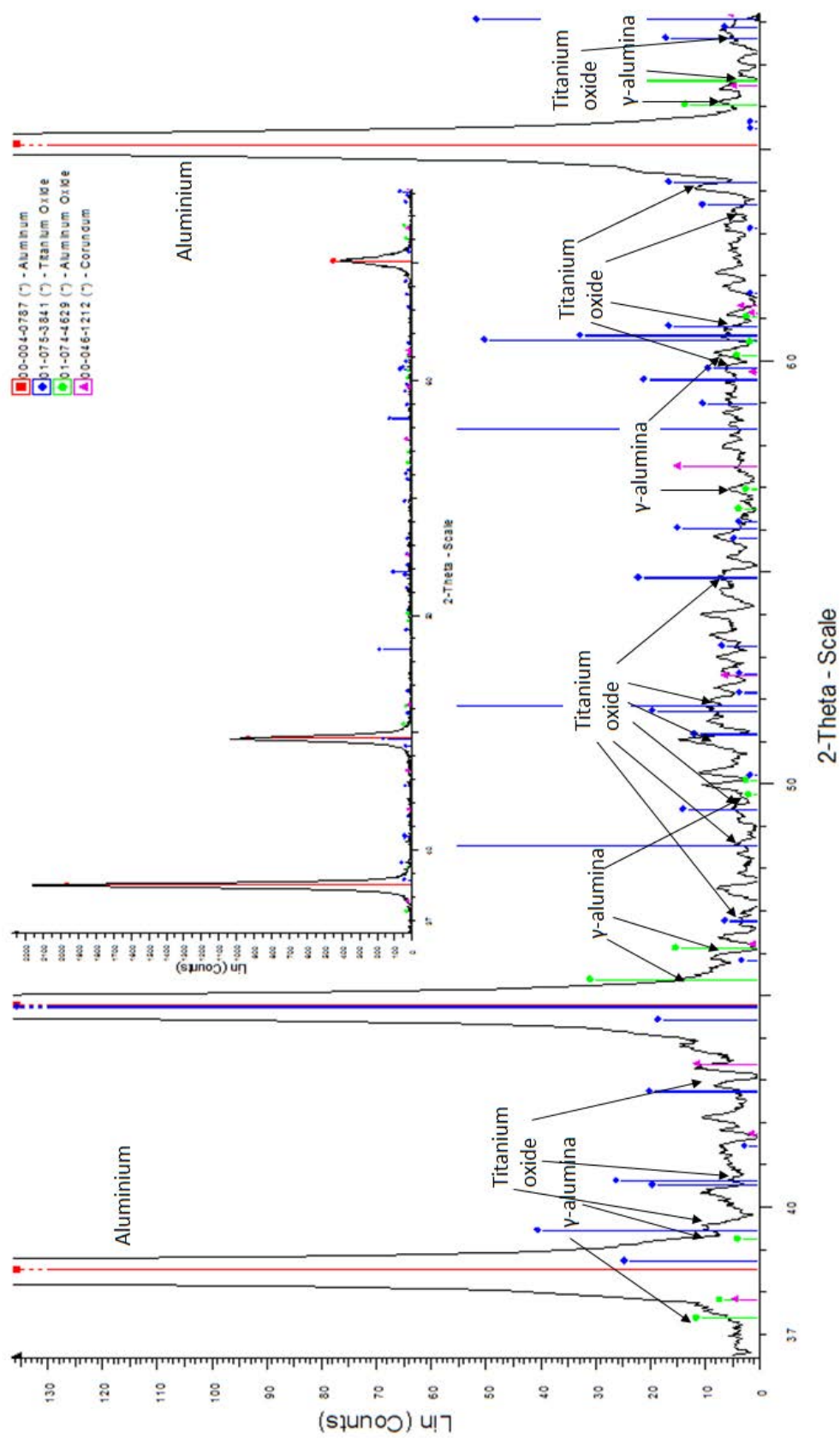
5 minutes

24 hours

**Al + Mo powder**

5 minutes
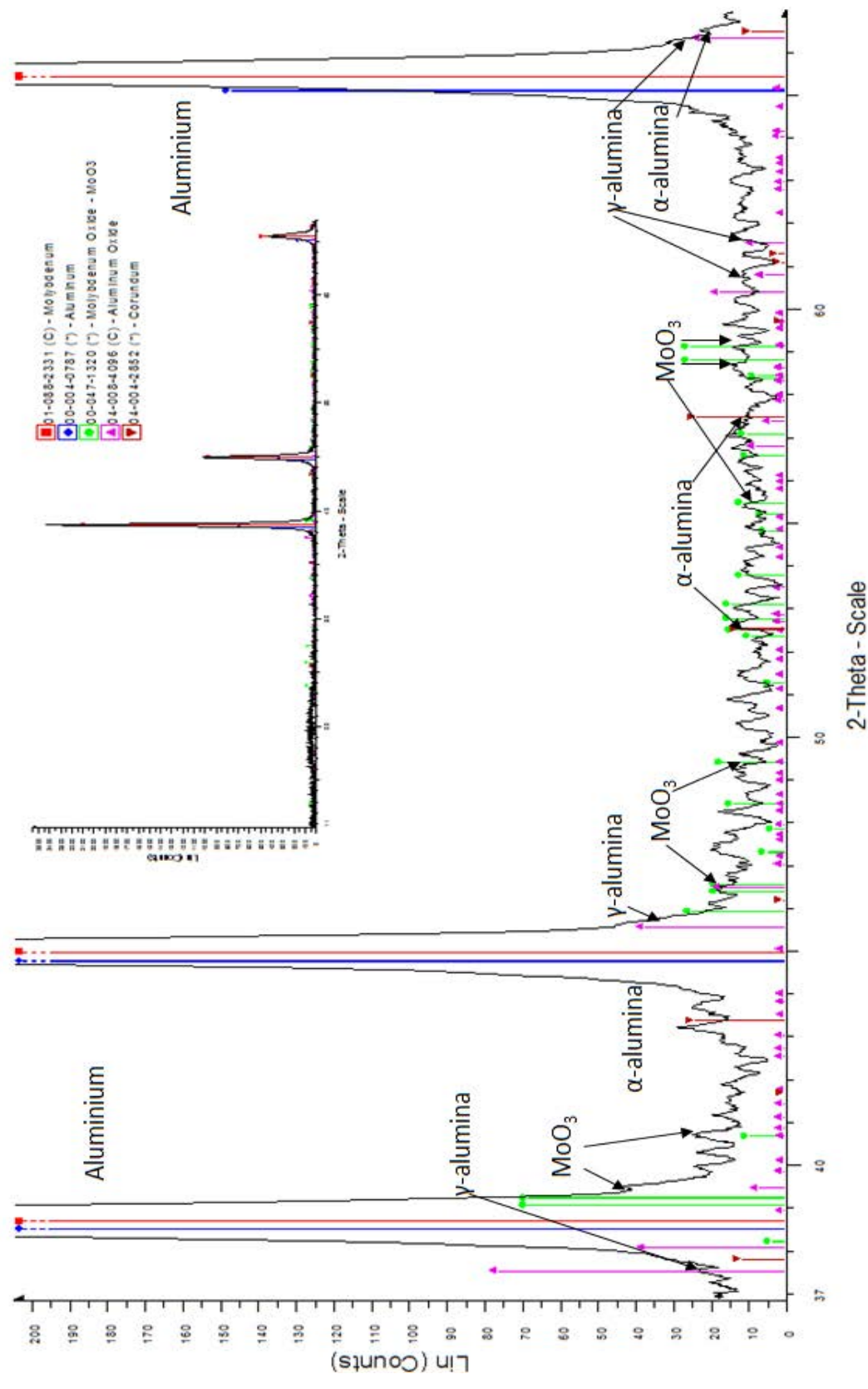
1 hour
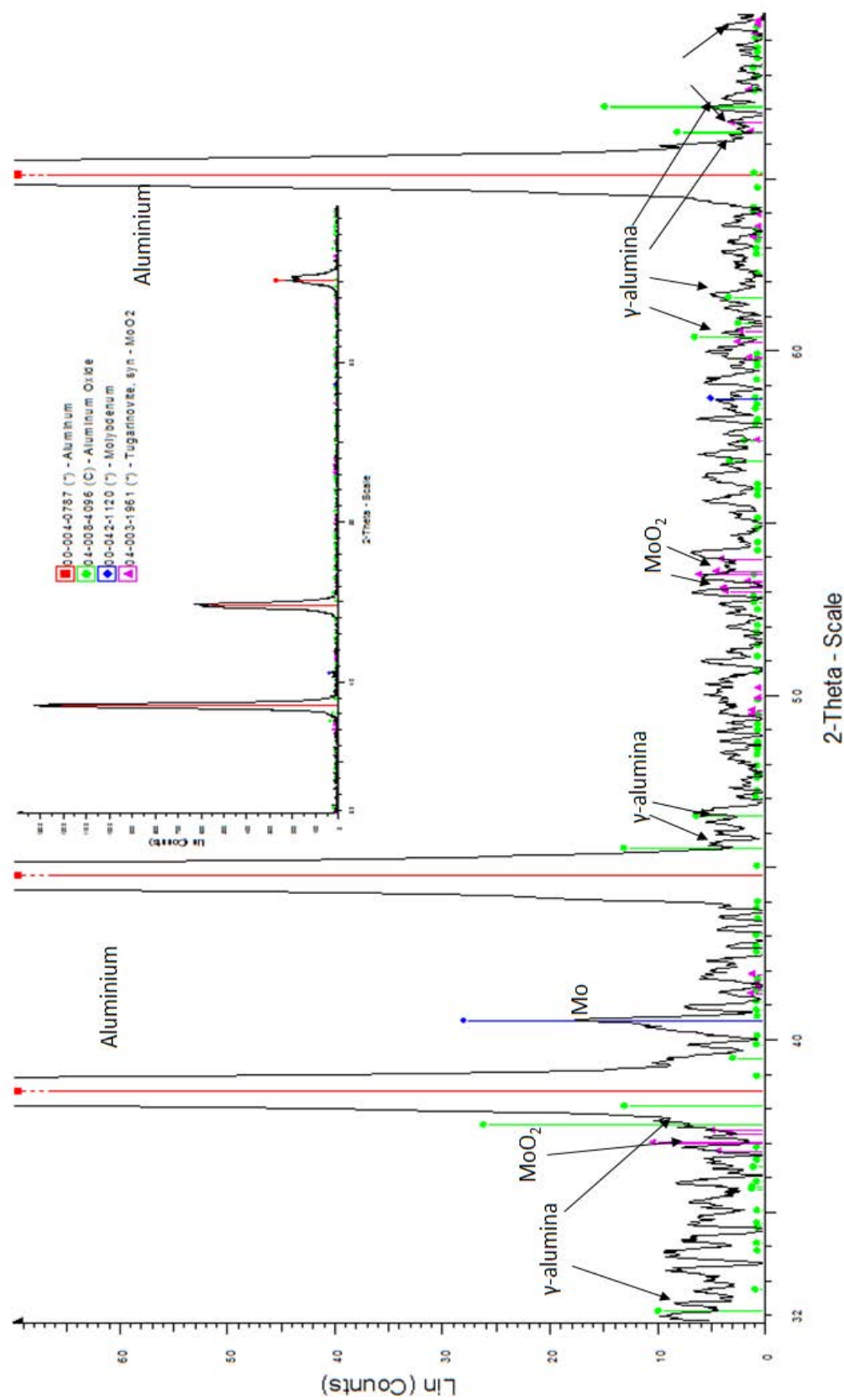
24 hours
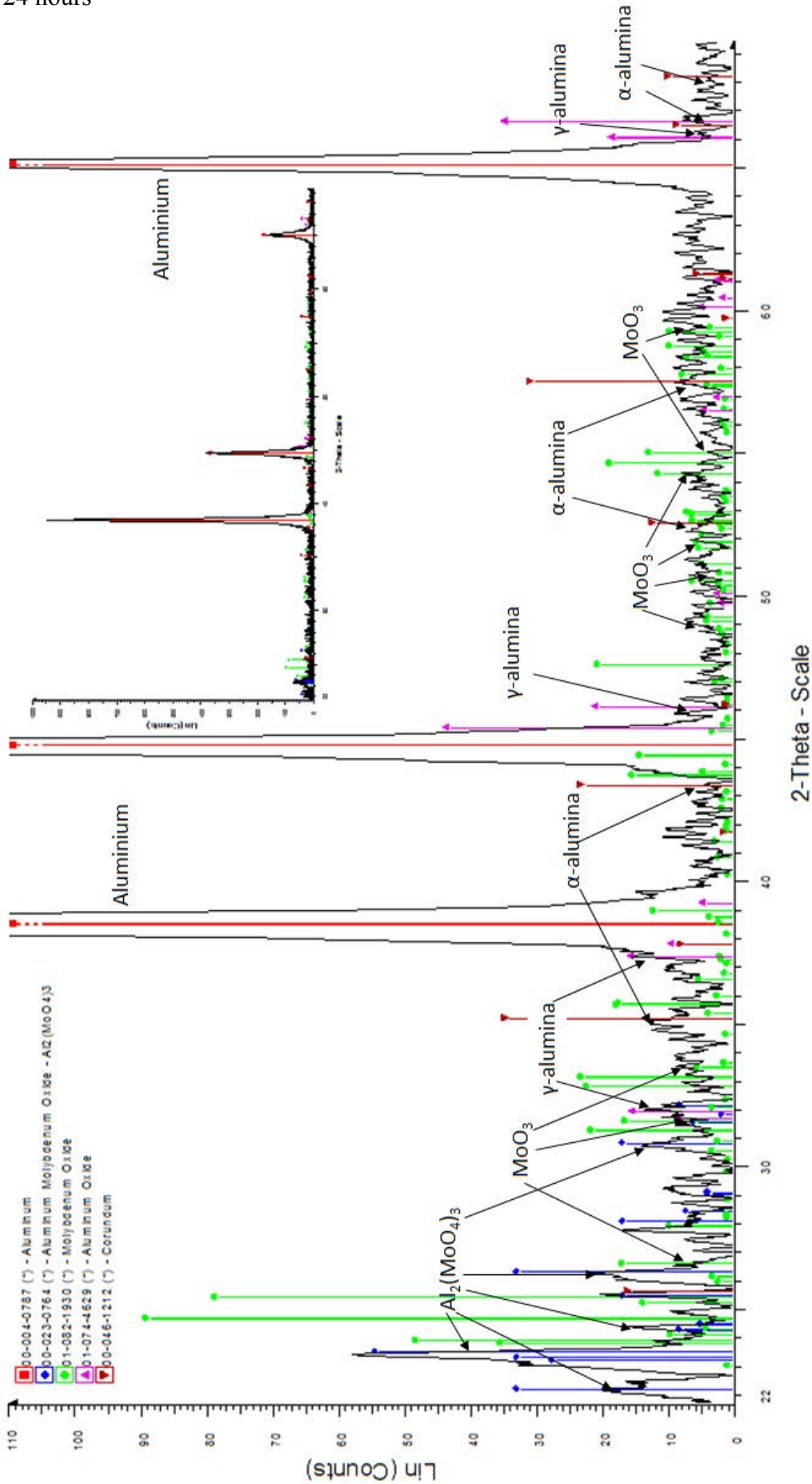
**Al-Mo**

5 minutes
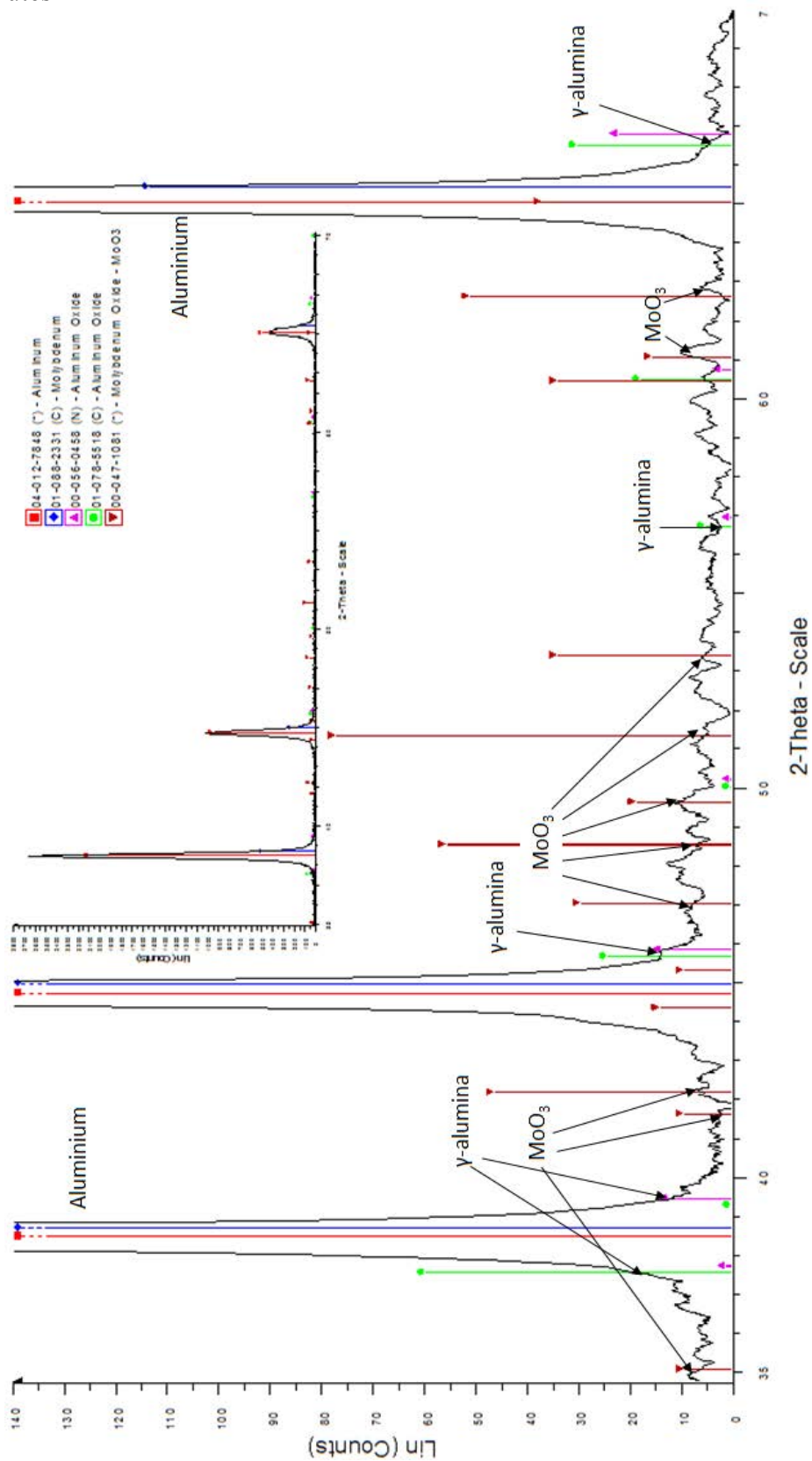
24 hours
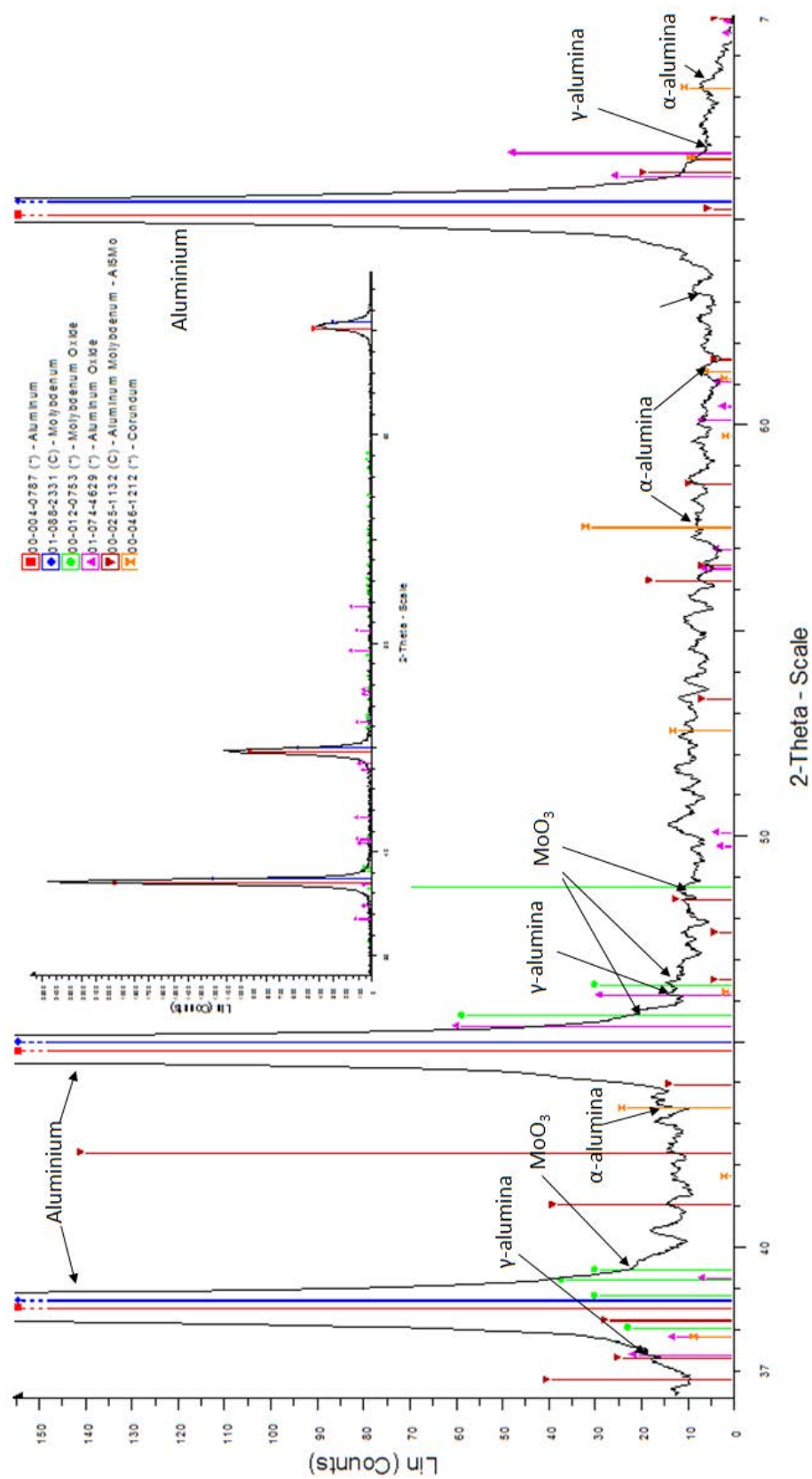
**Al-Si-Mg-Mo**
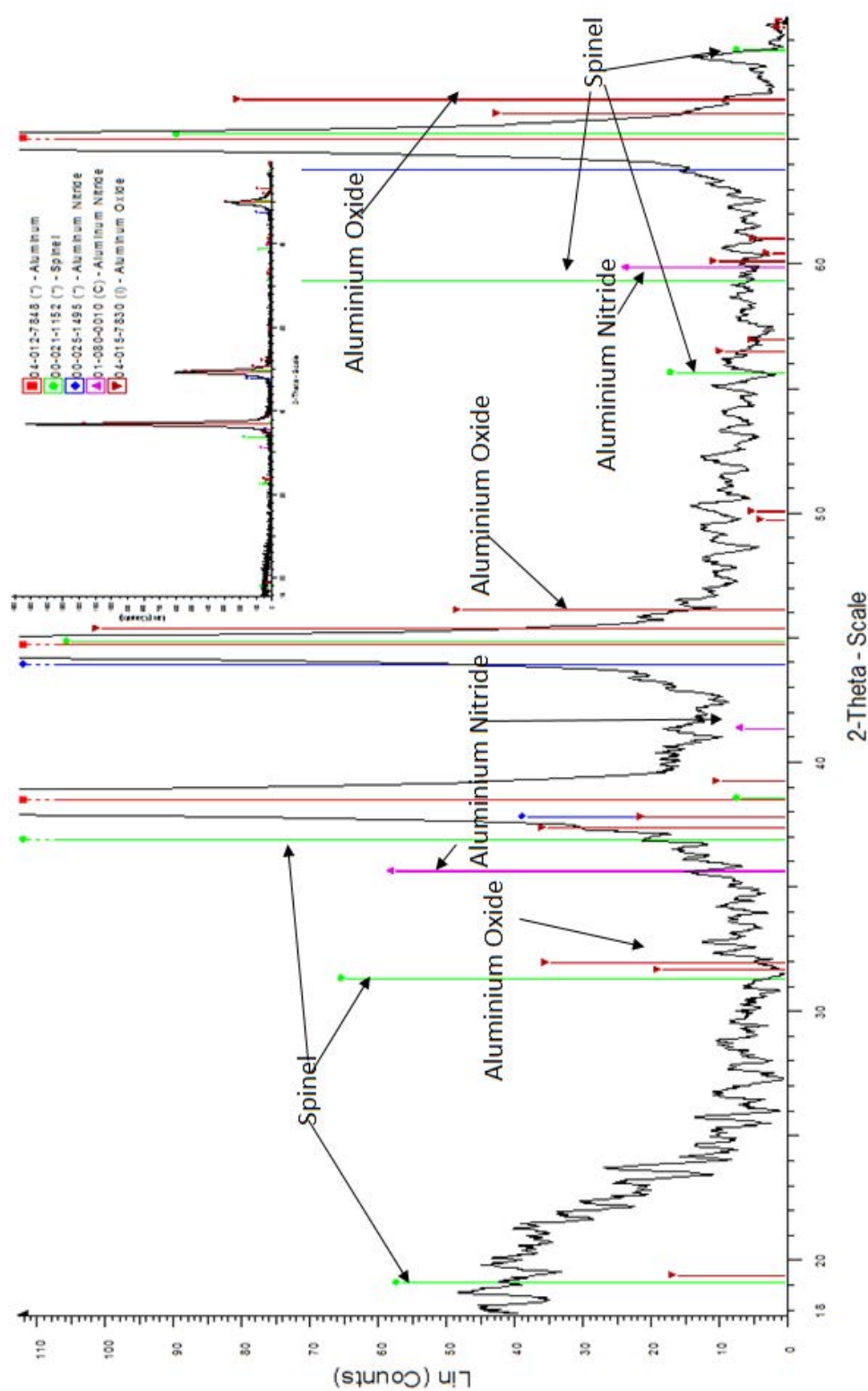
5 minutes
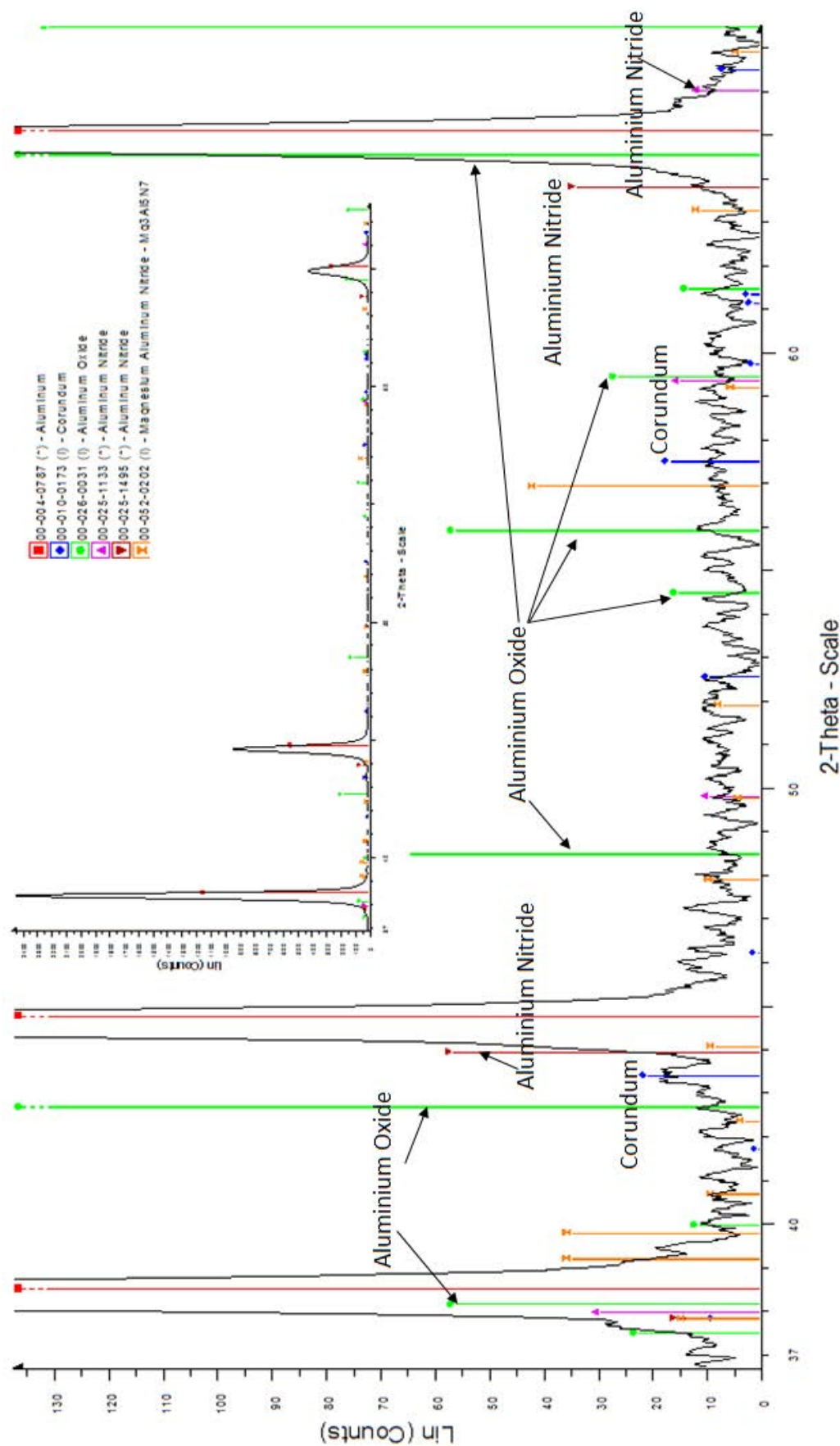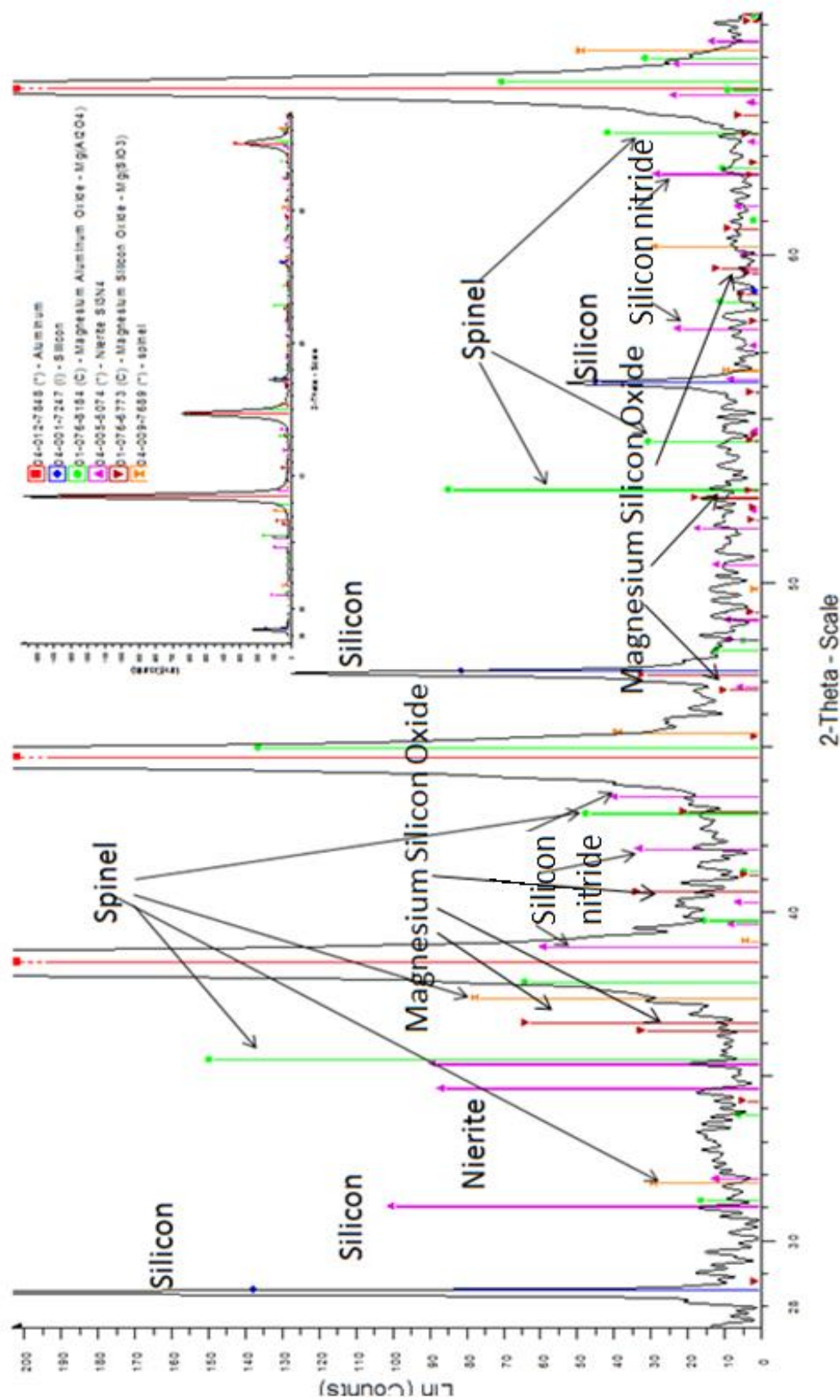
1 hour



230
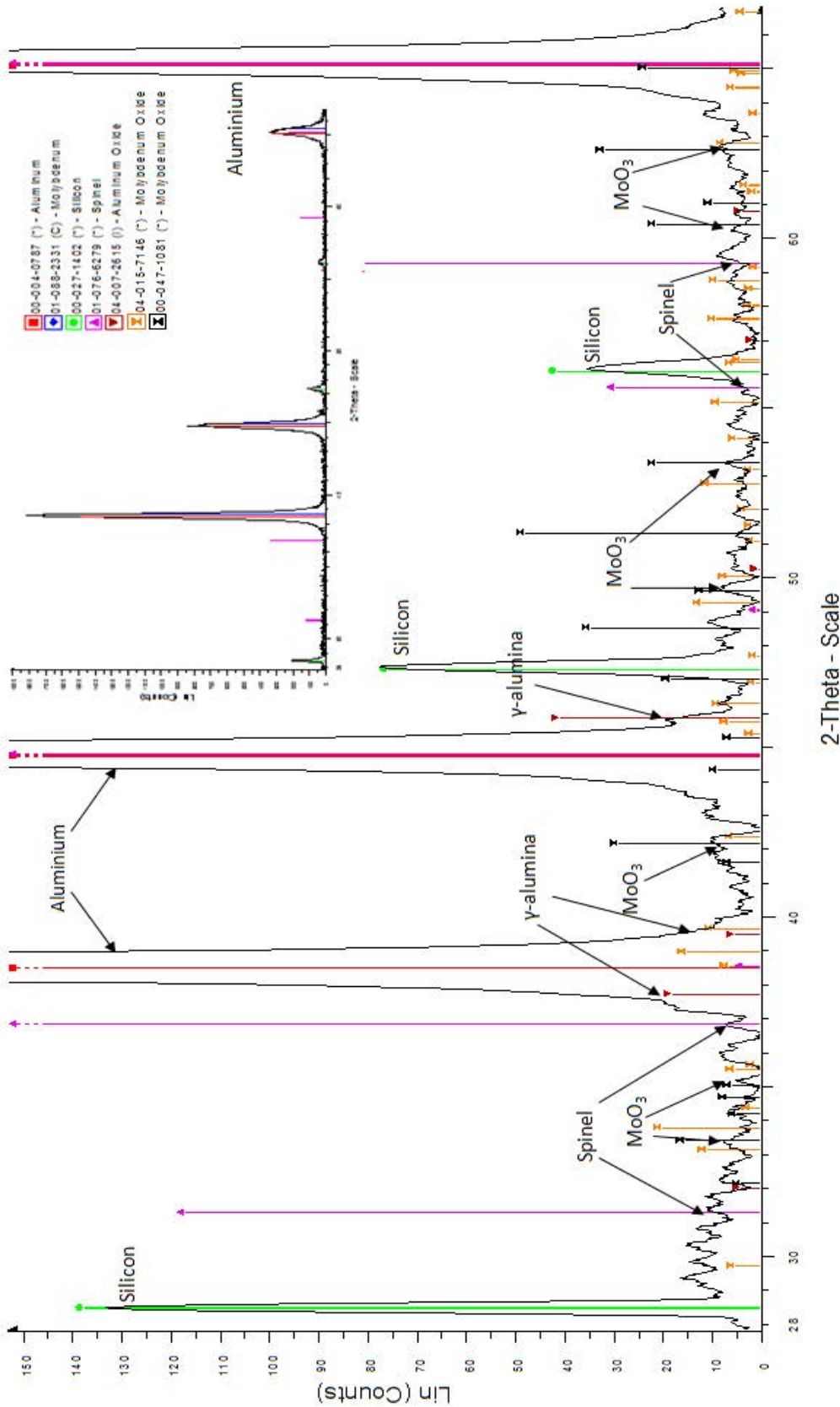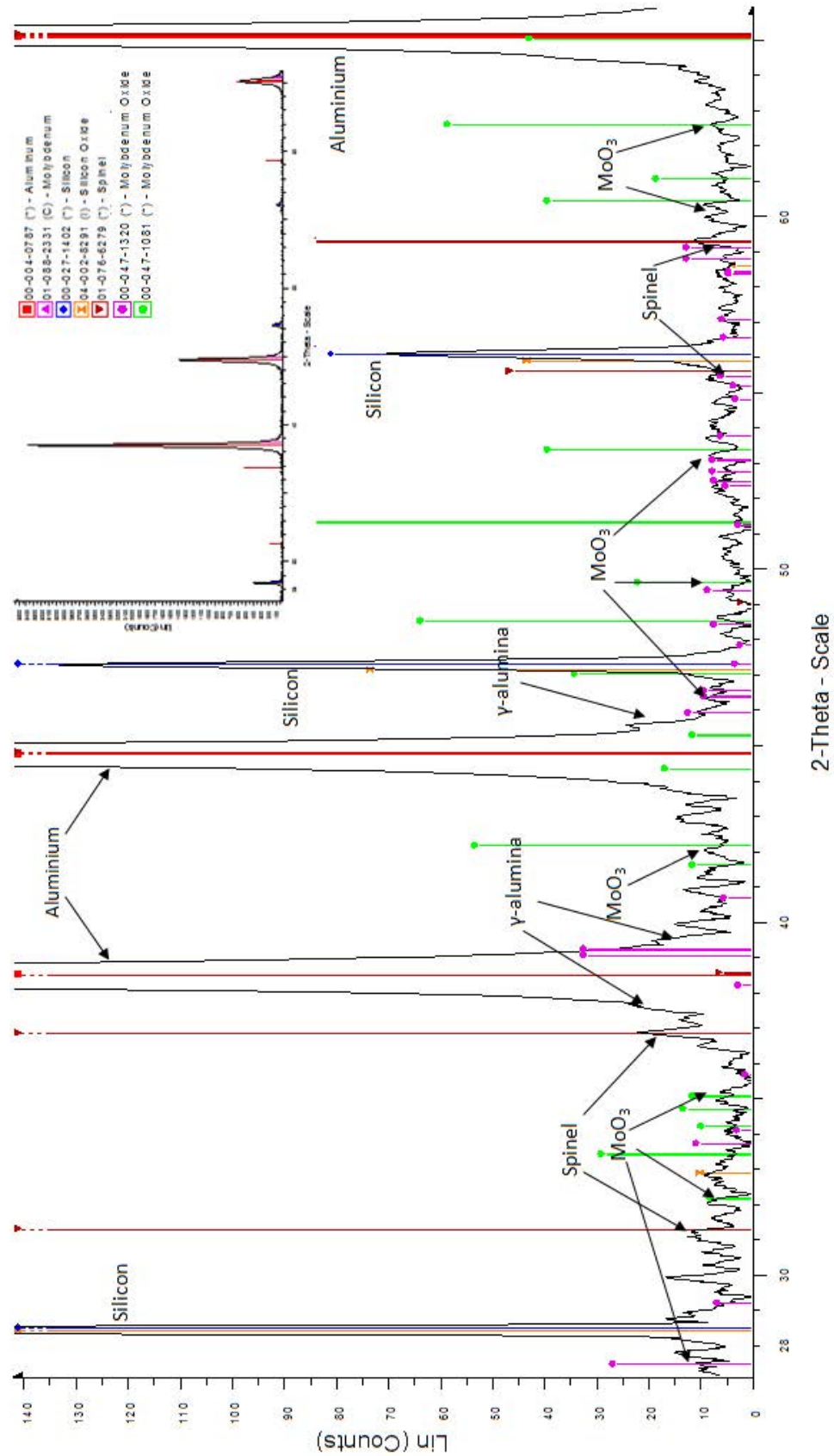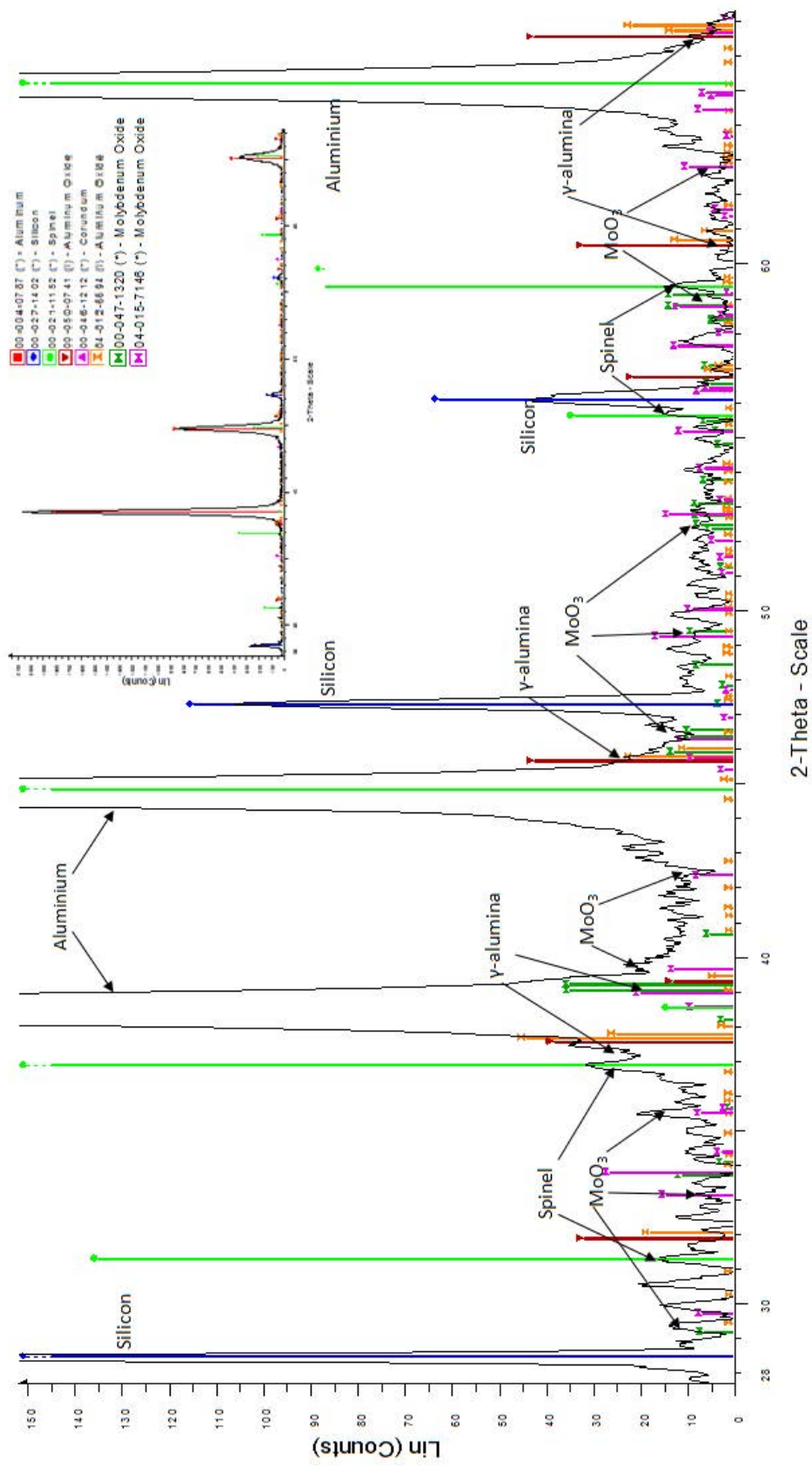
24 hours

**Al-N**

5 minutes
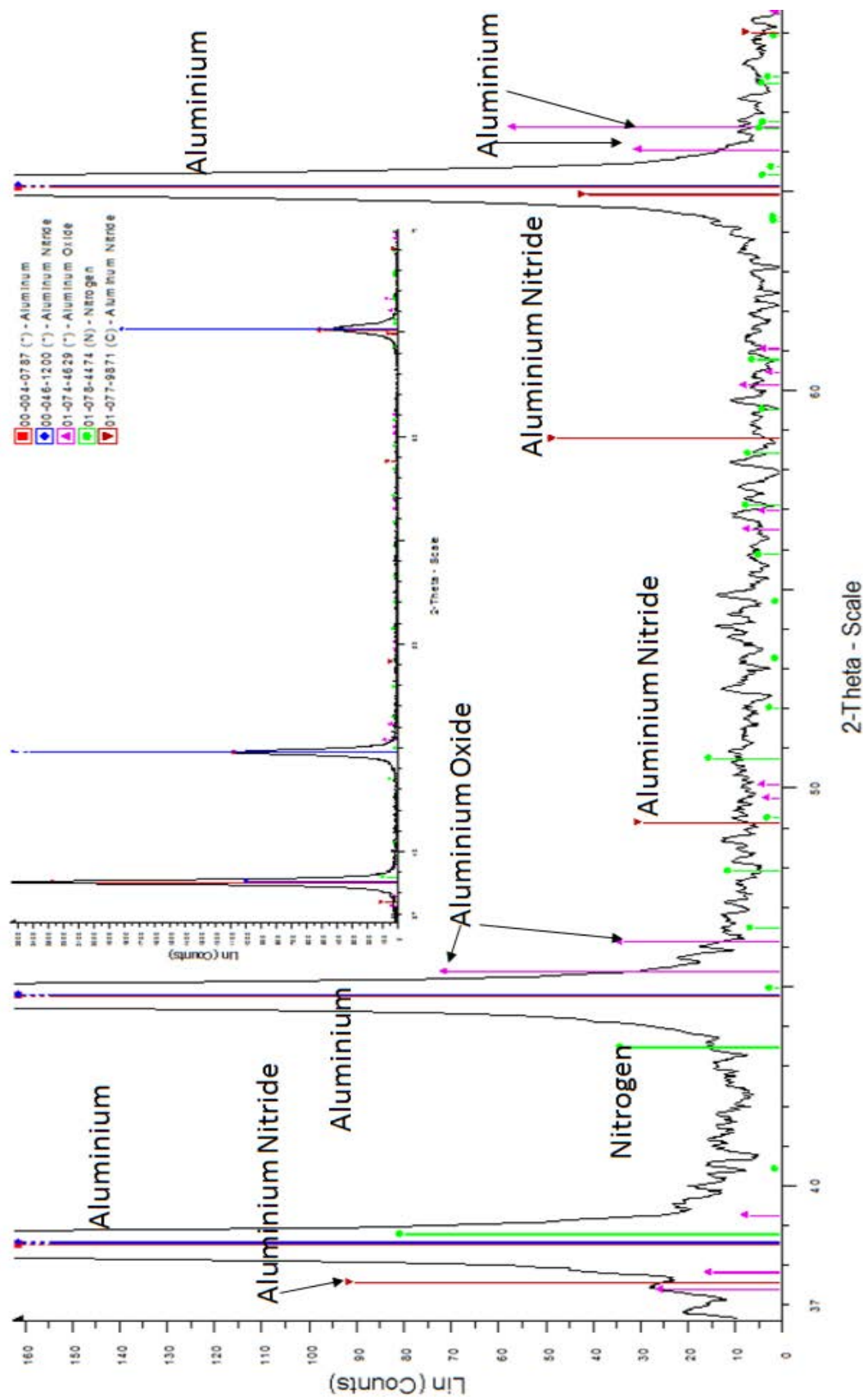
24 hours
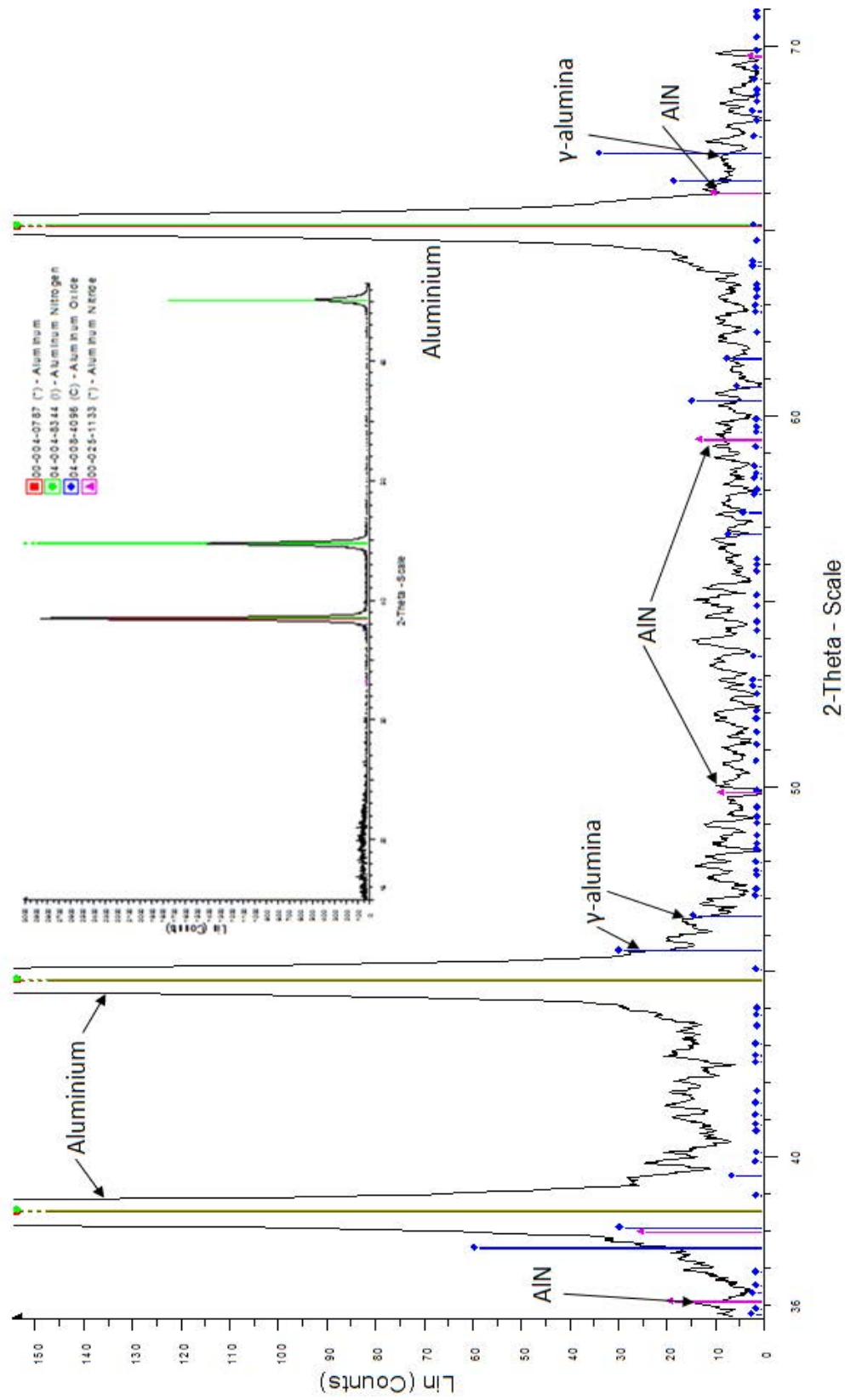
**Al-Mg-N**

5 minutes

24 hours

**Al-Si-Mg-N**

5 minutes

24 hours